Photoprotective & Solar Light Collecting Biomimetic Molecules

by

Katherine WongCarter

A Dissertation Presented in Partial Fulfillment
of the Requirements for the Degree
Doctor of Philosophy

Approved May 2014 by the
Graduate Supervisory Committee:

Ana Moore, Chair
Devens Gust
Ian Gould

ARIZONA STATE UNIVERSITY

August 2014

ABSTRACT

The first chapter reviews three decades of artificial photosynthetic research conducted by the A. Moore, T. Moore, and D. Gust research group. Several carotenoid (Car) and tetrapyrrole containing molecules were synthesized and investigated for excitation energy transfer (EET), photoregulation, and photoprotective functions. These artificial photosynthetic compounds mimicked known processes and investigated proposed mechanisms in natural systems. This research leads to a greater understanding of photosynthesis and design concepts for organic based solar energy conversion devices.

The second and third chapters analyze the triplet energy transfer in carotenoid containing dyads. Transient absorption, time-resolved FTIR and resonance Raman spectra revealed that in a 4-amide linked carotenophthalocyanine dyads the Car triplet state is shared across the larger conjugated system, which is similar to protein complexes in oxygenic photosynthetic organisms. In a carotenopurpurin dyad (CarPur) a methylene ester covalent bond prevents the purpurin (Pur) from influencing the Car triplet based on the transient absorption, time-resolved FTIR and resonance Raman spectra. Thus CarPur resembles the antenna proteins from anoxygenic photosynthetic bacteria. Additional examples of carotenoporphyrin dyads further demonstrates the need for orbital overlap for ultrafast triplet energy transfer and the formations of possible intramolecular charge transfer state.

The fourth chapter studies a 4-amino phenyl carotenophthalocyanine and its model compounds using high temporal resolution transient absorption spectroscopy techniques. EET from the Car second excited (S_2) state to the phthalocyanine (Pc) was determined to be 37% and a coupled hot ground state (S*)/Pc excited state spectrum was observed.

Excitation of the tetrapyrrole portion of the dyad did not yield any kinetic differences, but there was an S* signal during the excited states of the dyad. This demonstrates the EET and photoregulating properties of this artificial photosynthetic compound are similar to those of natural photosynthesis.

The last chapter covers the synthesis of silicon Pc (SiPc) dyes and the methods for attaching them to gold nanoparticles and flat gold surfaces. SiPc attached to patterned gold surfaces had unperturbed fluorescence, however the selectivity for the gold was low, so alternative materials are under investigation to improve the dye's selectivity for the gold surface.

DEDICATION

For my loving parents.

ACKNOWLEDGMENTS

I am grateful to Ana Moore for taking me under her wing to pursue my dream of working of artificial photosynthesis, and for giving me the chance to take my first steps towards being an independent researcher. I would like to express my gratitude to Tom Moore, Devens Gust, and Ian Gould for the insightful conversations and your encouragement through this graduate program.

I am indebted to many of our collaborators for their expertise and productivity. It was a pleasure to work with you: Alastair Gardiner, Richard Cogdell, Dario Polli, Denise Glazerano, Bruno Robert, Vladimiro Mujica, Hideki Hashimoto, Rienk van Grondelle, Dorota Kowalska, Nicodem Czechowski, Sebastian Maćkowski, and Erica Wee. Thanks to the Human Frontiers Science Project and Department of Energy for your financial support for this research. I'd like to thank Karl Weiss and Tim Karcher at the LeRoy Erying Center for Solid State Science, John Lopez and Zach Laughrey at the Proteomics and Protein Chemistry Facility, and Brian Cherry at the Magnetic Resonance Research Center for your technical prowess.

Thank you Smitha Pillai for teaching me just about everything I know about organic chemistry. All the way from my very first silica gel column to analyzing the dyad NMRs, you've been the most superb role model and mentor. Thanks to Gerdenis Kodis for your patience teaching me about many different spectroscopic techniques, and answering my numerous and repetitious questions. I'd like to thank Paul Liddell and Yuichi Terezano for your infinite synthetic wisdom. It was always a joy listening to your stories both chemistry related and otherwise. I would like to thank my labmate Brian Watson for reminding me about the big picture of our research and always dreaming big no matter how big the dirty

glassware pile was. I am grateful for my comrades, Antaeres Antoniuk-Pablant, Jaro Arero, Dalvin Méndez-Hernández, and John Tomlin, whom I enjoyed discussing chemistry, careers, computers, science policy, and life in general. Thank you for the fond memories studying for exams in the new graduate student room and the former coffee shop at the end of Mill Avenue, and our grasshopper talks in the break room. I hope you find much success and happiness wherever your endeavors take you. Thanks to Matthieu Kepof, Jesse Bergkamp, and Manuel Llonsola-Portolés, and all current and past members of the Moore/Moore/Gust group for showing me how to work-hard and play-hard.

Thank you to my climbing partners, hiking buddies, and fellow graduate students that have literally and figuratively caught me when I'd fallen and put me back on track. I'd like to thank my Grandfather, Roy Hayter, for the gentle nudge towards chemistry, and to my early science teachers, Mrs. Schwartz and Mrs. Lovelace, for making science spectacular. I grateful to thank Marilyn Murphy for encouraging me to pursue this PhD.

I owe my deepest gratitude to my parents for their endless encouragement to follow my heart, and for giving me the tools to go out and do just that. Thank you to my sister, Lisa, for sharing your advice and worldly experience. Your creative perspective always seems to turning everything upside-down and right-side up at the same time. And many thanks goes to my husband, Austin, for standing by me through the entire graduate school process and especially while writing this dissertation. Your attentive ear, supporting shoulders, and encouraging words kept me focused – even though I strayed so often! I hope this may be one of many adventures that we share together.

TABLE OF CONTENTS

CHAPTER Page

Page

LIST OF TABLES

Table Page

LIST OF FIGURES

Figure Page

Figure Page

Figure Page

Figure Page

Figure Page

CHAPTER 1

INTRODUCTION: LIGHT HARVESTING, PHOTOREGULATION, AND PHOTOPROTECTION IN SELECTED ARTIFICIAL PHOTOSYNTHETIC SYSTEMS

Katherine WongCarter, Manuel J. Llansola-Portolés, Gerdenis Kodis, Devens Gust, Ana L. Moore and Thomas A. Moore

Department of Biochemistry & Chemistry, Arizona State University, Tempe, Arizona 85287, USA

This document was submitted for publishing in *Light-Harvesting in Photosynthesis* by Taylor & Francis, New York, NY. Edited by R. van Grondelle and R. Croce.

Introduction to Artificial Photosynthesis

Artificial photosynthesis (AP) includes the design and synthesis of molecular systems that manifest selected aspects of the natural photosynthetic process[1]. The essential photochemistry of these synthetic systems follows from that of their natural counterparts: absorption of sunlight, energy transfer, regulation of energy flow, protection from photodamage and conversion of excited states to redox potential. Also, AP includes catalysis and ultimately self-repair and replication. Following the example from nature, the goal of AP is to assemble molecular systems into larger scale constructs capable of storing a fraction of the energy carried by sunlight in energy rich compounds.

AP is a diverse field that is in its infancy and already involves contributions from disciplines ranging from physics through chemistry and material science to synthetic biology. AP includes a future in which photosynthesis is reengineered for higher efficiency using the design principles developed in simpler artificial systems and new engineered

forms of life where heterotrophic organisms are converted to autotrophs by interfacing them to sources of electrons and electromotive force (emf)[1a, 2]. These hybrid constructs will have retained the essential features of living organisms including repair, replication and self-assembly, but their metabolism will be driven by solar photovoltaic (PV) cells[3].

AP research today is largely focused on the understanding and mimicry of the steps (processes) employed by photosynthesis to produce an energy rich fuel. These processes are linked to photosynthetic membranes where antenna pigments convert solar photons to excited states, regulate the flow of collected excitation energy to reaction centers (RC), and suppress the undesirable production of reactive oxygen species (ROS) such as molecular singlet oxygen. RCs use the excited states of specialized chlorophyll pigments to generate high-potential and low-potential redox species; electron flow down the resulting redox gradient is used to pump protons across the photosynthetic membrane, thereby generating proton motive force (pmf). In algae, photosynthetic cyanobacteria and higher plants, the electrons are used to reduce carbon dioxide. The source of electrons and hydrogen ions is water oxidation. AP systems designed today use these same sources of electrons and carbon. For the foreseeable future, this is certainly appropriate because the imperative to develop carbon-neutral energy and to draw down atmospheric CO_2 will require a source of electrons that can only be met by water oxidation.

One of many approaches to the assembly of AP model compounds is to use synthetic chromophores that are related to the natural pigments (bacteriochlorophylls, chlorophylls, carotenoids, etc.), but to use covalent bonds in place of the proteins that are used in natural systems to hold and organize the pigments. In the pigment protein complexes of natural photosynthetic membranes the electronic interactions, for example

between carotenoids and chlorophylls, that give rise to energy and electron transfer are in part a consequence of the proximity of their π electron systems, which is a function of the distance and geometry imposed on the pigments by the secondary, tertiary and quaternary protein structure. In general, these may be thought of as through space interactions, although protein moieties may play a part. In our model systems interchromophore distance and geometry are controlled by the linkage bonds joining the carotenoid and cyclic tetrapyrrole moieties. There are two limiting roles for the linker. In cases where the electronic structure of the linkage participates in the coupling, the interaction is referred to as through bond and, in cases where the linkage does not participate to a measureable extent, the coupling is referred to as through space. These two interactions are not mutually exclusive; AP models can be designed to involve both through space and through bond electronic couplings.

In our experience, regardless of whether the coupling is a consequence of through space or through bond interactions, in a wide variety of photophysical and photochemical measurements, our model systems have demonstrated the same essential features of electronic coupling required for the energy and electron transfer as are observed in the natural systems.

In this chapter we review a selection of the AP constructs developed in our laboratories that mimic many of the photochemical steps that occur in the natural

photosynthetic antenna systems. Reviews of our work in AP reaction centers, proton pumps, water oxidation, and proton reduction have been published elsewhere[1e, 1f, 1i].

Antenna Function

In nature, chlorophylls and bacteriochlorophylls are prevalent throughout the photosynthetic antenna, but they only absorb light strongly in the blue and red regions of the visible solar spectrum. By incorporating other pigments that collect photons from the remaining part of the available wavelengths of sunlight, plants, algae, and photosynthetic bacteria are able to collect more energy (Figure 1). Carotenoids play a key role in absorbing the green and yellow photons of the solar spectrum (400–550 nm region). An efficient energy transport mechanism is needed in order to pass the energy from the carotenoids and other pigments to the RC, where the excitation energy is transformed into chemical potential in the form of a charge separated state[4].

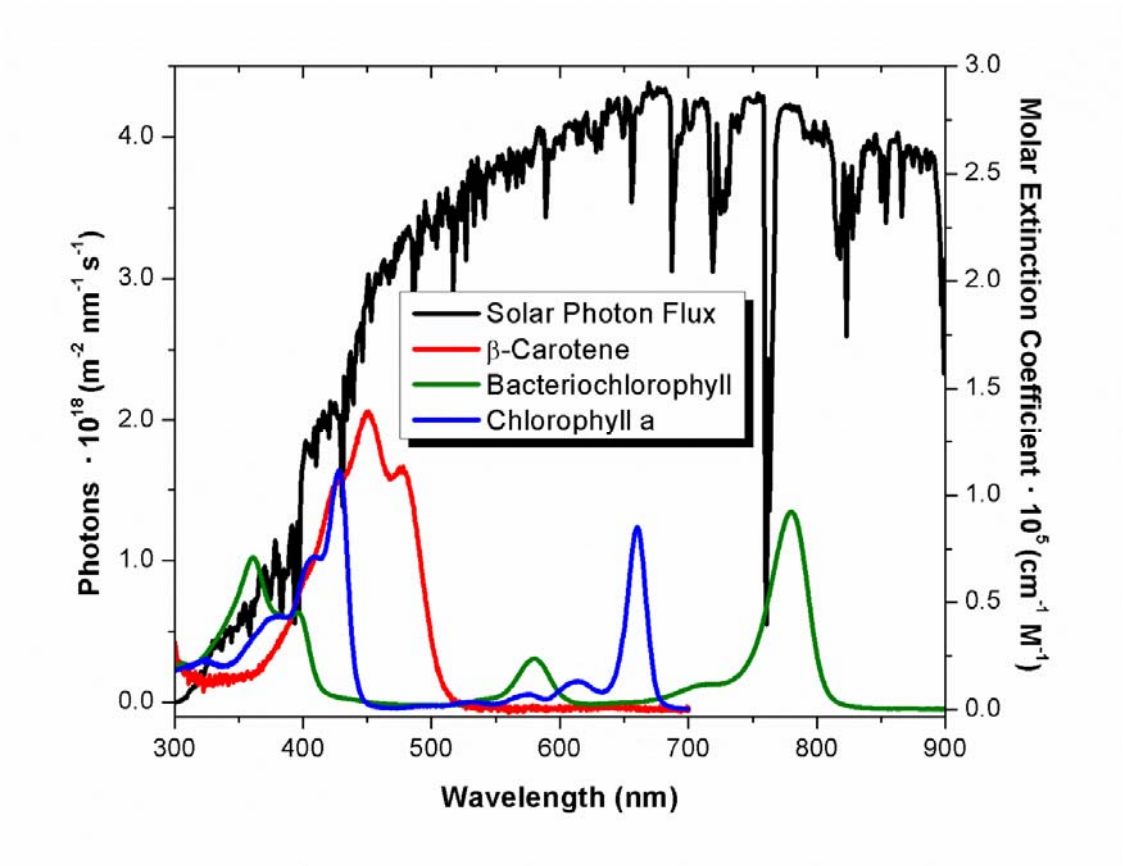

Figure 1. Solar irradiance spectrum (left axis) and absorption spectra of some photosynthetic pigments (right axis).

In this section we will describe a series of artificial antennas that exhibit very low excitation energy transfer (EET) efficiency and others where the efficiency reaches unity. The artificial antenna compounds are presented in chronological order to demonstrate the evolution of synthetic antenna design over time. The measured EET efficiency as a function of the electronic coupling between the chromophores guided the synthetic work.

Carotenoid based antennas. The first artificial antenna molecules synthesized by our research group were carotenoporphyrins[5]. These systems consisted of a porphyrin covalently attached to carotenoids with 6 or 10 carbon-carbon double bonds (db) conjugated with a phenyl ring (compounds **1** and **2** in Figure 2). Carotenoids with different

conjugation lengths, or number of db, were used to tune the wavelength of absorption. The absorption spectra of **1** and **2** are essentially identical to the sum of the spectra of related unlinked carotenoids and porphyrins, indicating that there is no strong electronic coupling between the chromophores. The ester linkage constrains the edges of the carotenoid and porphyrin π-orbitals to be close to one another and provides weak electronic coupling. Using steady state fluorescence excitation spectroscopy, it was found that in **1**, the efficiency of EET from the carotenoid to the porphyrin is 80%. However, this short carotenoid absorbs light in about the same spectral region as the porphyrin and hence does not add significantly to the spectral range used. The longer carotenoid employed in **2** collects light from an underutilized region of the solar spectrum, but none of the light absorbed by this carotenoid led to fluorescence emission from the porphyrin in dyad **2**,

indicating that EET was vanishingly small. This result suggests that a greater degree of electronic interaction between the energy donor and acceptor moieties is required.

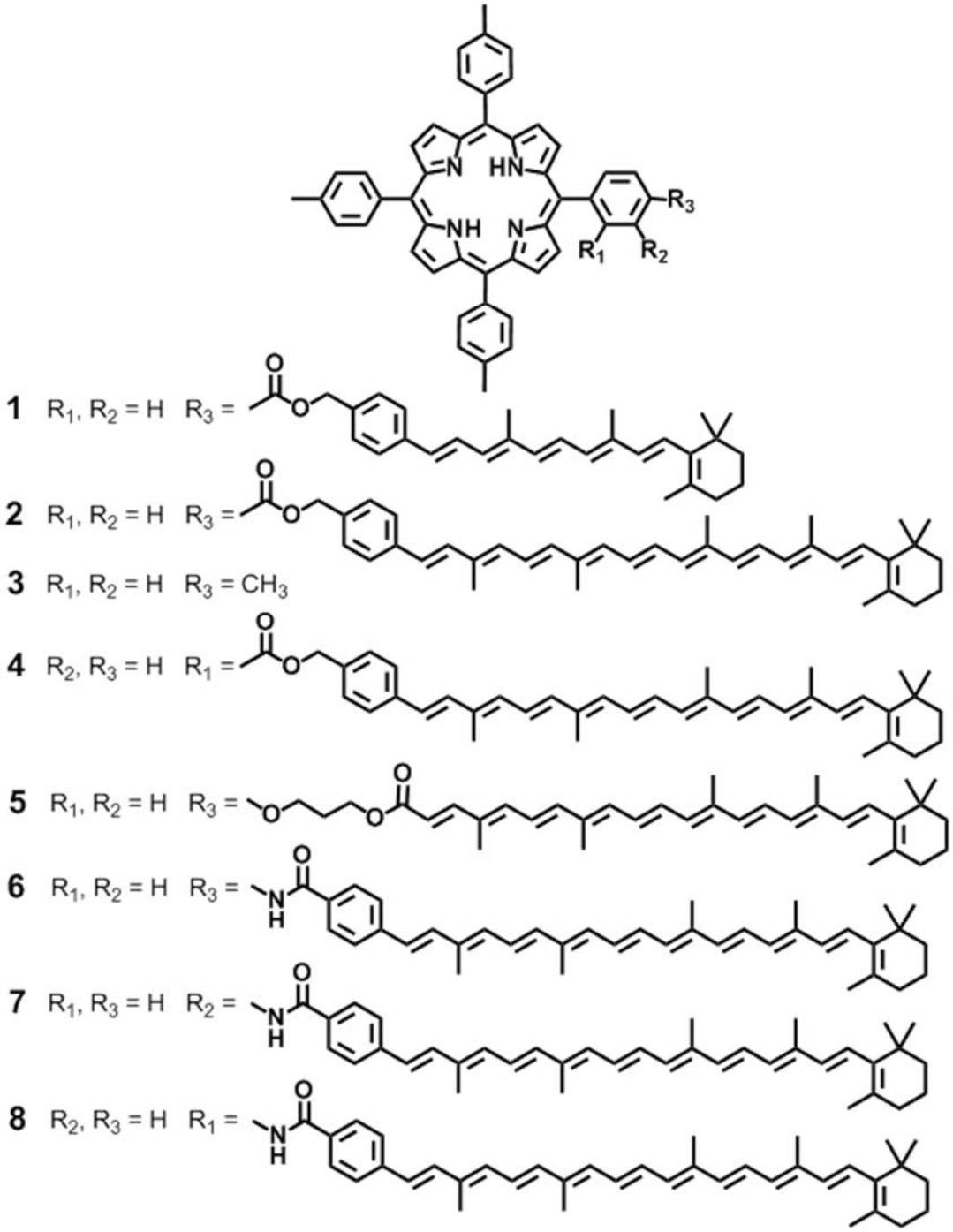

Figure 2. Molecular structures of carotenoporphyrin dyads and *meso*-tetra(*para*-tolyl)porphyrin (TTP), **3**.

A constitutional isomer of **2**, dyad **4** (Figure 2), wherein the carotenoid is attached to an *ortho* position of the *meso* aryl ring of the porphyrin was synthesized in order to achieve a closer interaction of the two chromophores, while maintaining the same ester linkage. Nuclear magnetic resonance (NMR) studies of **4** demonstrated that as a result of the *ortho* attachment of the carotenoid to the porphyrin *meso* aryl group, the carotenoid folds back across the porphyrin so that the π-systems are essentially in van der Waals contact. Molecular mechanics calculations determined that the separation of the two π-stacked systems is ~4 Å and the fluorescence measurements showed 25% EET efficiency.

Dyads **2**, and **4**, illustrate the use of through bond and through space coupling that can be accessed in models. The electronic coupling provided by the linkage, as reflected by the number of bonds and the hybridization of the atoms, is essentially the same in both cases, and is insufficient to mediate singlet energy transfer (antenna function) from the carotenoid to the porphyrin and fast triplet-triplet (T–T) energy transfer. However, by adopting a folded conformation dyad **4** acquires through space interactions between the π systems resulting in both singlet-singlet (S–S) energy transfer and ultrafast T–T transfer (*vide infra*). This clearly demonstrates that through space electronic interactions can be mimicked in covalently linked dyads, provided a conformation can be acquired that provides the necessary orbital overlap.

Dyad variations of the *para* and *ortho* positioned carotenoids with longer (propyl) linkers to the porphyrin (e.g. **5**) and to pyropheophorbide (a derivative of natural chlorophyll) were also investigated for their EET capability in low and high viscosity environments[6]. The overall results corroborate the previous observation, that significant EET requires relatively strong electronic interaction between the chromophores such as

that provided by van der Waals contact. Later, it was found that increased electronic interactions between the carotenoid and cyclic tetrapyrrole moieties can also be achieved by involving the linkage itself[7].

The potential involvement of the linkage in the electronic interaction of carotenoids and cyclic tetrapyrroles was investigated in a study of carotenoporphyrin dyads **6**–**8** (Figure 2). These dyads consist of identical carotenoid and porphyrin moieties, which are joined by a relatively rigid amide group, but the point of attachment of the carotenoid to the porphyrin *meso* aryl group was varied. The S-S energy transfer quantum yields, measured by fluorescence, were 0.17, 0.10, and 0.13 for **8**, **7**, and **6**, respectively. A lower energy transfer quantum yield, and therefore a slower singlet energy transfer rate, was observed for the *meta* isomer, **7**, than for *para* isomer, **6**, despite the fact that molecular mechanics calculations showed that the separation of the two chromophores is smaller for **7**. These results were consistent with energy transfer mediated by the linkage bonds rather than by a through-space mechanism.

Qualitatively, this superexchange, or through-bond, hypothesis was evaluated using simple Hückel molecular orbital theory assuming that the highest occupied (HOMO) and lowest unoccupied (LUMO) molecular orbitals of the linker were involved in the interaction. These results showed that for both HOMO and LUMO the coefficient of the wavefunction is greater at the *ortho* and *para* positions than at *meta* position.

One of the big challenges in building artificial photosynthetic antennas with carotenoids is the unique photophysics of linear polyenes. Carotenoids typically have very high extinction coefficients in the 450–500 nm spectral region (on the order of 10^5 M^{-1} cm^{-1}, see Figure 1). This strongly allowed transition is from the ground state, S_0 (A_g^-), to the

second excited singlet state, S_2 ($1^1B_u^+$) (group theory symbols for C_{2h} symmetry). As expected for an upper excited singlet state, the S_2 lifetime is extremely short (< 300 fs). The transition from the ground state, S_0 (A_g^-), to the lowest-lying excited singlet state of carotenoids, S_1 ($2^1A_g^-$), is single photon forbidden, and the state is populated by relaxation from S_2. The lifetime of the S_1 state, is on the order of 1-100 ps for most carotenoids and is inversely dependent on the length of the polyene. There are other dark excited states found in carotenoids, such as the $1^1B_u^-$ and 3^1Ag^- states that have been theoretically predicted and the S* and $S^‡$ that are readily seen in transient absorption experiments[4, 8]. In general, the unusual characteristics of the carotenoid excited states impose strict constraints on the electronic coupling and thermodynamics necessary for the energy and electron transfer processes between them and cyclic tetrapyrroles which are crucial to photosynthesis and AP.

9

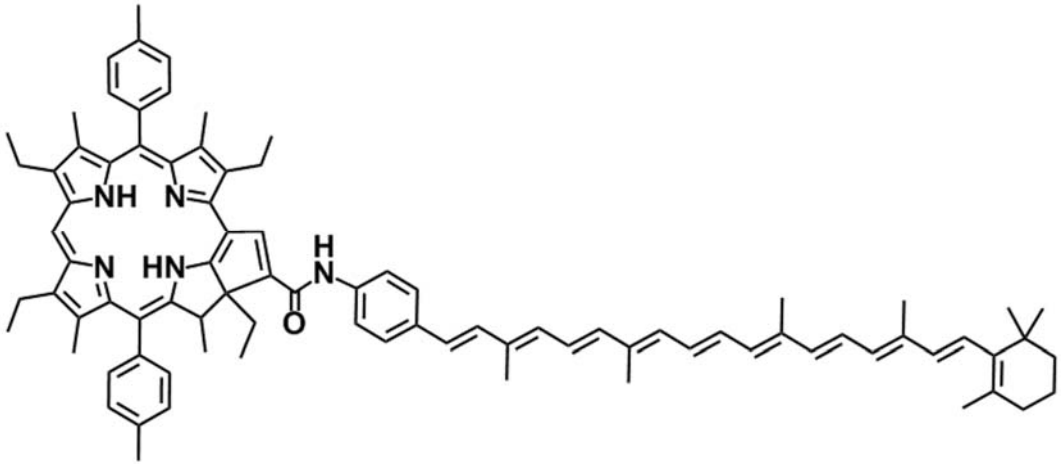

Figure 3. Molecular structure of dyad **9**, a 10 db carotenoid linked through a phenylamide group to the fused cyclopentadiene ring of a purpurin.

Even though the carotenoid S_2 state lifetime is extremely short, we were able to achieve efficient EET in dyad **9** (Figure 3) by careful attention to electronic coupling and thermodynamic parameters[9]. Measured by fluorescence upconversion spectroscopy, the S_2

lifetime of a model for the carotenoid in dyad **9**, a phenylacetamido substituted carotenoid with 10 db, was found to be 150 fs. In dyad **9**, the carotenoid moiety was found to have a considerably shorter lifetime, ~40 fs. If this quenching is attributed entirely to EET from the carotenoid S_2 state to the purpurin moiety, the quantum yield of this process would be 0.73 from:

$$\Phi = 1 - \frac{\tau_q}{\tau_f} \qquad \text{equation (1)}$$

where τ_q and τ_f are the S_2 lifetimes of the carotenoid moiety of the dyad and the carotenoid model alone, respectively. Indeed, steady-state fluorescence excitation measurements revealed that the quantum yield was in agreement with that calculated from the kinetics. The rate constant for EET in this system ($\sim 2 \times 10^{-13}$ s^{-1}) is of the order of that observed in natural light-harvesting antennas. Further evidence for EET from S_2 comes from the observation that the lifetime of the S_1 state of the carotenoid (7.8 ps) was the same in both a carotenoid model and the dyad. Moreover, the 10 db carotenoid S_1 state energy is below that of the lowest singlet excited state, Q_y, of the purpurin or the lowest singlet excited state, Q_x, of porphyrins (Platt's nomenclature for cyclic tetrapyrroles of D_{2h} symmetry)[10]. Therefore EET is only possible from the S_2 state of the carotenoid as depicted in Figure 4. We attribute efficient EET from S_2 to the electronic coupling provided by the amide group and the favorable thermodynamics achieved by overlap between the purpurin Q_x bands and the carotenoid S_2 state.

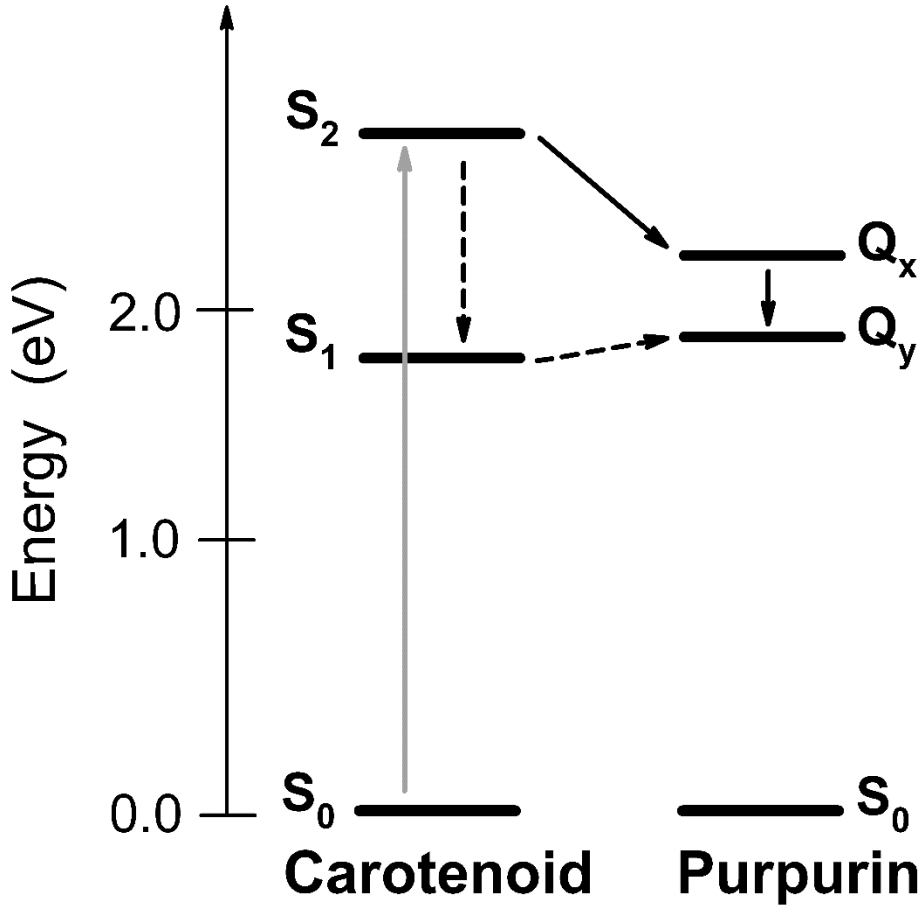

Figure 4. Singlet energy transfer pathways from the carotenoid S_2 state (solid arrow) or involving the carotenoid S_1 state route (dashed arrows, not observed) to the purpurin in dyad **9**. The grey arrow indicates the population of S_2 by direct excitation.

Triad **10** (Figure 5) was designed to address the question of energy transfer from carotenoids to cyclic tetrapyrroles as a function of the relative orientations of the pigments[11]. Inspiration for this series comes from the relative orientation of carotenoid to bacteriochlorophyll in the B800/B850 LH2 of *Rps. acidophila*, where the carotenoids are approximately perpendicular to the plane of the macrocycle in B800 and approximately parallel the plane in B850[12]. In triad **10**, two 9 db carotenoids are linked on opposite sides to a silicon phthalocyanine (Pc) through an ester linkage at the center of the macrocycle and extend axially at an angle of approximately 90° to the plane of the cyclic tetrapyrrole

(Figure 5). It was found that efficient EET was achieved by using both the S_2 and the S_1 states. To determine in detail how the carotenoid S_1 and S_2 excited states are involved in the flow of energy to Pc, the lifetimes of these excited states were measured in a model carotenoid and in triad **10**. By fluorescence upconversion spectroscopy it was demonstrated that the S_2 state of the carotenoid was quenched from 82 fs in the model carotenoid to 53 fs in **10**, resulting in an EET efficiency of 35% from the S_2 state. The contribution of S_1 was investigated by transient absorption measurements. The observed difference in the S_1 state lifetime of a carotenoid in triad **10** (2.6 ps) and the carotenoid model (24.4 ps), taking into account that the quantum yield of formation of the S_1 state was only 65%, gives the quantum yield of energy transfer from S_1 as ~58%. Thus, the overall quantum yield of EET from carotenoid to Pc from both the S_2 (35%) and S_1 (58%) states was 93%, in excellent agreement with the value estimated from steady state fluorescence excitation measurements[11]. As illustrated above, we note that steady state fluorescence excitation spectroscopy can only give the total EET efficiency. Time resolved methods are required to resolve the contributions from the individual states. As we shall demonstrate below, these contributions are a sensitive function of the electronic structure of the carotenoid moiety.

Extending the carotenoid conjugation by one double bond from 9 to 10 in triad **11** (Figure 5) reduced the overall EET efficiency from ~90% to 30%. This change is a result of the S_1 level in the longer carotenoid moving below that of the lowest singlet state, Q (for D_{4h} symmetry compounds)[10], of the Pc making energy transfer from the S_1 state of carotenoid to the Pc thermodynamically unfavorable. Thus, in triad **11** EET to Pc occurs only from the carotenoid S_2 state.

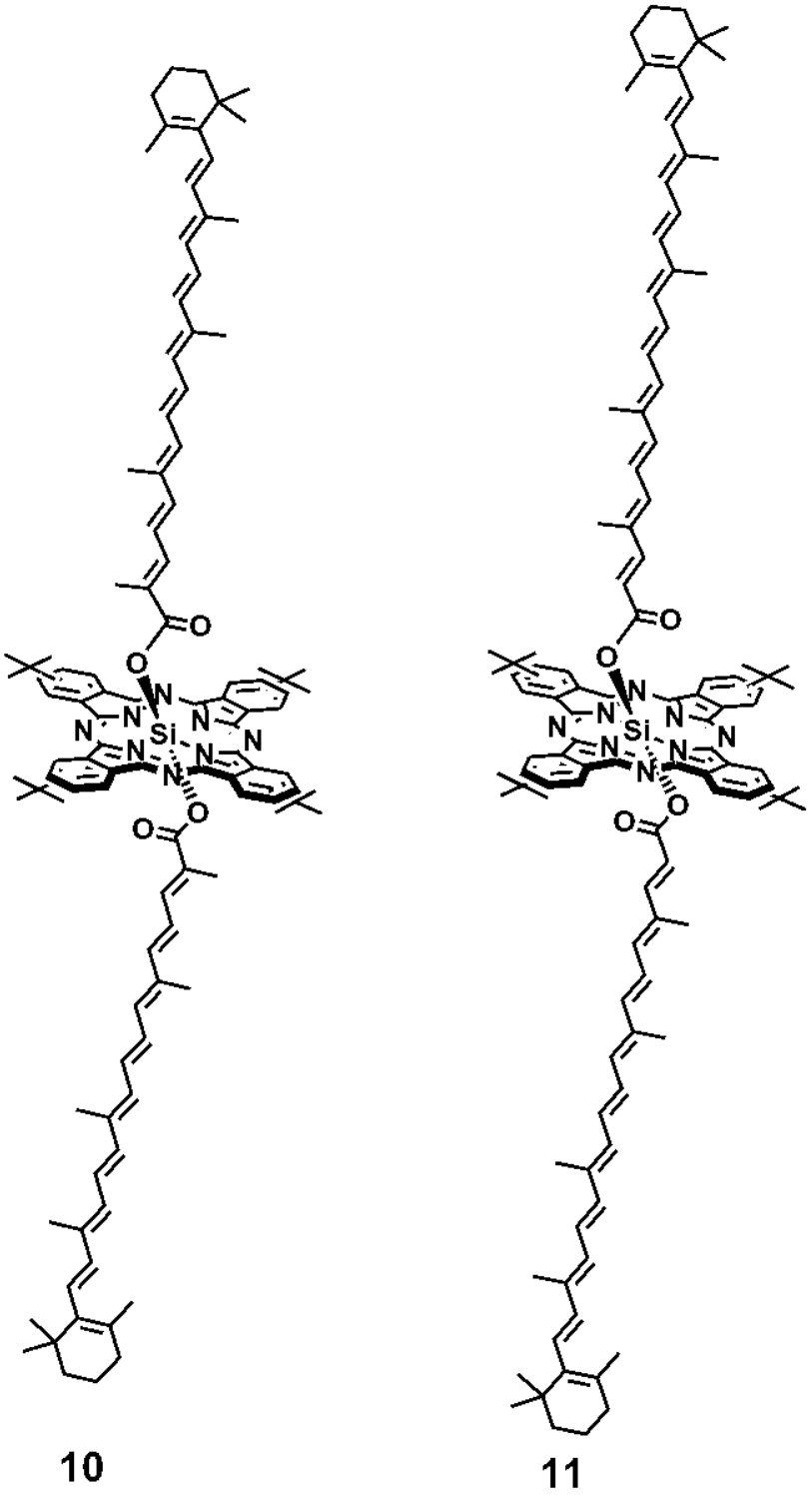

Figure 5. Axially substituted silicon phthalocyanine triads with 9 db, **10**, or 10 db, **11**, carotenoids.

Transient absorption studies on triads **10** and **11** also provided evidence for the formation of the S* state from S_2 in both of the triads, but not in the isolated carotenoid models. The S* state had a lifetime of ~26 ps in both triads[13]. Interestingly, in triad **10**, the decay of S* was associated with an increase in the Pc ground state bleaching near 690 nm, indicating that S* transfers energy to Pc in this case. The situation in triad **11** was different in that the Pc ground state bleaching and stimulated emission signals did not rise concomitantly with the decay of S* (26 ps). Thus, the efficient antenna function of the 9 db carotenoid in **10** is associated not only with the S_1 and S_2 states; all three states S_2, S_1, and S* contribute singlet electronic energy to Pc. This illustrates the importance of using multiple pathways for the EET process when using carotenoids in the construction of highly efficient artificial photosynthetic antennas.

Similar dependence of the EET from carotenoids to Pc on carotenoid length was observed in another set of dyads (Figure 6). In contrast to the case above where the carotenoids were axially linked to the Pc, in dyads **12**, **13** and **14**, with carotenoids having 9, 10, and 11 carbon–carbon db, respectively, the carotenoids were attached to the periphery of the macrocycle of a zinc Pc via an amide linkage[14]. This orientation is reminiscent of the relationship between the carotenoid and the bacteriochlorophyll in B850[12]. Ultrafast transient absorption spectroscopy and global analysis[15] of the data were used to evaluate the energy transfer and excited-state deactivation pathways following excitation of the allowed carotenoid S_2 state. The S_2 state rapidly relaxed to the S* and S_1 states. In all systems a pathway of energy deactivation within the carotenoid manifold in which the S* state acts as an intermediate state in the S_2 to S_1 internal conversion on a sub-picosecond time scale was detected. In dyad **12**, similar to the case with triad **10**, all

carotenoid singlet excited states, S_2, S* and S_1, contribute to singlet-singlet energy transfer to Pc, making the process very efficient (> 90%), while for dyads **13** and **14** the S_1 energy transfer channel is precluded by thermodynamic considerations and only S_2 was capable of transferring energy to Pc. Finding S* in our dyads and triads is particularly gratifying because the same state is seen in the natural systems; this is a further illustration that the essential features of the electronic coupling and spectroscopy in native antenna pigment-protein complexes is recapitulated in these models[16].

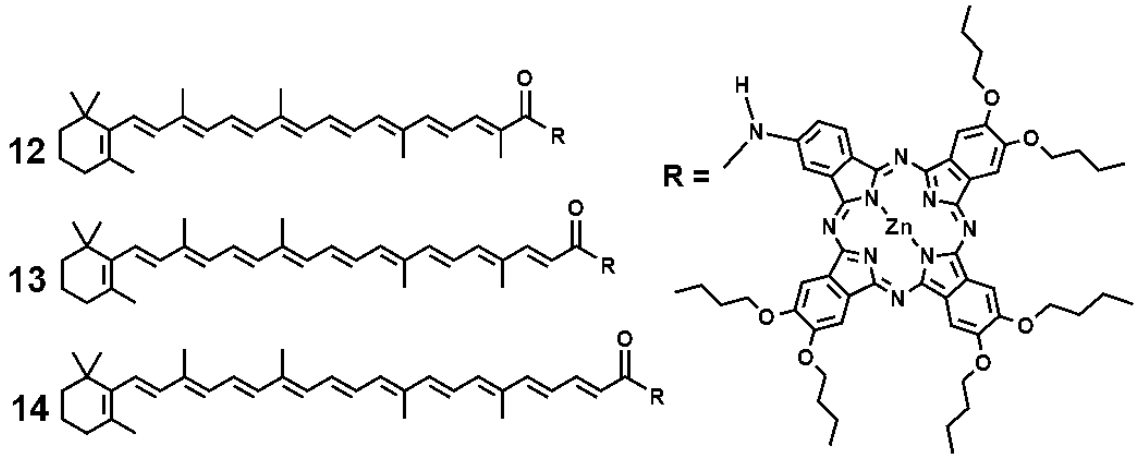

Figure 6. Three carotenophthalocyanine dyads where the two chromophores are connected via an amide linkage. Dyad **12** has 9 db, **13** has 10 db, and **14** has 11 db.

The fluorescence excitation spectra of carotenophthalocyanines **12** and **13** indicated a weak but measureable dependence of the energy transfer efficiency on excitation wavelength, suggesting an increase of energy transfer with excitation at the blue edge of the absorption band (to the higher vibronic states) of the carotenoid. This phenomenon was more evident in a series of carotenophthalocyanines where the two chromophores were tightly coupled through an arylamine moiety (dyads **26**–**29**, Figure 11). In addition to fluorescence excitation measurements, ultrafast transient absorption measurements also indicated that population of the carotenoid hot S_2 state results in enhanced energy transfer

to the Pc. It was hypothesized that the higher energy transfer efficiency with excess vibrational excitation results either from a decreased internal conversion rate to lower-lying optically forbidden states, or from enhanced coupling between higher vibrational S_2 states and Pc[17].

The spectroscopic results obtained for these model systems in conjunction with the crystallographic data which shows very close intermolecular contacts in natural antenna pigment-protein complexes, suggests that classical Förster theory is not adequate to explain the mechanism of singlet-singlet energy transfer between longer carotenoids and cyclic tetrapyrroles. First, at the short interchromophore distances necessary for EET, the Förster dipole approximation breaks down. At these distances coulombic coupling using transition monopoles is appropriate[18]. Furthermore, at the distances required for efficient energy and electron transfer there is clearly orbital overlap in the natural systems; this level of electronic coupling in synthetic models is provided by the linkage or a combination of the linkage and a conformation that brings the π systems into van der Waals contact (*vide supra*). Orbital overlap introduces contributions to the electronic coupling that arise from electron exchange interactions. Interestingly, both of these mechanisms may promote T–T as well as S–S energy transfer (see last paragraph of this chapter for evolutionary implications of this electronic coupling).

Tetrapyrrole antennas. EET between (bacterio)chlorophyll molecules within antennas and funneling of the energy to RCs is ubiquitous in light harvesting complexes of natural photosynthetic systems. In collaboration with J. Lindsey, we constructed antenna molecules consisting of four covalently linked zinc tetraarylporphyrins, e. g.

tetrad 15, and linked them to free base porphyrin-fullerene artificial RCs to give hexads **16** and **17**[19] (Figure 7).

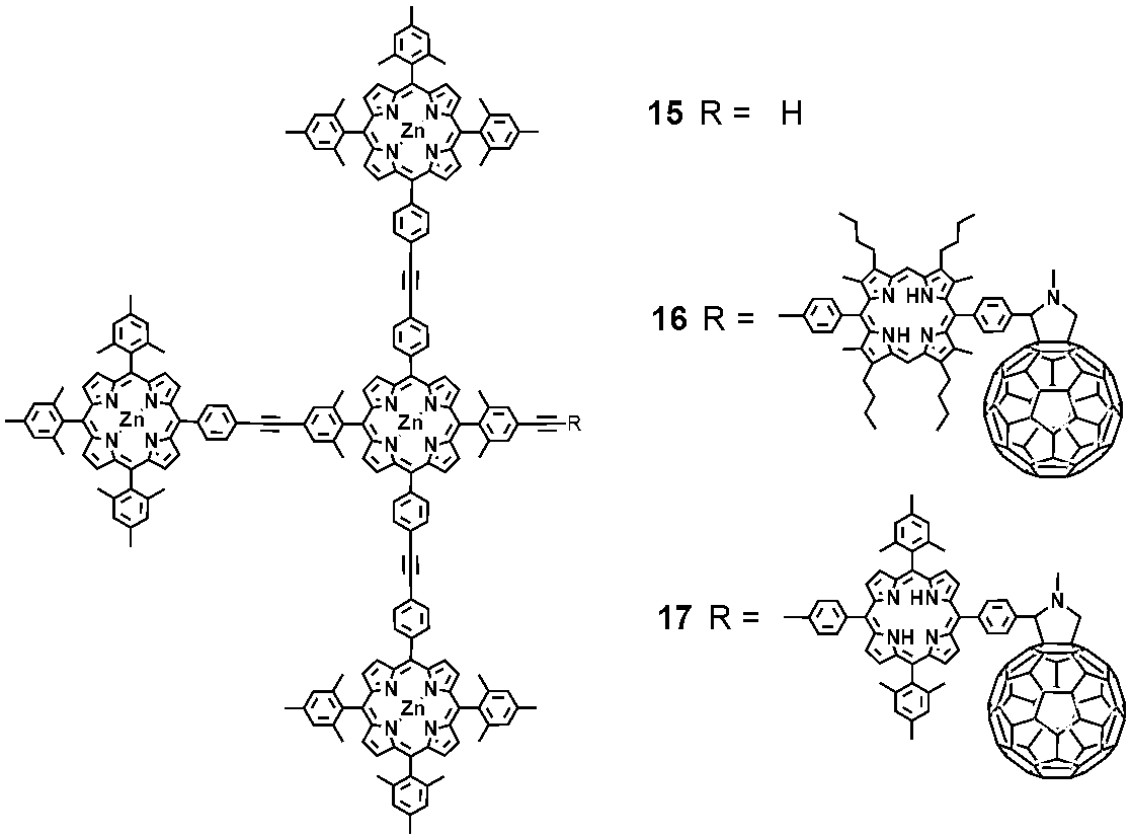

Figure 7. Structures of a tetrad antenna **15** and two different hexad antenna-reaction center models, one with an octalkyl-meso-diphenylporphyrin-C_{60} reaction center, **16**, and another with a *meso*-tetraaryl porphyrin-C_{60} reaction center, **17**.

Time-resolved absorption and emission studies showed that excitation of any peripheral zinc porphyrin moiety was followed by EET to the central zinc porphyrin with a time constant of ~50 ps. The excitation energy was then transferred to the free base porphyrin of **16** in 240 ps, which decayed by electron transfer to the fullerene with a time constant of 3 ps. The final charge-separated state had a lifetime of ~1 ns and was generated with a quantum yield of 0.69 based on light absorbed by the zinc porphyrin antenna.

We note that EET rate between the zinc porphyrin in the antenna of **16** and the free base porphyrin was relatively slow $(240\ ps)^{-1}$ compared with EET among the zinc porphyrins $(50\ ps)^{-1}$. Examination of the frontier molecular orbitals of the porphyrins involved in the linkage provides one feasible explanation. The symmetry of the HOMOs of porphyrins are either a_{2u}, which has lobes at the *meso* positions, or a_{1u} which has nodes at the *meso* positions. Indeed, there are examples of *meso*-linked arrays of porphyrins with a_{2u} HOMOs which undergo rapid energy transfer, whereas similar arrays of porphyrins with a_{1u} HOMOs undergo much slower energy transfer[19-20]. The presence of the eight β-alkyl substituents of the free base porphyrin of **16** results in the HOMO having a_{1u} symmetry and therefore diminished electronic coupling with the linker. Additionally, in molecules with β-alkyl substituents, steric effects result in an increased dihedral angle between the planes of the porphyrin ring and the *meso*-aryl ring. These factors undoubtedly reduced the electronic coupling and thereby reduced through bond mediated contributions to EET. In hexad **17** we addressed these issues by changes in the structure, which changed the symmetry of the HOMO and relaxed the steric-induced dihedral angle. The resulting EET from the antenna to the free-base porphyrin occurs in 32 ps, an 8-fold increase. Increasing the rate of this process by addressing the factors that control the symmetry of the HOMO and steric effects, and thereby the electronic coupling that mediates EET, is an example of using theory to guide design to optimize function. This strategy resulted in an increase in the yield of the final charge separated state from 69% in **16** to 90% in **17** [19a]. Following these and related principles it was possible to design antennas consisting of different multiple chromophores; with these systems efficient light harvesting throughout the visible spectrum was achieved[21].

The results described above demonstrate that it is possible to design and prepare synthetic antenna-reaction center complexes that mimic basic photochemical functions of natural photosynthetic light-harvesting antennas and reaction centers in simple, structurally well-defined constructs.

Photoregulation

Antennas are essential for collecting the photons that drive photosynthesis, but there are times when the antennas overdo their job, particularly under conditions of high light intensity. It is hypothesized that in the evolution of photosynthesis there was, and continues to be, a selective advantage for the organism to make optimum use of low light conditions to drive the relatively slow downstream metabolic reactions of legacy biochemistry[22]. Low light requires large antennas, resulting in a situation where during much of the day light in excess of that required to drive downstream metabolism is absorbed. If excess light energy is not dealt with properly, it would cause oxidative damage to the organism (see photoprotection section). As photosynthesis changed the earth's atmosphere from reductive to oxidative *ca.* 2.6–2 billion years ago, photosynthetic organisms developed myriad ways to prevent oxidative damage that occurs under excess light. One of these is known as non-photochemical quenching (NPQ)[23]. NPQ is a biological switch that results in the deactivation of the singlet excited states of chlorophylls in the antenna system. There are several triggers of NPQ including, in green plants, luminal acidification beyond the normal range required to maintain proton motive force. It is thought that essentially all oxygenic photosynthetic organisms have developed some form of NPQ[24].

Discovering the precise mechanisms of NPQ is an active research field. NPQ operates on several time scales from short times required for sensing and protein conformational changes to longer time scales for enzyme activation to even longer time scales for gene expression. Our models seek to mimic the rapid events known as the qe component of NPQ that results in quenching chlorophyll excited states and thereby interrupting EET to RCs. There is now general agreement that qe occurs following changes in the protein structure in pigment-protein complexes. These changes induce quenching of chlorophyll singlet excited states by interaction with specific carotenoids. In certain organisms under high light intensity it has been demonstrated that zeaxanthin, a carotenoid having 11 db, is formed by de-epoxidase enzymes in the xanthophyll cycle; it becomes the predominant carotenoid. It has been proposed that its longer conjugated system allows it to perform NPQ by some of the mechanisms discussed below[23, 25].

While NPQ is a necessary regulatory system in photosynthetic organisms, it is also one of the important factors responsible for the low overall efficiency of photosynthesis[1a, 22]. Anticipating that ways will be discovered to accelerate the rate-limiting downstream dark reactions, there will be a need to recalibrate NPQ to allow the photosynthetic process to proceed more efficiently. But, before that can be done it is imperative to understand the detailed mechanisms of NPQ. Studies with simple artificial light-harvesting antenna have helped in this regard and some examples of the systems and photophysical studies are briefly described in the following section.

Quenching of excited states of cyclic tetrapyrroles by electron transfer. Carotenoids have a paradoxical role in photosynthesis, they participate in EET to chlorophylls but when there is excess energy carotenoids are also responsible for

quenching the excited states of chlorophylls. Since the synthesis of our first carotenoporphyrin[5a] we observed quenching of the porphyrin fluorescence and speculated that electron transfer to the excited porphyrin from the carotenoid would be a reasonable explanation. As the synthesis of artificial photosynthetic antennas progressed, the attachment of the carotenoids, the nature of the porphyrins, and the number of conjugated db in the carotenoid were systematically changed. With carotenoporphyrins **6**–**8** (Figure 2), the degree of porphyrin fluorescence quenching depends on the position of carotenoid attachment to the *meso* aryl group of the porphyrin[7]. In addition to steady-state porphyrin fluorescence intensity measurements, the fluorescence lifetime was used to assess the quenching. The porphyrin model for dyads **6-8** has an 11 ns excited singlet state lifetime while the *ortho*, *meta*, and *para* isomers have shorter lifetimes (Table 1). This effect was observed with the dyads dissolved in toluene. When the solvent polarity was increased lifetimes got even shorter (Table 1). This quenching process was interpreted as a possible intramolecular electron transfer from the carotenoid to the porphyrin excited state via coupling through the linkage bonds. The *ortho* and *para* isomers were more strongly quenched and, as discussed above for EET, the *ortho* and *para* linked isomers have better electronic coupling[7]. Moreover, as will be shown in the photoprotection section below, the same pattern is observed for T-T energy transfer (see Figure 18).

Table 1. Fluorescence lifetimes for carotenoporphyrins in non-polar solvent (toluene) and polar solvent (acetonitrile)*.

Molecule	Toluene	Acetonitrile
Model Porphyrin **3**	11.0 ns	11.0 ns
Ortho Amide Dyad **6**	5.2 ns	1.0 ns**
Meta Amide Dyad **7**	7.2 ns	5.8 ns
Para Amide Dyad **8**	5.9 ns	3.9 ns

*All lifetimes were calculated from single exponential fits to the fluorescence decays.
In the case of **6 in acetonitrile three exponential components were required. The major (80%) component is reported.

No spectroscopic evidence for the formation of the radical pair species ($C^{\bullet+}$-$P^{\bullet-}$) was seen in **6**–**8**. In order to increase the probability of observing electron transfer, we designed dyad **18** which featured a powerfully oxidizing porphyrin. We reasoned that electron transfer would be in the Marcus normal region so that if more driving force for photoinduced electron transfer was available the process would be faster and the transient concentration of the charge separated species ($C^{\bullet+}$-$P^{\bullet-}$) would build up to a detectable level. In **18** three of the tolyl groups of the porphyrin were replaced by pentafluorophenyl groups and the carotenoid in **18** was a better electron donor than that in **6**–**8**. The driving force for the process C-*P → $C^{\bullet+}$-$P^{\bullet-}$ is estimated to be ~400 meV greater in **18** than in **6**–**8** [26].

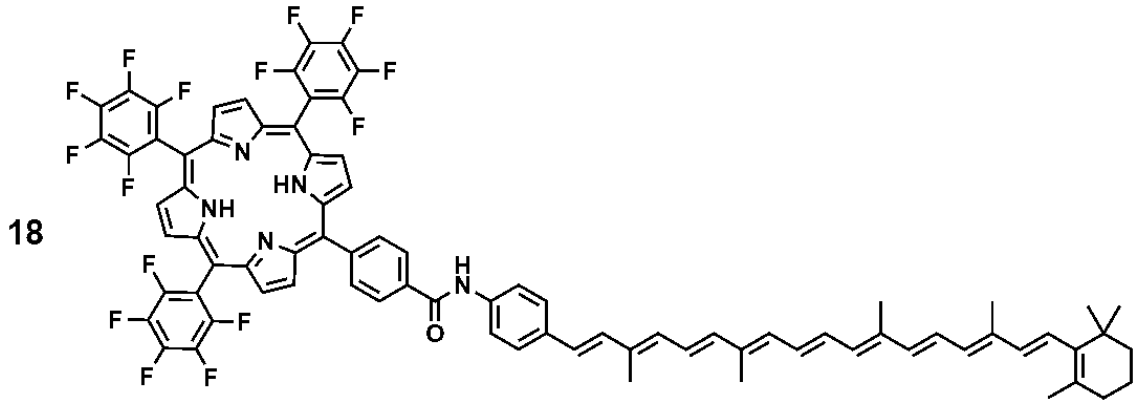

Figure 8. Molecular structure of dyad **18**; the fluorinated porphyrin is covalently attached to a carotenoid containing 10 db through an N-phenylamide linkage.

The porphyrin fluorescence in **18** was strongly quenched and using transient absorption spectroscopy we detected the formation and decay of the carotenoid cation radical, which has strong absorption at around 975 nm in butyronitrile. This construct demonstrated what has come to be called inverted kinetics in which the transient species decays faster than it forms. In this case the cation radical forms in ~50 ps and decays to the ground state in ~3 ps. We concluded that the necessary driving force for the 50 ps formation of the charge-separated state is provided by the combination of the high reduction potential of the fluorinated porphyrin and the low reduction potential of the carotenoid. This work established electron transfer quenching as a viable mechanism for cyclic tetrapyrrole quenching by carotenoids.

One consequence of inverted kinetics is that the concentration of the intermediate does not build up, making it difficult (and sometimes impossible) to detect. In the conclusion of this paper[26] we stated:

> the observation of porphyrin fluorescence quenching by electron transfer from a carotenoid provides a mechanism for similar energy-dissipating electron-transfer quenching *in vivo* and warns that because of the kinetics it could be very difficult to detect the transient species in pigment-bearing proteins. A rapid charge recombination process would be advantageous because it would preclude deleterious reactions of the radical ions in the photosynthetic membranes. Through energy dissipation, carotenoids could play a role in controlling photosynthetic energy flow.

Twelve years later in the laboratory of G. R. Fleming it was possible to detect the formation of the carotenoid radical cation in intact leaves under conditions necessary to induce NPQ[27].

Once the electron transfer mechanism was confirmed to operate in a carotenoporphyrin dyad, the length of the carotenoid conjugated system was studied in relation to its quenching ability. This study was relevant to NPQ because, as mentioned before, during the xanthophyll cycle it is the longer carotenoid (zeaxanthin with 11 db) that is presumably involved in the quenching of the chlorophyll excited state and not the shorter carotenoids (antheraxanthin and violaxanthin with 10 db and 9 db, respectively). A series of carotenoporphyrins were synthesized with carotenoids ranging from 5 to 11 db (Figure 9) and their porphyrin fluorescence quenching properties evaluated[28]. Steady state fluorescence studies showed that shorter carotenoids, between 5 and 7 db, do not quench the porphyrin fluorescence while longer carotenoids (8 to 11 db) are able to quench the porphyrin fluorescence (Figure 9B).

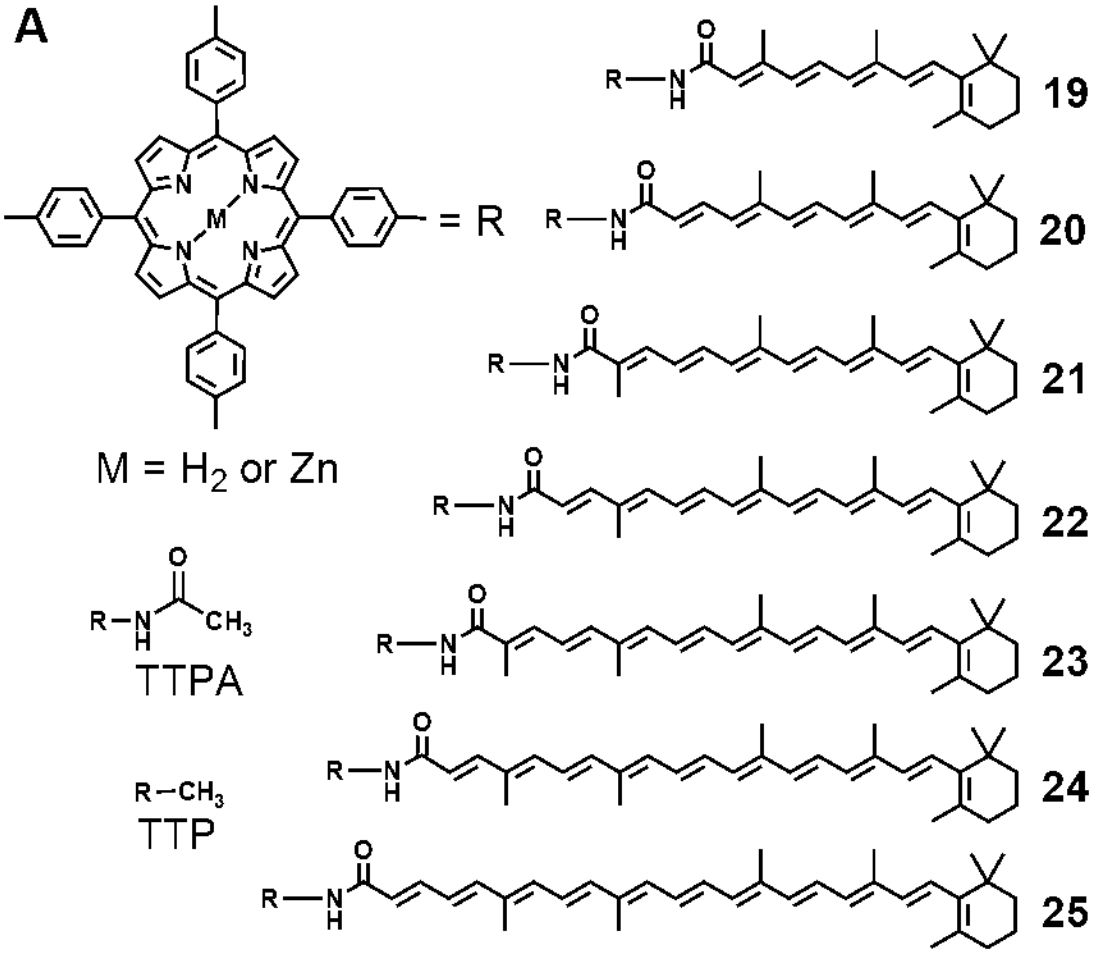
A
= R
M = H2 or Zn
TTPA
R–CH3
TTP
19
20
21
22
23
24
25

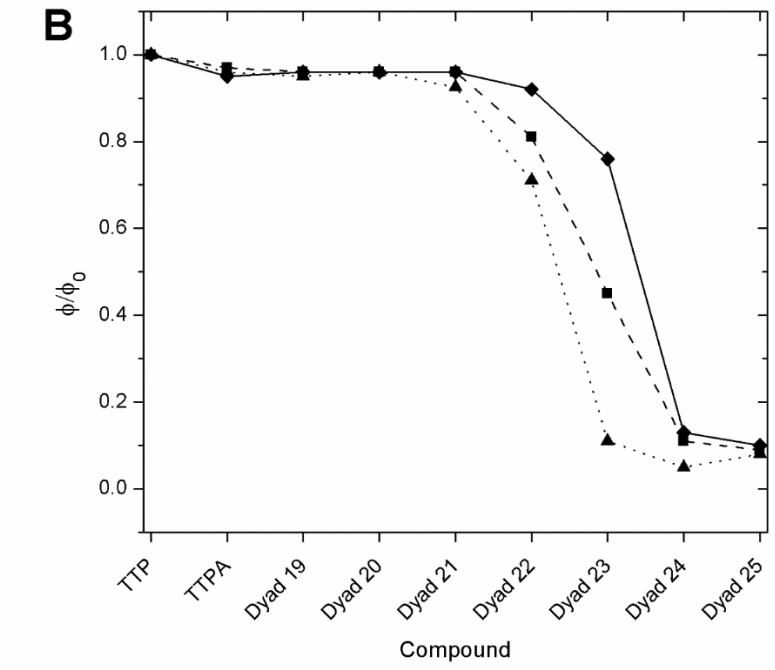
B
1.0
0.8
0.6
0.4
0.2
0.0
ϕ/ϕ0
TTP
TTPA
Dyad 19
Dyad 20
Dyad 21
Dyad 22
Dyad 23
Dyad 24
Dyad 25
Compound

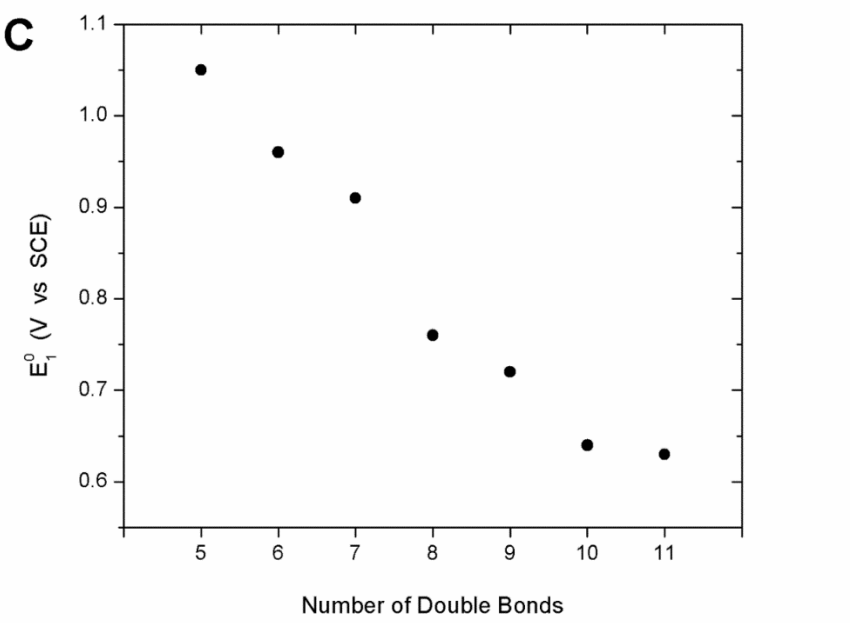

Figure 9. (A) Molecular structures of carotenoporphyrins with different numbers of db (**19**–**25**) and 5-(4-acetamidophenyl)-10,15,20-tris(4-methylphenyl)porphyrin (TTPA); (B) relative quantum yields of the porphyrin fluorescence of the carotenoporphyrins relative to free base or zinc tetra tolyl porphyrins (TTP): (◆) free base porphyrins and carotenoporphyrins in toluene, (■) free base porphyrins and carotenoporphyrins in acetonitrile, and (▲) zinc porphyrins and carotenoporphyrins in toluene; (C) correlation between the first oxidation potential of the carotenoid and the number of db of the carotenoid.

Electrochemical studies of the same set of carotenoporphyrin dyads and models for their carotenoid moieties resulted in data that are summarized in Figure 9C[29]. Carotenoids with more than eight double bonds can form charge separated states ($C^{\bullet+}$-$P^{\bullet-}$) that are lower in energy than the singlet excited state of a tetra-*para*-tolylporphyrin (TTP). If the formation of $C^{\bullet+}$-$P^{\bullet-}$ takes place it would explain the fluorescence quenching of the porphyrin. Although we did not detect the radical pair species directly, the solvent and redox potential dependence are good evidence that the quenching was by electron transfer to the excited state of the porphyrin. This work establishes the feasibility of NPQ based on controlling the chlorophyll quenching by controlling the number of conjugated db in the

carotenoid. As shown in Figure 9B, a change of one db changes the quenching by >5-fold; in the natural system, the change from zeaxanthin to violaxanthin is two db.

The radical pair species characteristic of electron transfer quenching was subsequently observed in polar solvents in triads **10** and **11**. The sensitivity of this quenching to the dielectric properties of the surrounding matrix provides another mechanism in the natural system for a protein conformational change to induce quenching. We also note that sensitivity to solvent dielectric is not necessarily specific to electron transfer quenching (see next section).

Quenching of the excited state of cyclic tetrapyrroles by energy transfer to the carotenoid S_1 state. We initiated the study of carotenophthalocyanine dyads expecting to further characterize electron transfer quenching. Phthalocyanine tetrapyrroles with their large extinction coefficients of the Q bands more closely resemble chlorophylls than porphyrins do and we were interested in exploring this feature for artificial reaction centers. Carotenophthalocyanines **12**, **13** and **14** with amide groups linking carotenoid moieties with 9, 10, or 11 carbon–carbon db, respectively, (see Figure 6) to the periphery of a zinc Pc were studied by transient absorption spectroscopy with excitation at 680 nm into the lowest Q band of the Pc[30]. The Pc fluorescence lifetimes indicated that carotenoids with 10 and 11 db quenched the singlet excited state of Pc, while the 9 db carotenoid did not. In dyad **13** (10 db) the Pc singlet lifetime is reduced by a factor of 10, to 300 ps, with respect to **12** (9 db, 3 ns) and in dyad **14** (11 db) the carotenoid becomes an even stronger quencher with a fluorescence lifetime of 56 ps.

As we mentioned above, the switch from non-quenching to quenching upon an increase in the conjugation length of the carotenoid by one double bond was a remarkable

observation and supports the hypothesis that the activation of NPQ in the violaxanthin cycle occurs by increasing the conjugation of the carotenoid. It only remained to show that the quenching mechanism was electron transfer as in the case of dyad **18**. However, repeated and careful time resolved measurements failed to detect the characteristic spectroscopic signature of the carotenoid radical cation expected from electron transfer quenching. Turning to target analysis, we used a reasonable kinetic scheme and were able to resolve the "pure" spectra of transient species and discovered the characteristic spectrum of the S_1 carotenoid species[15]. The spectral and kinetic parameters clearly showed that the carotenoid S_1 state is the quencher of the singlet excited state of Pc in dyads **13** and **14**. In other words, this is energy transfer quenching. This work provided the model for detecting the carotenoid S_1 state in these systems and similar techniques were subsequently used in a study of preparations isolated from LHCII, the major antenna of photosystem II of plants. In this natural system clear evidence of the S_1 state of one of carotenoids, lutein 1, acting as the quencher of the excited state of chlorophylls was found just a year later[31].

Figure 10 shows the energy level diagram summarizing the proposed Pc Q state quenching mechanism observed in dyads **13** and **14**. Dyad **12** is not able to quench the singlet excited state of Pc because the S_1 state of the carotenoid with 9 db is above the Q state of Pc. On the other hand, the S_1 state of the 9 db carotenoid of dyad **12** acts as energy donor and is responsible for ~20% of the EET from the carotenoid to the Pc[14]. This set of dyads provides a clear example of the "molecular gear shift" mechanism proposed by Frank and co-workers in 1994 to explain the quenching effect of zeaxanthin (11 db carotenoid) and the antenna function of violaxanthin (9 db carotenoid)[32].

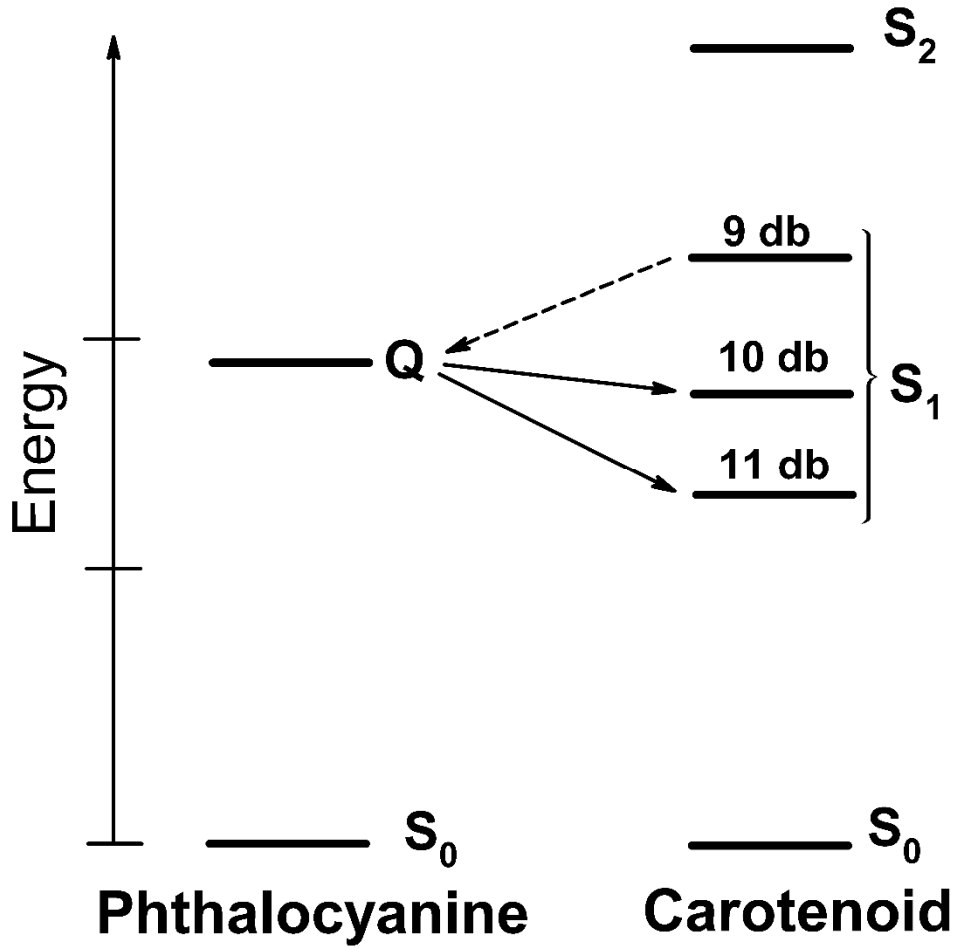

Figure 10. Energy diagram showing the relative energy levels of phthalocyanine (zinc Pc) and carotenoids with 9, 10, and 11 db. Solid arrows indicate energy transfer from the Pc Q state to the carotenoid S_1 states and the dashed arrow indicates energy transfer in the reverse sense from the carotenoid S_1 state to the Pc Q state.

It also was observed that quenching of Pc Q state occurs to a larger extent in more polar solvents such as acetone or DMSO. We interpreted this observation as evidence for involvement of a carbonyl carotenoid intramolecular charge transfer (ICT) state in the energy transfer mechanism. ICT involvement could be real or virtual; its energy is a function of solvent dielectric and as the dielectric increases it moves the ICT state closer to resonance between the S_1 and Q states. ICT states in carotenoids have been reported by Frank in a number of natural carotenoids containing carbonyl groups[4b, 33]. This finding

suggests that the "molecular gear shift" mechanism may be easily controlled by the environment surrounding carotenoids.

Quenching of the excited state of cyclic tetrapyrroles by excitonic coupling with the S_1 state of carotenoids. Dyads **12**, **13**, and **14** employed an amide linkage and therefore a carbonyl group was part of the structure. In order to determine whether the carbonyl group was essential to the energy transfer, we designed a series of dyads linked by an arylamino group[34] (Figure 11). The fact that such changes can easily be made in artificial systems highlights the flexibility of working with such systems.

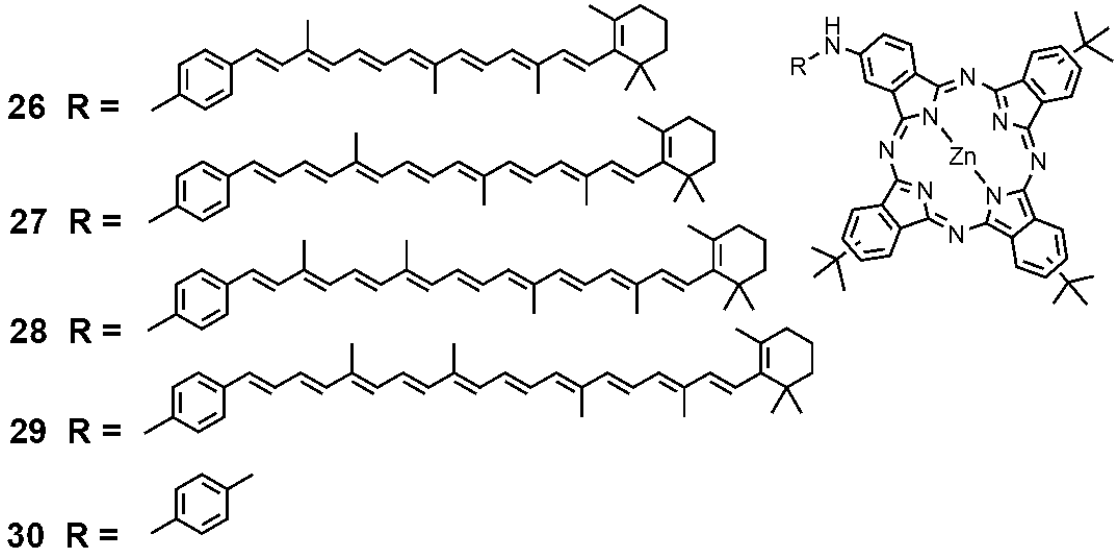

Figure 11. Molecular structures of carotenophthalocyanines with 8–11 db bond carotenoids with phenylamino linkages (**26**–**29**) to a zinc Pc and a model zinc Pc (**30**).

Transient absorption measurements of these dyads in toluene revealed completely different behavior from that observed with carotenophthalocyanines **12**–**14**. Even though the quenching of the Pc singlet state was a function of the number of db, in dyads **28** and **29** the spectral signature of the carotenoid S_1 state was present in the transient spectrum immediately after the excitation of the phthalocyanine with ~100 fs laser pulse[34]. In an attempt to resolve the rise time of the S_1 spectrum, dyad **28** was studied with ~30 fs time

resolution and the S_1 spectrum was fully developed on that time scale[35]. This observation indicates that on the 30 fs time scale the quenching of the Q state of Pc could not be described by a sequential ^{1}Pc to carotenoid S_1 energy transfer scheme as shown with the dyads **12**–**14** of Figure 6. This suggests that the quenching of Q was mediated through the formation of an exciton state, which is described as a composite or shared state between the phthalocyanine and the carotenoid. Such an exciton state would be a consequence of the strong electronic coupling between the chromophores in these systems. A schematic diagram showing formation and decay of the exciton state is depicted in Figure 12. Importantly, such a state can be populated from either the Pc Q state or the carotenoid S_1 state[34, 36]. Selective two photon excitation fluorescence experiments have provided evidence for the existence of such states in the natural systems[36-37].

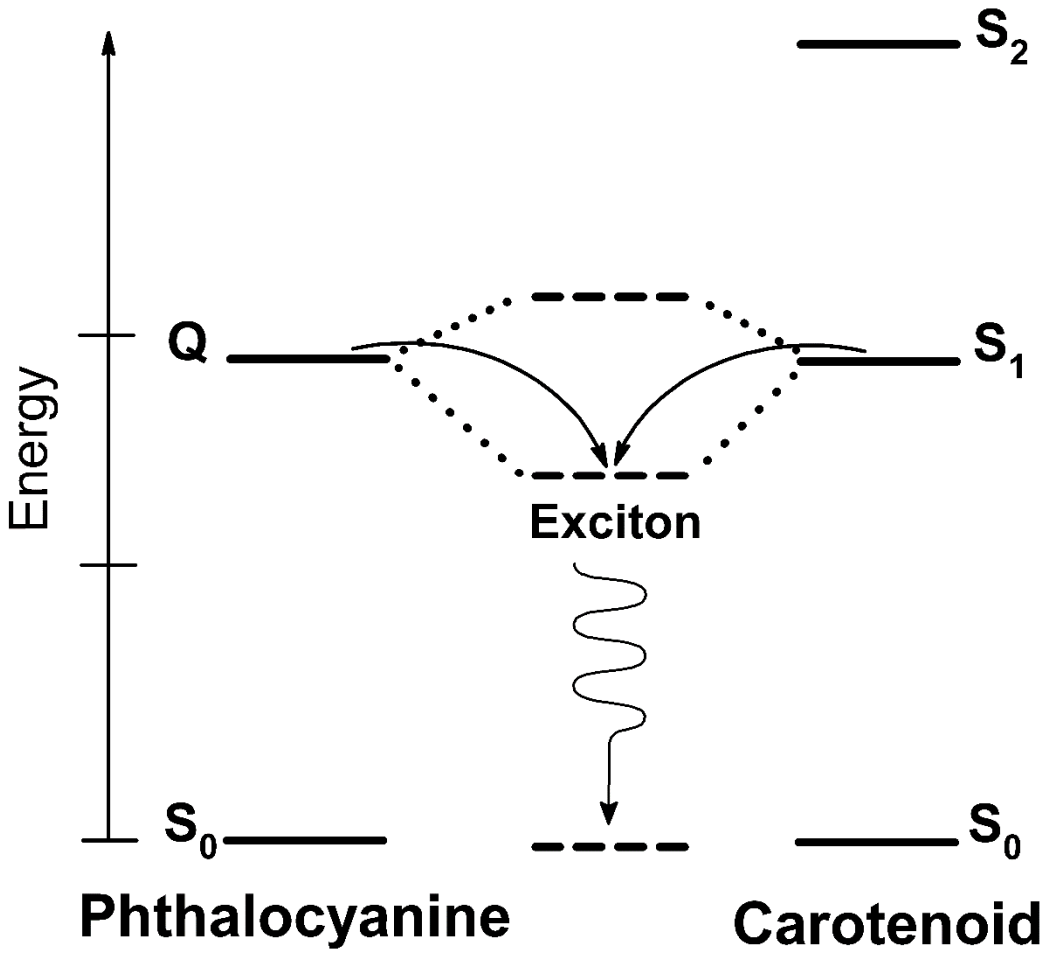

Figure 12. Energy diagram showing the exciton state formed in carotenophthalocyanine dyads which has contributions from the Pc Q and carotenoid S_1 states. After occupying the excitonic state (curved arrows) the excited energy is rapidly dissipated as heat and the system returns to the ground state.

Dyads **26**–**29** dissolved in THF showed the characteristic spectroscopic signatures of carotenoid radical cation species, indicating that photoinduced electron transfer contributes to the quenching for these dyads in more polar solvents.

In summary, on the basis of our work on various carotenophthalocyanine dyads we have identified three mechanisms of cyclic tetrapyrrole singlet excited state quenching by carotenoids in artificial systems:

1- Electron transfer from the carotenoid to the tetrapyrrole and fast recombination.

2- Energy transfer from the lowest Q state of the tetrapyrrole to the carotenoid S_1, followed by fast internal conversion to the carotenoid ground state.

3- Excitonic state formation between the lowest Q state of the tetrapyrrole and carotenoid S_1 state, followed by rapid internal conversion to the ground state.

The dominant quenching mechanism is a function of the molecular structure and dielectric environment. The study of these simple synthetic systems provides the basis for a detailed understanding of the interactions between carotenoids and cyclic tetrapyrroles and plays a role in the advancing our understanding of the control mechanisms that operate in natural photosynthetic systems.

Self-regulating artificial photosynthetic systems. We have designed and synthesized an artificial reaction center complex, **31** Figure 13, with an integral control element that demonstrates how the electron transfer process can be down regulated as a function of light intensity[38]. Molecular pentad **31** consists of two light-absorbing antenna moieties, a porphyrin primary electron donor, a fullerene electron acceptor and a photochrome control unit that functions as light intensity sensor. At low light intensities, the photochrome exists in a closed, dihydroindolizine (DHI) form that has no effect upon the photochemistry of the rest of the molecule. EET from the antenna dyes to the porphyrin is essentially 100% efficient. The porphyrin excited singlet state is quenched from 11.4 ns to 2.0 ns to form the $P^{\bullet+}$-$C_{60}^{\bullet-}$ charge separated state with a quantum yield of 82%. Increasing the actinic light intensity drives photoisomerization of the control unit from the DHI to the open form, betaine (BT). The betaine quenches the porphyrin excited state to 33 ps by EET. The betain reverts thermally to the DHI form. The fraction of pentads with the control unit in the BT form is a reversible function of the actinic light intensity and

temperature. This rapid quenching of the porphyrin primary electron donor effectively competes with photoinduced electron transfer to fullerene to dramatically lower the yield of charge separation involving the fullerene electron acceptor. Thus, this self-regulating molecule adapts its function as an artificial reaction center to the light level and mimics the regulatory mechanism observed in cyanobacteria promoted by the photoactive orange carotenoid protein (OCP)[39].

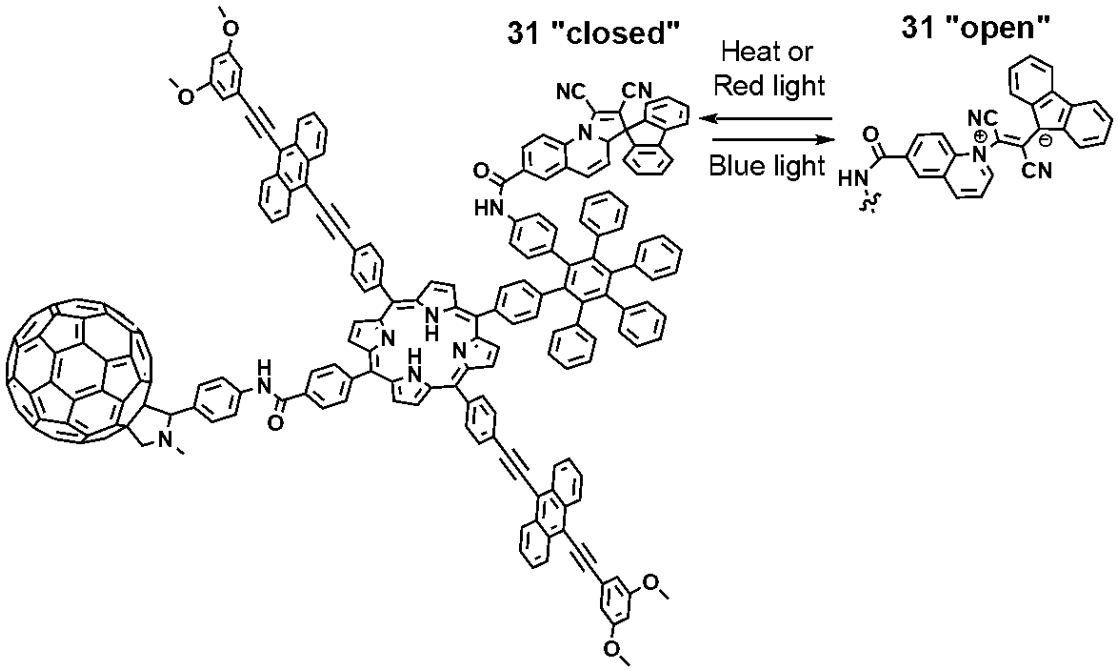

Figure 13. Structure of pentad **31** featuring a porphyrin as the primary electron donor linked to a fullerene electron acceptor and two bis(phenylethynyl)anthracene (BPEA) light-absorbing antennas. A photochromic control unit that can exist in two isomeric forms is an integral part of the structure.

Another self-regulating system, antenna **32**, consisting of five zinc porphyrin moieties and a pH sensitive control unit (Figure 14) was prepared and studied[40]. When dissolved in an organic solvent it absorbs light and exchanges singlet excitation energy among the porphyrins with a time constant of ~180 ps. The porphyrin excited states decay by the normal photophysical processes in ~2 ns, which is the fluorescence lifetime of a monomeric

zinc porphyin. Although not coupled to an artificial reaction center at this time, this excited state lifetime is certainly long enough to yield highly efficient charge separation. The control feature is demonstrated when acetic acid is added and the pH-sensitive control unit is protonated and converted to an open form that rapidly quenches the first excited singlet states of the antenna system to < 40 ps, rendering them kinetically incompetent to form charge separated states. The quenching process was ascribed to S-S energy transfer from the porphyrins to the pH sensitive dye and the transfer rates were consistent with those calculated using simple Förster theory. The resulting excited dye rapidly decays to the ground state, converting the excitation energy to heat. This system mimics the role of the antenna in NPQ triggered by low pH in the lumen of the thylakoid membrane. The quenching of the excited states of porphyrins in **31** and **32** is perfectly reversible and demonstrates that incorporation of self-regulation in response to external stimuli is possible in artificial photosynthetic constructs.

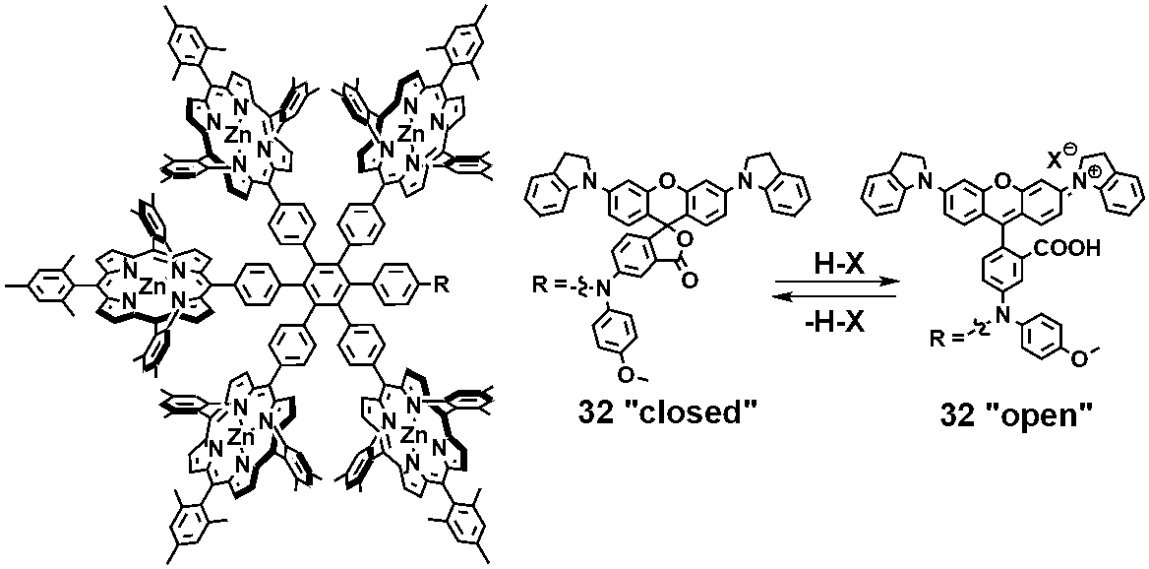

Figure 14. Structure of the hexad **32** featuring an integral pH sensor in either its closed or open form. HX is an acid that converts the pH sensor from closed to open.

Photoprotection

Molecular oxygen formed as byproduct of photosynthesis is an essential component of the biosphere. As a terminal electron acceptor in aerobic metabolism, it provides us with abundant energy. However, its reactivity is treacherous. The malevolent side comes from the facile sensitization of oxygen to yield its lowest excited state known as singlet oxygen ($^1O_2$). $^1O_2$ is an important member of the reactive oxygen species (ROS) family; it can damage lipids, proteins, co-factors and other cellular components and is a serious threat to living cells. In photosynthetic membranes, in addition to the small probability of intersystem crossing from chlorophyll singlet excited states under normal photosynthetic operation, conditions of excess light absorption can lead to radical pair recombination at reaction centers and the formation of triplet chlorophyll. In the oxygen-rich environment of the photosynthetic membrane, or in anaerobic photosynthetic bacteria and archaea, which adventitiously encounter an oxygenic environment, these triplet species can sensitize the formation of $^1O_2$. Control mechanisms such as NPQ are partially effective at dissipating excess energy at the chlorophyll singlet excited state level and thereby controlling chlorophyll triplet formation. But, because intersystem crossing and radical pair recombination do occur to a small extent, photosynthetic membranes have a second line of defense against $^1O_2$ involving carotenoid pigments as quenchers of chlorophyll triplet species and $^1O_2$ itself.

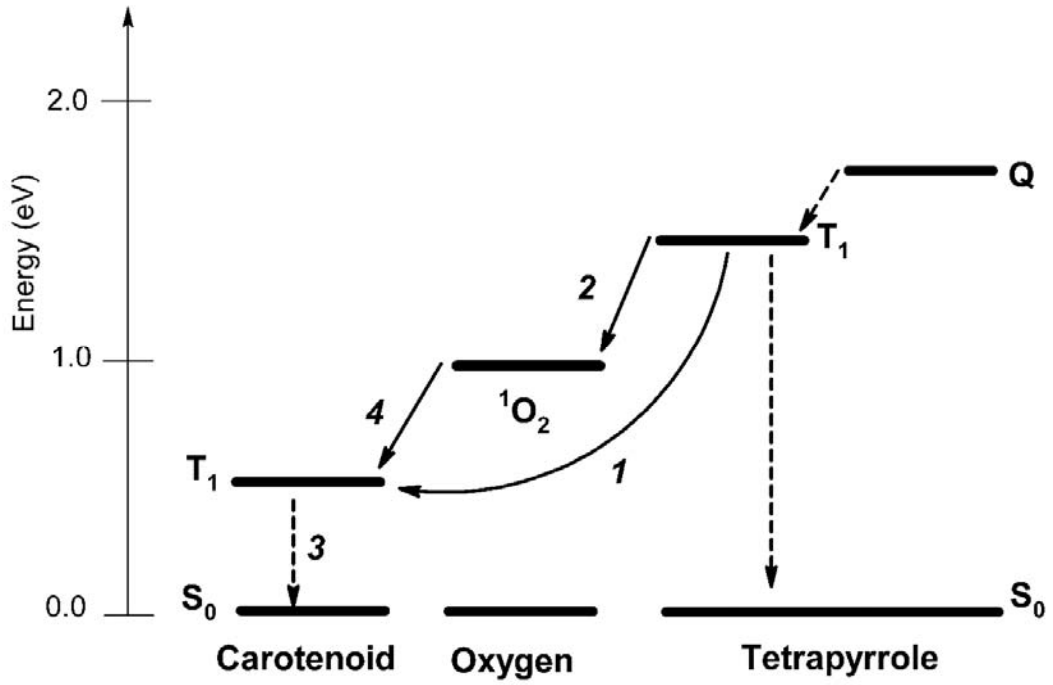

Figure 15. An energy level diagram with energy levels of a generic carotenoid and cyclic tetrapyrrole interacting with singlet oxygen ($^1O_2$). Photoprotective processes are represented by numbered arrows: dashed arrows are intersystem crossing events and solid arrows refer to energy transfers.

Figure 15 illustrates the photoprotective processes in photosynthetic membranes that suppress $^1O_2$ sensitization. The lowest excited triplet energy level of carotenoids (having > 8 db) is below that of chlorophyll and the $^1O_2$ energy level, which sets the stage for two distinct protective mechanisms:

1- The carotenoid ground state species can quench the chlorophyll triplet state by energy transfer (step 1), precluding sensitization by the triplet chlorophyll to form $^1O_2$ (step 2). The triplet carotenoid then decays harmlessly yielding heat and the ground state carotenoid (step 3).

2- The carotenoid can quench singlet oxygen by energy transfer (step 4), which returns the $^1O_2$ to its ground state; the resulting triplet carotenoid decays harmlessly

to its ground state (step 3). Additionally, carotenoids can act as chemical quenchers of $^1O_2$; β-carotene endoperoxide being a major oxidation product in PSII reaction centers[41]. This is considered a minor pathway in compared with the energy transfer mechanism.

Mechanism 1 actually prevents $^1O_2$ from forming and would appear to be the more effective of the two. It does require that T–T transfer be much faster than diffusion limited $^1O_2$ sensitization. The rate of this energy transfer process is controlled by thermodynamics and the electronic coupling between the pigments, which depends upon the extent of orbital overlap. In mechanism 2, the cell attempts to trap any $^1O_2$ that does form before it can damage cellular components. This is more risky and would depend on the carotenoid intercepting the trajectory of the $^1O_2$ before it finds a target. In any case, PSII is particularly vulnerable because the slow steps of water oxidation may lead to radical pair recombination at P680 and therefore triplet formation. These triplets cannot be protected by mechanism 1 because a carotenoid in van der Waals contact with P680 would be oxidized faster than the Mn cluster and would preclude water oxidation. This leaves only mechanism 2, which must be only partly effective because PSII frequently succumbs to oxidative damage at high light levels. Indeed, our studies of AP models indicated that mechanism 2 is not highly effective *vide infra* [42]. We also predicted that photoprotection in photosynthetic membranes would require van der Waals contact between carotenoid and (B)Chl pigments[5, 43]. The crystal structure of *R. sphaeroides* confirmed our prediction[44].

The effectiveness of mechanism 1 depends critically on the relative rates of the T–T energy transfer that quenches the chlorophyll triplet species and the diffusion limited rate of singlet oxygen sensitization. This is illustrated in Figure 16 in which sensitizers having

different T–T energy transfer rates to the attached carotenoid pigment were tested as $^1O_2$ sensitizers[45]. As a control, TTP with no carotenoid present and therefore no photoprotection was used; it can be seen (Figure 16, □) that $^1O_2$ was produced at a high rate. β-carotene added to the TTP solution (△) partially quenched singlet oxygen and protected the $^1O_2$ indicator dye, diphenylisobenzofuran (BPDH), by some combination of mechanisms 1 and 2, but at the concentrations used, primarily by mechanism 2. Dyad **2** (Figure 2, ●) having porphyrin to carotenoid T–T energy transfer with a 1.5 μs time constant showed better photoprotection of the BPDH than β-carotene in solution, but some $^1O_2$ was produced. The amount produced is qualitatively consistent with diffusion-limited collisions between oxygen and the porphyrin during its triplet state lifetime of 1.5 μs (note that spin statistics limit the collisions producing $^1O_2$ to 1/9 of the Debye diffusion limited collisions). Qualitatively, mechanism 2 played a minor role in quenching $^1O_2$ even though the carotenoid pigment was nearby. Consistent with the multitude of expected trajectories of $^1O_2$ following the sensitization collision with the triplet porphyrin moiety, we can assume that most of the trajectories of the nascent $^1O_2$ were not intercepted by the attached carotenoid. In trace ■ an isomer of dyad **2**, dyad **4** (Figure 2), in which T–T energy transfer is ultrafast demonstrated no $^1O_2$ sensitization, that is, complete photoprotection of the DPBH. We assign the photoprotection of DPBH to mechanism 1.

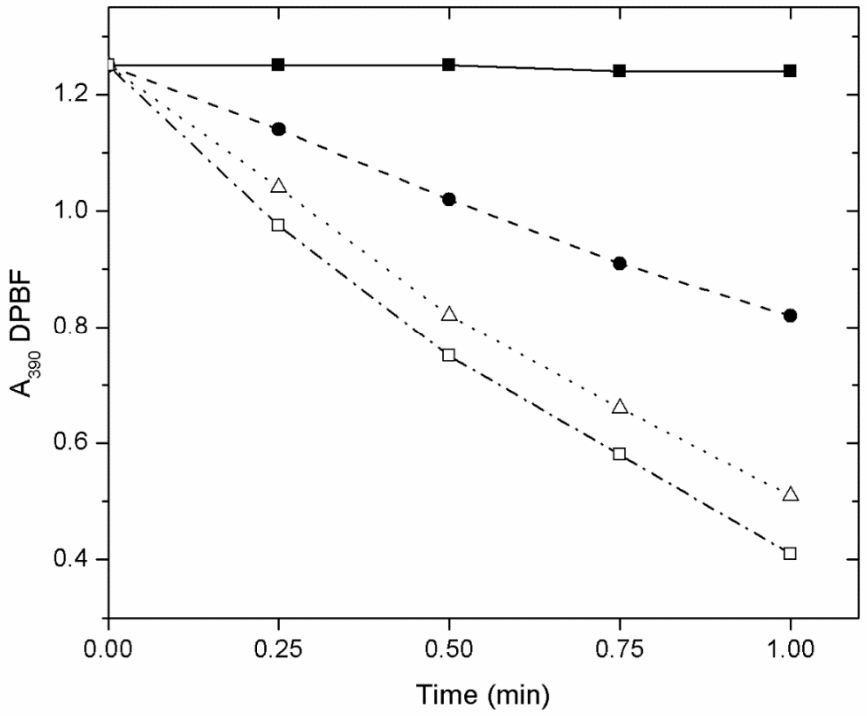

Figure 16. Change in absorbance measured at 390 nm due to the bleaching of diphenylisobenzofuran (DPBF), a singlet oxygen indicator, in the presence of (■) *ortho*-ester carotenoporphyrin **4**, (●) *para*-ester carotenoporphyrin **2**, (□) TTP **3**, or (△) mixture of TTP and β-carotene in toluene.

This work exploring the relative efficiencies of $^1O_2$ sensitization as a function of the T–T energy transfer rates, and therefore the electronic coupling, between cyclic tetrapyrrole and carotenoid has taken on new significance. It has been reported that in the cases looked at to date, T–T energy transfer rates are slower in anaerobic bacteria than in oxygenic photosynthesis[46]. Assuming that photoprotection is a fitness parameter in evolutionary selection, this would suggest that in the pigment protein complexes binding chlorophyll and carotenoid pigments, the electronic coupling necessary for adequate photoprotection is driven by the ambient levels of molecular oxygen, O_2. If this is the case, then oxygenic photosynthesis today may need improved photoprotection when

reengineered to provide improved efficiencies. A ten-fold increase in photosynthetic efficiency would mean a ten-fold increase in O_2 flux and therefore a greater challenge for quenching whole arrays of chlorophyll triplet states.

As mentioned above in connection with $^1O_2$ suppression, T–T energy transfer in the reaction center of *R. sphaeroides*, which was found to depend on temperature[47], has been explored using our model systems. In this case, the atomic level of reaction center crystal structure provided a clue. In fact, the carotenoid is located in van der Waals contact with an accessory bacteriochlorophyll, which is near the reaction center primary donor (the so-called special pair of bacteriochlorophylls), but on the "inactive branch" with respect to electron flow processes. The second lowest triplet level in the system is located on the special pair (the carotenoid triplet is the lowest excited state). A triplet formed on the special pair by radical pair recombination must migrate to the accessory bacteriochlorophyll, an endergonic process, before spontaneously migrating to the carotenoid pigment.

In order to mimic this triplet energy transfer relay[42] and to take advantage of the subtle variations in structure afforded by models to fully explore the kinetic and thermodynamic parameters controlling $^1O_2$ suppression, we designed triad **33** and its derivative, **34**, as triplet relay constructs in which the energetic landscape of the triplet levels includes an endergonic step (Figure 17). Triad **33** features a free base porphyrin and triad **34** a zinc porphyrin. The pyropheophorbide lowest triplet excited state energy level is lower than that of either porphyrin; it is a mimic of the special pair and the porphyrins are mimics of the accessory bacteriochlorophyll in the *R. sphaeroides* reaction center. Following excitation of the triad, singlet excitation is localized on the pyropheophorbide

where intersystem crossing forms the triplet state and activated T–T energy transfer occurs to populate the carotenoid triplet level. Because the zinc porphyrin has a higher triplet exited state energy level than the free base, energy transfer to the carotenoid in triad **34** is slower than in **33**.

Generally, we observed the same thermally activated flow of triplet energy in these triads that was observed in the natural system. In all cases at 77 K there was no evidence of T–T energy transfer. At room temperature, $^1O_2$ sensitization was suppressed in triad **33** but not prevented. In the case of **34**, due to slow T–T energy transfer to the carotenoid, the quantum yield of $^1O_2$ formation was not suppressed by the attached carotenoid pigment. We conclude that even though the carotenoid is near the site of $^1O_2$ formation, it is not effective at $^1O_2$ suppression, implying that mechanism 2 is not effective.

It is worth noting that the temperature dependence establishes that the accessory bacteriochlorophyll in the natural system and the porphyrins in triads **33** and **34** are real, not virtual, intermediates in the triplet energy transfer process.

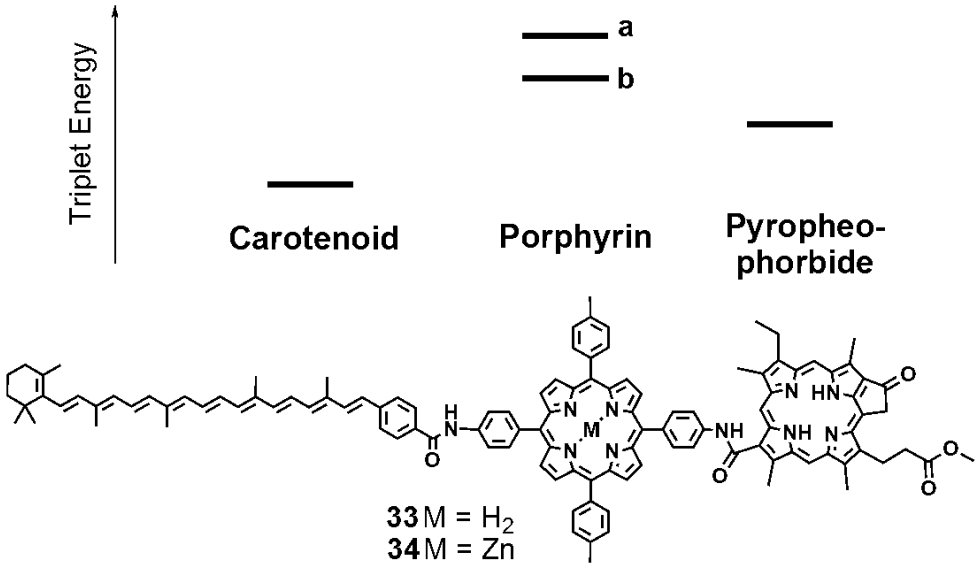

Figure 17. Energy diagram for triad **34**, which contains a zinc porphyrin with a higher porphyrin triplet energy level (a) than triad **33** (b).

Interestingly, the necessary conformation for electronic coupling need not be the most stable one, provided sufficient thermally activated conformations are available for the dyad to transiently acquire the required orbital overlap. In 1982 we reported a carotenoporphyrin[6d] (dyad **5,** Figure 2) in which the linkage between the chromophores was electronically insulating but sufficiently flexible to allow the dyad to transiently "fold" and undergo electron exchange mediated T–T energy transfer. Freezing these dyads to restrict thermal motion completely abolished the T–T energy transfer. But, because the carotenoid singlet states are very short lived, the thermal motion required for electronic coupling is not sufficiently fast to mediate S–S energy transfer; the efficiency of S–S transfer from the carotenoid to the porphyrin was vanishingly low.

As mentioned above in connection with singlet energy transfer and photoregulaton, the role of electron exchange interactions in mediating energy and electron transfer is further illustrated by the series of *ortho*, *meta*, and *para* amide-linked dyads **6**, **7**, and **8**[7] (Figure 2). In each case, the number of bonds and the hybridization of the atoms in the bonds are the same. As shown in Figure 18 and Table 1 the photophysics of the three isomers depend in the same way on the attachment point of the linkage to the aryl group. This dependence is adequately explained by electronic coupling terms that depend upon the overlap integrals that arise in electron exchange interactions, which are a sensitive function of the *ortho, meta*, and *para* positions on the aromatic ring, as explained above.

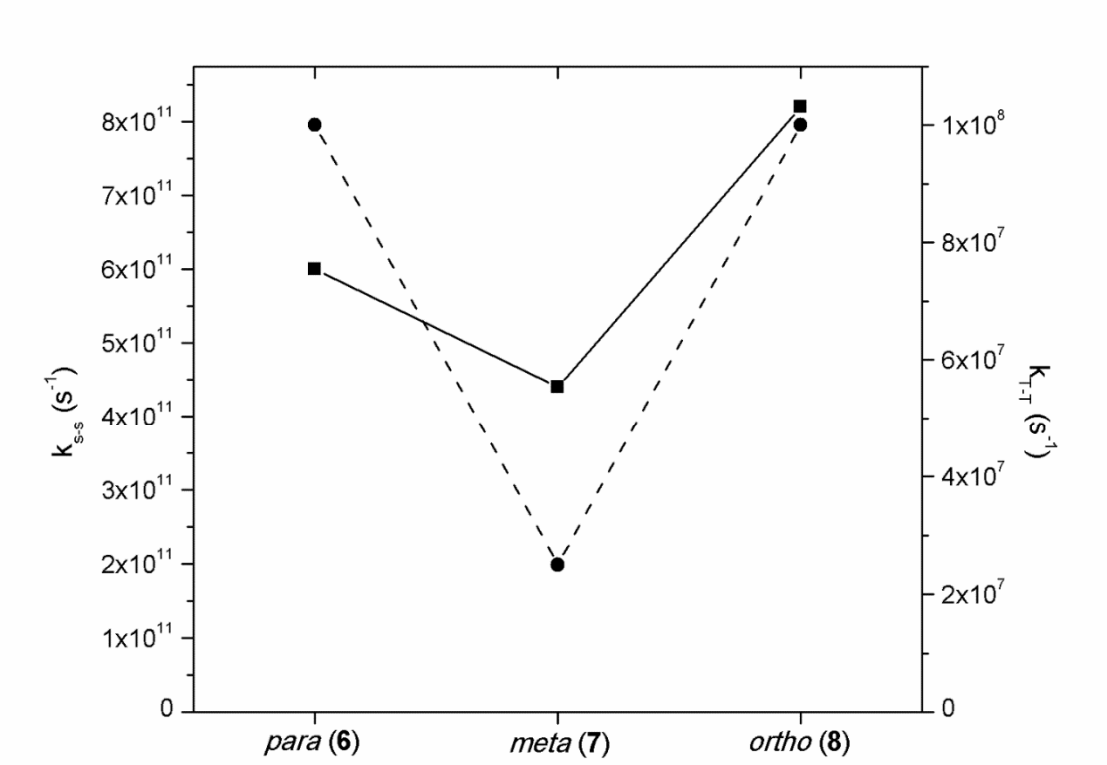

Figure 18. Singlet-singlet ($k_{S\text{-}S}$, ■) and triplet-triplet energy transfer rates ($k_{T\text{-}T}$, ●) measured for three carotenoporphyrin amide isomers. See also Table 1.

Mimicking the photophysics of non-adiabatic processes in photosynthesis involves managing the thermodynamic parameters controlling the process as well as the electronic coupling. The thermodynamic parameters in EET and T-T energy transfer are quantitatively characterized by using spectral overlap to evaluate the density of states term in the Fermi Golden Rule. Here, we present one example where the thermodynamics of electron transfer, specifically the reorganization energy, played a pivotal role in biomimicry. In the reaction centers of photosynthetic purple bacteria, radical pair recombination to yield a triplet state localized on the special pair was one of the most intriguing and characteristic electron transfer processes observed in the early events of photosynthesis. The role of radical pair recombination was touched on in the

photoprotection section above. Both transient absorption and magnetic resonance techniques have been used to characterize the exchange coupling and dynamics that lead to charge recombination involving triplet excited states[48]. In a series of papers we reported the requisite conditions in artificial reaction centers for observing such recombination[49]. We found that observing recombination to a triplet energy surface in these systems depends crucially on the reorganization energy. When the internal reorganization energy was low, implemented in our system by using a C_{60} moiety as the electron acceptor and a porphyrin as primary donor in carotenoporphyrin-C_{60} triad **35** (Figure 19), the solvent dielectric could be varied to modulate the yield of recombination to the triplet species from vanishingly small to almost 100%. Unexpectedly, understanding in detail the photophysics, dynamics and thermodynamics of recombination in these triads could play an important role in unlocking some of the secrets of navigation in migrating birds[50]!

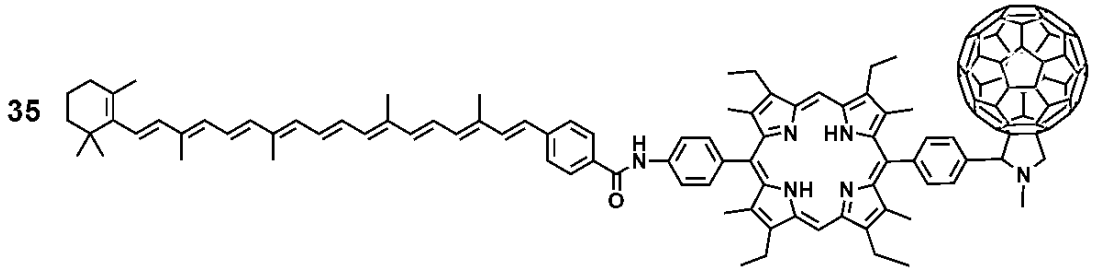

Figure 19. An AP reaction center: carotenoporphyrin–C_{60} triad **35**. It undergoes photoinduced charge separation that recombines to the carotenoid triplet state.

Conclusion

In conclusion, the fundamental photochemical interactions among chromophores that are used in photosynthesis for light gathering and photoprotection can be realized and studied in small, covalently linked model systems. The study of these simpler systems contributes to the understanding of energy flow in the much more complex natural systems.

In addition, the principles embodied in the synthetic molecules could be used to engineer photosynthesis-like functions into artificial photosynthetic solar energy conversion devices.

We also hypothesize that the photoprotective role of carotenoids is an example of evolutionary exaptation. We imagine that in the beginning the only photophysical properties important in nature's involvement with carotenoids were the highly allowed absorption to S_2 and the highly forbidden nature of S_1. The strong absorption of S_2 for light gathering was advantageous for the nascent solar powered organisms. In fact, even shorter carotenoids were finding their way into photoprocesses as revealed by the ubiquitous distribution of rhodopsins in the biosphere. Even in the early anoxic atmosphere, photosynthesis began the process of freeing organisms from the requirement of a redox gradient in the Earth's crust to drive their metabolism. Solar powered organisms surely thrived. Because carotenoid S_2 and S_1 states are very short lived, making use of those states in light harvesting required the strong electronic coupling to the chlorophyll pigment system as described in this review. Evolutionary pressure drove this coupling to the point where light harvesting acquired the necessary efficiency for a particular organism to be reproductively successful in its environmental niche.

Serendipitously, the carotenoid pigments came with another photophysical property, a triplet level below $^1O_2$ [51]. Because the evolution of photosynthesis occurred in an anoxic atmosphere, there was no selective pressure for $^1O_2$ suppression. But fortunately, the electronic coupling necessary to make the combination of carotenoid S_2 and S_1 states successful at singlet energy transfer to the chlorophyll system assured the electronic coupling necessary for T–T energy transfer and photoprotection. Thus, the stage was set

for the evolution of water oxidation and O_2 production. In other words, photoprotection was in place before it was needed: it preexisted. Water oxidation and O_2 production were a huge success for photosynthetic organisms and, ironically, resulted in the extinction of what must have been a wonderful cornucopia of anaerobic life forms.

CHAPTER 2

CAROTENOTETRAPYRROLE DYADS MIMIC PHOTOSYNTHETIC TRIPLET-TRIPLET ENERGY TRANSFER

Denise Galzerano[1], Katherine WongCarter[2], Ana L. Moore[2], Maxime Alexandre[3], John Kennis[3], Dalvin Méndez-Hernández[2], Vladimiro Mujica[2], Smitha Pillai[2], Paul A. Liddell[2], Gerdenis Kodis[2], Devens Gust[2], Rienk van Grondelle[3], Winfried Leibl[1], Thomas A. Moore[2], Bruno Robert[1*]

[1] : Institut de Biologie et de Technologie de Saclay, CEA, UMR 8221 CNRS, Université Paris Sud, CEA Saclay 91191 Gif sur Yvette, France

[2] : Department of Chemistry and Biochemistry, Arizona State University, Tempe, AZ 85287-1604 USA

[3] : Department of Physics and Astronomy, Faculty of Sciences, VU University Amsterdam, Amsterdam, The Netherlands

[*]: to whom correspondence should be sent.

Bruno Robert, Institute of Biology and Technology of Saclay, CEA-Saclay, 91191 Gif/Yvette Cedex, France,

tel: 33-169089015

email: bruno.robert@cea.fr

This document was modified for this thesis and will be submitted for publishing.

Introduction

During the first steps of the photosynthetic process, the absorption of photons by antenna pigment-protein complexes and the subsequent transfer of the excitation energy to the reaction centers are both intimately linked with the potential production of dangerous oxidative species. Although its yield is low, production of (bacterio)chlorophyll ((B)Chl) triplet excited states by intersystem crossing from (B)Chls excited singlet states is a major source of singlet oxygen in photosynthetic organisms, one of the most dangerous chemical species for living organisms[52]. In photosynthetic pigment-protein complexes, this sensitization reaction is precluded by transfer of the triplet excited state from (B)Chls to carotenoid molecules, which feature a triplet state energy below that of singlet oxygen. This quenching reaction reduces the lifetime of the (B)Chl triplet state by many orders of magnitudes[53].

In the light-harvesting (LH) proteins from most (anoxygenic) purple bacteria, the triplet-triplet (T-T) energy transfer from BChl to carotenoid molecules occurs in the nanosecond range[54]. By contrast, in light-harvesting complexes (LHC) from oxygenic organisms, we recently showed that this transfer is ultrafast, the chlorophyll triplet state decaying faster than it is formed[46]. The mechanisms underlying this ultrafast T-T energy transfer, which was proposed to represent an adaptation of oxygenic photosynthetic organisms to their oxygen-rich environment, are not yet fully understood. Some relevant observations are that when ultrafast T-T energy transfer occurs between chlorophyll and carotenoid molecules, the presence of the triplet state on the carotenoid has an usually strong influence on the chlorophyll Q_y electronic transition, and the decay of this perturbation decays with the carotenoid lifetime[54a, 55]. Moreover, the carotenoid triplet state

exhibits an abnormal resonance Raman signature, suggesting a partial loss of its typical triplet state character. Finally, when time-resolved infrared absorption experiments were performed on these complexes, clear chlorophyll contributions are observed to decay in parallel with the decay of the carotenoid triplet state. From these observations, it was tentatively proposed that the triplet state could be delocalized over the carotenoid/chlorophyll couple, and thereby shared between these molecules[46]. Understanding in detail the relationship between photoprotective T-T energy transfer mechanisms and the exposure of the photosynthetic organism to oxygen is essential in order to extend those mechanisms to reengineered photosynthetic systems where the production of oxygen and therefore the steady state level of oxygen in the membranes would be much higher than current levels.

Over the last three decades, large numbers of carotenoid/tetrapyrrole synthetic dyads have been designed and synthesized, in which the absorption of a photon is followed by the formation of a triplet state by intersystem crossing at the level of the tetrapyrrole, and subsequent transfer of the tetrapyrrole triplet energy to the carotenoid[6b, 45, 56]. In these dyads, depending on their precise chemical properties and on the way the tetrapyrrole and the carotenoid molecules are linked, the T-T energy transfer kinetics range from tens of microseconds to the sub-nanosecond range in which the actual T-T energy transfer rate was not determined because intersystem crossing in the tetrapyrrole is the rate limiting step[43a, 45, 56b]. In this work, we have studied both slow and fast T-T energy transfer in dyads using a combination of vibrational and transient absorption spectroscopic methods and have found they mimic the dynamics and spectroscopic signatures characteristic of the natural systems.

Methods

Synthesis. The synthesis of the carotenophthalocyanine **1** and the phthalocyanine **3** model have been reported previously[30]. The carotenopurpurin ester **2** and purpurin model **4** were synthesized starting with 5,15-bis(3,5-dimethoxyphenyl)-10-(methyl-3-propenoate)-2,8,12,18-tetrabutyl-3,7,13,17-tetramethylporphyrin, following a published procedure[57]. This porphyrin was cyclized to form the purpurin macrocycle, and the purpurin model **4**, before the methyl-ester was hydrolyzed to the carboxylic acid for coupling to a carotenoid benzyl alcohol. The esterification reaction of the purpurin acid and the 7'-apo-7-(4-hydroxymethylphenyl)-β-carotene took place via a triazine adduct. The synthesis of the apo-carotenoid was based on procedures previously published[58]. Synthetic details are reported in the Supplementary Information document.

Absorption Spectroscopy. Steady-state absorption spectra were measured on a Shimadzu UV-3101PC UV-vis-NIR spectrometer. The nanosecond-millisecond transient absorption measurements were made with excitation from an optical parametric oscillator driven by the third harmonic of a Nd:YAG laser (Ekspla NT342B). The pulse width was ~4–5 ns, and the repetition rate was 10 Hz. The detection portion of the spectrometer (Proteus) was manufactured by Ultrafast Systems. The instrument response function was 5 ns.

The transient absorption data analysis was carried out using ASUFIT[59] developed in a MATLAB environment (Mathworks Inc.). Evolution-associated-difference spectra (EADS) were obtained by global analysis of the transient absorption data using a kinetic model consisting of sequentially interconverting species, e.g. 1 → 2 → 3 → …, where the arrows indicate successive mono-exponential decays with increasing time constants, which

can be regarded as the lifetimes of each species. Associated with each species is a lifetime and a difference spectrum. Each EADS corresponds in general to a mixture of states and does not portray the spectrum of a pure state or species. This procedure enables us to describe the evolution of the transient states of the system. The global analysis procedure described here has been extensively reviewed[15]. Random errors associated with the reported lifetimes obtained from transient absorption measurements were typically ≤5%.

Resonance Raman. Resonance Raman spectra were obtained using excitations provided by a 24 W Sabre laser (Coherent, Palo Alto, California), and recorded at room temperature with 90° signal collection using a two stage monochromator (U1000, Jobin Yvon, Longjumeau, France), equipped with a front-illuminated, deep-depleted CCD detector (Jobin Yvon, Longjumeau, France). Low temperature (77 K) resonance Raman spectra were recorded using a Helium flow cryostat (Air Liquide, Sassenage, France). Resonance Raman spectra of the ground and triplet state of the carotenoid moiety of the dyads were recorded as extensively described by Gall *et al*.[46].

FTIR. FTIR difference spectra were recorded at room temperature using a step-scan FTIR spectrometer (Vertex 80V). A global infrared (IR) source and a fast pre-amplified photovoltaic MCT detector (16 MHz, KV 100, Kolmar Technologies) were used. The IR light impinging on the sample was sent through 1850 cm^{-1} and 4000 cm^{-1} low-pass filters. The detector signal was recorded with an external digitizer (PAD 82a; Spectrum Labs, Rancho Dominguez, CA; 100 MHz) and with the internal digitizer (96 kHz, 24 bit A/D converter. A 10 Hz Nd: YAG laser (5 ns, 100 mJ at 355 nm, Surelite Continuum, Santa Clara, CA) was used to pump an optical parametric oscillator (Surelite Continuum), producing tunable visible light from 400-700 nm, with pulse duration of 5-7 ns. This light

was attenuated to ~2 mJ/cm^2 (for all excitation wavelengths), weakly focused to a spot of 5 mm in diameter and overlapped with the IR probe beam. The temporal resolution for this set up is 12.5 μs. All the measurements were performed at 10 °C by using a Harrick thermo regulated liquid cell.

Computational Calculations. Using Gaussian 09, density functional theory (DFT) calculations were performed in order to optimize the ground state structure of the carotenoid dyads and models. From the optimized ground state structures, bond order calculations were performed for the ground state and first excited triplet state electronic configurations. All calculations were done in the gas phase at the B3LYP/6-31G* level of theory.

Results

A

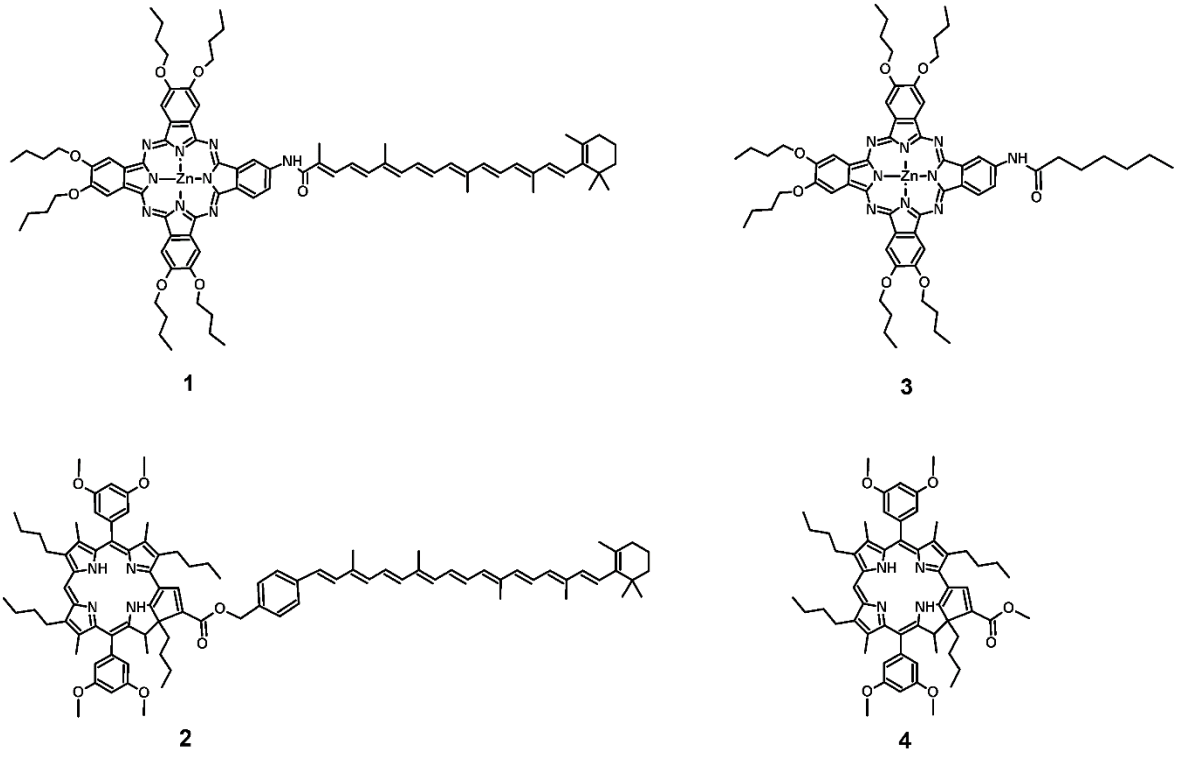

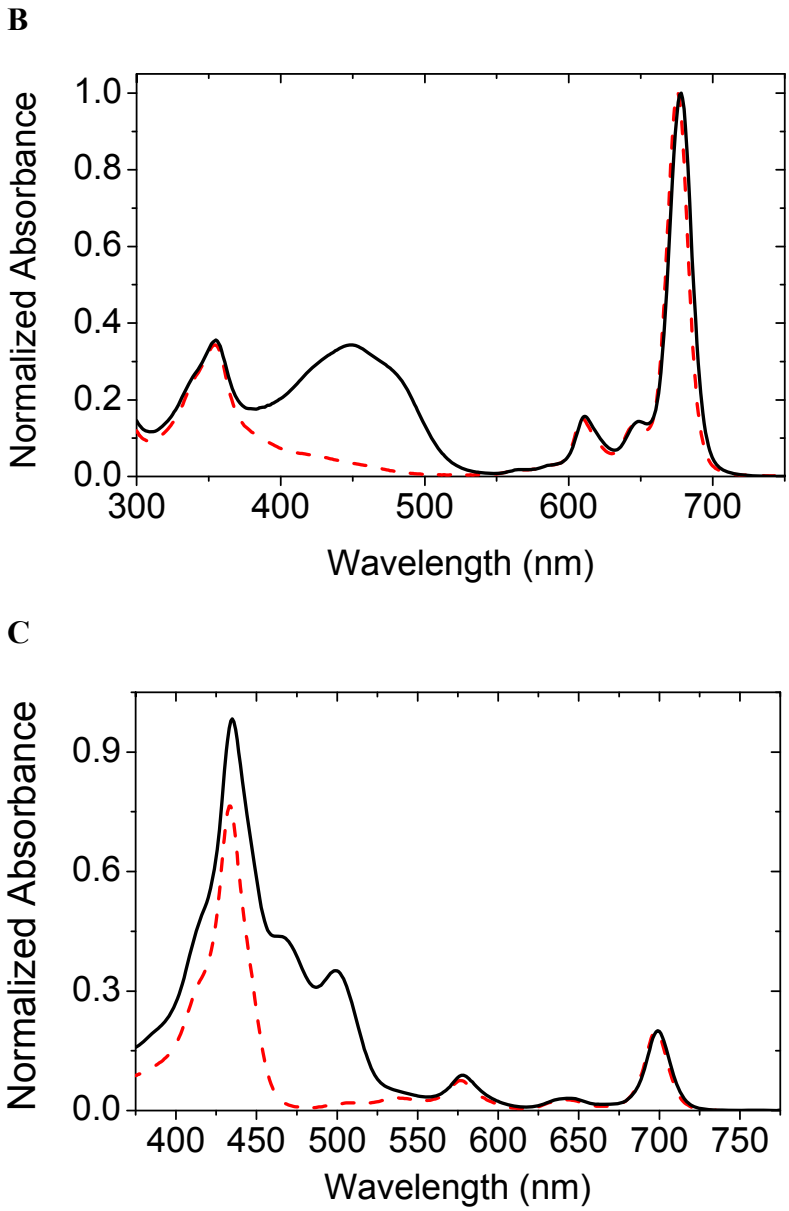

Figure 1: Molecular structure (A) of carotenophthalocyanine dyad (**1**) and model phthalocyanine (**3**), carotenopurpurin dyad (**2**) and model purpurin (**4**). Room temperature electronic absorptions in methyl-THF of carotenophthalocyanine, dyad **1**, (solid line), model phthalocyanine **3** (dash line) (B) and carotenopurpurin, dyad **2**, (solid line), model purpurin **4** (dash line) (C).

Carotenophthalocyanine, dyad 1. Dyad **1** comprises a carotenoid having 9 conjugated double bonds linked to a phthalocyanine by an amide bond (see Figure 1). Excitation of the phthalocyanine at 680 nm is followed by intersystem crossing over the

500 ps phthalocyanine singlet lifetime to yield the phthalocyanine triplet state, which immediately decays by T-T energy transfer to the linked carotenoid[14]. The phthalocyanine triplet spectrum was not observed as an intermediate between the decay of the phthalocyanine singlet and the rise of the carotenoid triplet and therefore the dynamics of the triplet transfer process were not determined. Based on the detection limits and our experience with this system, we estimate that the T-T energy transfer is at least 10-times faster than the 500 ps lifetime of the phthalocyanine singlet state. The lifetime of 7.3 μs (Figure 2, second EADS) is assigned to a species closely resembling the carotenoid triplet. The position of the T_1/T_n transition, deduced from these time-resolved experiments, peaks at about 510 nm and the carotenoid ground-state bleach is centered at around 440 nm[55a, 60] (Figure 2). The population of the carotenoid triplet state (or carotenoid triplet-based state, *vide infra*) is associated with a perturbation of the phthalocyanine Q transitions as shown by the noticeable bleaching located at 610 and 680 nm (7.3 μs EADS). This bleaching decays with the same 7.3 μs time constant as the carotenoid triplet excited state (see kinetics in Figure 2, inset). The third non-decaying EADS corresponds to the decay of triplet excited state of small amount of free, unattached phthalocyanine impurity or decomposition product. Global analysis also yielded a 1.1 μs EADS, showing the same spectral features at 440 nm and 515 nm, and a slightly larger perturbation of the phthalocyanine Q transitions. This EADS is likely to be associated with a relaxation of the carotenoid triplet-based excited state in the dyad.

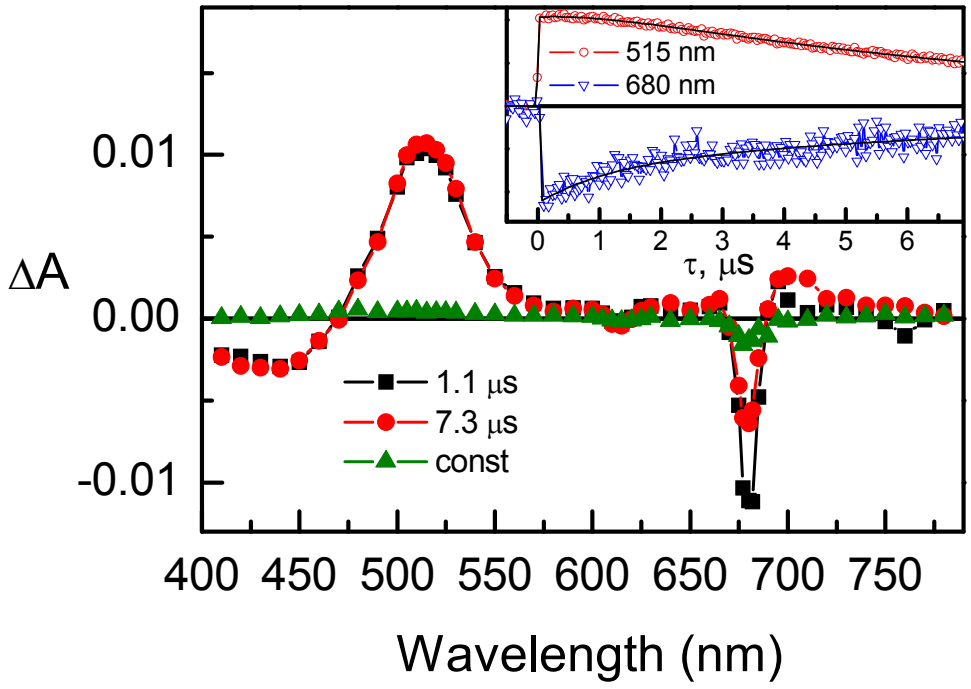

Figure 2: Evolution-associated-difference spectra (EADS) for the carotenophthalocyanine, dyad **1**, with excitation at 680 nm in argon bubbled (30 min) methyl-THF solution. Inset shows kinetics at 515 and 680 nm with solid lines as fits.

Resonance Raman spectra of this dyad dissolved in THF were performed with various excitation conditions, ranging from 457 nm to 528 nm. Figure 3A displays resonance Raman spectra obtained with 501 and 514 nm excitations. As these excitation lines match the position of the S_0/S_2 electronic transition of the carotenoid in the dyad, they are expected to enhance the contribution of this part of the molecule only. These spectra actually contain the four groups of bands typical from carotenoid molecules. The ν_1, observed at 1531 cm^{-1} arises from the C=C stretching modes, the ν_2, at 1160 cm^{-1}, which arises from a combination of C–C stretching modes and in-plane C-bending modes, the ν_3 at about 1000 cm^{-1} from in-plane rocking vibrations of the methyl groups attached to the conjugated chain and the weak ν_4 band, at about 950 cm^{-1}, from C–H out-of-plane wagging motions coupled with C=C torsional modes. The frequency of ν_1 and the structure of ν_2 are

exquisitely sensitive to the carotenoid configuration[61]. Both of these bands indicate that the carotenoid in the dyad is in *all-trans* configuration. Of course, as carotenoid *cis* isomers do not absorb exactly at the same position as the *all-trans*, these particular conditions of resonance may favor the *all-trans* carotenoid. However, as the same conclusion may be drawn at every excitation used (namely 457, 476, 488, 496, 501, 514 and 528 nm, data not shown), we safely conclude that the carotenoid configuration in this dyad is *all-trans* only. These spectra do not change upon dyad illumination at 77 K or at room temperature (data not shown), indicating that no light-induced *cis-trans* isomerization occurs, although the carotenoid triplet state is populated at the end of the excitation energy decay cascade.

A

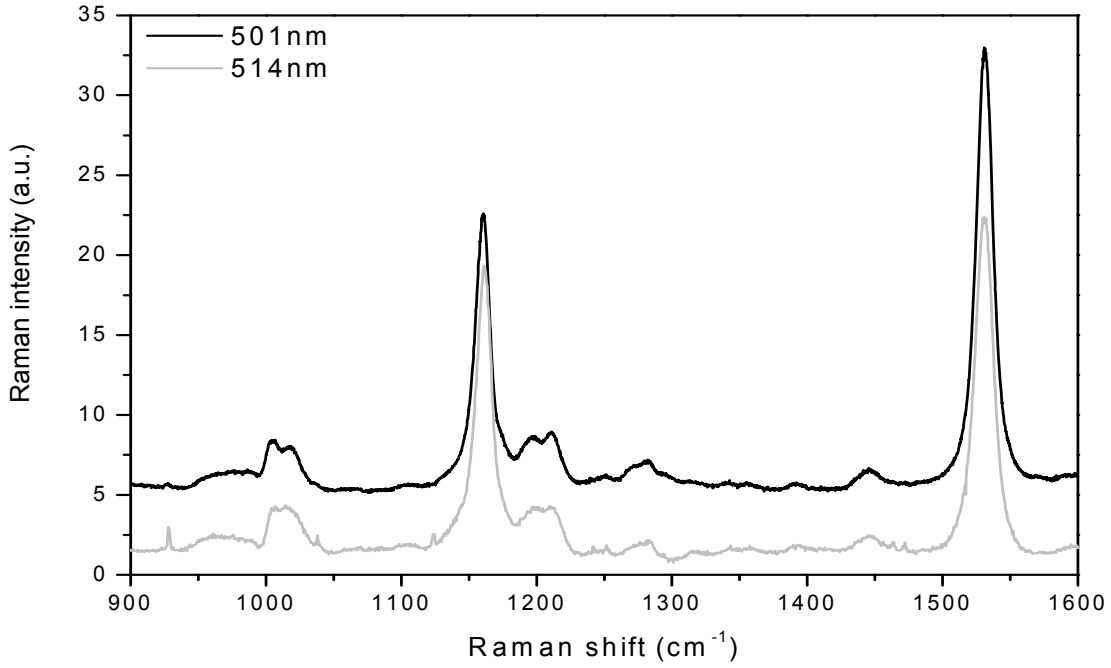

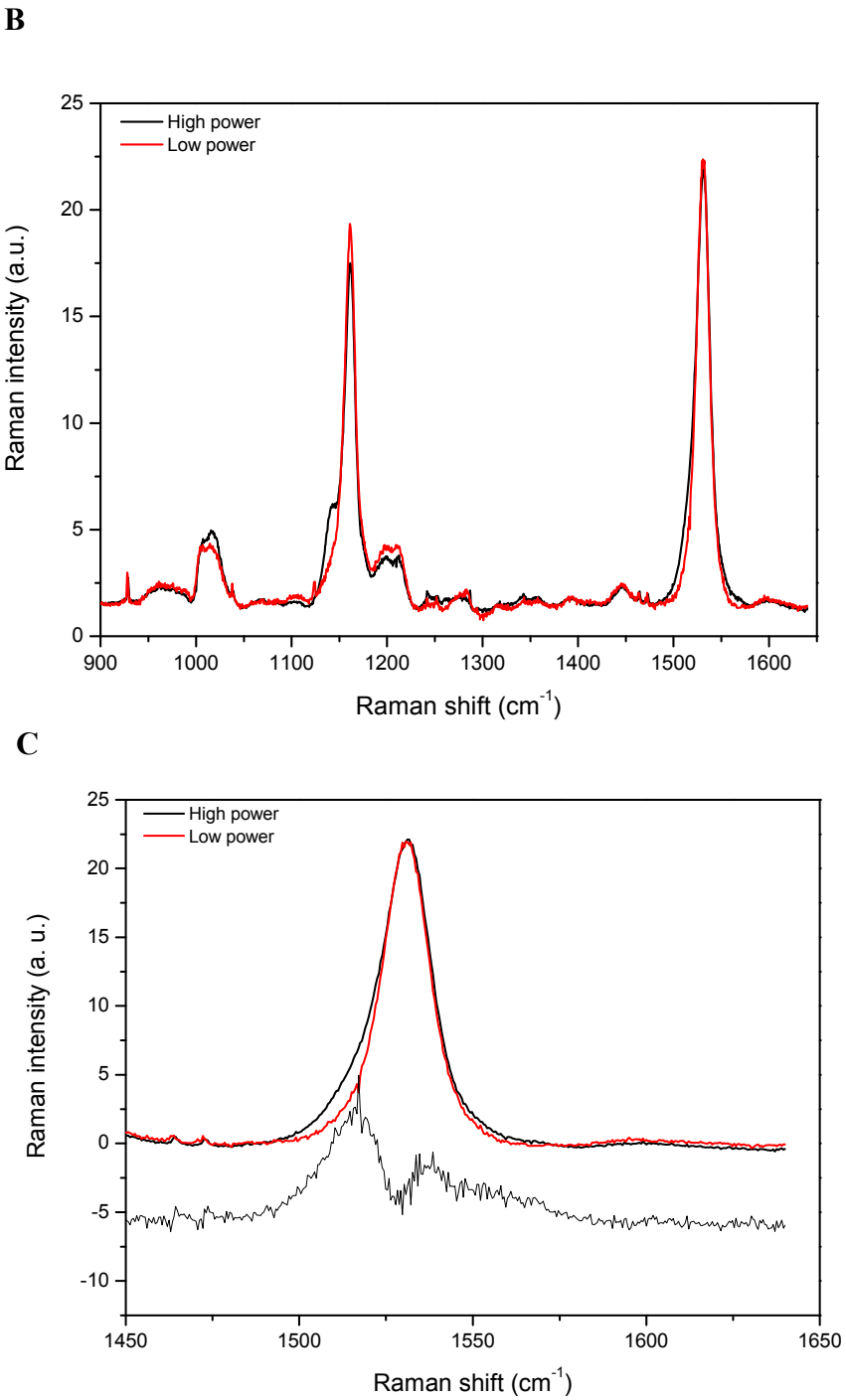

Figure 3. Resonance Raman spectra of the carotenophthalocyanine, dyad **1**, in THF excited at 501 and at 514 nm (A). Resonance Raman spectra of the carotenophthalocyanine, dyad **1**, in THF obtained with 514 nm excitation, at low and high laser power (see text). B: full spectra (900-1600 cm^{-1}). C: high frequency region (1450-1650 cm^{-1}) with computed spectral difference on the bottom.

With increasing laser power, using an excitation at 514 nm, located close to the T_1/T_n transition of the carotene, a number of small bands appear in the spectrum (Figure 3B). As discussed extensively by Gall *et al*.[46], the observed power dependence of the appearance of these features is consistent with progressive, dynamic accumulation of a transient state, and the bands observed at higher laser intensity are characteristic of the resonance Raman spectra of carotenoid molecules in their triplet states[62]. Figure 3B, right, displays the ν_1 region of the resonance Raman spectra obtained with a 514.5 nm excitation at low and high power, together with the computed difference. The ν_1 frequency of the dyad carotenoid triplet is at 1515 cm^{-1}, i.e., 16 cm^{-1} downshifted as compared to that of the carotenoid ground state (located at 1531 cm^{-1}). As discussed by Gall *et al*.[46], the build-up of a 'normal' triplet state of a carotenoid induces a 24 cm^{-1} downshift of that band, due to the transition of one electron from the bonding highest occupied molecular orbital (HOMO) to an antibonding orbital. The build-up of the carotenoid triplet state in this dyad thus induces a smaller downshift of this mode.

In order to better characterize the carotenoid triplet state in the carotenophthalocyanine dyad, we recorded the FTIR difference spectrum [triplet – ground state] of the dyad and of the phthalocyanine model in THF obtained 12 μs after excitation by a 670 nm flash (Figure 4). Due to the ultrafast T-T energy transfer time, at 12 μs the triplet state should be located on carotenoid moiety. The difference FTIR spectrum obtained for the dyad is obviously similar – but not identical – to that of model phthalocyanine, indicating that the phthalocyanine makes a major contribution to these spectra. We note that the major differences between the spectrum of the dyad and the spectrum of the model phthalocyanine are an intense positive signal at 1475 cm^{-1} and a

negative signal at 1455 cm^{-1}, accompanied by positive features at 1410, 1355, and 1274 cm^{-1}. These five features (although not exactly at the same frequencies) are found in the FTIR difference spectra of carotenoids bound to purple bacteria LH2 (Galzerano *et al*., in preparation). The same experiment was performed with a 100 ns time resolution (data not shown). The average of the spectra collected in the first 3 μs after the flash, even though quite noisy, show the same features of the spectra obtained with the 12 μs time resolution, indicating that the latter can be satisfactorily representative of the dynamics occurring in the first microseconds after the laser flash.

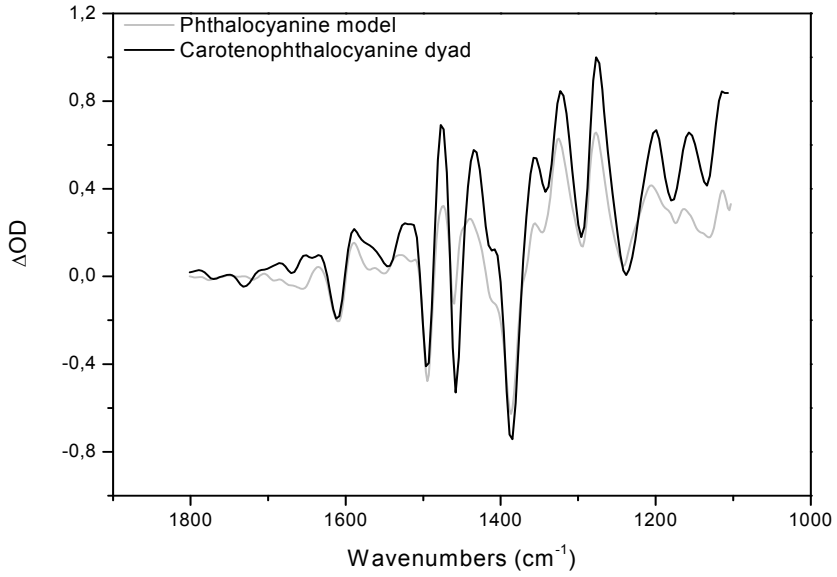

Figure 4. Time-resolved FTIR difference spectra ([triplet – ground state) performed on the phthalocyanine model **3**, compared to the carotenophthalocyanine, dyad **1**, in THF obtained with excitation at 670 nm.

As discussed below, we tentatively interpret the similarities between the spectra of the dyad and the model phthalocyanine as an indication of contributions to the phthalocyanine electronic structure by the triplet carotenoid moiety of the dyad. This finding is in contrast to the case of dyad **2** presented below.

Carotenopurpurin, dyad 2. Dyad **2** comprises a purpurin linked by a methyl ester to a 10 double bond phenyl apocarotenoid (Figure 1). For this dyad, dissolved in methyl-THF, excitation by a laser flash at 578 or 699 nm populates the purpurin singlet excited state (see absorption spectrum, Figure 1B), which undergoes intersystem crossing followed by T-T energy transfer to yield the carotenoid triplet state (Figure 5). The 42 ns EADS has the characteristic shape of the purpurin triplet excited state, with Soret and Q_y bleaching around 435 and 700 nm, respectively. With a 42 ns time constant the purpurin triplet spectrum is transformed into the carotenoid triplet spectrum, which shows an intense induced absorption around 530 nm and broad ground state bleaching around 460 nm, and decays in 5.8 μs. There are two other minor EADS required for a satisfactory fit of the data. The non-decaying one can be associated with the decay of triplet excited state of a very small amount of free (unattached) purpurin and the 1 μs EADS is possibly due to relaxation of the carotenoid triplet excited state and/or slower T-T energy transfer between purpurin and carotenoid in some minor dyad population. In the case of dyad **2**, the triplet state of the carotenoid moiety does not significantly perturb the purpurin electronic absorption spectrum, as shown by minimal Q_y bleaching signal in the 5.8 μs EADS.

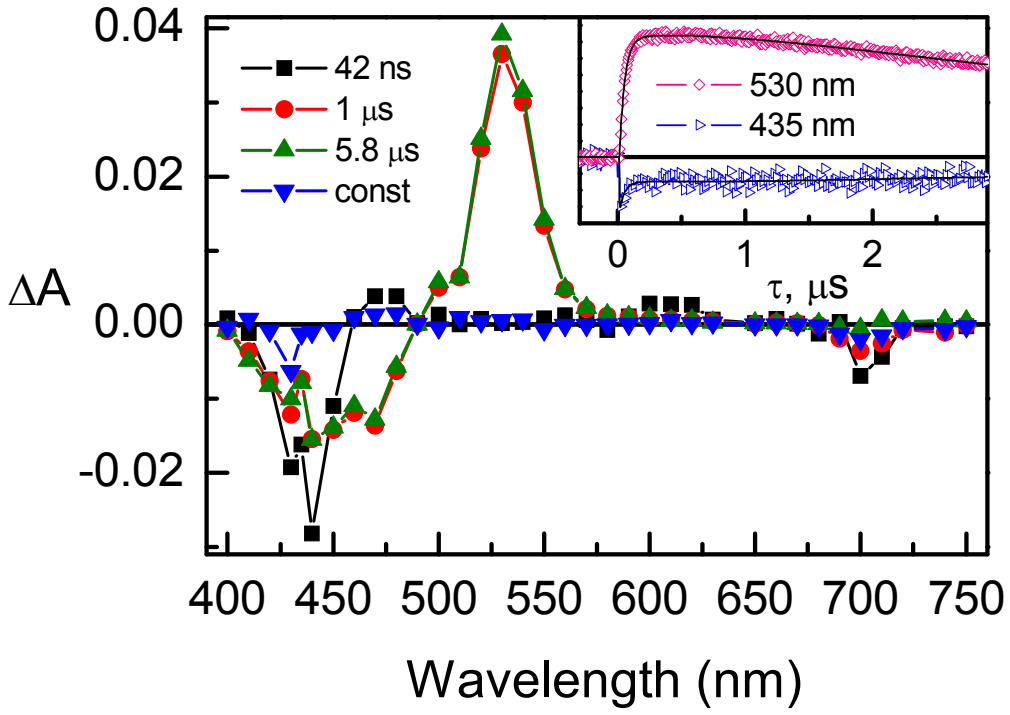

Figure 5: Evolution-associated-difference spectra (EADS) for the carotenopurpurin, dyad **2**, with excitation at 699 nm in argon bubbled (30 min) methyl-THF solution. Inset shows kinetics at 435 and 530 nm with solid lines as fits.

Resonance Raman spectra of this dyad dissolved in THF were performed with various excitation conditions, ranging from 457 nm to 528 nm. Figure 6A displays, as an example, a resonance Raman spectra of this dyad obtained with a 528 nm excitation at low laser power. As was the case for dyad **1**, the resulting resonance Raman spectra of the carotenoid indicated an *all-trans* configuration, even after extensive illumination of the dyad at 77 K or room temperature.

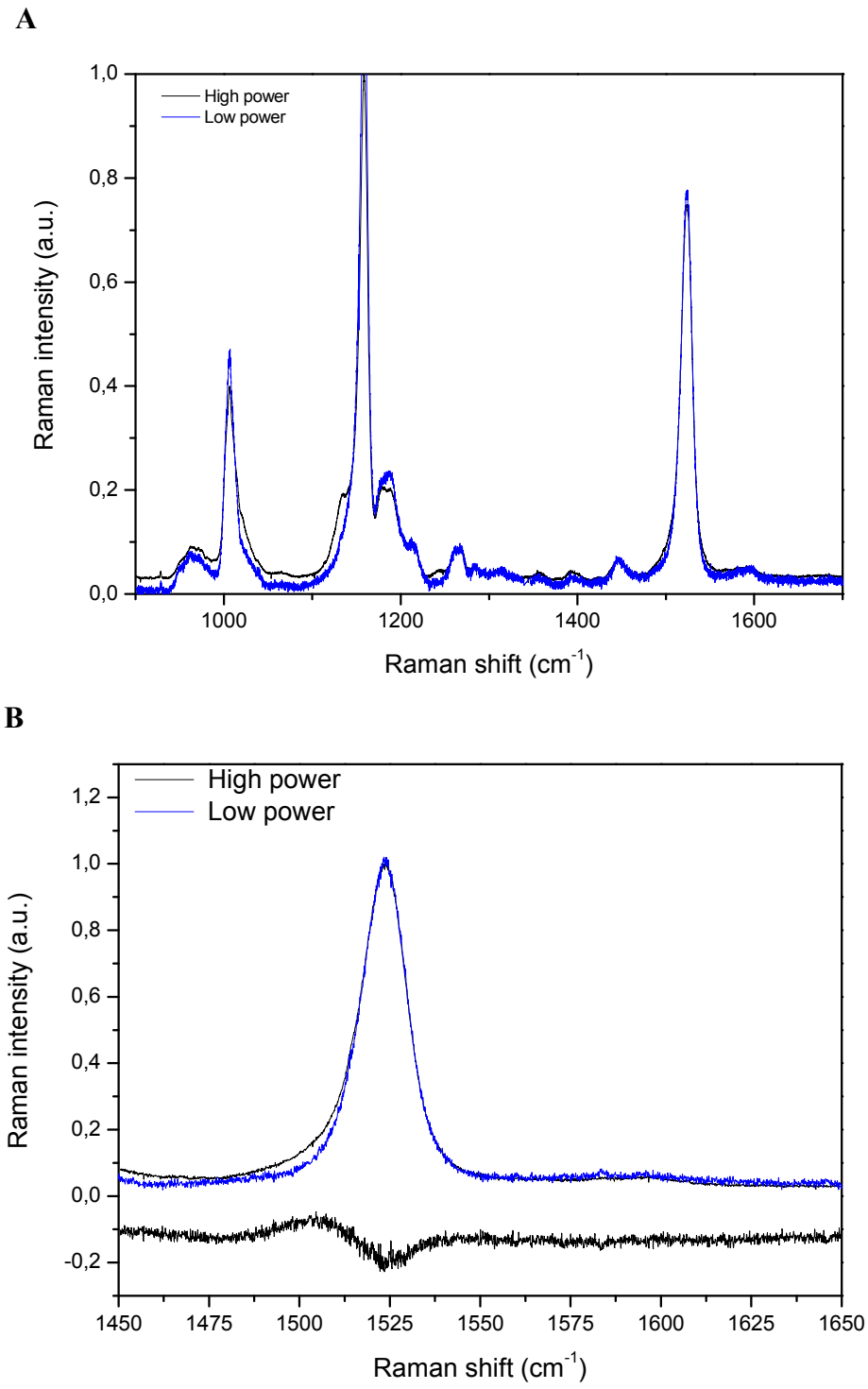

Figure 6. Full spectrum (900-1700 cm^{-1}) (A) and High frequency region (1450-1600 cm^{-1}) with computed spectral difference on the bottom (B) resonance Raman spectra of carotenopurpurin, dyad **2**, in THF excited at 528 nm.

With increasing laser power, using excitation at 528 nm, located close to the T_1/T_n transition of the carotenoid, a number of small bands appear in the spectrum (Figure 6A). Figure 6B displays the ν_1 region of resonance Raman spectra obtained at this excitation at low and high power. The ν_1 frequency of the carotenoid triplet (Figure 6B), which appears at high power, is centered at about 1502 cm^{-1} *i.e.,* downshifted by 24 cm^{-1} as compared to that of the carotenoid ground state (located at 1524 cm^{-1}). This value is very similar to that observed upon the build-up of an unperturbed triplet state of isolated β-carotene in THF[62b].

The FTIR difference spectrum of the carotenopurpurin dyad in THF was recorded 12 μs after a 435 nm flash, exciting the purpurin Soret transition. On this timescale the triplet state should be essentially 100% located on the carotenoid moiety. Figure 7 presents the FTIR difference spectrum obtained for dyad **2** and model purpurin **4** in THF. The difference FTIR spectrum of dyad **2** is qualitatively different from that of the model purpurin; it reveals major features not present in the model purpurin. Outside of an intense carbonyl signal, located at 1663 (-)/1630 (+), some of the main contributions are located at 1455 (-), 1420 (+), 1349 (+) and 1260 (-) cm^{-1} and are reasonably consistent with what is observed in the FTIR difference spectra of carotenoid bound to purple bacteria LH2 (Galzerano *et al*., paper in preparation).

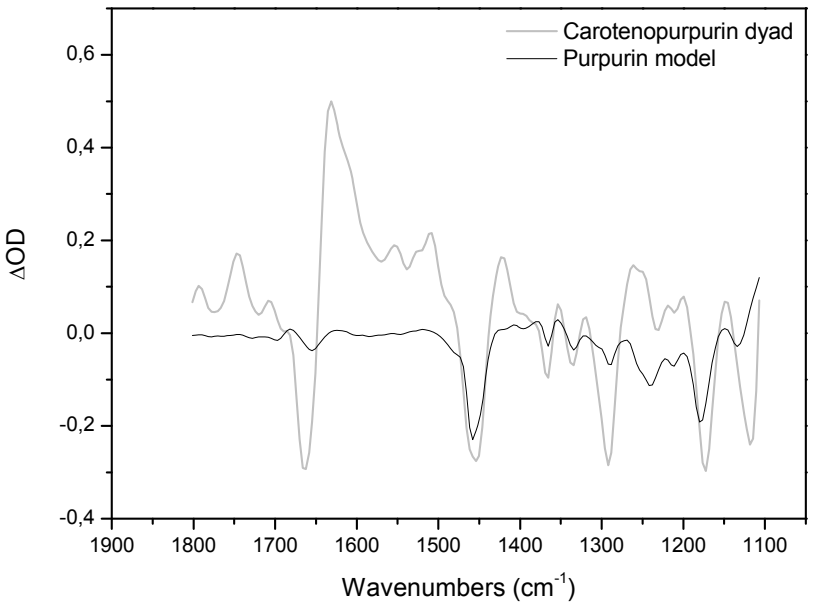

Figure 7. Time-resolved FTIR difference [triplet – ground state] measurements in THF performed on the purpurin model **4,** compared to carotenopurpurin, dyad **2**, obtained with excitation at 435 nm.

Discussion

Transient absorption spectroscopy. Cartenopurpurin, dyad **2,** is a new artificial photosynthetic dyad designed to have weaker electronic coupling between the chromophores than in the case of carotenophthalocyanine dyad **1**. The coupling is a function of the linkage between the carotenoid and the tetrapyrroles, the purpurin and phthalocyanine. In the carotenopurpurin, a methylene ester was used to link pigments resulting in a dyad with very weak through bond coupling and slow T-T energy transfer[45]. In carotenophthalocyanine, an amide linkage was used, which greatly increases the coupling yielding much faster triplet transfer lifetimes[7].

From the absorption spectra (Figure 1B) there are similarities between the tetrapyrroles: their Soret electronic transition is located in the blue region, their Q bands in

the red/NIR, and there is minimal overlap between these transitions and the carotenoid absorption bands. In carotenopurpurin **2** the carotenoid with 10 C=C absorbs maximally at 467 nm, which is at longer wavelength than that of carotenophthalocyanine **1** which has 9 C=C and maximally absorbs at 448 nm.

In the case of carotenophthalocyanine **1** efficient and fast singlet energy transfer and intersystem crossing limited triplet energy transfer was observed[30]. The carotene triplet lifetime was found to be 7.3 μs. The same intersystem-crossing-limited triplet energy transfer phenomenon occurs in the LHCII of green plants[46, 55a]. In addition, the Q band bleach of the phthalocyanine that occurs during the lifetime of the dyad **1** carotenoid triplet state imitates the chlorophyll Q band bleach observed during the carotenoid triplet lifetime in LHCII[55a]. Thus, with respect to these spectroscopic features, dyad **1**, mimics the behavior of LHCII.

In the case of dyad **2** the purpurin triplet state decay is accompanied by the rise of the carotene triplet species. The triplet energy transfer lifetime is 42 ns. Unlike dyad **1**, there is minimal purpurin Q band bleach at around 700 nm observed during the lifetime of the carotenoid triplet state. Taken together, these features indicate weaker coupling between the chromophores, which is consistent with previous observations in dyads using this linkage[6b, 7]. The behavior of dyad **2** mimics that observed in LH2 of many purple photosynthetic bacteria where the T-T energy tranfer is slower (nanosecond time scale) and the triplet carotenoid has very limited influence on the Q band from BChl[54a].

Resonance Raman & DFT calculations. Using power-resolved experiments similar to those used in the natural systems[46] (Gall *et al*., 2011), we were able to accumulate carotenoid triplet states in both dyads and to measure the corresponding resonance Raman

spectra. The typical ν_1 transition for an unperturbed carotenoid is downshifted 25 cm^{-1} due to the lower C=C bond order resulting from a change in excited state electronic structure[62b]. As discussed below, both the ν_1 shift and the IR difference spectra are interpreted as indicators of the electronic coupling between the chromophores. In this view, the coupling arises from charge transfer (CT) interactions in which the electron in the carotenoid-based LUMO (an antibonding orbital) is shared with the nearby tetrapyrrole. As the electron is shared, the antibonding character is reduced, which increases the C=C bond order resulting a smaller ν_1 shift. Therefore, the ν_1 shift is inversely proportional to the electronic coupling between the chromophores.

The resonance Raman spectrum of the carotenoid-based triplet state in the carotenophthalocyanine **1** (Figure 3B) shows that ν_1 undergoes only a 16 cm^{-1} downshift, which is much less than that observed for unperturbed carotenoids[62b]. Nearly the same triplet downshift of the ν_1 C=C frequency was measured in green plants by Gall *et al*.[46]. Thus, in dyad **1** the electronic coupling is strong and, as measured by the shift in ν_1, mimics quantitatively that found in LHCII. In both cases T-T energy transfer is very fast. For dyad **2**, the ν_1 frequency downshift is 24 cm^{-1} (Figure 6) which is similar to that expected for unperturbed *β*-carotene ($\Delta\nu_1$ -25 cm^{-1})[62b] and matches the frequency shift found in LH2 proteins[46]. Thus, in dyad **2** the electronic coupling is much less, and it quantitatively mimics that found in in LH2. In both dyad **2** and LH2, T-T transfer is relatively slow.

We note that the natural system relies on Van der Walls contact between the carotenoid and tetrapyrrole for the orbital overlap necessary for coupling, whereas in dyad **1** the coupling is provided by the amide bond and the much weaker coupling found in dyad **2** is provided by the methylene ester linkage[7].

DFT calulations of dyad **1** in the ground state show LUMO orbital amplitudes over both the carotenoid and phthalocyanine (Figure 8A). As a first approximation, it can be expected that in such systems the excited state, either singlet or triplet, in which the LUMO is singly occupied will be delocalized between both the carotenoid moiety and the attached tetrapyrrole. This delocalization may be considered charge transfer between the chromophores. In contrast, DFT calulations of dyad **2** show orbital amplitude exclusively on the carotenoid moiety in both the HOMO and LUMO (Figure 8B). Additionaly, the C=C bond order difference between the ground singlet state (GSS) and excited triplet states (ETS) of dyad **1**, dyad **2**, and a model carotenoid were calculated (Figure 9). The overall change in bond order between the ETS and the GSS electronic configuration is significantly lower for dyad **1** than for the model carotenoid and dyad **2**. We attribute this difference to the delocalization or sharing of the LUMO between the phthalocyanine and carotenoid. This sharing or CT contribution to the electronic structure *increases* the bond order in the carotenoid because it results in less electron density in the antibonding LUMO orbital in the C=C bonds of the carotenoid. For the carotenoid model and dyad **2**, an electron in the more localized LUMO antibonding orbital reduces the bond order in the ETS (and presumably in the excited singlet state as well but our experiments did not probe that state) causing a larger change in the bond order, which is reflected in the larger down frequency shift observed in dyad **2**.

FTIR. Qualitatively, the IR difference spectra report the change in the bond orders making up the normal modes that accompany the change in electronic structure from ground state in which the HOMO is doubly occupied to the triplet state in which the HOMO and LUMO are singly occupied. Although predicting the quantitative changes in the IR

spectrum is beyond the scope of this report, we interpret common features in the IR difference spectrum between the model tetrapyrrole and the dyad as an indication of triplet electronic structure characteristic of the tetrapyrrole but found when the dyad is nominally in the carotenoid-based lowest triplet state. In other words, the greater the similarity of the IR difference spectra, the more the electronic structure of the tetrapyrrole has triplet character. As discussed above, we propose CT interactions in which the shared LUMO is occupied by an electron from the carotenoid as the mechanism for delocalizing the triplet over the two chromophores.

FTIR time-dependent spectroscopic measurements were made 12 μs after exciting the phthalocyanine moiety of carotenophthalocyanine dyad **1** at 670 nm. Based on the information obtained from the transient absorption mesaurements, T-T energy transfer is very fast and the triplet of the carotenoid decays in 7.3 μs. Thus at 12 μs when the FTIR spectra were measured, the dominant state is the carotenoid-based triplet. The minor contribution of the free phthalocyanine, which was observed in transient absorption spectroscopy (Figure 2), is considered too small to contribute significantly to the FTIR difference spectrum. Comparing the dyad **1** FTIR difference spectrum (Figure 4) with that of the model phthalocyanine, vibrational signals and intensities occuring at 1610, 1500, 1390, 1260, and 1240 cm^{-1} are found in both samples and provide evidence that the phthalocyanine electronic structure in dyad **1** has characteristics in common with those of the model phthalocyanine. We interpret this similarity as an indication of the partial presence of an electron in the LUMO of dyad **1** even though the dyad lowest triplet state is nominally the carotenoid triplet. DFT calculations (Figure 8A) further support this

interpretation by indicating that the LUMO orbital amplitudes are spread over the carotenoid and phthalocyanine components.

Similar IR difference results have been reported in oxygenic photosynthetic complexes. In these complexes, namely peridinin-chlorophyll protein (PCP) and LHCII, where the T-T energy transfer between chlorophyll and carotenoid molecules is sub-nanosecond, FTIR difference spectra in the microsecond timescale also yielded mainly signals arising from chlorophyll molecules[46, 63]. Thus dyad **1** mimics the fast T-T energy transfer and the IR difference spectrum "fingerprint" of electronic coupling found in LHCII and PCP, both oxygenic photosynthetic systems.

The triplet state of carotenopurpurin dyad **2** was populated by T-T energy transfer from the excited purpurin with a 42 ns time constant. Therefore, 12 μs after the excitation laser pulse the excited state must reside on the carotenoid molecule. As shown in Figure 7, in this case the differences between the purpurin model difference spectrum and the dyad difference spectrum are qualitatively obvious. For example, the features at 1790, 1660, 1625 cm^{-1} were not observed in the purpurin model difference spectrum but are seen in dyad **2**. Thus the vibrational transitions observed in dyad **2** indicate a purpurin electronic structure that has little in common with the triplet electronic structure of the purpurin model. This would be expected if the electronic structure of the two chromophores is not extensively shared or delocalized in the triplet state. This can be explained by the weak coupling provided by the methylene ester linkage between the two chromophores, which effectively isolates the LUMO wavefunction on the carotenoid. Indeed, DFT calculations predict that the LUMO is localized on the carotenoid moiety (Figure 8B).

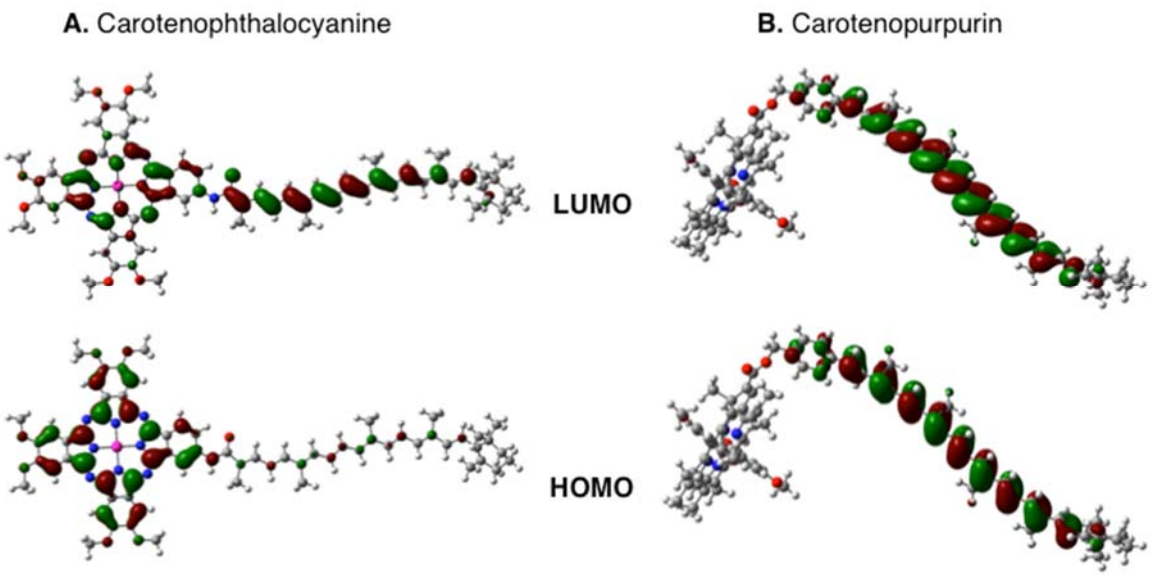

Figure 8. Orbital diagrams of the carotenophthalocyanine, dyad **1**, (**A**) and the carotenopurpurin, dyad **2** (**B**) calculated using DFT (B3LYP/6-31G*).

The behavior of dyad **2** is reminiscent of that found in LH2 proteins from purple bacteria in which the IR difference spectrum of LH2 is very different from that of the (BChl) (Galzerano *et al*., paper in preparation). Dyads **1** and **2** demonstrate that by controlling the coupling, artificial photosynthetic systems can be designed to mimic their natural counterparts.

Conclusions

In dyad **1** both FTIR difference spectra and Raman shifts indicate a triplet electronic structure shared between the carotenoid and tetrapyrrole moieties. This coupling gives rise to ultrafast T-T energy transfer. Similar results were found in pigment-protein complexes from oxygen evolving photosynthetic organisms. We postulate that a shared electronic structure is essential for protection from singlet oxygen sensitization in photosynthetic membranes in oxygenic organisms. In the carotenopurpurin, dyad **2**, in which the linkage provides less electronic coupling, T-T energy transfer is slower and there is much less

spectroscopic evidence of a delocalized triplet state. This mimics the behavior of the BChl and carotenoids in the LH2 complexes of anaerobic photosynthetic bacteria in which the exposure to oxygen is intermittent and much lower.

Altogether, our experiments indicate a remarkable similarity between the electronic structure required for the coupling necessary for ultrafast T-T energy transfer in photosynthetic proteins and in synthetic dyads. These results are encouraging for artificial systems because efficient water oxidation will expose membranes to high levels of oxygen production and this work demonstrates that nature's mechanism for protection can be provided in artificial photosynthetic constructs.

Acknowledgements

This work was supported by EU program Marie Curie (FP7 Initial Training Network HARVEST), by the ERC funding agency (PHOTPROT project), and by the National Research Agency (ANR, Cyanoprotect Project). This work was supported by the French Infrastructure for Integrated Structural Biology (FRISBI) ANR-10-INSB-05-01. The synthesis, computational calculations, and transient absorption spectroscopy were funded by the US Department of Energy (FG02-03ER15393) and the Human Frontiers Science Program Grant Number RGP0005. This work was supported as part of the Center for Bio-Inspired Solar Fuel Production, an Energy Frontier Research Center funded by the US Department of Energy, Office of Science, Office of Basic Energy Sciences (award DE-SC0001016). D.D.M.H. was supported by the National Science Foundation Graduate Research Fellowship Program (NSF-GRFP; grant no. DGE-0802261), by the More Graduate Education at Mountain States Alliance (MGE@MSA) and by the Alliance for

Graduate Education and the Professoriate (AGEP), National Science Foundation Cooperative agreement no. HRD-0450137.

Supplementary Information

Synthesis of the carotenopurpurin. Performed by Paul Liddell.

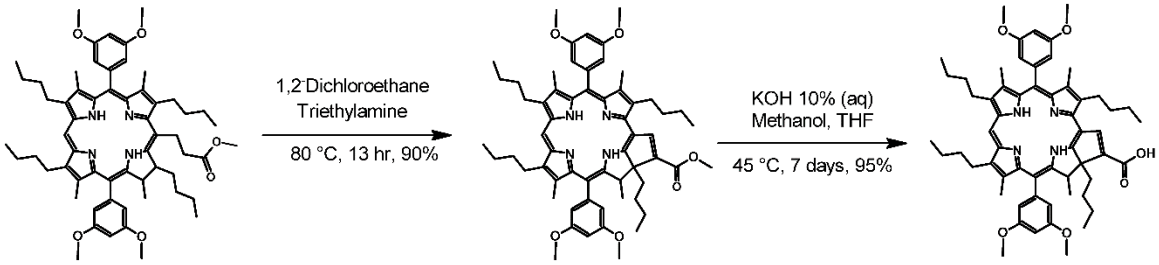

Scheme S1. Synthesis of the purpurin acid.

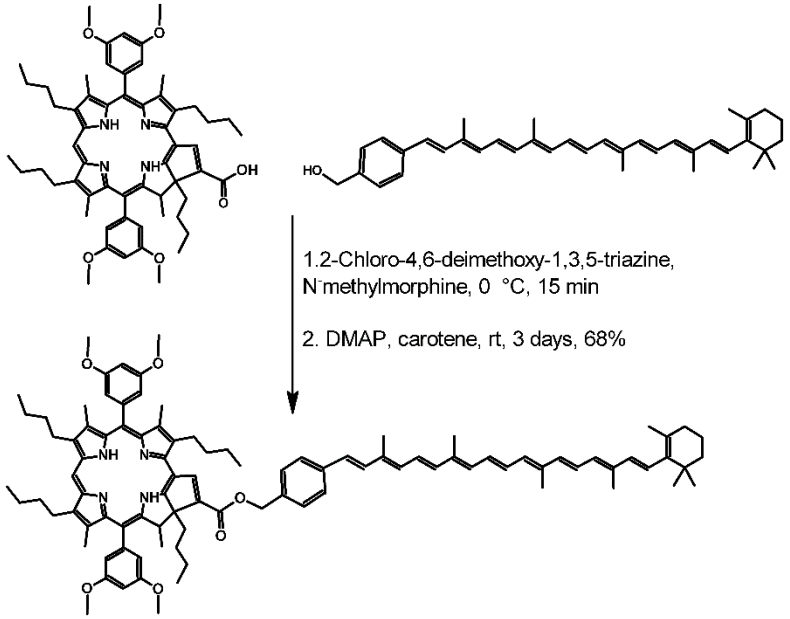

Scheme S2. Synthesis of the carotenopurpurin dyad.

5,15-Bis(3,5-dimethoxyphenyl)-10-(methyl-3-propenoate)-2,8,12,18-tetrabutyl-3,7,13,17-tetramethylporphyrin (1). This compound was synthesized according to the general procedure outlined by M. J. Gunter and B. J. Robinson. ^{1}H NMR (300 MHz, $CDCl_3$) δ -1.62 (2H, brs, -NH), 0.93 (6H, t, J = 8Hz, -CH_3), 1.02 (6H, t, J =

8Hz, -CH_3), 1.43 (4H, sextet, *J* = 7Hz, -CH_2-), 1.61 (4H, sextet, *J* = 7Hz, -CH_2-), 1.74 (4H, quintet, *J* = 7Hz, -CH_2-), 1.97 (4H, quintet, *J* = 7Hz, -CH_2-), 2.24 (6H, s, -CH_3), 2.38 (6H, s, -CH_3), 3.40 (4H, t, *J* = 8Hz, -CH_2-), 3.71 (4H, t, *J* = 8Hz, -CH_2-), 3.93 (3H, s, -CO_2CH_3), 3.95 (12H, s, -OCH_3), 6.03 (1H, d, *J* = 15Hz, vinyl-H), 6.86 (4H, t, *J* = 2Hz, Ar-H), 7.23 (2H, m, Ar-H partially obscured by the $CHCl_3$ peak), 9.57 (1H, s, meso-H), 10.09 (1H, d, *J* = 15Hz, vinyl-H); MALDI-TOF-MS m/z calcd for $C_{60}H_{74}N_4O_6$ 947, obsd 948; Uv/vis (DCM) 440, 530, 608, 688 nm.

Purpurin (2). To a tube containing 200 mg (0.211 mmol) porphyrin (1) was added 1,2-dichloroethane (30 mL) and triethylamine (4 mL). The contents were flushed with nitrogen and the tube then sealed with a Teflon screw cap. The reaction mixture was then warmed to 80 ^oC for 13 hours. The solvent was removed under vacuum and the residue chromatographed on silica gel (toluene containing 3-5% ethyl acetate). The isolated material was recrystallized from dichloromethane/methanol to give 180 mg (90% yield) of purpurin (2): ^1H NMR (300 MHz, $CDCl_3$), δ -0.60 (1H, m, -CH_2-), -0.08 (1H, s, -NH), 0.21 (3H, t, *J* = 8Hz, -CH_3), 0.30-0.50 (2H, m, -CH_2-), 0.56-0.67 (1H, m, -CH_2-), 0.84 (1H, s, -NH), 1.03 (3H, t, *J* = 9Hz, -CH_3), 1.06 (3H, t, *J* = 9Hz, -CH_3), 1.09 (3H, t, *J* = 9Hz, -CH_3), 1.38-1.47 (1H, m, -CH_2-), 1.60-1.74 (6H, m, -CH_2-), 1.67 (3H, d, *J* = 9Hz, -CH_3), 1.90-2.10 (6H, m, -CH_2-), 2.30 (3H, s, -CH_3), 2.40 (3H, s, -CH_3), 2.41 (3H, s, -CH_3), 2.4-2.5 (1H, m, -CH_2-), 3.54-3.84 (6H, m, -CH_2-), 3.75 (3H, s, -OCH_3), 3.86 (3H, s, -OCH_3), 3.97 (3H, s, -OCH_3), 3.98 (3H, s, -CO_2CH_3), 4.05 (3H, s, -OCH_3), 4.49 (1H, quartet, *J* = 9Hz, C-H), 6.41 (1H, t, *J* = 2Hz, Ar-H), 6.75 (1H, t, *J* = 3Hz, Ar-H), 6.84 (1H, t, *J* = 3Hz, Ar-H), 6.92 (1H, t, *J* = 2Hz, Ar-H), 7.30 (1H, t, *J* = 2Hz, Ar-H), 7.49 (1H, s, Ar-H), 9.45 (1H,

s, meso-H), 9.51 (1H, s, vinyl-H); MALDI-TOF-MS m/z calcd for $C_{60}H_{74}N_4O_6$ 947, obsd 947; Uv/vis (DCM) 436,538, 580, 642, 660, 700 nm.

Purpurin Acid (3). To a flask containing 350 mg (0.370 mmol) purpurin (2) was added THF (250 mL), methanol (60 mL) and 12 mL 10% aqueous potassium hydroxide. The solution was stirred at 45 ^oC under a nitrogen atmosphere for 7 days. After cooling, the volume of the reaction mixture was reduced to about 100 mL then diluted with dichloromethane (300 mL) and washed with dilute citric acid. The organic layer was washed with water three times and then concentrated to give 328 mg (95% yield). The material was used without further purification.

Carotenopurpurin (4). To a flask containing 300 mg (0.322 mmol) purpurin acid (3) was added dichloromethane (10 mL) and 67 μL (0.64 mmol) N-methylmorpholine. The solution was cooled to 0 ^oC under a nitrogen atmosphere followed by the addition of 68 mg (0.386 mmol) 2-chloro-4,6-dimethoxy-1,3,5-triazine. Stirring at 0 ^oC continued for 15 min then at room temperature for 3 hours. TLC indicated that all of the purpurin acid had been converted to the triazine adduct. 7'-apo-7-(4-hydroxymethylphenyl)-β-carotene (200 mg, 0.386 mmol) and 79 mg (0.63 mmol) 4-dimethylaminopyridine were added and stirring continued. After 3 days the TLC showed that the reaction was complete. The solvent was evaporated and the residue chromatographed on silica gel (toluene containing 1-2% ethyl acetate). The material obtained was recrystallized from dichloromethane/methanol to give 312 mg (68% yield) of the carotenopurpurin (4): ^1H NMR (500 MHz, $CDCl_3$) δ -0.6 (1H, m, $-CH_2-$), -0.58 (1H, brs, -NH), 0.21 (3H, t, J = 7Hz, $-CH_3$), 0.34-0.43 (2H, m, $-CH_2-$), 0.86 (1H, s, -NH), 1.00-1.07 (15H, m, Car 16-CH_3, Car 17-CH_3, 3x-CH_3), 1.42 (1H, m, $-CH_2-$), 1.46-1.48 (2H, m, Car 2-CH_2-), 1.60-1.67 (12H,

m, Car 3-CH_2-, -CH_3, 3x-CH_2-), 1.72 (3H, s, Car 18-CH_3), 1.90-2.03 (15H, m, Car 20-CH_3, Car 20^1-CH_3, Car 19-CH_3, 3x-CH_2-), 2.03 (3H, s, Car 19-CH_3), 2.29 (3H, s, -CH_3), 2.39 (6H, s, -CH_3), 2.47 (1H, m, -CH_2-), 3.56-3.73 (6H, m, -CH_2-), 3.75 (3H, s, -OCH_3), 3.85 (3H, s, -OCH_3), 3.96 (3H, s, -OCH_3), 4.04 (3H, s, -OCH_3), 4.50 (1H, quartet, J = 7Hz, -CH-), 5.35 (1H, d, J = 12Hz, Ar-CH_2-), 5.47 (1H, d, J = 12Hz, Ar-CH_2-), 6.12-6.96 (18H, m, 14x vinyl-H, 4x Ar-H), 7.30 (1H, s, Ar-H), 7.49 (5H, s, Ar-H), 9.48 (1H, s, meso-H), 9.50 (1H, s, vinyl-H); MALDI-TOF-MS m/z calcd for $C_{97}H_{118}N_4O_6$ 1436, obsd 1436; Uv/vis (DCM) 373, 438, 472, 504, 582, 644, 700 nm.

CHAPTER 3

INTERMOLECULAR CHARGE TRANSFER CHARACTER IN CAROTENOTETRAPYRROLE TRIPLET STATES

Katherine WongCarter, Gerdenis Kodis, John J. Tomlin, Edgar Reyes, Smitha Pillai, Paul Liddell, Devens Gust, Thomas A. Moore, Ana L. Moore

Department of Chemistry & Biochemistry and The Center for Bioenergy and Photosynthesis, Arizona State University, Tempe, Arizona 85287-1605, United States

Introduction

Carotenoids are important for removing reactive oxygen species (ROS), such as singlet oxygen, in the photosynthetic protein complexes as discussed in Chapter 1. Carotenoids have a low lying first excited triplet state that can quench singlet oxygen and return it to the benign ground state. Alternatively, the formation of ROS can be prevented by immediately transferring triplet energy from a (bacterio)chlorophyll to a carotenoid, this was also discussed in the previous chapter. Chapter 2 also highlighted the importance of this ultrafast triplet energy transfer in a carotenophthalocyanine artificial photosynthetic dyad and its similarities to the triplet energy transfers in LHCII of green plants. This chapter investigates a possible intramolecular charge transfer (ICT) character of the carotenoid triplet state in several carotenotetrapyrrole dyads.

An ICT state is a partial charge transfer state where there is a partial negative charge (δ^-) on one part of the molecule and a partial positive charge (δ^+) in the other part[64]. This occurs when there is an electron donor and an electron acceptor that have some electronic coupling between them thus allowing an electron flow between the two parts of the

molecule. Thus when the orbitals of the donor and acceptor interact they form a polarized state that can be stabilized in polar solvents by lowering the energy of the ICT state[65]. Similar ICT states were observed in carotenoids in natural protein complexes. It is thought that the twisting of the carotenoid polyene by the protein environment[66], and/or carbonyl functional groups[4a] are responsible for the ICT character in some carotenoids. ICT states were observed in artificial photosynthetic compounds using ultrafast transient absorption spectroscopy. For example, in a carotenophthalocyanine dyad with a carotenoid with 11 double bonds (db) in addition to a carbonyl group, the phthalocyanine singlet excited state was more quenched in polar solvents. This effect was assigned to the phthalocyanine singlet excited state energy transfer to a carotenoid ICT state, which energy was lowered below the normal carotenoid singlet excited state in polar solvents[30]. The formation of triplet excited state and its possible ICT character in the dyads are investigated here using nanosecond-millisecond transient absorption spectroscopy.

Three sets of dyads were measured and analyzed for their carotenoid triplet state properties. The first set contains carotenopurpurin dyads (Figure 1). One is an amide carotenopurpurin, **CPur1**, which was studied previously by our group for its efficient antenna properties[9]. It was determined that the triplet energy transfer is limited by the intersystem crossing rate of the purpurin. The other carotenopurpurin dyad, **CPur2** is a methylene ester analogue described in Chapter 2. The other two dyads are classical artificial photosynthetic systems containing carotenoid and porphyrin moieties covalently bound at isomeric *ortho* (**CPor3**) and *para* (**CPor4**) positions (Figure 2). Their synthesis was updated and yield improved in order to perform these spectroscopic studies. The last set of dyads (Figure 3) contains carotenophthalocyanine dyads (**C9Pc**, **C10Pc**, **C11Pc**) that

have been previously studied for the photoregulatory and NPQ properties[14, 30]. As the energy levels of excited states vary depending on the length of the carotenoid, the effect of change in length on carotenoid and phthalocyanine triplet states coupling in dyads was investigated.

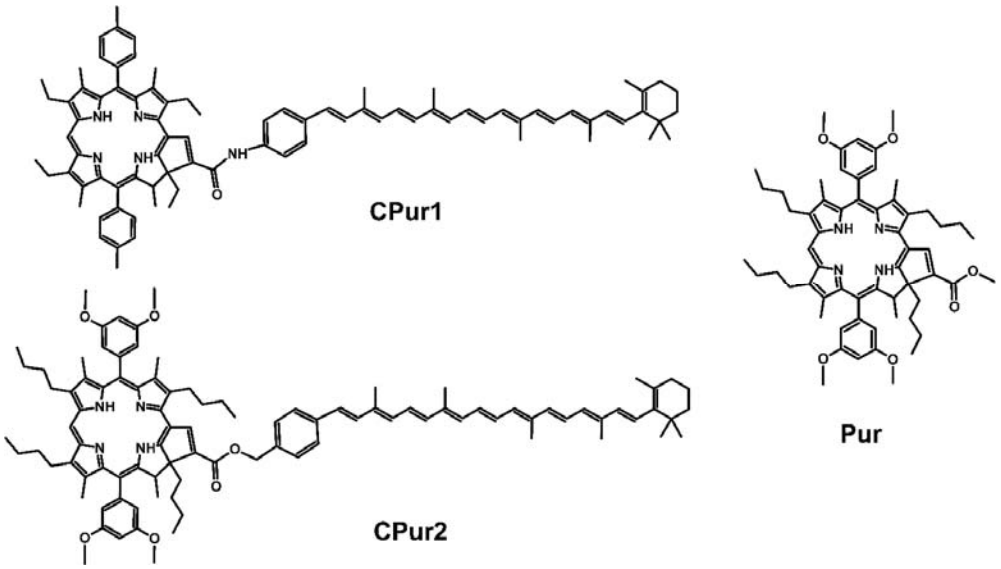

Figure 1. Molecular structure of the amide (**CPur1**), ester (**CPur2**) carotenopurpurin dyads, the model purpurin (**Pur**).

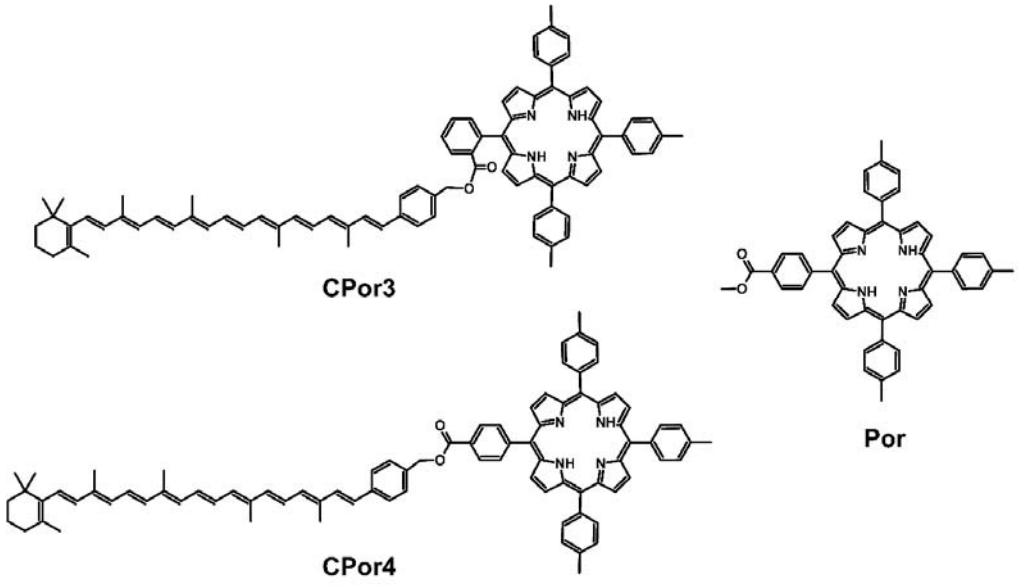

Figure 2. Molecular structure of the *ortho*- (**CPor3**), *para*-carotenporphryin (**CPor4**) dyads, and the model porphyrin (**Por**).

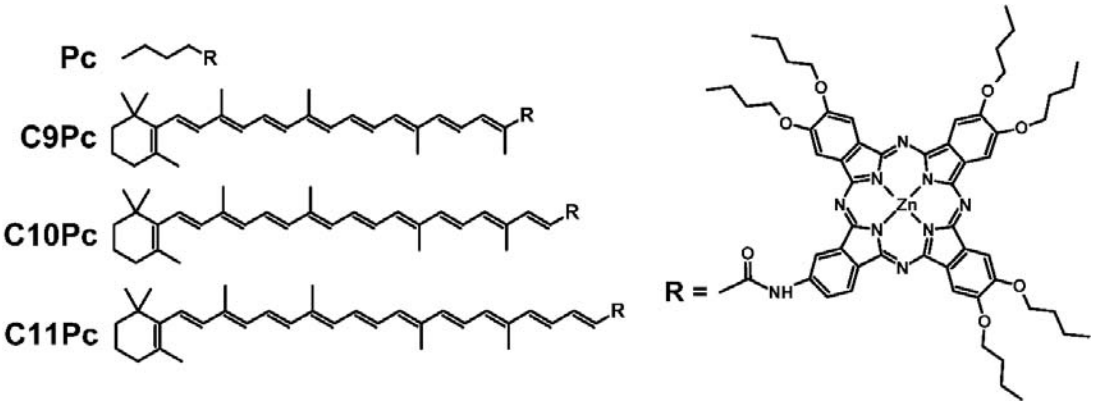

Figure 3. Molecular structure of the phthalocyanine model compound (**Pc**), and the carotenophthalocyanine dyads with carotenoids containing 9 (**C9Pc**), 10 (**C10Pc**), and 11 (**C11Pc**) double bonds.

The change in the solvent polarity induces changes in the spectral features of the triplet state suggesting formation of the solvent stabilized triplet state with ICT character. Those findings may be important for future applications in artificial photosynthesis and broaden our understanding of processes in natural photosynthetic systems.

Materials & Methods

Synthesis. The synthesis of the amide carotenopurpurin, **CPur1**, was previously reported by Macphearson *et al*.[9] and the synthesis of the ester carotenopurpurin, **CPur2**, was reported in Chapter 2.

The carotenoporphyrin dyad synthesis (Scheme 1) was updated and improved based on procedures previously developed[67]. The tri-tolyl-porphyrins and model porphyrin (**Por**) were synthesized using a general porphyrin condensation procedure[68]. The synthesis of the benzyl-hydroxy apo-carotenoid was based on procedures previously published[6b]. The esterification reaction of the porphyrin acid and the 7'-apo-7-(4-hydroxymethylphenyl)-β-carotene took place via an EDCI and DMAP coupling reaction to produce **CPor3** and **CPor4**.

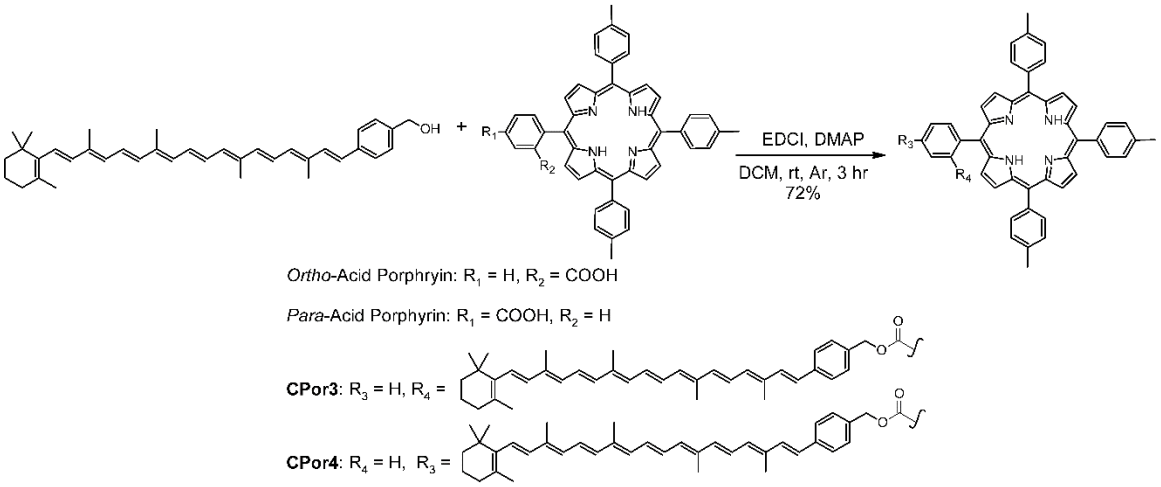

Scheme 1. Synthesis of *ortho*- (**CPor3**) and *para*-carotenoporphyrins (**CPor4**).

Synthesis of the **C9Pc**, **C10Pc**, and **C11Pc** carotenophthalocyanines, and the phthalocyanine model were reported previously[30].

Spectroscopy. All samples were purified by prep-TLC and dissolved in several solvents: Sigma-Aldrich anhydrous cyclohexane, freshly distilled methyl-THF over LiH, and Sigma-Aldrich Chromasolv® HPLC grade benzonitrile. Once dissolved, the samples were bubbled with a steady stream of argon for 30 minutes to remove oxygen from the solution before performing the pump-probe experiments. At the conclusion of each experiment the integrity of the oxygen-free environment was checked by adding air and observing the quenching of triplet states by molecular oxygen present in air.

Steady-state absorption spectra were measured on a Shimadzu UV-3101PC UV-vis-NIR spectrometer. The nanosecond-millisecond transient absorption measurements were made with excitation from an optical parametric oscillator driven by the third harmonic of a Nd:YAG laser (Ekspla NT342B) using wavelengths that would excite the tetrapyrrole transitions to induce tetrapyrrole triplet state formation and triplet energy transfer to the carotenoid. The pulse width was ~5 ns and the repetition rate was 10 Hz.

The detection portion of the spectrometer (Proteus) was manufactured by Ultrafast Systems. The instrument response function was 5 ns.

The transient absorption data analysis was carried out using ASUFIT[59] developed in a MATLAB environment (Mathworks Inc.). Evolution-associated-difference spectra (EADS) were obtained by global analysis of the transient absorption data using a kinetic model consisting of sequentially interconverting species, e.g. $1 \rightarrow 2 \rightarrow 3 \rightarrow \ldots$, where the arrows indicate successive mono-exponential decays with increasing time constants, which can be regarded as the lifetimes of each species. Associated with each species is a lifetime and a difference spectrum. Each EADS corresponds in general to a mixture of states and does not portray the spectrum of a pure state or species. This procedure enables us to describe the evolution of the transient states of the system. The global analysis procedure described here has been extensively reviewed[15]. Random errors associated with the reported lifetimes obtained from transient absorption measurements were typically ≤5%.

Results

Carotenopurpurin model and dyads. The purpurin model, **Pur**, absorption spectrum has the typical features for this class of cyclic tetrapyrroles, a Soret at 433 nm, and several Q bands, the largest is the red-most Q band at 698 nm (Figure 4). The purpurin model is a synthetic precursor for the ester carotenopurpurin **CPur2** and is slightly different than the purpurin in the amide carotenopurpurin **CPur1**. The solubilizing groups at *beta* positions around the purpurin macrocycle in **CPur1** do not affect the absorption properties of the tetrapyrrole because the Soret and Q bands occur at the same wavelengths (Figure 4). With the addition of the apo-carotenoid moiety the dyads have an increased absorbance

between 430 and 520 nm, and the purpurin absorption transitions do not shift, which is typical for these carotenotetrapyrrole dyads.

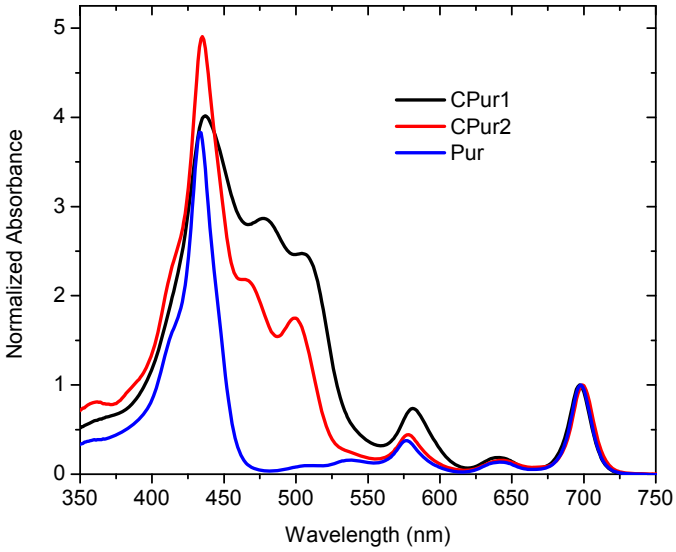

Figure 4. Amide carotenopurpurin (**CPur1**), ester carotenopurpurin (**CPur2**), and model purpurin (**Pur**) normalized absorption spectra in methyl-THF.

The purpurin model triplet has a lifetime of 99 μs (Figure 5) in argon saturated solutions. The purpurin triplet spectrum shows a large ground state bleach at the Soret and red-most Q band. The purpurin triplet spectrum also has photoinduced absorption between 430 and 620 nm, which is offset by some ground state bleach by the other Q bands at 560 and 610 nm.

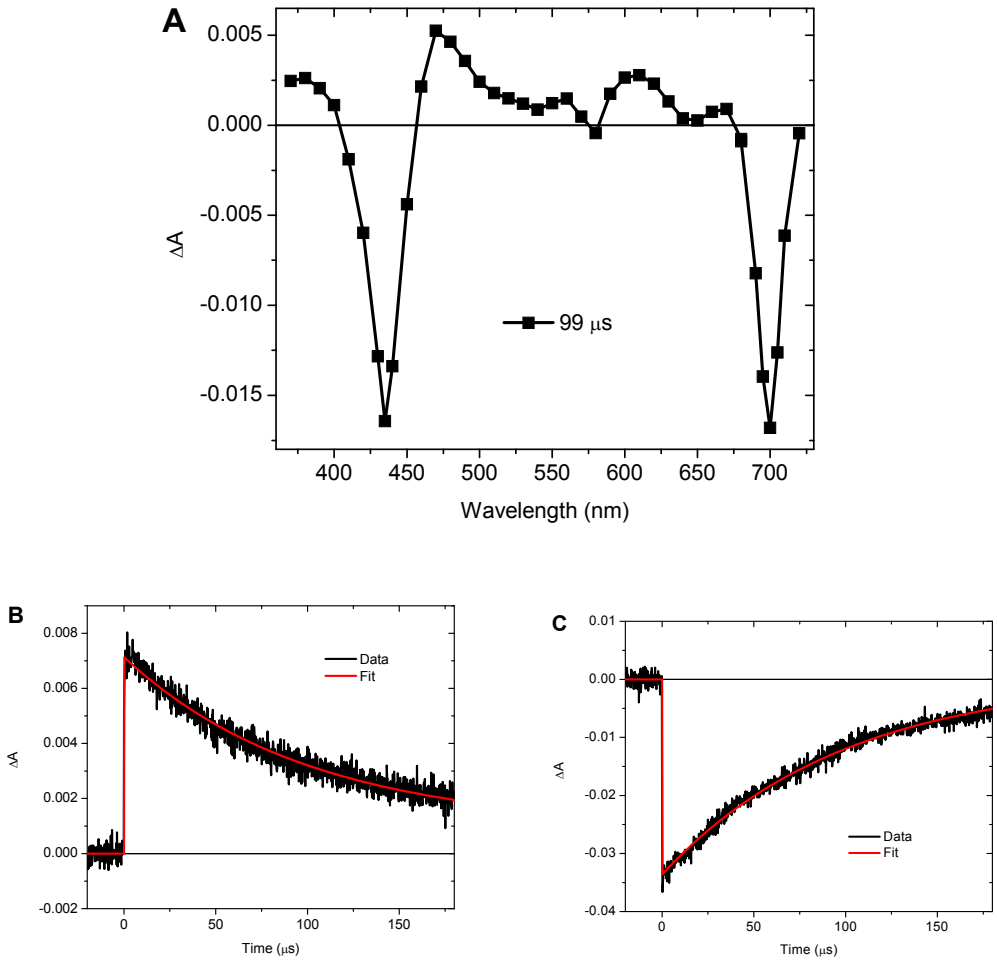

Figure 5. Transient spectrum at 5 ns delay time (A) and kinetic traces at 490 nm (B) and 700 nm (C) resulted from exciting the purpurin model (**Pur**), at wavelengths 577 or 698 nm in argon saturated methyl-THF.

CPur1 contains a carotenoid with 10 db attached to a *para*-aminophenyl group that forms an amide bond with the carboxylic group of the external ring of a purpurin, the E ring (Figure 1). The absorption spectra in three different solvents (benzonitrile, methyl-THF, and cyclohexane) are very similar (Figure 6). The purpurin has a Soret at 440 nm, and Q bands at 580, 640, and 700 nm. The carotenoid moiety of **CPur1** has additional absorption bands at 475 and 505 nm in methyl-THF and cyclohexane, but they are shifted bathochromically to 490 and 515 nm in benzonitrile.

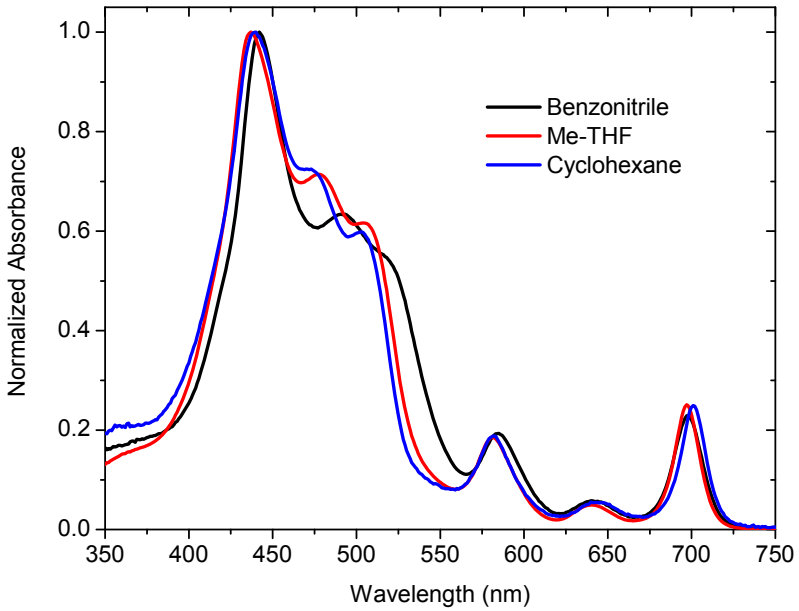

Figure 6. Amide carotenopurpurin (**CPur1**) absorption spectra in methyl-THF, cyclohexane, and benzonitrile.

Global analysis of the transient absorption data with excitation at 580 and 700 nm of **CPur1** in cyclohexane resulted in three EADS with 0.64, 4.41 and 128 μs decay lifetimes (Figure 7). The 4.41 μs EADS is characteristic to carotenoid triplet and shows a carotenoid photoinduced bleach centered around 465 nm and a T_1/T_n induce absorption centered at 540 nm[55a, 60]. The 0.64 μs EADS has a very similar spectrum to that of the 4.41 μs EADS and is interpreted as a relaxation of carotenoid triplet excited state. In addition, the long-lived purpurin triplet state from degraded dyads was observed and was responsible for the 128 μs EADS. The triplet energy transfer from the purpurin to the carotenoid is faster than the detection limit of the nanosecond flash photolysis instrument. Lastly, there is little to no bleaching of the purpurin Q_y band or influence of the purpurin on the carotenoid triplet spectrum on the dyad in cyclohexane (Figure 7, inset).

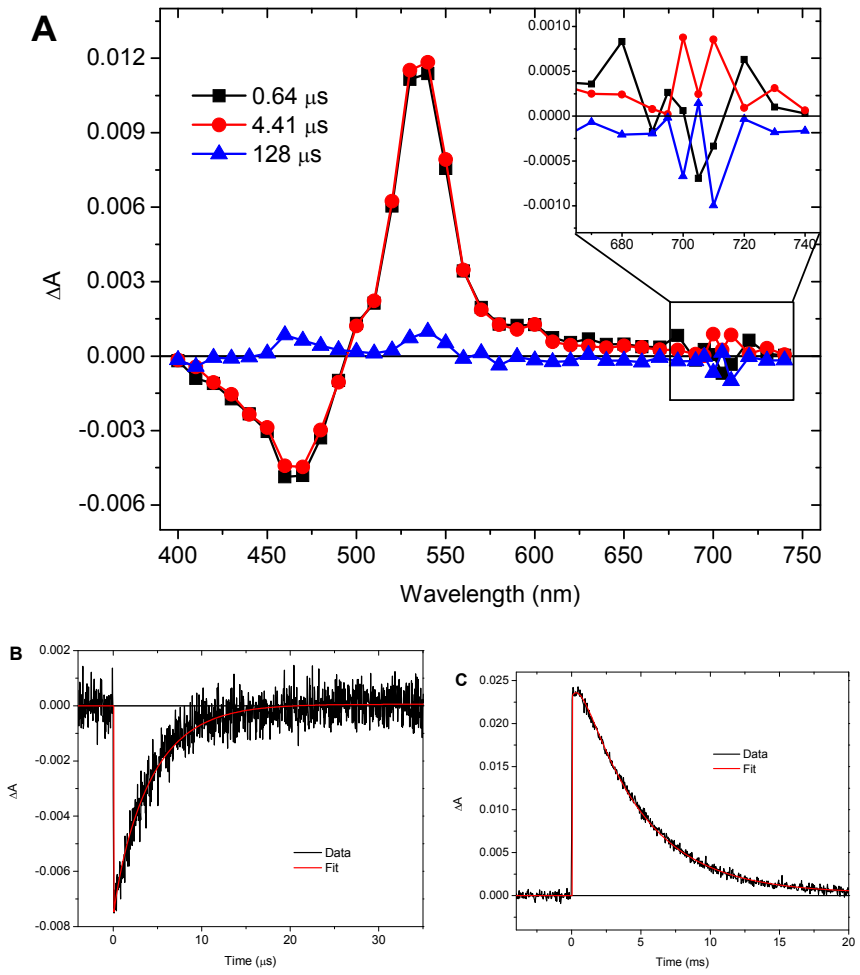

Figure 7. EADS (A) and kinetic traces at 450 nm (B) and 530 nm (C) resulted from exciting the amide carotenopurpurin, (**CPur1**), at 580 and 700 nm in argon saturated cyclohexane.

Transient absorption spectroscopy was performed on amide dyad **CPur1** in methyl-THF and resulted in three decay lifetimes (Figure 8). The 5.54 µs EADS corresponds to the carotenoid triplet spectrum and shows a photoinduced bleach at 460 nm and triplet induced absorption around 540 nm. In addition, there are ground state bleach bands at 440 nm and 700 nm due to the purpurin Soret and Q_y band transitions, respectively, which decay at the same time as the carotenoid triplet. The non-relaxed carotenoid triplet intermediate state was measured to decay in 0.648 µs and a long 1000 µs lifetime decay was assigned to the purpurin triplet from dyads with degraded carotenoids.

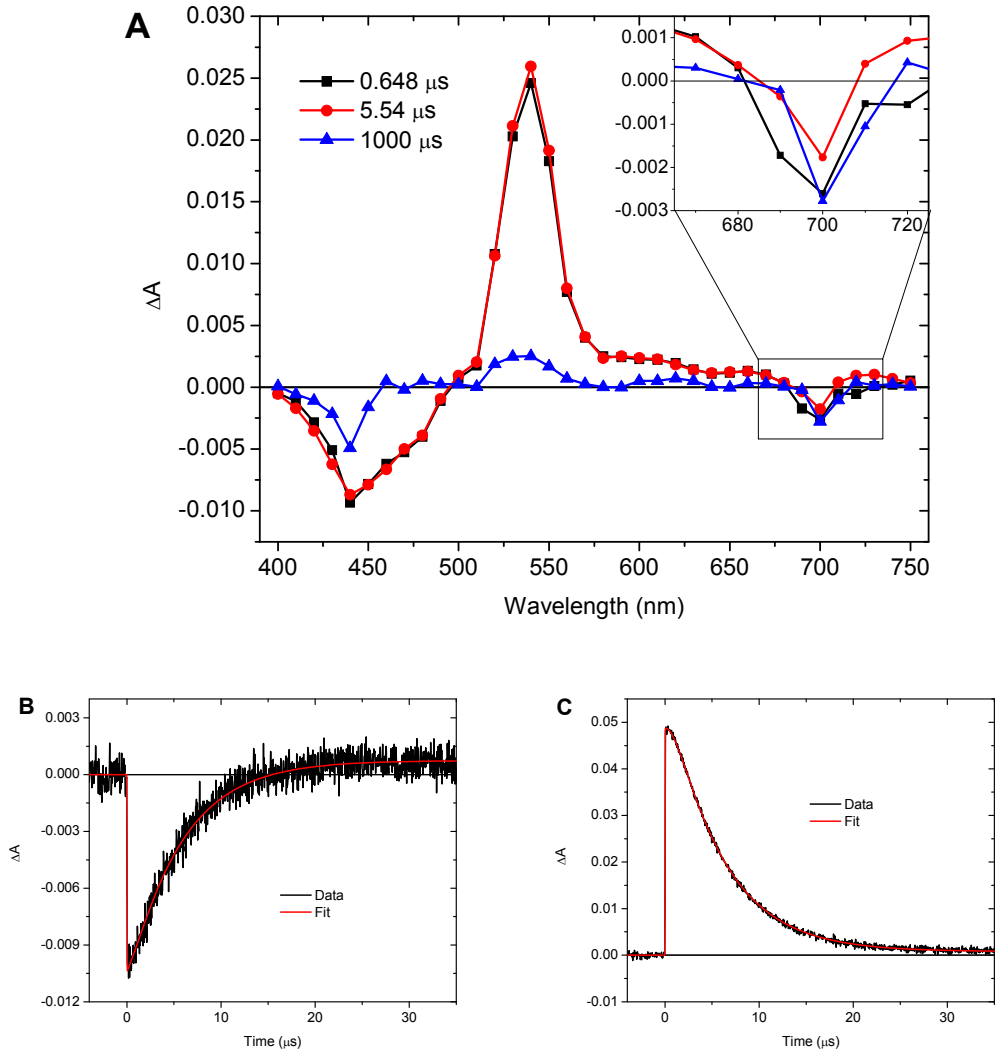

Figure 8. EADS (A) and kinetic traces at 470 nm (B) and 540 nm (C) resulted from exciting the amide carotenopurpurin (**CPur1**) at 580 and 700 nm in argon saturated methyl-THF.

Transient absorption spectroscopy was also carried out on the amide carotenopurpurin **CPur1** in benzonitrile, which resulted in three decay components (Figure 9). The first 0.648 µs EADS is due to the relaxation of carotenoid triplet excited state with relatively large purpurin bleach contributions at 440 and 695 nm. The second 5.54 µs EADS corresponds to the carotenoid triplet; it has the characteristic ground state bleach centered at 475 nm and induced T_1/T_n absorption around 550 nm, with the addition of the purpurin Soret at 440 nm, and Q_y band bleach at 700 nm. It is interesting that the Q band

is red shifted and less intense in the relaxed carotenoid triplet state than in non-relaxed state. The 100 μs EADS lifetime has transitions similar to that of the purpurin triplet (Figure 5A), with some carotenoid absorption, and is possibly due to degraded dyads. It is clear that there is a larger contribution of the purpurin on the carotenoid triplet state in benzonitrile than in methyl-THF and cyclohexane.

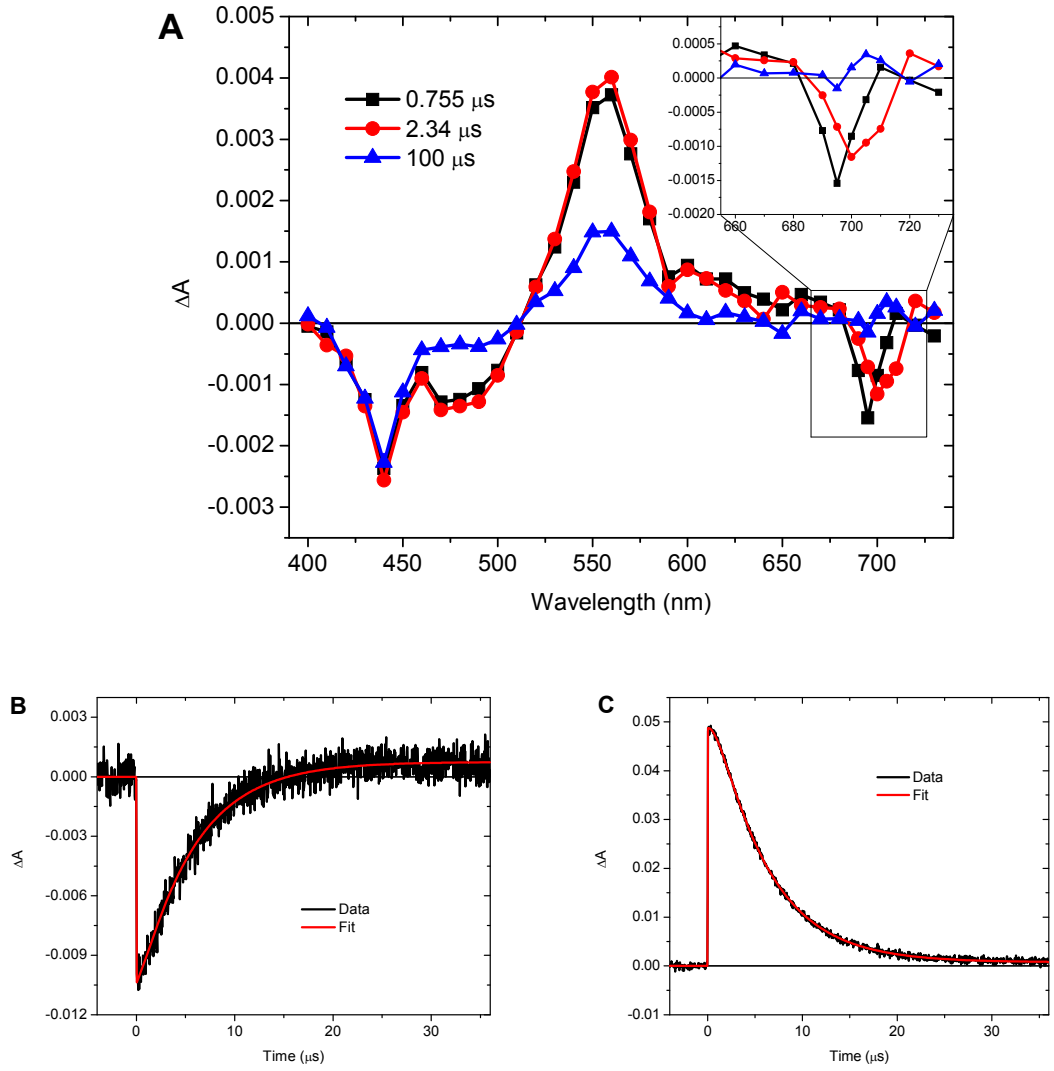

Figure 9. EADS (A) and kinetic traces made at 470 nm (B) and 540 nm (C) resulted from exciting the amide carotenopurpurin, **CPur1,** at 584 and 700 nm in argon saturated benzonitrile.

The ester carotenopurpurin, **CPur2**, is comprised of the same apo-carotenoid moiety with a phenyl ring at the proximal end, covalently attached to a methylene ester on the external ring of a purpurin. The purpurin is essentially the same as the purpurin in the amide dyad; the alkane chains and aromatic groups in the *beta* positions are intended to improve solubility while keeping the same absorption properties (Figure 10). The purpurin Soret and Q bands are around 435, 578, 646, and 700 nm, respectively. While in cyclohexane and methyl-THF the carotenoid transitions are around 468 and 500 nm, they shift to 480 and 512 nm in benzonitrile.

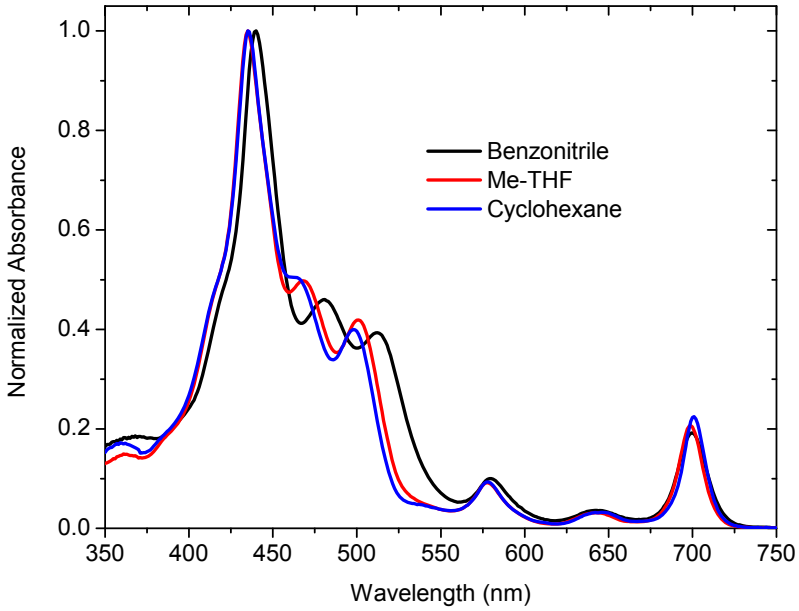

Figure 10. Normalized absorption spectra of the ester carotenopurpurin (**CPur2**) in methyl-THF, cyclohexane, and benzonitrile.

In this case the triplet energy transfer process was detected because the carotenoid and purpurin moieties are less-coupled (Figure 11). The first 51 ns EADS corresponds to that of the purpurin triplet with the Soret bleach at 440 nm and the Q_y band bleach at 700 nm. The purpurin triplet decays in 51 ns to form the carotenoid triplet. There are two EADS which correspond to the carotenoid triplet excited state: the non-relaxed triplet excited state

which relaxes in 0.71 μs and the relaxed carotenoid triplet which decays in 3.51 μs. The last 16.2 μs EADS most likely corresponds to the purpurin triplet from degraded dyads. There is minimal influence of the purpurin on the carotenoid triplet state.

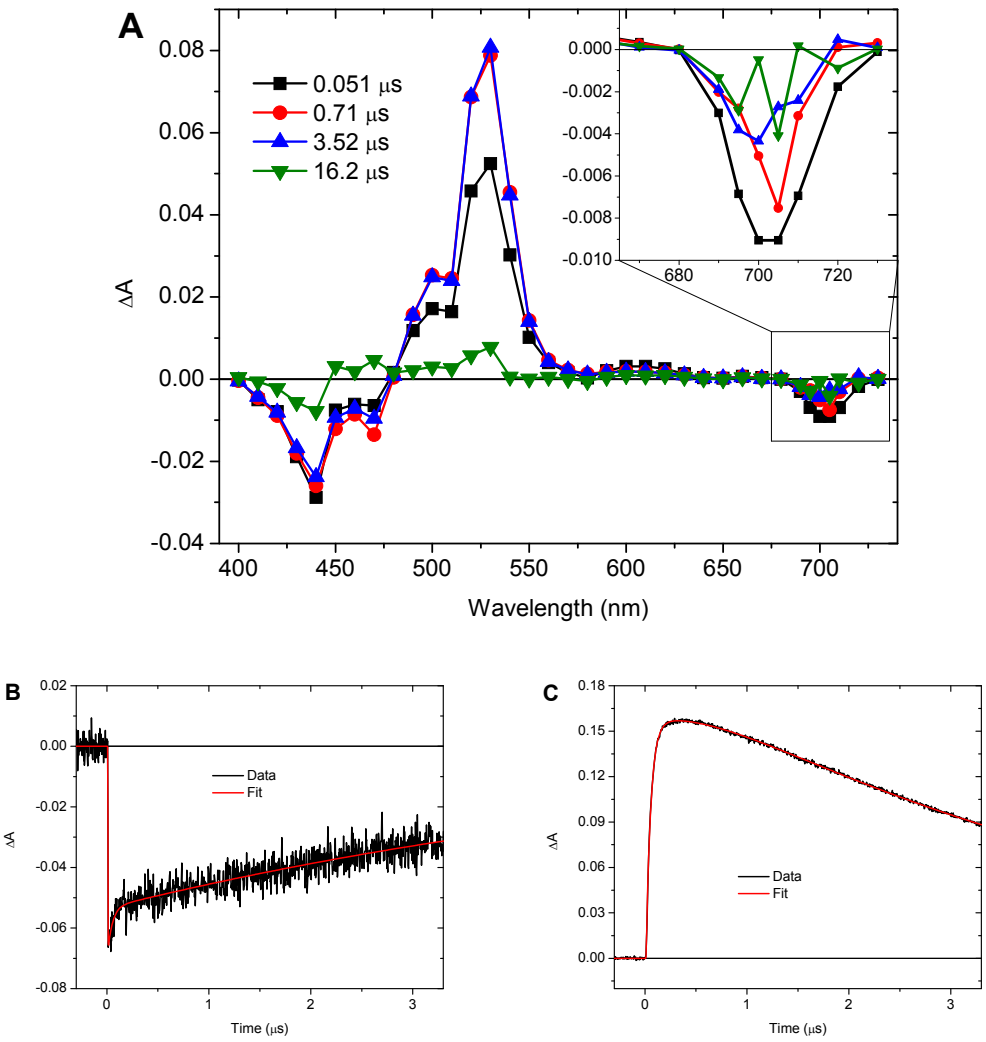

Figure 11. EADS (A) and kinetic traces at 440 nm (B) and 530 nm (C) resulted from exciting the ester carotenopurpurin, **CPur2,** at 578 and 700 nm in argon saturated cyclohexane.

Figure 12 shows four EADS resulting from the carotenopurpurin ester dyad (**CPur2**) in methyl-THF. The 42 ns EADS matches that of the purpurin with a Soret and Q_y band photoinduced bleach (inset). The 0.91 μs EADS is similar to that of the major 5.8

μs EADS, both have a photoinduced bleach around 450 nm and T_1/T_n absorption at 540 nm, but there is less purpurin Q_y band bleaching in the relaxed carotenoid triplet than in the non-relaxed. The non-decaying EADS is due to the purpurin triplet resulting from carotenoid degradation in the dyad. The EADS in cyclohexane and methyl-THF are very similar.

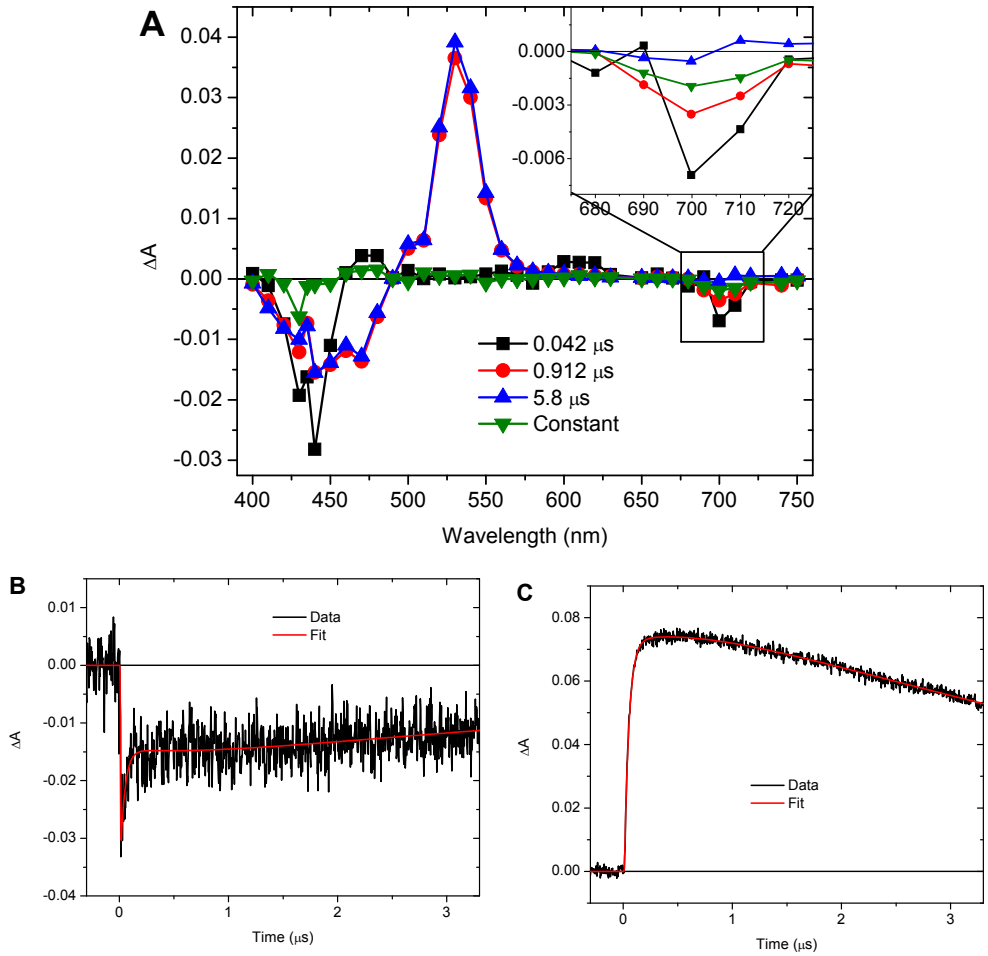

Figure 12. EADS (A) and kinetic traces made at 435 nm (B) and 530 nm (C) resulted from exciting the ester carotenopurpurin, **CPur2,** at wavelengths 580 and 700 nm in nitrogen bubbled methyl-THF.

In benzonitrile, the triplet-triplet energy transfer was measured to be 34 ns (Figure 13). The purpurin triplet decays and the carotenoid triplet rises simultaneously. The non-relaxed carotenoid triplet state and relaxed triplet state shows similar spectral features as

before, including a decrease in the Q_y band bleach as the triplet state relaxes (Figure 13, inset). The 80.6 µs EADS corresponds to the purpurin triplet from detached or degraded dyads. The resulting EADS in benzonitrile has similar lifetimes and similar spectral features as those in the less polar solvents measured.

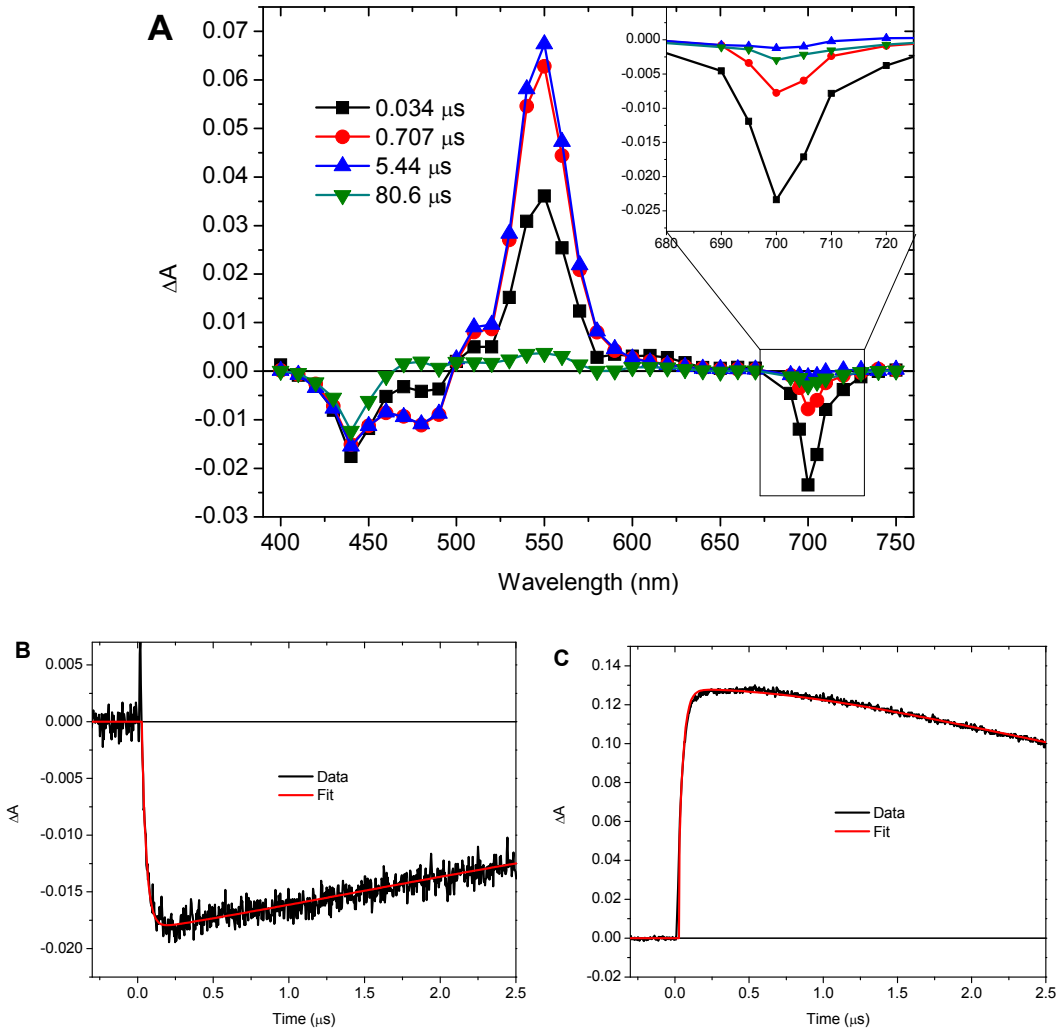

Figure 13. EADS (A) and kinetic traces at 490 nm (B) and 550 nm (C) resulted from exciting the amide carotenopurpurin, **CPur1,** at 700 nm in argon saturated benzonitrile.

Carotenoporphyrin model and dyads. The porphyrin model **Por** absorption spectrum has a Soret at 419 nm and four Q bands, at 516, 552, 591, and 647 nm (Figure 14). **Por** is the synthetic precursor for **CPor4**, but it is spectroscopically the same as the porphyrin used to make **CPor3**; the position of the methyl ester on the benzene ring relative to the porphyrin *meso*-position does not change the absorption properties of the tetrapyrrole. The Soret and Q band transitions of both carotenoporphyrin dyads, **CPor3** and **CPor4**, occur at the same wavelengths as the model porphyrin.

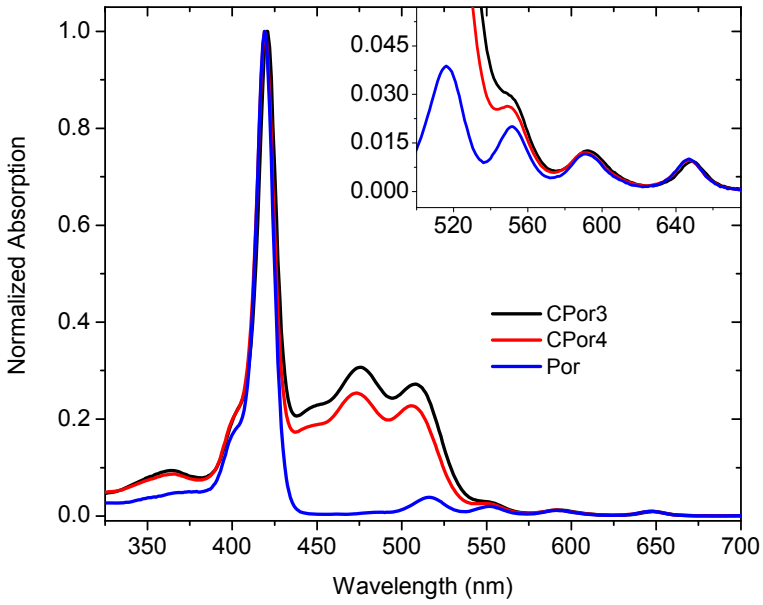

Figure 14. Ortho-Carotenoporphyrin (**CPor3**) *para*-carotenoporphyrin (**CPor4)** and model porphyrin (**Por**) absorption spectra in methyl-THF.

The porphyrin triplet decays in 172 μs (Figure 15). Similar to the purpurin triplet spectrum there is a photoinduced absorption between 440 and 620 nm, and ground state bleaching from the Soret and Q bands.

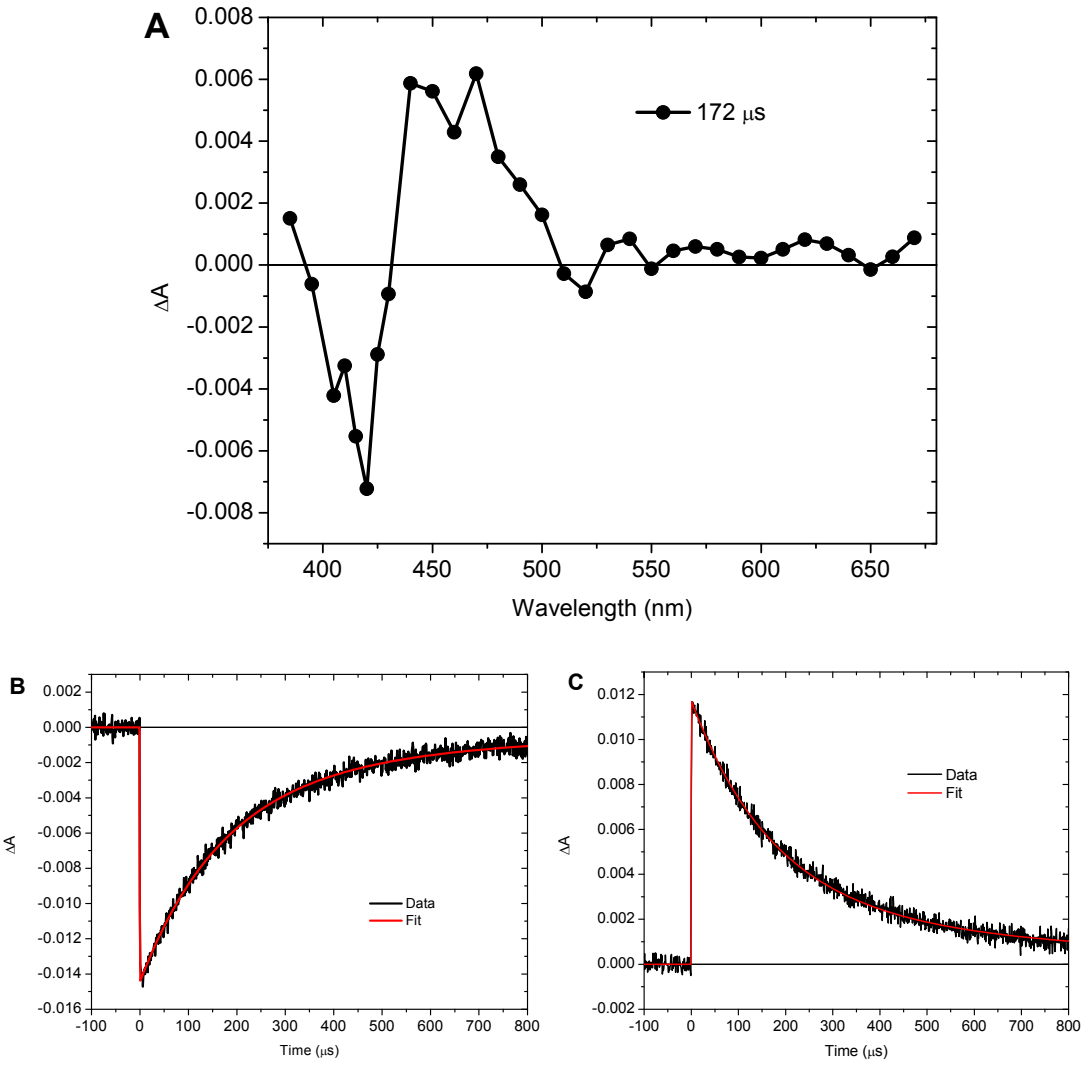

Figure 15. Transient absorption at 5 ns delay time (A) and kinetic traces made at 420 nm (B) and 440 nm (C) resulted from exciting the porphyrin model, **Por,** at 514, 592, and 648 nm in nitrogen saturated methyl-THF.

The *ortho*-carotenoporphyrin, **CPor3**, consists of a 10 double bond containing apo-carotenoid with a terminal phenyl group attached through a methylene ester to the *ortho* position on an aryl group positioned on the *meso* position of a tri-tolyl free base porphyrin. Its absorption spectrum in cyclohexane and methyl-THF has a Soret at 420 nm, Q bands at 550, 594, and 650 nm, and carotenoid transitions at 470 and 505 nm (Figure 16). The *ortho*-carotenoporphyrin dyad in benzonitrile has a slightly red-shifted absorption spectrum: the

Soret is at 424 nm, the Q transitions are same (Figure 16, inset), but the carotenoid transitions occur at 483 and 516 nm.

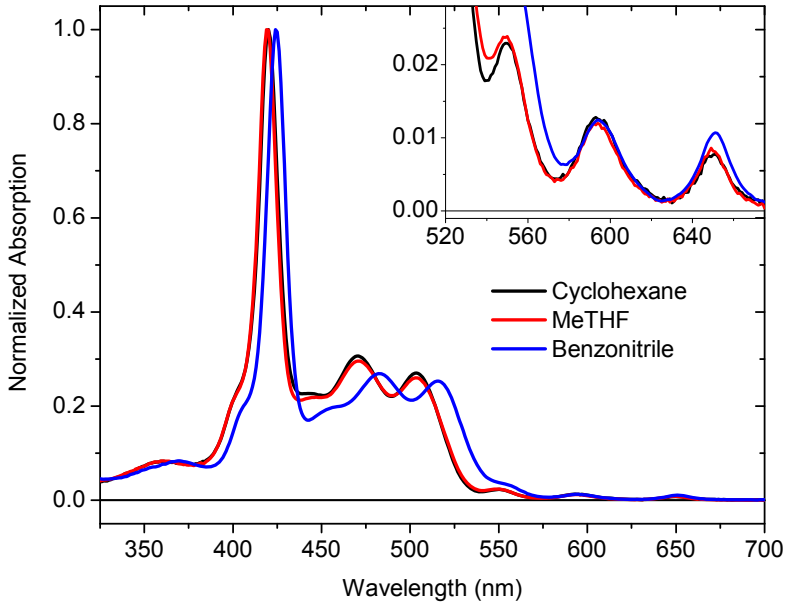

Figure 16. Ortho-Carotenoporphyrin, **CPor3**, absorption spectra in methyl-THF, cyclohexane, and benzonitrile.

Global analysis of transient absorption data of *ortho*-carotenoporphyrin **CPor3** shows two decay lifetimes in cyclohexane (Figure 17). The 4.84 μs EADS shows a porphyrin photoinduced bleach around 420 nm, a carotenoid ground state bleach centered at 470 nm, and a photoinduced absorption at 530 nm. The 25 μs EADS corresponds to the degraded dyad.

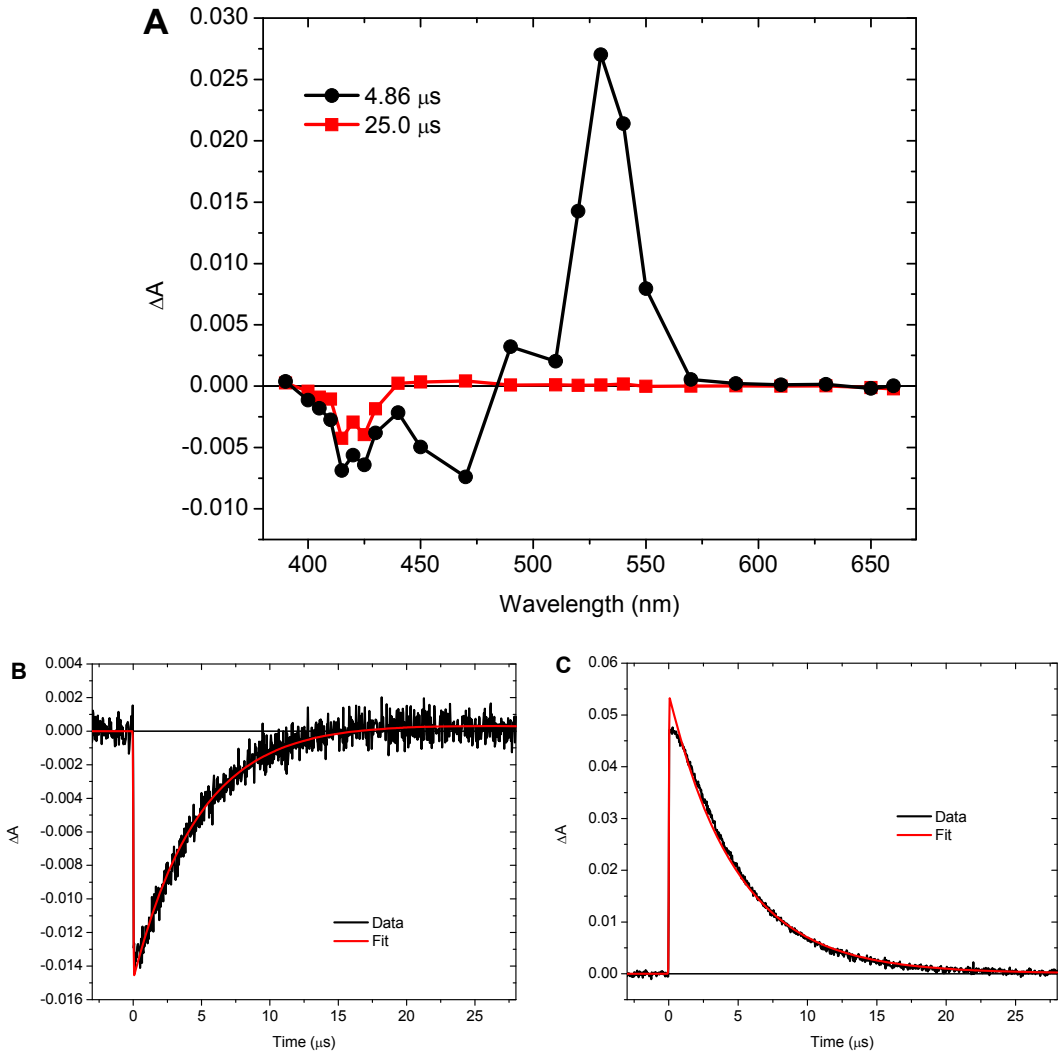

Figure 17. EADS (A) and kinetic traces at 470 nm (B) and 530 nm (C) resulted from exciting the o*rtho*-carotenoporphyrin (**CPor3**) at 415 nm in argon saturated cyclohexane.

Upon excitation of the *ortho*-carotenoporphyrin (**CPor3**) in methyl-THF a similar EADS result (Figure 18). The 6.11 μs EADS shows both carotenoid (ground state bleach and T_1/T_n absorption) and porphyrin characteristics (Soret ground state bleach at 425 nm). However, the porphyrin triplet feature here has relatively larger intensity than that measured in cyclohexane. This carotenoid triplet decay is followed by a long lived porphyrin triplet from the degraded dyad.

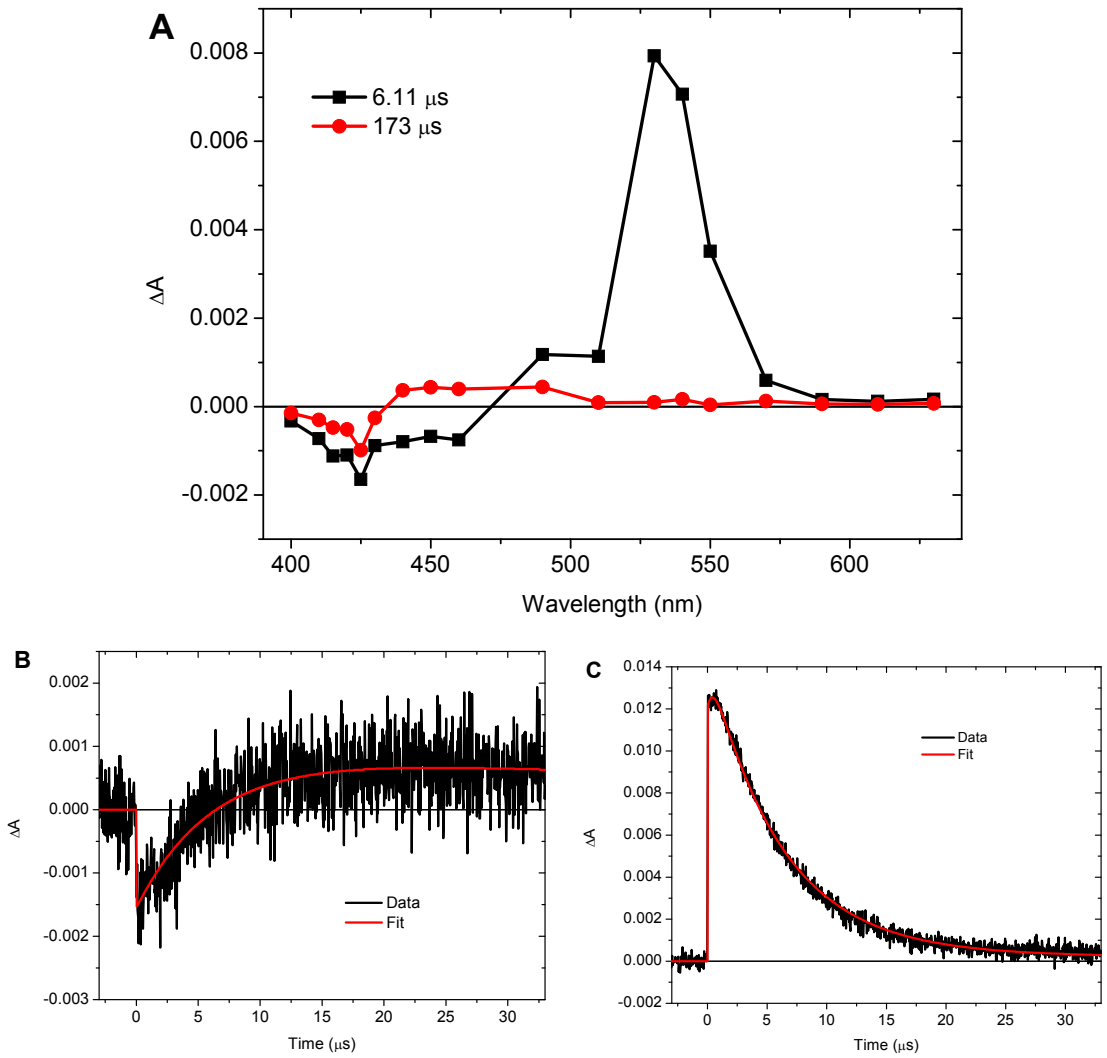

Figure 18. EADS (A) and kinetic traces measured at 460 nm (B) and 540 nm (C) resulted from exciting the *ortho*-carotenoporphyrin (**CPor3**) at 413 and 515 nm in argon saturated methyl-THF.

A large porphyrin Soret ground state bleach is evident in the EADS corresponding to the carotenoid triplet when the *ortho*-carotenoporphyrin (**CPor3**) was measured in benzonitrile (Figure 19). The carotenoid triplet decays in 5.36 μs, and during this lifetime there is an intense porphyrin Soret ground state bleach at 425 nm, a carotenoid induced bleach (460 nm), and a T_1/T_n absorption (540 nm). There is a long-lived porphyrin triplet that lasts 228 μs due to dyad decomposition as well.

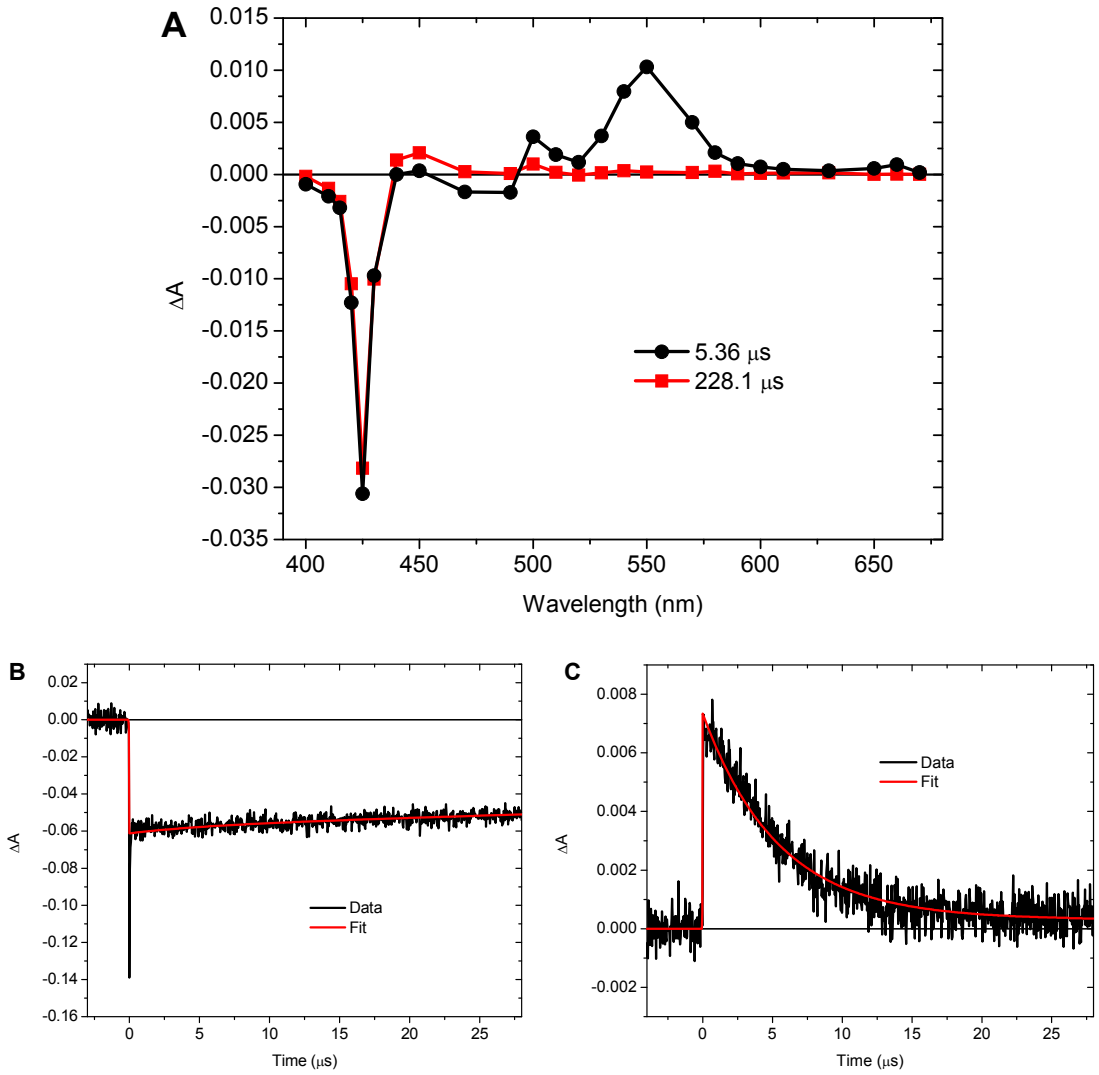

Figure 19. EADS (A) and kinetic traces measured at 425 nm (B) and 530 nm (C) resulted from exciting the *ortho*-carotenoporphyrin, **CPor3,** at 428 or 433 nm in argon saturated benzonitrile.

The *para*-carotenoporphyrin, **CPor4**, contains the same apo-carotenoid, methylene ester linkage, and tri-tolyl porphyrin, however the methylene ester linkage is positioned on the *para* position to the porphyrin. Its absorption spectrum is very similar to that of the *ortho*-carotenoporphyrin (Figure 14), and the spectrum has a bathochromic shift in benzonitrile (Figure 20). In cyclohexane and methyl-THF the porphyrin moiety absorbs at 418, 548, 594, and 648 nm, while the carotenoid absorbs at 467 and 499 nm. In benzonitrile,

the porphyrin Soret transition is centered at 424 nm, while the Q bands are centered at 593 and 649 nm, and the carotenoid transitions occur at 483 and 515 nm.

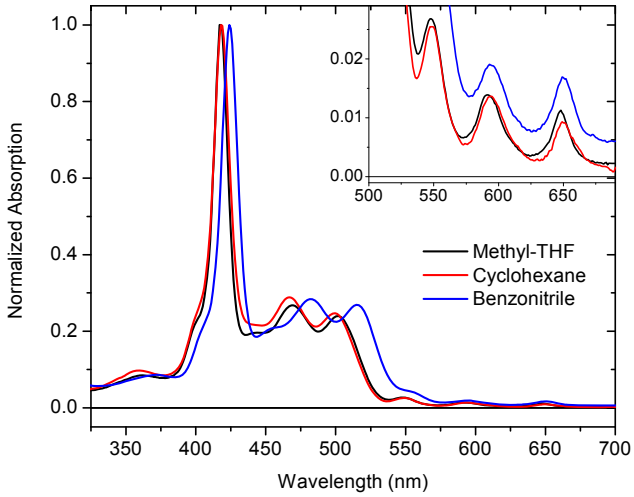

Figure 20. Para-carotenoporphyrin (**CPor4**) absorption spectra in methyl-THF, cyclohexane, and benzonitrile.

When **CPor4** is in cyclohexane, two decay lifetimes were measured for the *para*-carotenoporphyrin (Figure 21). The first 3.47 µs EADS corresponds to the porphyrin triplet and shows a Soret bleach at 420 nm. As the porphyrin triplet decays, the carotenoid triplet develops due to the triplet-triplet energy transfer between the two chromophores, which is well known[6d, 9, 45]. The carotenoid triplet decays in 4.18 µs, and its corresponding EADS has photoinduced ground state bleach at 450 nm and T_1/T_n absorption at 530 nm.

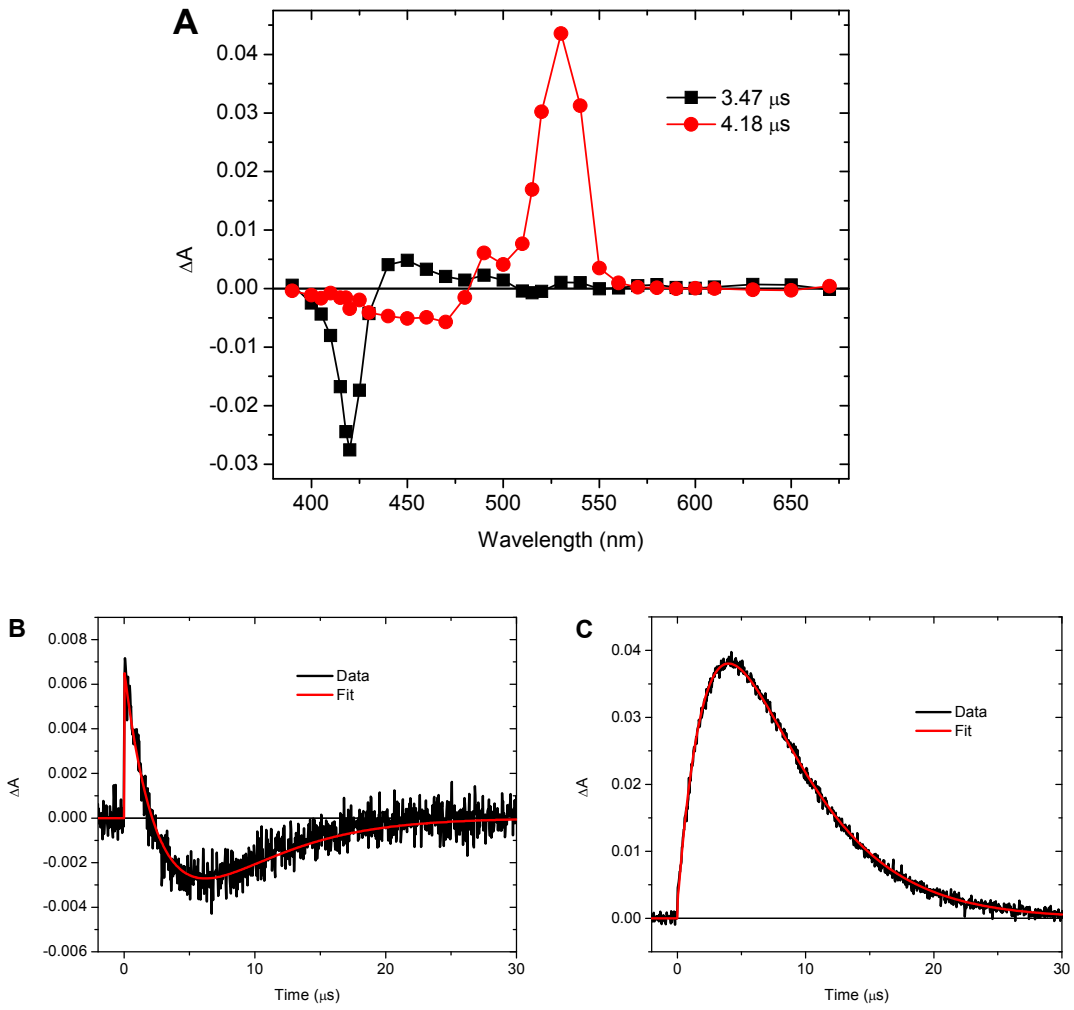

Figure 21. EADS (A) and kinetic traces measured at 460 nm (B) and 530 nm (C) resulted from exciting the *para*-carotenoporphyrin, **CPor4,** at 418 and 548 nm in argon saturated benzonitrile.

Upon 417 nm excitation, **CPor4** presents three decay lifetimes (Figure 22). A porphyrin triplet spectrum (first EADS) shows the Soret ground state bleach at 420 nm, and decays in 3.50 μs due to the triplet-triplet energy transfer. The carotenoid triplet spectrum does not have any major contributions from the porphyrin Soret during its 5.34 μs decay lifetime. The 5.34 μs EADS shows the same carotenoid photoinduced bleach and

T_1/T_n absorption as was observed for other carotenoporphyrin dyads. A 173 µs EADS results from unattached porphyrin or degraded dyads.

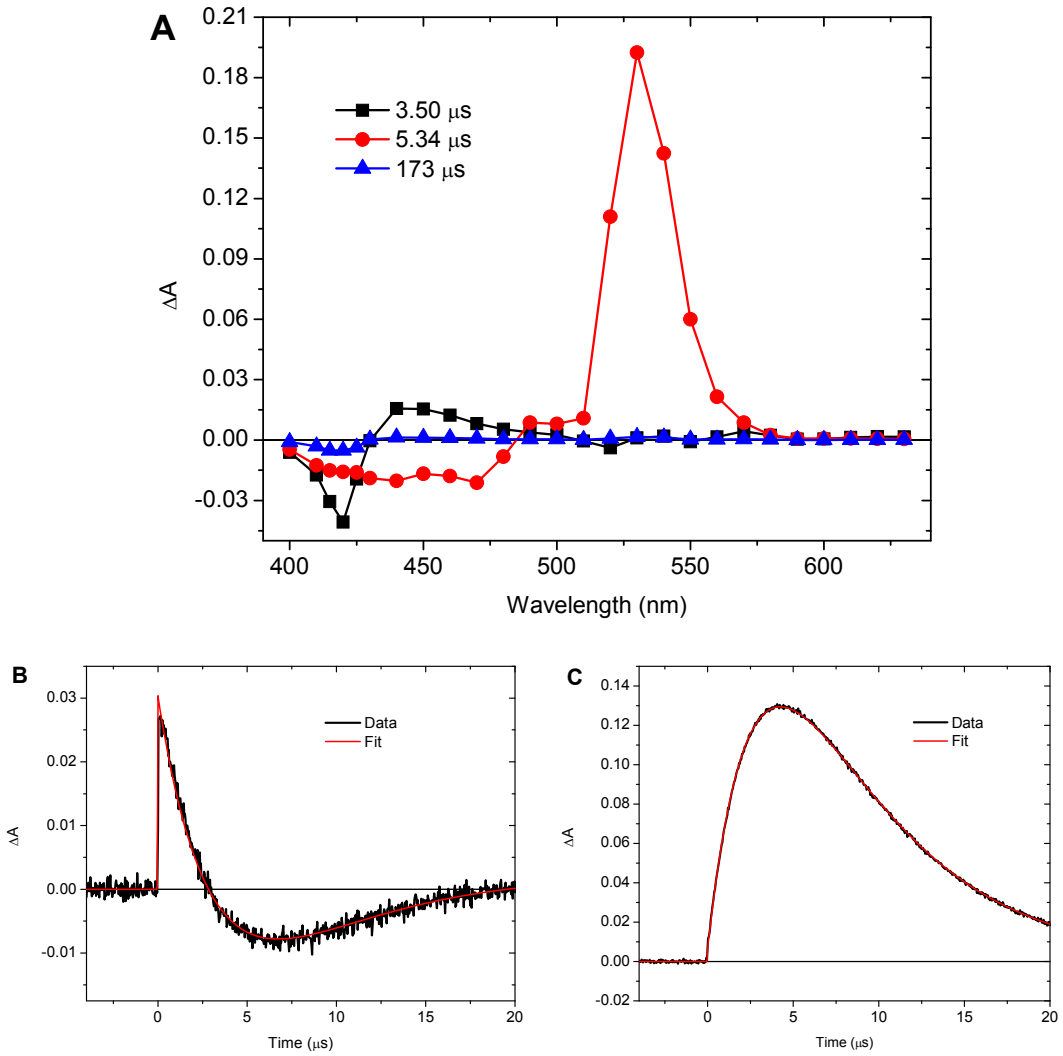

Figure 22. EADS (A) and kinetic traces measured at 450 nm (B) and 540 nm (C) resulted from exciting the *para*-carotenoporphyrin (**CPor4**) at 417 nm in argon saturated methyl-THF.

The *para*-carotenoporphyrin **CPor4** transient absorption measurements give three decay lifetimes in benzonitrile (Figure 23), much like those observed in methyl-THF. First 3.05 µs EADS corresponds to the porphyrin triplet spectrum, it has a large Soret ground state bleach at 425 nm due to the bathochromic shift of the absorption spectrum in the polar

solvent. The second 4.89 μs EADS corresponds to carotenoid triplet, which has minimal influence from the porphyrin in the Soret region. The last EADS is due to the decomposed dyad or unattached porphyrin which has a decay lifetime longer than the time scale of the measurement and is labeled as constant.

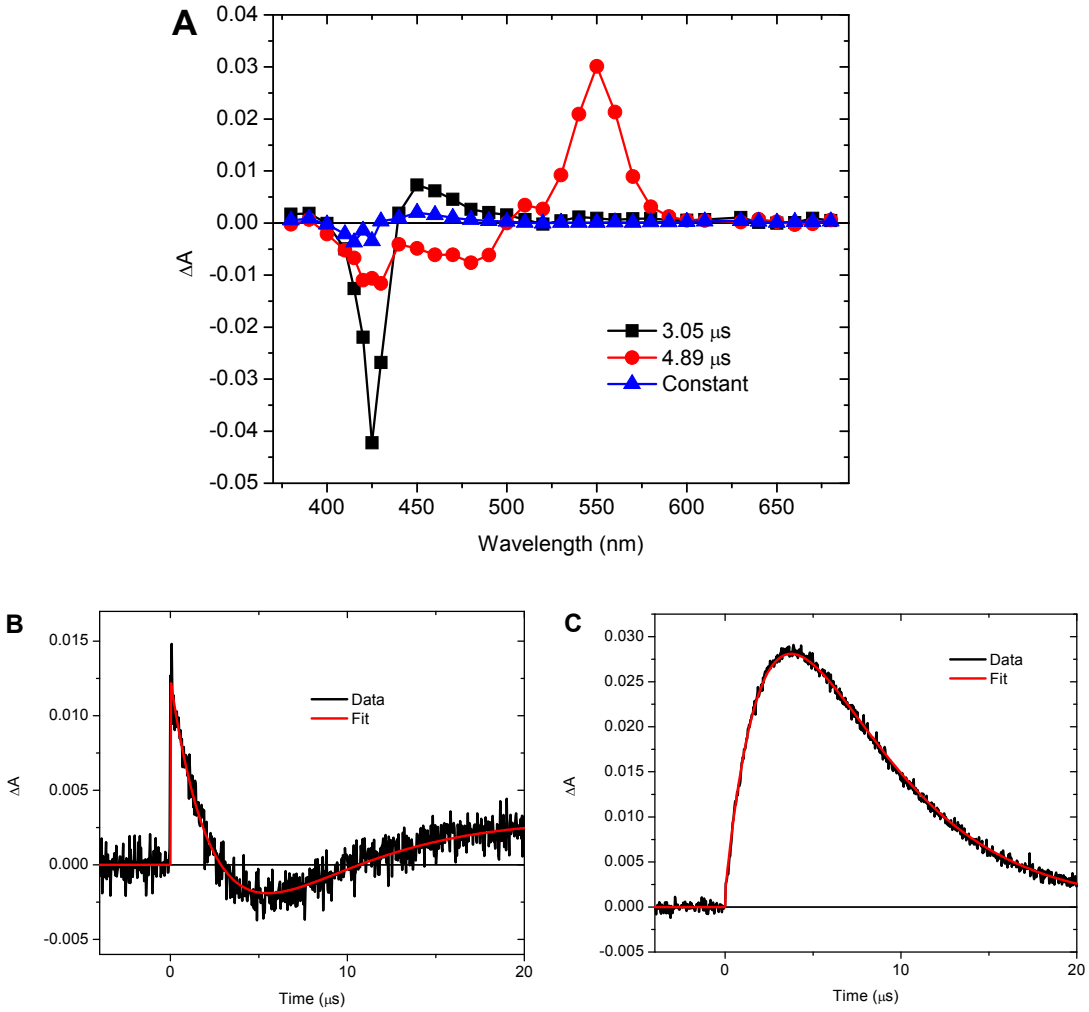

Figure 23. EADS (A) and kinetic traces measured at 460 nm (B) and 550 nm (C) resulted from exciting the *para*-carotenoporphyrin, **CPor4,** at 424 or 593 nm in argon saturated benzonitrile.

Carotenophthalocyanine model and dyads. Three carotenophthalocyanine dyads, **C9Pc**, **C10Pc**, and **C11Pc**, were analyzed for their degree of coupling which is

reflected in the carotenoid triplet state spectrum as was observed in other dyads. The absorption spectrum of the phthalocyanine model (**Pc**) and the carotenoid containing dyads are similar in that they both contain **Pc** features but the dyads also absorb light from the carotenoid moiety (Figure 24). In the **Pc**, the Soret transition occurs at 355 nm and it does not change in the dyads. The Q_x band has a slight bathochromic shift in the dyads and when the carotenoid length is increased; the phthalocyanine model Q_x band occurs at 676 nm, in the **C9Pc** dyad the Q_x band is at 678 nm, while the same Q_x band in **C10Pc** and **C11Pc** dyads occur at 680 nm. The same trend is observed at the Q_y absorption band, which maximally absorbs at 609 nm for the phthalocyanine model. As the carotenoid increases in conjugation length, it is expected that the carotenoid absorption red shift as the number of double bonds increase. The carotenoid maximum for the **C9Pc** dyad occurs at 449 nm, the **C10Pc** dyad at 473 nm, and at 483 nm for the **C11Pc** dyad.

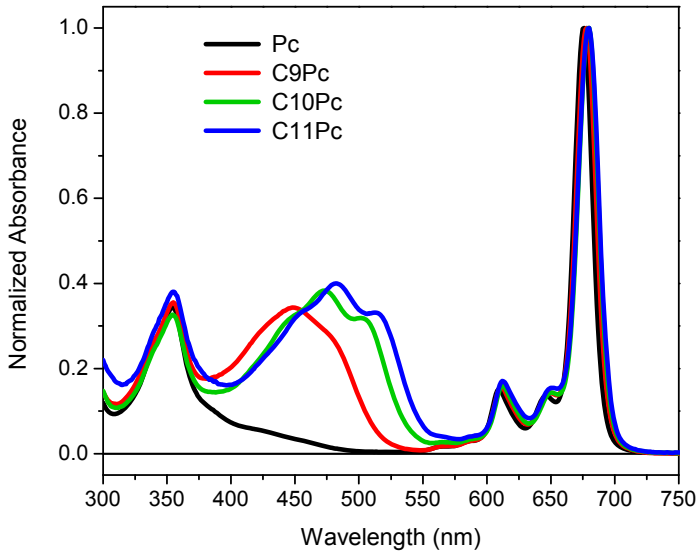

Figure 24. The normalized absorption spectra of the phthalocyanine model (**Pc**), and carotenophthalocyanine dyads (**C9Pc**, **C10Pc**, **C11Pc**) in methyl-THF.

The phthalocyanine model Pc triplet has a lifetime of 233 μs (Figure 25). Triplet spectrum has one main feature - the Q_x ground state bleach centered at 675 nm. In addition, there is some photoinduced absorption between 400 and 600 nm, and a Q_y bleach at 610 nm.

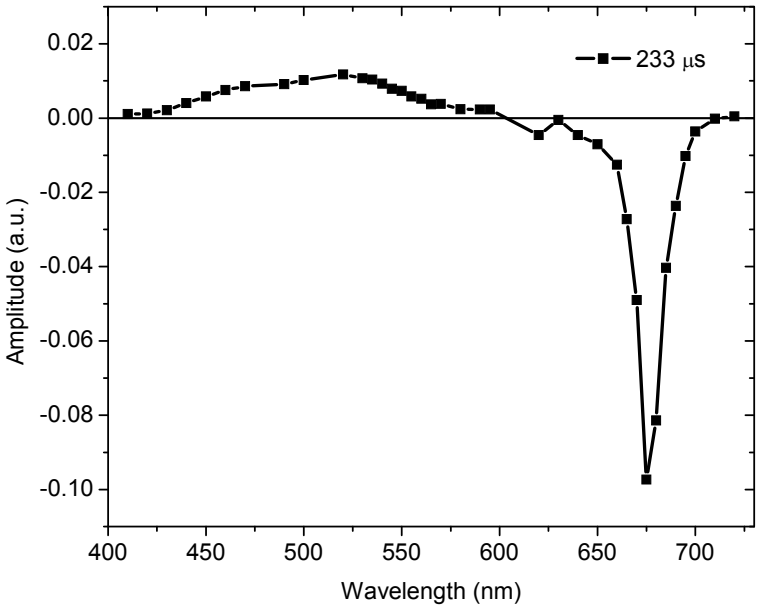

Figure 25. Transient absorption spectrum at 5 ns delay time after exciting the phthalocyanine model **Pc** with 610 nm laser pulse in argon saturated methyl-THF.

Transient absorption of each dyad showed one decay lifetime and the spectrum was assigned to the carotenoid-phthalocyanine coupled triplet state (Figure 26). The transient absorption spectra were normalized to the carotenoid photoinduced bleach between 430 and 530 nm in order to compare the degree of the phthalocyanine bleach. **C9Pc** has the longest triplet lifetime of 7.8 μs due to the shorter conjugation of the carotenoid and has the smallest phthalocyanine Q_x bleach. Both the **C10Pc** and **C11Pc** dyads have shorter triplet lifetimes and sequentially larger Q_x bleaches centered at 680 nm.

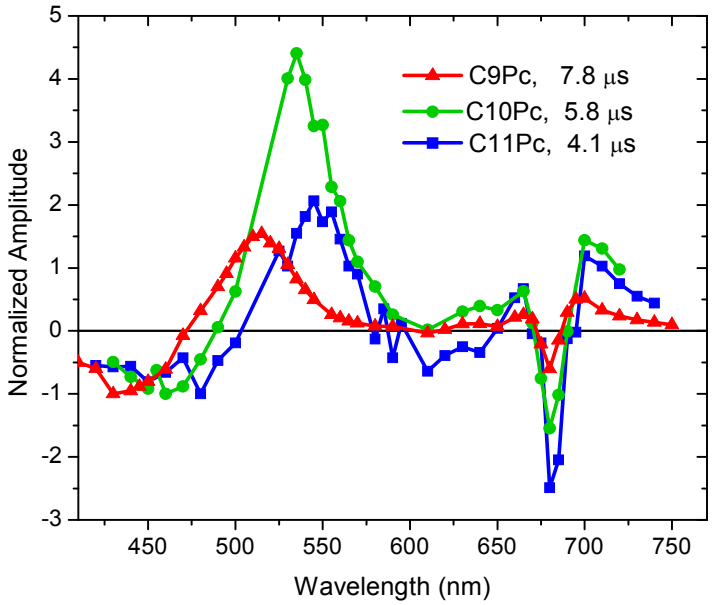

Figure 26. The normalized decay associated spectra (DAS) of the **C9Pc**, **C10Pc**, and **C11Pc** carotenoid triplet spectra in argon saturated methyl-THF.

Discussion

Amide vs. ester carotenopurpurin dyads. The amide carotenopurpurin **CPur1** was initially used to study singlet energy transfer from the S_2 and S_1 states of the carotenoid to the purpurin[9]. Based on previous experiments on dyads and triads the amide bond is known to allow for efficient energy transfer from very short lived singlet excited states[7]. This was the motivation for making an amide carotenopurpurin dyad. Our research group also rationalized that the partial conjugation through the amide bond allows electronic coupling between the two chromophores, but it also allowed them to keep their spectroscopic identities[7]. This is seen in the absorption spectrum (Figure 4) of the dyads which have the same Soret and Q band transitions as the model purpurin **Pur** that of the dyads.

The triplet energy transfer from the purpurin to carotenoid in the amide dyad **CPur1** was not observed because it is limited by the intersystem crossing rate of the purpurin. Our

research group observed the decay of the S_1 purpurin in 1.4 ps and the immediate rise of the carotenoid triplet state in 1.4 ps using femtosecond resolution by fluorescent upconversion and picosecond time scale transient absorption techniques[30]. Thus the triplet energy transfer is faster than the intersystem crossing process such that as soon as intersystem crossing occurs the energy is transferred to the carotenoid triplet state. This is an extremely effective photoprotective mechanism and an efficient method of preventing ROS formation.

Due to the narrow spectral range of the previous experiments, the purpurin transitions were not observed in the amide carotenopurpurin **CPur1** triplet transient. The transient absorption experiments performed here extended the spectral region to include the purpurin Q absorption. By expanding the spectral region, we were able to measure the carotenoid triplet spectra containing features characteristic to both carotenoid and purpurin, which supports the idea of a coupled triplet state. In this well-coupled dyad, the triplet state occupies orbitals that are in both moieties of the molecule (see Chapter 2). The charge in the excited state is not distributed evenly and can reside on one side of the dyad more than the other creating an ICT-like state, which is stabilized by polar environments. For example, polar solvents can lower the activation energy for absorption transitions such that the change in absorption measured increases in the transient absorption spectra[64]. When comparing the ratio between the carotenoid T_1/T_n induced absorption and the Q_y bleach of the purpurin for the amide dyad **CPur1**, this ratio increased with solvent polarity (Table 1).

Table 1. Numbers are from EADS assigned to the carotenoid triplet state and are calculated by dividing the ΔA of the purpurin Q_y bleach (700 nm) by the ΔA of carotenoid triplet absorption (540 or 550 nm).

SOLVENT	AMIDE DYAD **CPUR1**	ESTER DYAD **CPUR2**
Benzonitrile	0.41	0.02
Methyl-THF	0.07	0.01
Cyclohexane	0.00	0.05

Conversely, the ester carotenopurpurin **CPur2** was designed with the expectation for a slow energy transfer due to the insulating methylene ester group. For all three solvents, the purpurin triplet spectrum decay and concomitant rise of the carotenoid triplet was measured and determined to be the triplet energy transfer rate. The methylene-ester bond does not provide strong enough coupling to cause the coupled triplet state between two chromophores therefore there are minimal perturbations of the carotenoid triplet spectrum by the purpurin Soret and Q_y band transitions; the carotenoid and purpurin have two distinct triplet states in this dyad. The ratio between the carotenoid triplet absorption and the purpurin Q_y band bleach in the carotenoid triplet state (Table 1) essentially does not change with increasing solvent polarity. This demonstrates that there is a no triplet delocalization in **CPur2** even though the methylene ester group brings the purpurin and carotenoid within a good distance to transfer triplet energy through space.

These dyads mimic photoprotective triplet energy transfer in natural photosynthetic systems. The amide carotenopurpurin **CPur1** mimics the triplet energy transfer in LHCII from green plants, which is ultrafast and limited by intersystem crossing process[46]. This ultrafast triplet energy transfer is beneficial for aerobic systems to reduce the formation of ROS. For anaerobic systems, like that in purple photosynthetic bacteria, there is a lower concentration of oxygen which reduces the urgency or evolutionary advantage of

performing an ultrafast triplet energy transfer. Purple photosynthetic bacteria perform triplet energy transfer between their bacteriochlorophyll and carotenoid molecules in the nanosecond time scale[54], which is similar to the triplet energy transfer kinetics measured for the ester carotenopurpurin, **CPur2**.

***Ortho*- vs. *para*-carotenoporphyrin dyads.** These molecules were studied for their triplet-triplet energy transfer properties previously by our research group[6d, 45]. It was found that the *ortho*-carotenoporphyrin **CPor3** has a folded conformation which situates the two chromophores ~4 Å apart and allows π-π interactions for favorable energy transfer. The *para*- isomer **CPor4** is spatially separated and has less favorable interactions, which results in triplet energy transfers in the microsecond time scale[6d, 45]. Similar transient absorption studies were performed here on the same carotenoporphyrins and its model porphyrin. The porphyrin triplet state was measured from the porphyrin model (Figure 5A) and its spectrum was used to identify the porphyrin triplet that precedes the carotenoid triplet formation in the *para*-carotenoporphyrin **CPor4**. Triplet energy transfer rates from the porphyrin to the carotenoid between 3.05 and 3.50 μs were measured, which is longer than that observed by Bensasson *et al*.[45] in deoxygenated benzene (1.5 μs). The *para*-carotenoporphyrin **CPor4** has a flexible methylene group resulting in conformations that allow the π systems of the carotenoid and porphyrin to interact in limited ways[6d]. Due to the folded conformation of the *ortho*-dyad **CPor3**, porphyrin triplet state and triplet energy transfer was faster than the detection limit of the transient absorption equipment used and was not observed in cyclohexane, methyl-THF, or benzonitrile.

The porphyrin Soret ground state bleach during the carotenoid triplet spectrum is a phenomenon that was not previously observed due to the narrow spectral window used[6d].

The *ortho*-carotenoporphyrin **CPor3** has a photoinduced bleach that corresponds to the Soret ground state bleach transition that decays during the same lifetime as the carotenoid triplet. This phenomenon was measured in carotenophthalocyanine[30] and carotenopurpurin **CPur1** dyads as well, and provides evidence for electronic coupling in the triplet state. If there is sufficient electronic coupling between the carotenoid and porphyrin in the *ortho*-dyad **CPor3**, then their spectra should have contributions from both moieties (see Chapter 2). This is in fact what was observed in three different solvents (Figures 13, 14, and 15).

A molecular complex shows ICT character when one region of the complex has a partial positive charge and another region has a partial negative charge. The energy of this ICT state can be lowered and the absorption transitions made more favorable in solvents with high dielectric constants[64]. The stabilization of this ICT state across the coupled dyad increases the perturbation of the carotenoid triplet by the porphyrin and shows up as an increase in the relative intensity of porphyrin spectral signatures, for example the Soret bleach, in the carotenoid triplet spectrum of the dyad. Table 2 compares the relative change in absorption for each carotenoporphyrin dyad; the ratio between the porphyrin Soret bleach and the T_1/T_n transition of the carotenoid triplet, assuming that the carotenoid triplet is equivalent in all dyads since they contain the same carotenoid. The *ortho*-carotenoporphyrin (**CPor3**) has a larger Soret bleach to carotenoid triplet absorption ratio than the *para*-dyad (**CPor4**) in all the solvents due to the close contact between two chromophores. In methyl-THF and cyclohexane the ratio is the same for **CPor4**, and it increases four-fold in benzonitrile. This could be due to the flexible nature of the methylene group which could allow shorter through space contact and therefore stronger coupling between the carotenoid and the porphyrin in this solvent. Thus when the dyad is in

benzonitrile this coupled complex is stabilized and has a larger Soret photoinduced bleach. The *ortho*-carotenoporphyrin (**CPor3**) also has an increase in the porphyrin Soret bleach and carotenoid T_1/T_n transition ratio, and it is ten-fold higher in benzonitrile than in cyclohexane and methyl-THF (Table 2). The dramatic increase in the porphyrin Soret reflects the fact that the dyad is extremely coupled and that the ICT state is favorable.

Table 2. Numbers are from the EADS associated with the carotenoid triplet and are calculated by dividing the ΔA of the porphyrin Soret bleach (420 or 425 nm) by the ΔA of carotenoid triplet absorption (530 or 550 nm).

SOLVENT	*ORTHO* DYAD **CPOR3**	*PARA* DYAD **CPOR4**
Benzonitrile	2.97	0.35
Methyl-THF	0.21	0.08
Cyclohexane	0.23	0.08

The differences in the proximity of the carotenoid and the porphyrin macrocycle in the carotenoporphyrins are similar to the charge transfer state measured by Stark fluorescence spectroscopy on LHCII trimers and trimer aggregates[69]. In the presence of an external magnetic field the aggregated LHCII trimer protein complexes had a shift in their Stark fluorescence, which indicates a large dipole or charge transfer state. It was proposed that a carotenoid-chlorophyll exciton was formed in the aggregated protein complexes, possibly due to closer proximity of the two molecules. By bringing a carotenoid within the π-system of a tetrapyrrole may lead to a Dexter type electron exchange and facilitate the formation of such charge transfer in the form of an ICT state in the *ortho*-dyad.

Carotenophthalocyanine dyads. It is well known that when a molecule extends its conjugated system the absorption spectrum red shifts and the energy gap between the frontier molecular orbitals decreases. This is evident by the bathochromic, or red shift, of the carotenoid moiety between 400 and 530 nm in Figure 24. In addition, the lifetimes of

the carotenoid excited state decreases with the increase of its conjugation length[4a]. The **C9Pc** dyad has a carotenoid triplet lifetime of 7.8 μs, while the **C11Pc** dyad has the shortest (4.1 μs) lifetime for the triplet carotenoid (Figure 26).

The phthalocyanine absorbance is moderately affected by the attachment of the carotenoid to the periphery of the macrocycle. When comparing the model compound to the carotenoid dyads there is a slight bathochromic shift in both the Q_x and Q_y bands. Adding the 9 db carotenoid shifts the Q_x and Q_y bands 2 nm, and the 10 and 11 db carotenoids the Q bands shifts 4 nm with respect to the phthalocyanine model. These slight shifts are due to the amide bond attached to the macrocycle of the phthalocyanine, which partially extends the conjugation into the carotenoid due to the partially conjugated nature of the amide bonds.

Our research group previously observed that the carotenoid and phthalocyanine moiety have coupled states by using ultrafast spectroscopic measurements[14, 30]. Similar couplings were measured using vibrational spectroscopic techniques in Chapter 2, however, only shorter carotenoids with 9 or 10 db were investigated with different tetrapyrroles and covalent linkers making it difficult to correlate the length to their coupling abilities. The length of a carotenoid has been shown to be effective for photoregulation in natural[48b] and artificial systems[14, 30]. More specifically, there was an increased coupling between the carotenoid S_1 and ICT state, which lead to the formation of an S_1/ICT state, in the carotenophthalocyanine with the longest carotenoid **C11Pc**. In addition, this coupled state was confirmed to be an ICT state instead of a complete charge transfer state because the carotenoid radical cation spectral signature was not observed in the near infrared region.

Figure 26 contains the carotenophthalocyanine triplet spectra which have features associated with the carotenoid triplet, ground state bleach around 450 nm and induced absorption around 530 nm, as well as the phthalocyanine Q_x ground state bleach centered at 680 nm. The spectra are normalized to the carotenoid photoinduced bleach due to the lack of phthalocyanine spectral features in this region and to allow a simple comparison between spectra. **C9Pc** has the smallest Q_x bleach, while the **C10Pc** and **C11Pc** have sequentially larger phthalocyanine Q_x bleaches. This trend was quantified in Table 3 by dividing the amplitude of the phthalocyanine bleach by the amplitude of carotenoid bleach for each dyad. This assumes that the carotenoid bleach is the same in all the dyads after the triplet energy transfer. As the length of the polyene extends the greater the phthalocyanine bleach transition occurs. This increased phthalocyanine Q_x perturbation in the carotenoid triplet spectrum provides evidence that the coupling between the two chromophores in the triplet state increases with carotenoid conjugation length. It would be interesting to see if there is an optimal carotenoid length for this carotenoid-phthalocyanine triplet state coupling or if this trend continues as the polyene length extends (see Appendix A).

Table 3. Numbers are calculated by dividing the ΔA of the Pc Q_x bleach (680 nm) by the ΔA of carotenoid triplet bleach (435 to 490 nm).

DYAD	CAROTENOID BLEACH/ PC Q_X BLEACH RATIO
C9Pc	0.60
C10Pc	1.54
C11Pc	2.49

Conclusions

Three sets of artificial photosynthetic dyads demonstrated different degrees of a carotenoid- tetrapyrrole triplet state coupling. The coupling strength depended on the length of the carotenoid and solvent polarity. The carotenopurpurin dyads provided examples of well-coupled (**CPur1**) and less-coupled (**CPur2**) systems using different covalent bonds to promote or deter electronic connectivity between the two components. For comparison, the carotenoporphyrin triplet energy transfer depended on their spatial separation. The *para*- isomer (**CPor4**) contained the same methylene ester linkage between the porphyrin and the carotenoid as the *ortho*- isomer (**CPor3**), however the isomeric position of attachment of the two chromophores and thus the distance across the connecting benzene ring prevent orbital interactions in **CPur4**. The carotenoid in the *ortho*-carotenoporphyrin (**CPor3**) is positioned closest to the porphyrin and has a folded conformation over the macrocycle of the porphyrin such that large H^1-NMR shifts due to the porphyrin ring current could be detected. In this case there is a through space electronic coupling similar to the through bond coupling due to partial conjugation through the amide bond of the amide carotenopurpurin (**CPur1**). Additional amide carotenophthalocyanine dyads (**C9Pc**, **C10Pc**, **C11Pc**) with different carotenoid lengths were compared to see how the length of the carotenoid affected the coupling in the triplet state between chromophores.

There are different types of carotenoids with different photophysical and photochemical properties useful for photoprotection. Each set of dyads also illustrates the different types of connections one can use to attach an apo-carotenoid to a tetrapyrrole or artificial reaction center to provide antenna and photoprotective properties. Carotenoids have an untapped potential for applications in solar cells.

CHAPTER 4

ULTRAFAST ENERGY TRANSFER AND EXCITED STATE COUPLING IN AN ARTIFICIAL PHOTOSYNTHETIC ANTENNA

Margherita. Maiuri[†,⊥], Joris J. Snellenburg[‡,⊥], Ivo H. M. van Stokkum[‡], Smitha. Pillai[§], Katherine WongCarter[§], Devens Gust[§], Thomas A. Moore[§], Ana L. Moore[§], Rienk van Grondelle[‡], Giulio Cerullo[†], Dario Polli[†]

[†]IFN-CNR, Dipartimento di Fisica, Politecnico di Milano, Piazza L. da Vinci, 32, 20133 Milano, Italy

[‡]Department of Physics and Astronomy, VU University Amsterdam, De Boelelaan 1081, 1081HV Amsterdam, The Netherlands

[§]Department of Chemistry & Biochemistry and The Center for Bioenergy and Photosynthesis, Arizona State University, Tempe, Arizona 85287-1605, United States

Author Contributions:

[⊥]These authors contributed equally to this work.

Article first published 1 November 2013 DOI 10.1021/jp401073w

Reprinted (adapted) with permission from Maiuri, M.; Snellenburg, J. J.; van Stokkum, I. H. M.; Pillai, S.; WongCarter, K.; Gust, D.; Moore, T. A.; Moore, A. L.; van Grondelle, R.; Cerullo, G.; Polli, D. Ultrafast Energy Transfer and Excited State Coupling in an

Artificial Photosynthetic Antenna. *The Journal of Physical Chemistry B* **2013,** *117,* (46), 14183-14190**. © 2013 American Chemical Society.** See Appendix C.

My contribution to this work was the synthesis of the phthalocyanine model for spectroscopic measurements and editing of the manuscript.

Introduction

Photosynthetic light harvesting involves the absorption of sunlight to create electronic excitations in the peripheral antennas of photosynthetic systems and the subsequent rapid excitation energy transfer (EET) to a reaction center[70]. EET occurs through highly engineered, sophisticated and extensive networks of pigment-protein complexes, made of densely packed chromophores held in precise configurations by the surrounding protein scaffold. The chromophores present in natural antennas are carotenoids (Cars) and (bacterio)chlorophylls ((B)Chls). Cars absorb light in the blue-green region of the spectrum and transfer the electronic excitation to the (B)Chls, thereby increasing the overall efficiency of the light-harvesting process. In addition, Cars play crucial roles in photoprotection of the photosynthetic apparatus[71]. First, they scavenge the highly reactive singlet oxygen and limit its generation by quenching its precursor (B)Chl triplet state. Second, they are involved in the so-called non-photochemical quenching (NPQ) mechanism[72], that allows the photosynthetic organisms to adapt to the changing light levels by down-regulating their photosynthetic activity under high illumination conditions. Although the precise mechanism of NPQ is still under debate and may vary from one system to another[27, 31, 73], there is now a general agreement that it occurs by quenching the Chl singlet states via interaction with Cars.

The main features of Car photophysics can be described by a model based on two low-lying excited singlet states, denoted S_2 and S_1[74]. In this picture, the transition from the ground state S_0 (with $1^1A_g^-$ symmetry) to the excited state S_2 ($1^1B_u^+$) is optically allowed and leads to a strong absorption band in the visible region. The transition from S_0 to the lower-lying S_1 ($2^1A_g^-$) state is one-photon forbidden for reasons of symmetry. Following photoexcitation, energy relaxes from the S_2 state into the S_1 state by internal conversion (IC) in a few hundreds of femtoseconds; then, S_1 decays back to S_0 on a slower, picosecond time scale[4b]. Within the photosynthetic apparatus, EET from Cars to (B)Chls can occur from both S_2 and S_1 states[4a]. Despite extensive investigations, the details of the electronic structure of carotenoids are still a matter of ongoing debate[8]. Recently, a growing number of experiments on Cars, both in solution and within light harvesting complexes call for a scenario which challenges the simple three-level picture, with additional excited states[75] required for a full description of their photoinduced dynamics.

Synthetic chemistry has made possible the development of artificial complexes which mimic many of the functions of natural light-harvesting[13, 76]. In these systems the chromophores, i.e. Cars and tetrapyrroles (porphyrins/phthalocyanines), are linked by covalent bonds rather than being held in position by the protein scaffold. The study of such artificial antennas is interesting on the one hand because they allow the investigation of the fundamental mechanisms of natural light-harvesting while working on simpler and more controlled systems. On the other hand, they can be considered as the main building blocks of future bioinspired artificial systems that can be used to convert light into stored chemical energy[1f].

In this work we focus on a prototypical artificial dyad, which mimics the light harvesting process in natural photosynthesis, in order to address two fundamental roles of Cars in photosynthesis: EET and photoprotection via NPQ. We study a dyad composed of a Car with 10 conjugated double bonds, serving as light harvester, linked to a phthalocyanine (Pc), acting as energy acceptor, through a phenylamino group, resulting in an effective conjugation length $N \approx 11$. Recently the same artificial complex has been studied by Kloz et al.[17, 34] in different solvents, but information about the initial events that occur directly after photo-excitation was limited by the 100-fs time resolution of the conventional transient spectrometers employed.

Thanks to the ≈30 fs temporal resolution of our measurements, we are able to resolve the dynamics of the extremely fast Car → Pc EET and $S_2 \rightarrow S_1$ IC processes, not observed by Kloz *et al*.[17] due to the limited 100-fs time resolution. In addition, upon selectively pumping the Pc with sub-20 fs pulses, we detect the instantaneous appearance of transient features characteristic of the Car S_1 state, confirming the results of Kloz *et al.*[34] but with 3 times better time resolution. The observation of an instantaneous Car signal upon photoexcitation of the Pc strongly suggests the existence of excited state coupling between the Q_x state of the Pc and the S_1 state of the Car. Taken together, our results highlight the similarity between artificial and natural supramolecules both in terms of light-harvesting and photoprotective functions.

Materials and Methods

Synthesis. The chemical structure of the dyad is shown in the inset of Figure 1. The dyad and the two isolated reference compounds, Pc and Car, were synthesized as previously described[7]. The dyad consists of a 10-double-bond polyene terminated with a *para*-phenylene group that is attached to an amino group at a peripheral position of Pc. The reference Pc is identical to the dyad but the polyene chain is replaced by a methyl group and in the reference carotenoid the Pc moiety of the Car-Pc is replaced by a tolyl group. The dyad actually exists as a mixture of isomers in which the positions of the various *t*-butyl groups varies. This is not expected to significantly affect the photophysics of the molecule.

The dyad and its two reference compounds were dissolved in toluene for the spectroscopic measurements described below. The ground-state absorption spectrum of the dyad is reported in Figure 1 as a solid black line: the Car $S_0 \rightarrow S_2$ transition lies in the blue-green (450-550 nm wavelength region), while the Pc moiety has its main absorption peak at ≈690 nm (due to its Q_x transition), with a small replica at ≈625 nm (due to its Q_y transition). We note that in Pcs the Q_x/Q_y name ordering is reversed as compared to (B)Chls.

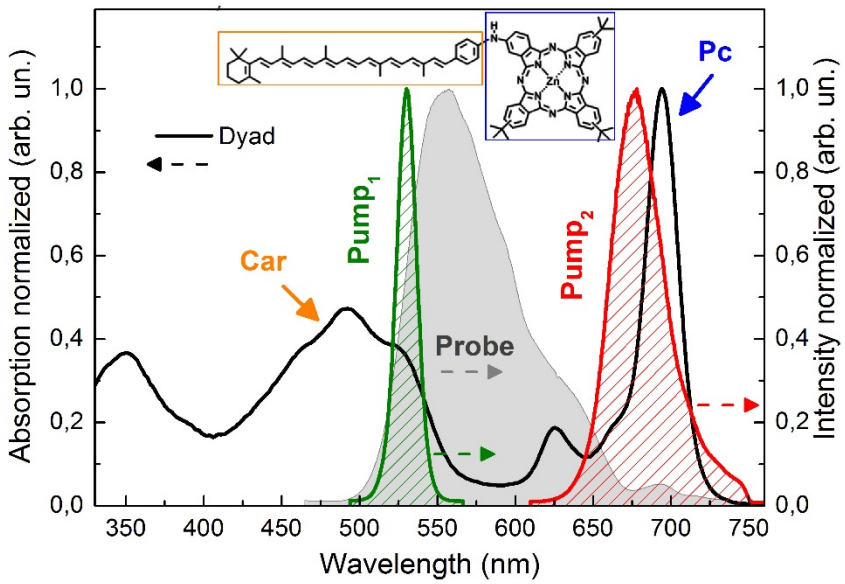

Figure 1. Chemical structure, absorption spectrum (black solid line) of Pc-Car dyad diluted in toluene and probe spectrum (gray area) used in the experiments; $Pump_1$ and $Pump_2$ represent the different pump pulses used for excitation at 530 and 680 nm (green and red dashed curves, respectively).

Ultrafast spectroscopy. The high time resolution experimental apparatus is based on two synchronized noncollinear optical parametric amplifiers (NOPAs)[77] pumped by a regeneratively amplified mode-locked Ti:Sapphire laser system delivering pulses with 150-fs duration, 500-μJ energy, at 1-kHz repetition rate and 780-nm central wavelength. The first NOPA generates 15-fs pulses peaked at 530 nm ($Pump_1$ in Figure 1), in resonance with the $S_0 \rightarrow S_2$ transition of the Car. The same NOPA can be tuned to generate 15 fs pulses at 680 nm ($Pump_2$ in Figure 1) in order to selectively excite the Pc. The second NOPA provides ultra-broadband probe pulses with ≈7 fs duration spanning the 500-700 nm wavelength range (grey filled spectrum in Figure 1), thus covering both the Car and Pc absorption bands. Both NOPAs are compressed to their transform-limited duration by multiple bounces on custom-designed chirped mirrors. The beams are focused onto the sample contained in a cuvette with 200-μm-thick fused-silica windows. After the sample,

the probe beam is selected by an iris and focused onto the entrance slit of a spectrometer with single-shot detection capability at 1 kHz[78]. By recording the probe spectrum with and without the pump, one can obtain the transient absorption (TA) spectrum, defined as: $\Delta A(\lambda,\tau) = - ln[T_{on}(\lambda,\tau)/T_{off}(\lambda))]$, as a function of probe wavelength and delay.

Data analysis. For this study a total of four measurements (Car and dyad with excitation at 530 nm, Pc and dyad with excitation at 680 nm) were analyzed by a combination of global and target analysis[15]. Software to perform this kind of analysis is freely available in the form of the Glotaran software package[79]. The TA spectra of the dyad and the isolated Car excited at 530 nm were recorded in a 50 ps time window, then analyzed simultaneously using a specific kinetic scheme (target analysis), resulting in the estimated species associated difference spectra (SADS) of the pure molecular states. For this set of measurements the instrument response function (IRF) was fitted to a Gaussian of 42 fs full width at half maximum (FWHM) for both samples.

With 680-nm excitation the TA spectra of the dyad and the isolated Pc were recorded in a 100 ps time window, and then analyzed simultaneously using a sequential kinetic model ($1 \rightarrow 2 \rightarrow 3 \rightarrow \ldots$) in which the arrows indicate successive mono-exponential decays with increasing time constants (global analysis). Each component is characterized by its evolution associated difference spectrum (EADS). The first EADS then corresponds to the time-zero TA spectrum. Only three components were required to describe the spectral evolution in the 100 ps measurement window. Because no detailed kinetic scheme is imposed, the EADS may reflect mixtures of molecular species, and in fact for the dyad this is most certainly the case as is explained in the Results section. For this set of measurements the IRF was fitted to a Gaussian of ≈60 fs FWHM for both the

Dyad and the Pc samples. Given the IRF and the signal-to-noise ratio of our data, we can conservatively estimate a time resolution of at least 30 fs.

Results

Carotenoid-phthalocyanine energy transfer. The Car→Pc EET process in the dyad can in principle occur from the bright S_2 excited state as well as from the dark S_1 state of the Car; in both cases, it competes with IC processes towards lower-lying states. To establish the relative weight of these two deactivation pathways, we compare the excited state dynamics of the isolated Car (where only the IC process occurs) with that of the dyad (where both the IC process and the EET channel are active).

Figure 2a shows the ΔA heat map of the isolated Car in toluene solution: we observe the prompt rise of a negative signal, which we assign to ground state photobleaching (PB) and to stimulated emission (SE) from S_2 to S_0. This signal rapidly decays, giving rise to a positive photoinduced absorption (PA) band peaking at 610 nm, the formation of which is completed within ≈400 fs. This PA band is well known in Cars and assigned to a transition from S_1 to a higher-lying S_n state[4b], thus providing a signature of the population of the S_1 state through the IC process. The PA band shows a faster build-up in the red compared to the blue, and undergoes spectral narrowing within the first 500 fs. These effects are due to intramolecular vibrational relaxation (IVR) within S_1 associated with dissipation of the excess energy deposited as a result of the IC process[80].

Figure 2b shows the ΔA heat map of the dyad in toluene solution, following excitation of the Car moiety at 530 nm. In this case, the temporal evolution of the TA signals occurs on a significantly shorter time scale as compared to the isolated Car, indicating a much faster decay of the population out of the initially excited Car S_2 state

(see comparison of time traces in Figure 2c). In particular, within ≈100 fs following excitation a nearly stationary TA spectrum is formed, which displays not only the expected $S_1 \rightarrow S_n$ PA from the Car but also (i) a negative PB signal peaking at around 690 nm, reflecting excitation of the Pc moiety and thus indicating Car → Pc EET, and (ii) an increased PA shoulder in the blue (peaking at ≈555 nm), representing a new deactivation pathway within the Car manifold towards an additional intermediate excited state, denoted as S*. A spectrally similar state, which in our experiments is not observed in the isolated Car (Figure 2a), has been observed in other Cars in the same spectral region, both in solution[8] or when embedded in light-harvesting systems[16, 66a, 81].

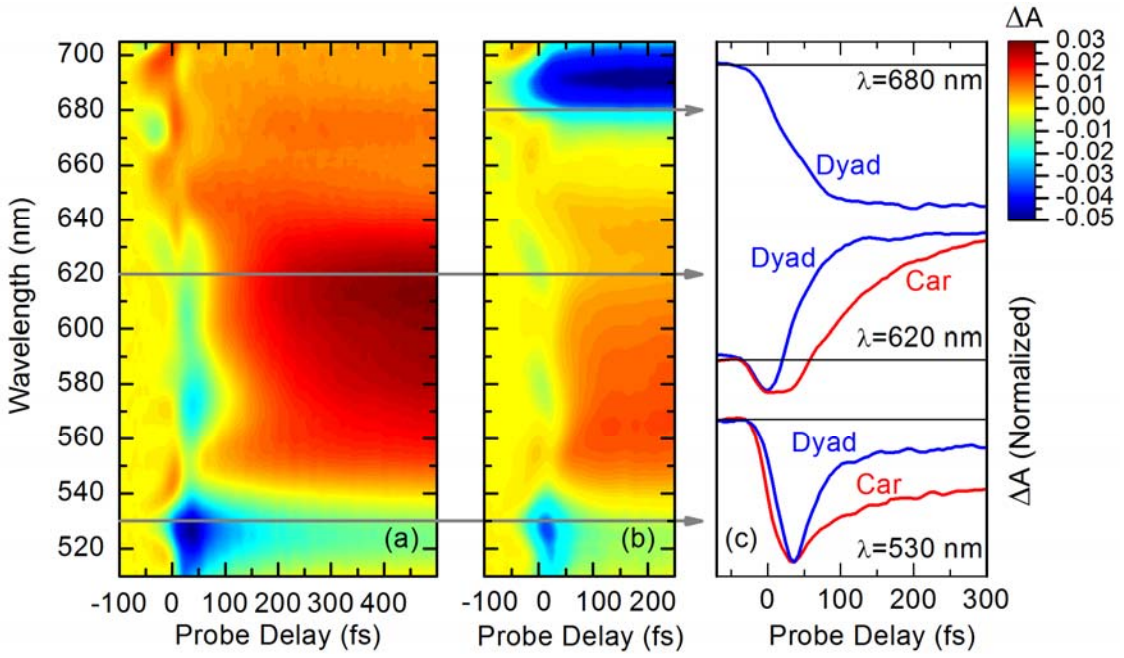

Figure 2. ΔA heat maps as a function of probe wavelength (vertical) and probe delay (horizontal) for the isolated Car (a) and the dyad (b) in toluene; excitation at 530 nm. As indicated in the color map, the zero level is coloured in yellow, red indicates positive signals (i.e. photo-induced absorption) and green/blue denote negative signals (i.e. decrease in absorption due to stimulated emission and/or ground-state photo-bleaching). Time traces at selected probe wavelengths (c).

Figure 3a depicts the compartmental model used for the target analysis of the 530 nm excitation data, using the minimum number of components that were necessary to satisfactorily fit the data. Alternative models were initially considered and investigated and then discarded based on the decreased quality of fits and/or physical interpretability of the estimated parameters (rate constants and SADS). S_2, hot S_1, S_1 and S* are SADS associated with Car, while Pc1 and Pc2 are associated with the phthalocyanine. Spectral evolutions of hot $S_1 \rightarrow S_1$ and Pc1 $\rightarrow$ Pc2 were taken into account in order to include IVR processes within the two species: as a consequence of $S_2 \rightarrow S_1$ IC or Car $\rightarrow$ Pc EET, excess energy is initially deposited both in the Car S_1 state and in the Pc, due to the excitation of the Car S_2 state via the 530 nm pump pulse. Both for the isolated Car and for the dyad the model did not require the inclusion of additional excited states of the Car (such as the $1^1B_u^-$ state), which in some cases have been proposed to mediate the $S_2 \rightarrow S_1$ IC process[75]. The estimated population time profiles and corresponding SADS are shown in Figure 3b and 3c, respectively. Figure S1 reports the same SADS of Figure 3c but vertically offset to improve readability. Car $S_2 \rightarrow$ hot $S_1 \rightarrow S_1 \rightarrow S_0$ IC rate constants and associated SADS were constrained to be equal in the analysis of the isolated Car and the dyad. This approach is based on the assumption that, when covalently linking the two molecules, their excited states are not significantly affected. Without this assumption it would be very difficult to compare the experiments in the dyad with those of the isolated moieties. The first SADS can be identified as the S_2 state of the Car, with a PB at 525 nm and SE from 550 until 650 nm. From the S_2 state of the Car three different species are populated in the dyad: the hot S_1 of the Car, the first excited state of the Pc species (Pc1), and the additional excited state S* of the Car. The lifetime of the S_2 state is 39 ± 2 fs in the dyad. The S* state subsequently

decays in 320 ± 10 fs to the ground state, presumably via an IC process. Based on previous results[16, 66a, 81-82], the Car S* state is restricted to only contribute to the fit for wavelengths shorter than 585 nm. The hot S_1 state evolves in ≈440 fs into the relaxed S_1 state, which subsequently decays to the ground state in 7.5 ps. Analogously, the hot Pc (Pc1) evolves in ≈3 ps into the relaxed Pc state (Pc2), which relaxes to the ground state on a much longer time scale. The excellent fit quality of the simultaneous target analysis is demonstrated in Figure S2.

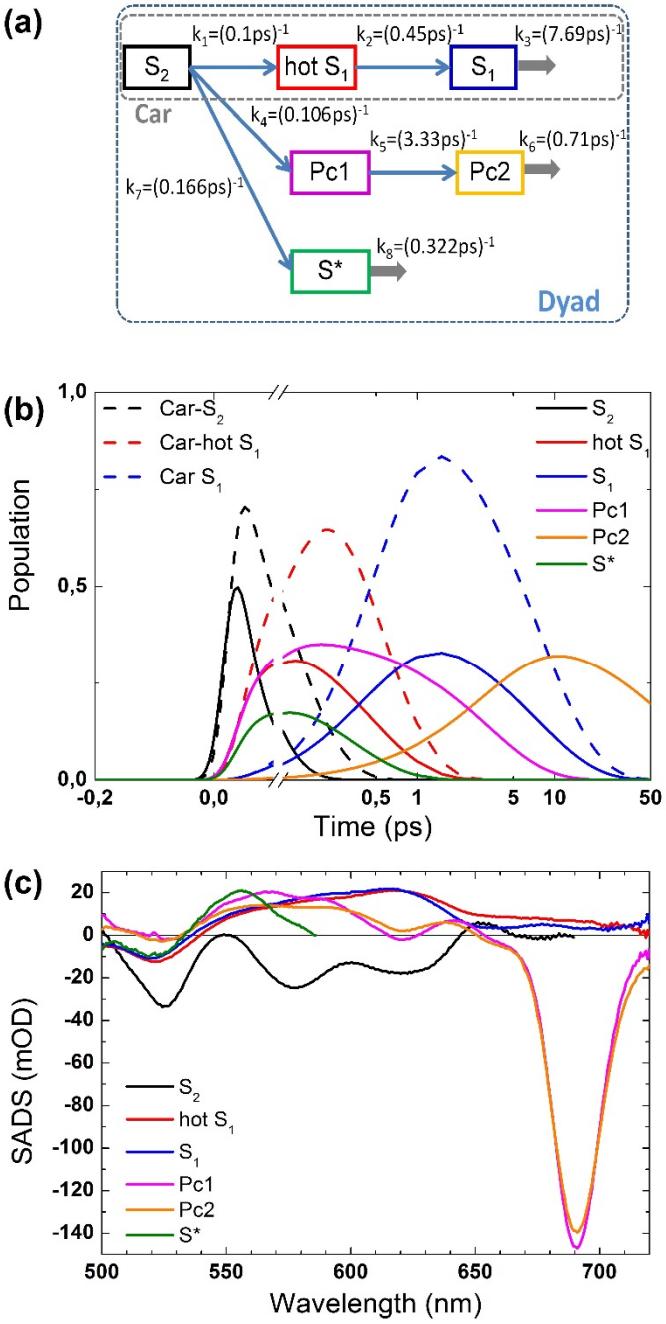

Figure 3. (a) Kinetic scheme used for target analysis of the 530 nm excitation data. The estimated rate constants (in 1/ps) are indicated in the figure; the global lifetimes are 0.1 ps (S_2, Car), 0.039 ps (S_2, Dyad), 0.44 ps (hot S_1), 7.5 ps (S_1), 3.3 ps (Pc1), 73 ps (Pc2) and 0.32 ps (S*). (b) The population profiles and (c) estimated SADS. Note that the time axis is linear until 0.1 ps and logarithmic thereafter. The dashed population profiles in (b) correspond to the isolated Car and the solid ones to the Car-Pc dyad.

Carotenoid-phthalocyanine coupling. To investigate the possible coupling between the excited states of the Pc and Car moieties in the dyad, we compare TA measurements on the dyad with those of the isolated Pc, both excited at a wavelength of 680 nm, corresponding to the peak of Pc absorption and with negligible absorption from the Car. Figure 4 reports the EADS obtained from the simultaneous global analysis of both measurements; the raw data in the form of kinetic traces and fits are reported in Figure S3.

The interpretation of these EADS is quite straightforward. Upon 680 nm excitation of the isolated Pc molecule, the photogenerated excited state Pc1 with a 94 fs time constant undergoes a tiny red-shift, attributed to IVR, evolving to Pc2, which decays in 54 ps into a long-lived component Pc3 which does not evolve in our time window. IVR occurs because the pump spectrum is broader than the Pc absorption and the excitation pulse peaks at a wavelength slightly blue-shifted with respect to the Pc absorption maximum (see Figure 1). The dyad undergoes a similar evolution on the same timescale, but with the PB signals of the Pc moiety in the dyad clearly red-shifted by approximately 5 nm with respect to the isolated Pc molecule. The same red-shift is observed in the ground-state absorption spectrum and is assigned to the effect of the linkage joining the Pc to the carotenoid. For the isolated Pc, the EADS show two PB bands, at ≈690 and ≈620 nm, assigned to the Q_x and Q_y transitions, respectively, and a broad and almost featureless PA band extending to the blue.

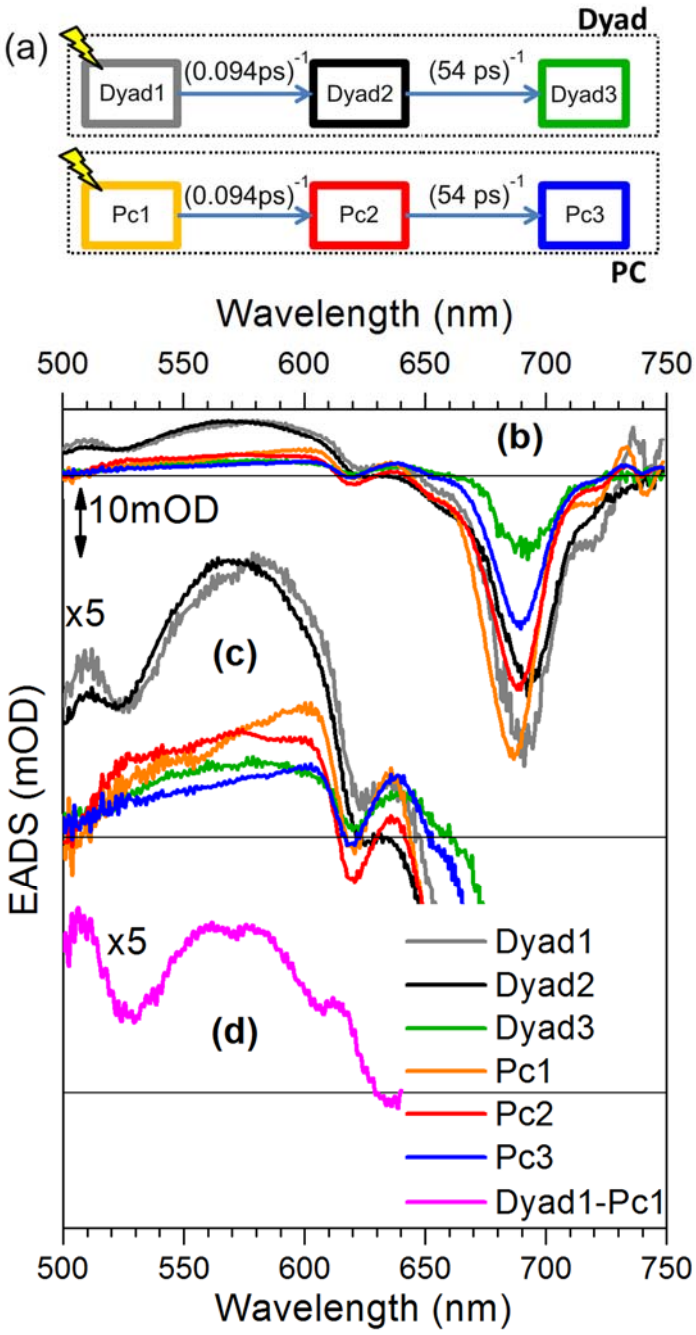

Figure 4. (a) Kinetic scheme used for target analysis of the 680-nm excitation data. The dynamics was modeled with three sequential decays. The time constants were linked between the experiments and found to be 0.094 ps (for Pc1 and Dyad1), 54 ps (for Pc2 and Dyad2) and long-lived (for Pc3 and Dyad3). (b) EADS resulting from the simultaneous analysis of the measurements collected for the isolated Pc moiety (Pc1, Pc2 and Pc3; yellow, red and blue curves) and the dyad (Dyad1, Dyad2 and Dyad3; grey, black and green curves) at 680 nm excitation; (c) EADS magnified 5 times; (d) Dyad1 EADS minus the Pc1 EADS (magenta curve).

The EADS for the dyad are qualitatively similar but, as shown expanded in the middle panel, with clear differences in the PA signal. To better highlight these differences, we subtracted the isolated Pc EADS from the dyad EADS (panel c). When this difference EADS (pink curve in Figure 4d) is compared qualitatively with the estimated SADS from Figure 3c, it is clear that the extra spectral signature observed in the dyad (i.e. a PA signal between 540 and 620 nm) closely matches the Car S_1 excited state TA spectrum (blue SADS in Figure 3c). We also observe additional negative features around 530 nm and around 630 nm. The former corresponds to the PB of the Car $S_0 \rightarrow S_2$ transition, while the latter can be explained by a shift of the Q_y absorption band of the Pc in the dyad. All these additional features in the dyad EADS do not display any rise time within our ≈30 fs temporal resolution but are immediately present following photoexcitation of the Pc moiety. As discussed below, we take them as a clear evidence of electronic coupling between the Pc excited state and the S_1 excited state of the Car.

Discussion

Carotenoid-phthalocyanine energy transfer. EET between Cars and (B)Chls in natural light-harvesting complexes has been studied in detail using ultrafast spectroscopy, as recently reviewed by Polivka and Frank[4a]. At first sight, one would expect EET from Cars to be a rather inefficient process. On the one hand, the S_2 lifetimes are rather short (ranging from 50 to 300 fs depending on the number of double bonds *N*), providing an efficient parallel deactivation channel via IC to S_1 and on the other hand, the $S_0 \rightarrow S_1$ transition is optically forbidden, so that one would expect that direct dipole-coupled Förster transfer from S_1 should be inefficient. However, the S_2 EET channel is always found to be active, while the S_1 channel is activated only in specific systems. The reason for the high

efficiency of EET from S_2 lies in the optimization of the Car-(B)Chl distance, which, combined with the large value and proper orientation of the S_2 dipole moment, results in rather large Förster EET rates[83]. The most studied systems for EET are the peripheral LH2 complexes of purple bacteria, due to the availability of detailed structural information and to the well separated absorption spectra of the different pigment groups. In the prototypical purple bacterium *Rhodopseudomonas (Rps.) acidophila*, containing the carotenoid rhodopin glucoside ($N = 11$), EET has been investigated in many studies and its efficiency has been found to be around 50% from S_2[80b, 84]. In other bacteria this efficiency has been found to be different. When the Car conjugation length increases, the S_2 lifetime becomes shorter, thus reducing the EET efficiency. For our dyad, the EET efficiency from the Car S_2 state to the Pc can be calculated as $\eta_{ET2} = \frac{k_4}{k_1 + k_4 + k_7} = 37\%$, highlighting the similarity of our artificial antenna with natural light-harvesting complexes[85]. This number agrees very well with independently performed fluorescence excitation measurements where the energy transfer efficiency for this system was found to be 42% integrated over the relevant spectrum (Gerdenis Kodis (ASU), private communication). Without the loss channel from S_2 to S* (k_7 in Figure 3a) the energy transfer efficiency would be higher than 60%.

In some purple bacteria the EET channel from S_1 is activated because the Car to BChls distance is smaller than the molecules themselves, so that the charge density locally changes and the Förster transfer becomes permitted (one should consider the full donor/acceptor Coulomb coupling). In particular, it is found to be quite efficient for bacteria having Cars with $N < 11$, while it is not significant for longer Cars[4a, 86]. We considered EET from S_1 to Pc in our dyad molecule but we found this contribution not to

be present: the S_1 dynamics were found to be unchanged between the isolated Car and the dyad. This means that no EET process occurs from the S_1 state of the Car, i.e. $\eta_{ET1} \cong 0$. We note that, with respect to LH2 complexes, where the first excited state Q_y of the accepting BChl molecule absorbs at 800/850 nm, here the Pc lower state (Q_x) is higher in energy (it absorbs at ≈690 nm). The Car S_1 state energy (measured in many samples using fluorescence, two-photon absorption, Raman or infrared S_1-S_2 absorption) depends on the conjugation length (the higher *N*, the lower its energy). For example in spheroidene having $N = 10$, the S_0-S_1 gap would correspond to a one-photon transition at 700-750 nm[4b]. In the dyad, the phenyl group linkage between the Car and Pc results in an increased conjugation length, thus further decreasing the S_0-S_1 gap. This points to an unfavorable uphill energy landscape for the $S_1 \rightarrow$ Pc EET.

The TA data in the dyad clearly show an additional decay pathway for the S_2 state of the Car, towards an excited state resembling S*. The S* state was discovered about a decade ago in spirilloxanthin ($N = 13$)[66a], both in solution and bound to the LH1 complex of *Rhodospirillum rubrum*, and later observed in other carotenoids[14, 16, 81, 87]. It is characterized by a PA band blue-shifted with respect to the S_1-S_n band but red-shifted with respect to the optically allowed S_0-S_2 transition. Despite alternative assignments of S* to a hot ground state[81, 88], there is now a general consensus in interpreting it as a separate excited state, generated from S_2 in competition with S_1, and often leading to the formation of a long-lived triplet state in Cars[89]. Generally, S* is found to have a longer lifetime with respect to S_1; here, on the other hand, its lifetime (0.3 ps) is measured to be significantly shorter than the S_1 lifetime (7.5 ps). Niedzwiedzki, *et al*.[90] considered the hypothesis of S* as a distorted S_1 state, but more research is needed to decide on the nature of this short-

lived S* state. We note that such short-lived S* state, acting as a quencher for the carotenoid S_2 state, could play an important role in the carotenoid/(B)Chl interaction found in photosynthetic bacteria and higher plants. The fact that we do not detect it in the isolated carotenoid could indicate that fine energetic tuning could be actively used in nature (maybe even in the NPQ mechanism) to activate or suppress this energy deactivation channel. Alternative target models, considering the absence of S* state in the dyad or its presence also in the Car, were considered (see Figure S4 and S5 in the Supporting Information and relative discussion) but discarded based on the decreased quality of fit and the physical interpretability of the estimated parameters.

Carotenoid-phthalocyanine excited state coupling. NPQ is the mechanism employed by plants and algae to self-protect from the adverse effects of high light intensity. It is based on the quenching of Chl singlet excited states via enhanced nonradiative internal conversion to the ground state. The molecular processes underlying NPQ are not yet fully understood and are hotly debated, but there is a general agreement regarding the fact that Car-Chl electronic interactions are involved. A possible pathway is EET from Chl to the S_1 dark state of the lutein carotenoid, enabled by conformational changes in the peripheral, trimeric major light-harvesting antenna of photosystem II, called LHCII[31]. Alternatively, a charge transfer mechanism has been proposed, with charge separation followed by recombination occurring in the minor antenna complexes after energy transfer to a Chl/zeaxanthin heterodimer[27, 73a]. Recently in LHCII the formation of coupled excitonic states between the S_1 state of the Car and the Chl, which decrease the excited state lifetime of Chl, has been proposed to mediate NPQ[37].

In order to shed light on the mechanisms of NPQ in natural systems, it is interesting to investigate an artificial dyad such as the one addressed in this study as a model system containing only one Car and one tetrapyrrole unit. The advantage resides in the fact that in this case the pure quenching kinetics can be directly studied because they are shorter than the decay times of the tetrapyrrole excited states by their intrinsic photophysical pathways. On the other hand, in the natural light-harvesting systems, such kinetics are obscured because the excitation must first slowly transfer (in hundreds of picoseconds) from the large pigment pool to the Cars/Chls in the quenching site, where it rapidly decays. This results in an inverted kinetics, for which the TA signal from the Car S_1 state is small and convoluted with the exciton dynamics in the pigment pool.

In Car/tetrapyrrole dyads all the three aforementioned quenching mechanisms have been observed, depending on the exact molecular architecture and solvent environment:

(1) EET from Pc to the S_1 state of the Car, possibly passing through an intramolecular charge-transfer state, followed by fast internal conversion to the Car ground state[30, 34]; this occurs only for carotenoids with sufficiently large conjugation length to lower the S_1 energy, analogously to the "molecular gear shift mechanism" proposed for the xanthophyll cycle[32].

(2) Electron transfer from Car to Pc followed by rapid charge recombination on the picosecond time scale, occurring especially in polar solvents[13, 91]

(3) Excitonic coupling between the Pc and the S_1 state of the Car and ensuing internal conversion to the ground state of the Car. This mechanism has been proposed to occur in the Pc/Car dyad that we are studying on the basis of two complementary experimental results: (i) in a pump-probe study, upon Pc excitation the TA signal

from the Car S_1 state immediately appeared within the 100 fs instrumental temporal resolution, indicating Pc → Car interaction[34]; (ii) in a fluorescence experiment, upon direct Car S_1 population (using two-photon excitation) a strong emission from Pc was observed, indicating Car → Pc interaction[36a]. Such a bidirectional Car ↔ Pc EET evidences excitation energy sharing between the two moieties and is a very strong indication for excited state interactions. Such excited state coupling ultimately depends on a delicate balance of the Car S_1/Pc relative energies and on thermal fluctuations. In more polar environments (THF) such coupled states have been observed and tentatively assigned as precursors of charged separated states[34].

The experimental results presented in Figure 4c clearly show that upon Pc excitation an additional TA signal immediately appears in the dyad with respect to the pure Pc sample. With the help of our target analysis reported in Figure 3c we can clearly identify this band as PA from the Car S_1 state (blue SADS in Figure 3c). We also observe PB of the Car $S_0 \rightarrow S_2$ transition at 530 nm. These bands appear within our temporal resolution of ≈30 fs, corresponding to a three-fold improvement with respect to the findings of Kloz *et al.*[34]. Three possible scenarios could explain this observation: (i) extremely rapid Pc → Car S_1 EET, which would result in equally rapid deactivation of Pc, not observed in our experiments; (ii) Pc → Car S_1 EET slower than Car S_1 deactivation, resulting in an inverted kinetics; in this case, however, the S_1 signal would rise with a time constant corresponding to the S_1 lifetime, which is much longer (on the several picosecond timescale, see Figure 3a,b) than our temporal resolution; (iii) excited state coupling between Pc and Car S_1, which is then our proposed explanation.

Conclusion

In this work we performed a comprehensive study of excited state dynamics in a carotenoid-phthalocyanine dyad which acts as an artificial photosynthetic antenna. By the use of our state-of-the-art pump-probe system with high temporal resolution it was possible to completely time resolve the ultrafast excited-state dynamics of the isolated Car and of the dyad system, occurring within the ≈100 fs time scale. The combination of experimental results and their simultaneous comparison by means of global and target analysis enabled us to evaluate the EET pathways and efficiency (as high as ≈37%) from the Car to the Pc. In addition, by exciting Pc moiety in the dyad we observe, within the ≈30 fs time resolution of the experiments, features in the transient absorption spectrum which closely match those of the S_1 excited state of the Car. This result strongly suggests that in this dyad there is electronic coupling between the Pc excited state and the S_1 excited state of the Car, a mechanism that has been recently proposed to mediate NPQ in the LHCII complexes of higher plants. Excited state coupling has been reported in several natural photosynthetic systems such as Fenna–Matthews–Olson (FMO) bacteriochlorophyll complex[92], light-harvesting proteins isolated from marine cryptophyte algae[93] and the trimeric light-harvesting complex II (LHCII)[94] from *Arabidopsis Thaliana* using two-dimensional electronic spectroscopy (2DES). Oscillations were observed in these experiments, and interpreted as a long-lived superposition (coherence) of exciton states. These observations were made possible by the fact that 2DES signals are recorded at the amplitude level, so that the quantum phase of the system can be directly accessed, thereby providing evidence of quantum coherence effects. For these reasons, the dyad system studied in this work is an ideal candidate for future 2DES measurements: the excitonic coupling between the

carotenoid and the PC we observed here using pump-probe spectroscopy could in principle manifest itself as a coherence in the 2DES signal.

This study highlights once again the similarity between artificial and natural photosynthetic complexes in terms of two fundamental functions: light harvesting and photoprotection. These results show that artificial complexes are promising for future application for controlling natural photosynthesis.

Acknowledgements

T.A.M., A.L.M. and D.P. acknowledge financial support by the Human Frontiers Science Program Grant Number RGP0005. This project was carried out in part within the research programme of BioSolar Cells, cofinanced by the Dutch Ministry of Economic Affairs (J.J.S., I.H.M.v.S., and R.v.G.). I.H.M.v.S., R.v.G. and G.C. acknowledge financial support of the European Research Council: Advanced Grant proposal 267333 (PHOTPROT) to R.v.G. and Advanced Grant proposal 291198 (STRATUS) to GC. This work was supported by the U. S. Department of Energy (FG02-03ER15393). Gerdenis Kodis is acknowledged for providing the number for energy transfer efficiency as determined by independent fluorescence excitation measurement.

Supporting Information

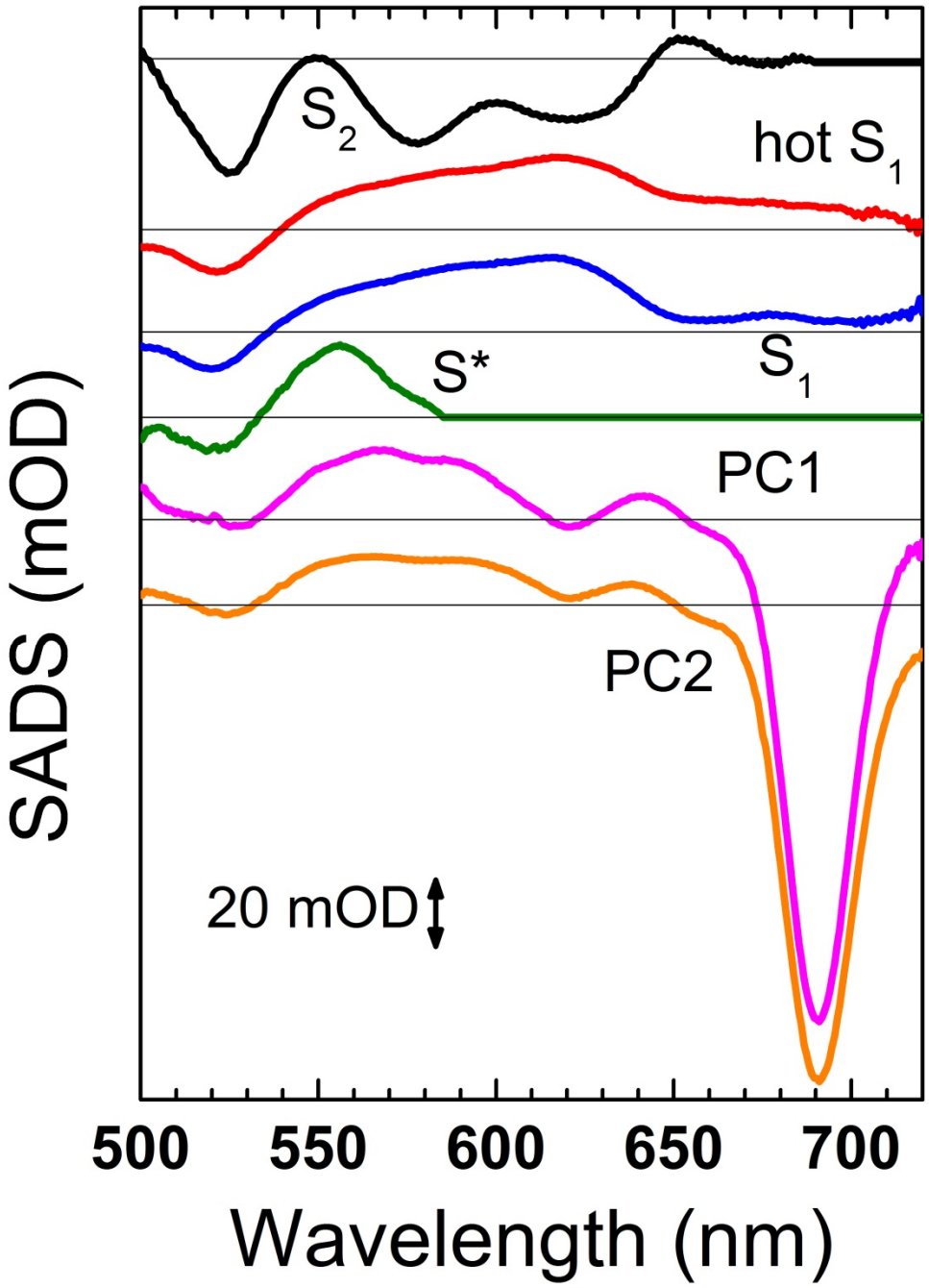

Figure S1. The same SADS of Fig. 3c are here plotted separately (vertically shifted) to help the reader in appreciating the fine details of the spectra.

In the following a complete comparison of data and fits is reported, in the form of kinetic traces at several selected wavelengths for the carotenoid and the dyad excited at 530 nm (Figure S1) and for the Pc and the dyad excited at 680 nm (Figure S2).

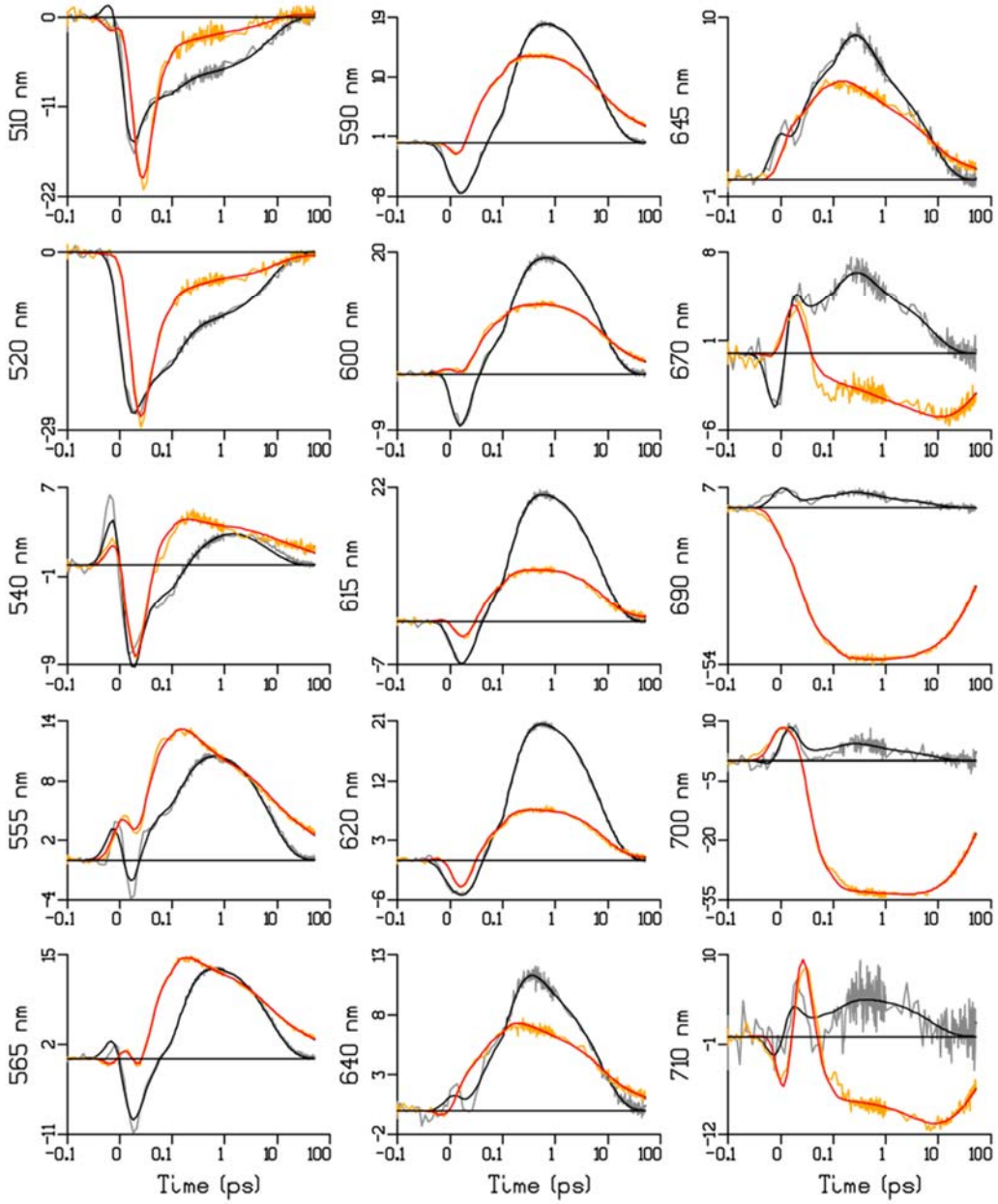

Figure S2: Kinetic traces at selected wavelength upon 530 nm photoexcitation for both the Carotenoid, gray (data) and black (fit) curves, as well as for the dyad , orange (data) and red (fit); vertical axes is expressed in mOD. Please note that the time axis is linear from -0.1 to 0.1 ps (with respect to the maximum of the IRF) and logarithmic thereafter.

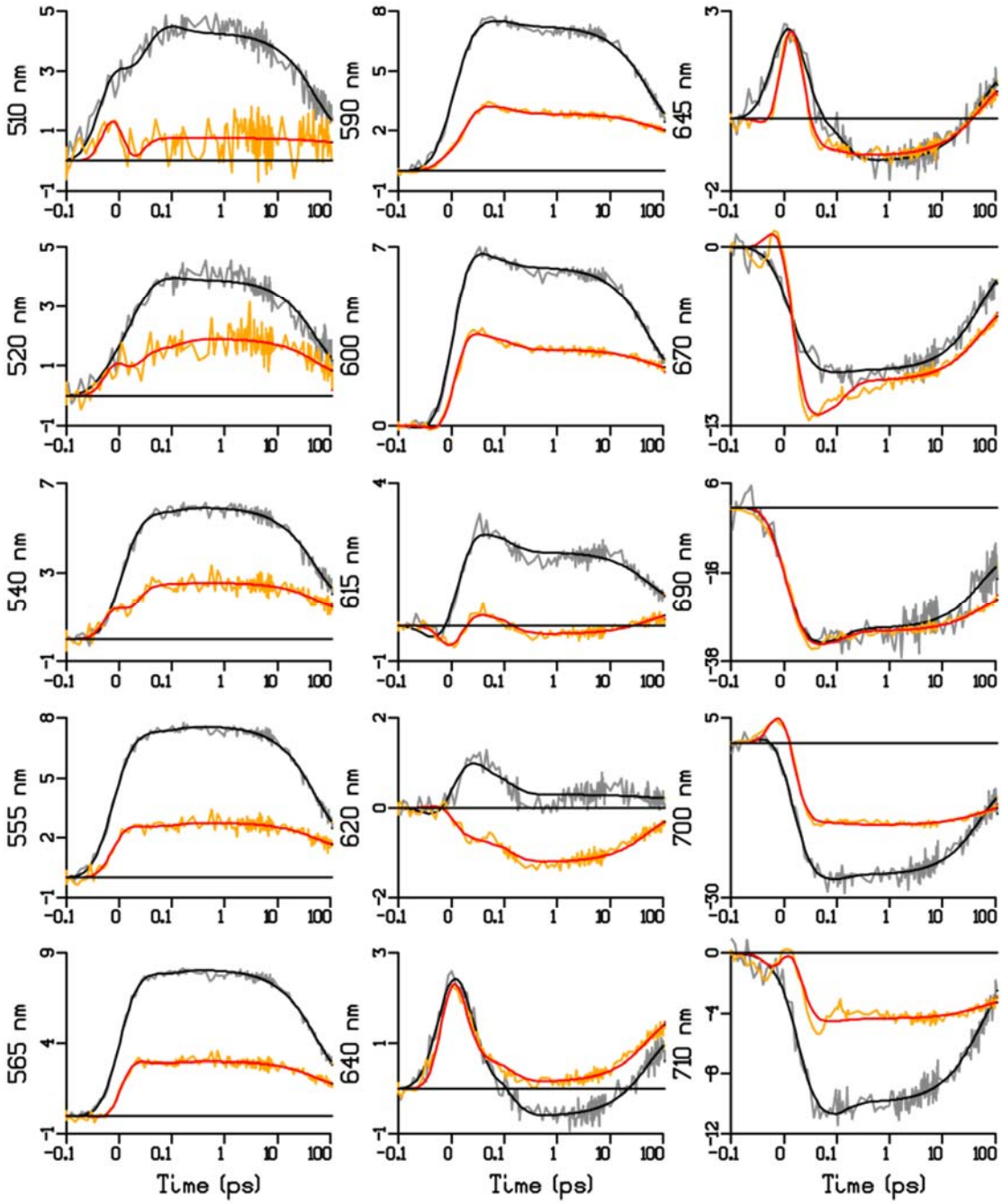

Figure S3. Kinetic traces at selected wavelength upon 680 nm photoexcitation for both the dyad , gray (data) and black (fit) curves, as well as for the Pc , orange (data) and red (fit) curves; vertical axes is expressed in mOD. Please note that the time axis is linear from -0.1 to 0.1 ps (with respect to the maximum of the IRF) and logarithmic thereafter.

Analysis of alternative target models

The target model used in the analysis of the 530 nm excitation experiment describes both measurements simultaneously: (1) the isolated carotenoid as well as (2) the Car-Pc Dyad. Part of the model accounts for the carotenoid features in both measurements (Car-S_2, hot S_1 and S_1), and part accounts for those features only present in the Dyad measurement (PC1, PC2 and S*). We have also tested two alternative target models, namely:

a) Absence of S* state both for the isolated carotenoid and for the dyad (Figure S4 below)

b) Presence of S* state both for the isolated carotenoid and for the dyad (Figure S5 below)

We discarded them and chose the present model for the following reasons:

1) Quality of the fit: the rms error of the fit increases by about 1% in cases a) and b).

2) Over fitting: there is no need to include an extra compartment (S*) to describe the data acquired in the isolated carotenoid: the fit is already perfect without its involvement, no spectral/temporal feature remains unexplained. Including this compartment anyways results in a very noisy SADS for the S* state.

3) Interpretability of the SADS: in case a) the target analysis provides an increased shoulder in the first Pc specie (PC1) which is not physical because it strongly differs from its counterpart, namely the EADS associated with the isolated Pc sample excited at 680nm, which presents a broad unstructured and almost flat spectral shape in the 540-600 nm region. In case a) also the lifetime of the PC1 specie results subsequently shortened. This means that the S* feature is indeed present in the dyad

and discarding it results in a distorted fit, where this component is picked up by the PC1 SAS.

4) Estimated energy transfer efficiency: in the current model (including the short lived S* state in the Dyad only) an energy transfer efficiency from Car to Pc of ≈37% is predicted, in line with independent fluorescence excitation measurements performed on this dyad (data not shown), whereas the two alternative models both predict an energy transfer efficiency in excess of 60% (upon excitation at 530nm).

Model (a): no S* in the isolated Car and in the dyad:

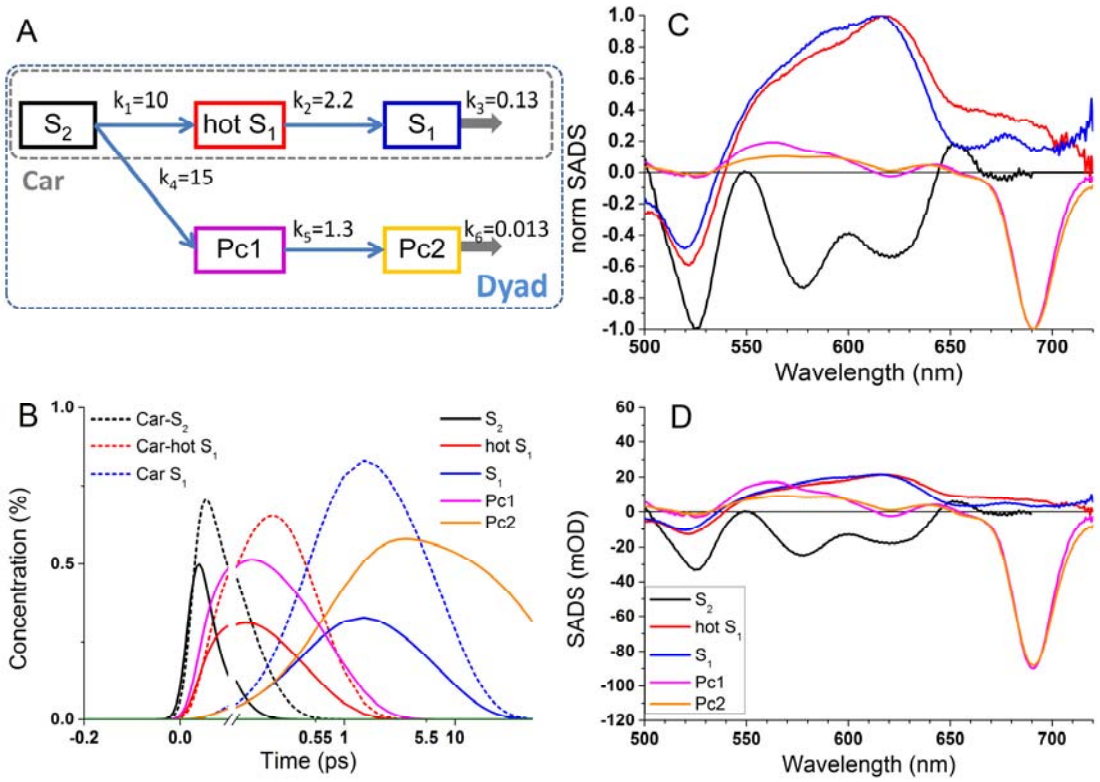

Figure S4: The figure depicts the effect of leaving the S* out of the model altogether on the estimated rate constants and the resulting SADS. (A) shows the target model with the new estimated rate constants between the compartments, most notably the effect of leaving out the S* compartment is a much increased energy transfer efficiency from Car to Pc in the Dyad (in this case estimated to be ≈60%), the PC1 lifetime is shortened and the PC1 SADS has picked up a significant amount of amplitude in the 650 nm region.

Model (b): Presence of S* in both the isolated Car and dyad:

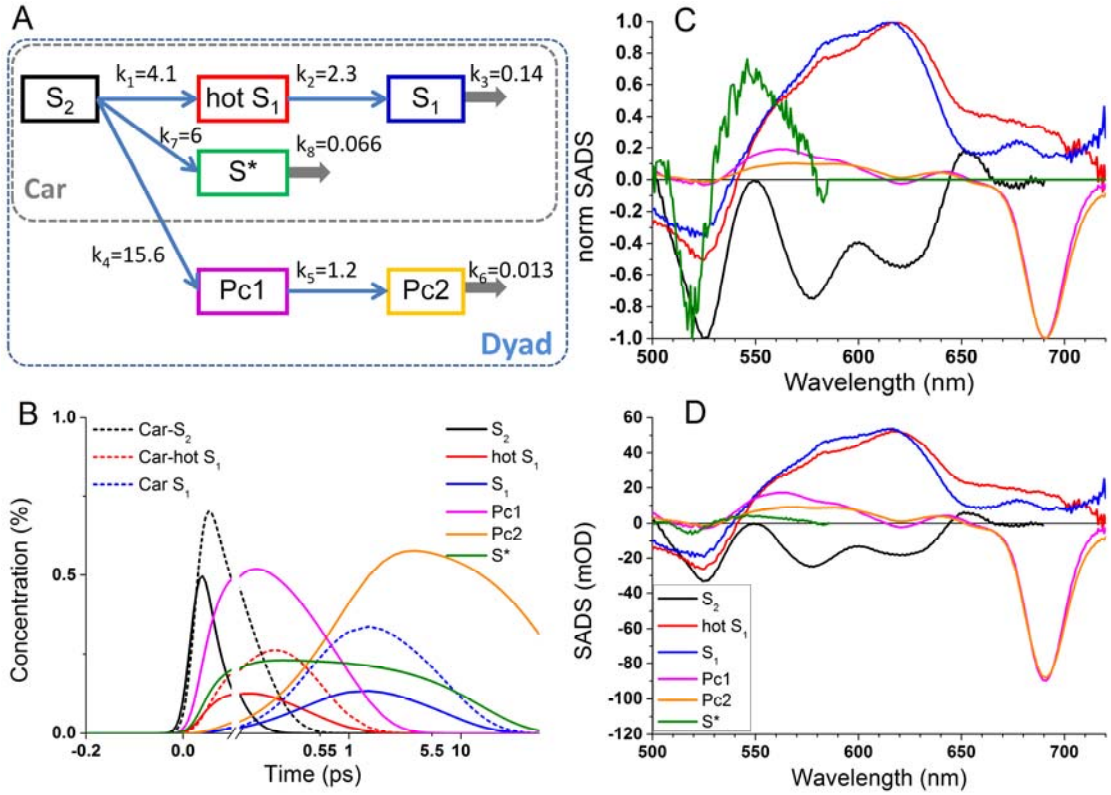

Figure S4. The figure depicts the effect of fitting the S* species common to both datasets (Car and Dyad) to the estimated rate constants and the resulting SADS. (A) shows the target model with the new estimated rate constants between the compartments, most notably the S* compartment now has a lifetime longer than S_1 but the quality of the corresponding SAS as shown in panels B (normalized) and D is reduced. Again there is a much increased energy transfer efficiency from Car to Pc in the Dyad (in this case estimated to be ≈61%). Moreover, the amplitude of the PC1 SAS in the 560 nm region is now much increased with respect to the spectrum of the isolated PC.

CHAPTER 5

SYNTHESIS AND ATTACHMENT OF SILICON PHTHALOCYANINES TO GOLD SURFACES FOR SOLAR ENERGY COLLECTION

Katherine WongCarter[a], Manuel J. Llansola-Portolés[a], Gerdenis Kodis[a], Erica Wee[b], Alastair Gardiner[c], Richard Cogdell[c], Dorota Kowalska[d], Nicodem Czechowski[d], Sebastian Maćkowski[d], Hideki Hashimoto[e], Thomas A. Moore[a], Ana L. Moore[a]

a: Department of Chemistry & Biochemistry and The Center for Bioenergy and Photosynthesis, Arizona State University, Tempe, Arizona 85287-1605, United States

b: Centre for Catalysis Research and Innovation, Department of Chemistry, University of Ottawa, Ottawa, Ontario K1N 6N5, Canada

c: Institute of Molecular Cell and Systems Biology, University of Glasgow, G12 8TA, United Kingdom

d: Optics of Hybrid Nanostructures Group, Institute of Physics, Nicolaus Copernicus University, 87-100 Toruń, Poland

e: Department of Physics, Osaka City University, Osaka 558-8585, Japan

Introduction

The sun has the potential to provide a sustainable energy source for human needs because the light that irradiates the Earth's surface in one hour (89,300 TW) can provide enough energy to power all of human kind's current energy demands for a year (17 TW)[95]. One of the challenges with using solar energy is to efficiently collect the sun's photons to

produce electricity or fuel. Sunlight is very diffuse, 1.1 x 10^{21} photons $m^{-2}s^{-1}$ between 400 and 700 nm, but nature has developed antenna structures to collect and focus this energy towards reaction centers to produce charge separated states and eventually a fuel[48b]. The goal of this project is to identify the design concepts used in light harvesting proteins for solar energy collection and recreate the supramolecular assembly for an efficient artificial photosynthetic system. This would be applied to devices that replace fossil fuel energy sources and provide energy for human needs from the sun.

An excellent system for studying solar energy harvesting is purple non-sulfur photosynthetic bacteria. This is because their photosynthetic units contain circular antenna protein complexes to achieve fast, irreversible energy transfers toward their reaction centers[12, 96]. The antenna protein complex light harvesting protein 2 (LH2) funnels energy, through Förster resonance energy transfer, toward light harvesting protein 1 (LH1) which has the reaction center protein located inside its cavity. The LH2 is particularly interesting because it contains two separate rings of bacteriochlorophyll *a* (BChl) molecules that absorb energy at different wavelengths, due to their protein environment and coupling with nearby BChl molecules (Figure 1). Nine BChl molecules arranged side-to-side in LH2 maximally absorb light at 800 nm, this ring is called BChl 800 (B800). A second ring, called BChl 850 (B850), contains eighteen BChl molecules in a face-to-face orientation, which brings the centers of the chromophores within 9 Å of each other allowing them to couple and red shift their absorption spectrum. The circular structure allows the antenna to transfer energy in any direction which is advantageous for efficient energy transfer from the LH2 proteins to the LH1 and reaction center[12, 96].

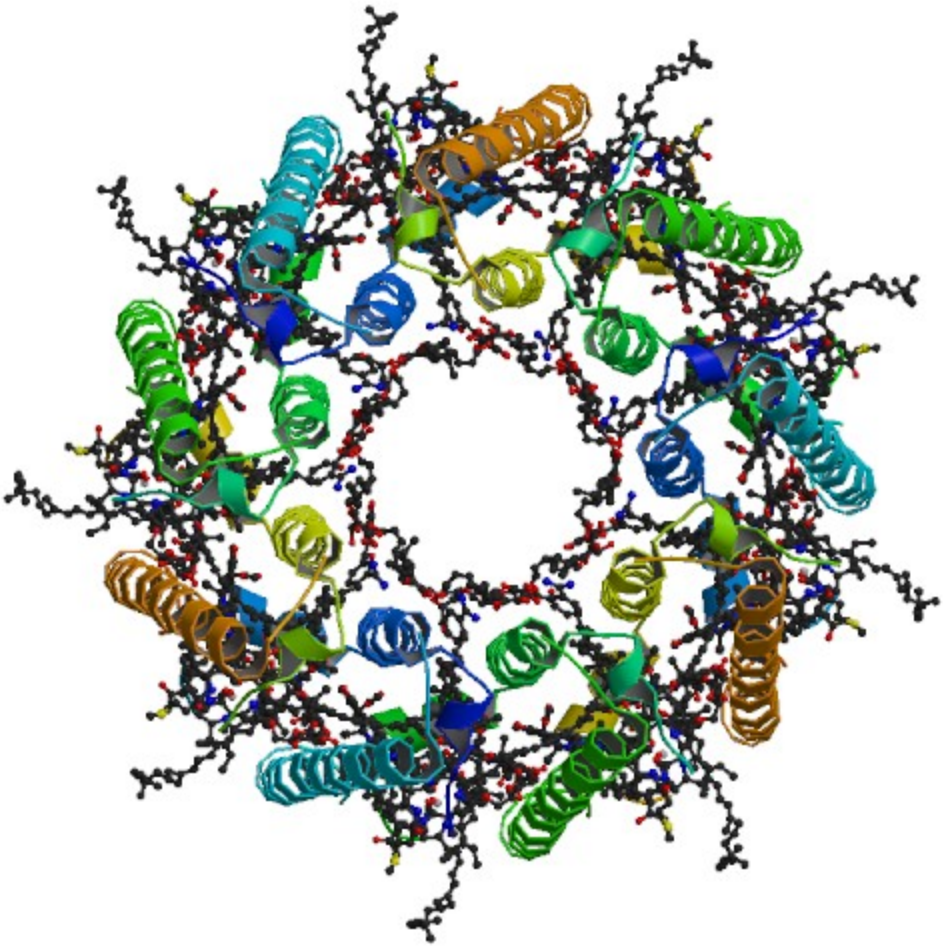

Figure 1. The crystal structure of LH2 from *Rhodopseudomonas acidiphila*[97].

Crystal structures provided valuable information about the structure and function of how the antenna proteins work. There are now additional methods to further understand how these proteins are able to transfer energy so efficiently. Atomic force microscopy (AFM) was able to image the proteins directly in the cell membrane as opposed to the crystal structures which are heavily treated for crystal formation. The AFM imaging shows that there is some irregularity in the protein assembly within the same membrane as well as between different species. For example, the number of subunits in LH2 and the elliptical shapes of LH1 instead of circles[98]. This means that the time-resolved studies that measured

the energy transfer rates resulted from an average of all the different chromophore interactions in all the different structures possible. This makes it difficult to accurately determine which distances and configurations of BChl are the most efficient systems. This is why we must explore the different structures on the nanoscale to understand which natural system is the most efficient, with the added benefit of learning how to start making solar harvesting devices.

There are several methods of creating nanoscale structures and patterns. For example, photolithography is able to print a variety of shapes and patterns on a glass surface[99], and there are many methods for creating nanoparticles with different metals and sizes[100]. Gold is a convenient metal for making nanoscale materials and is known to adsorb thiol compounds[99, 101]. Thus a method for attaching chromophores similar to that of the bacteriochlorophylls (BChl) in LH2 would require a thiol functional group to attach to the surface of these gold patterns in order to test their energy transfer kinetics and compare to the naturals system.

Phthalocyanine (Pc) absorb light in the blue, red, and near infrared regions of the electromagnetic spectrum which is similar to the absorption properties of the BChl in LH2. Pcs can also be synthesized with anchoring groups at different positions on the macrocycle to change its orientation relative to a surface. For example, Pc have been attached to glass slides using silane groups connected at the end of a long alkane chain at the periphery, or the edge, of the macrocycle[102]. Carotenoids have been attached peripherally to the Pc macrocycle[14], and axially through a silicon atom inserted into the middle of the Pc macrocycle[103]. Previous studies applying silicon phthalocyanines (SiPc) to a flat gold surface with thiol linkers positioned on the periphery and axially have been studied[104].

However their fluorescence was not investigated and the fluorescent properties are an important characteristic for singlet energy transfer in the LH proteins and is a process that we would like to recreate with supramolecular organization.

The crux of this project is the attaching of SiPc dyes to nanoscale surfaces. Several SiPc compounds and one porphyrin with short linkers were made first, and tested (Figure 2). The poor fluorescent and adsorption properties of this first set of compounds resulted in a mixed monolayer approach with longer alkane thiol ligands. This required the synthesis of SiPc molecules with long aliphatic linkers (Figure 3). They were mixed with supporting ligands on several different kinds of gold nanoparticles (AuNP) and patterned gold surfaces. Gold surface chemistry is an area that continues to develop as different compounds and materials are combined[105].

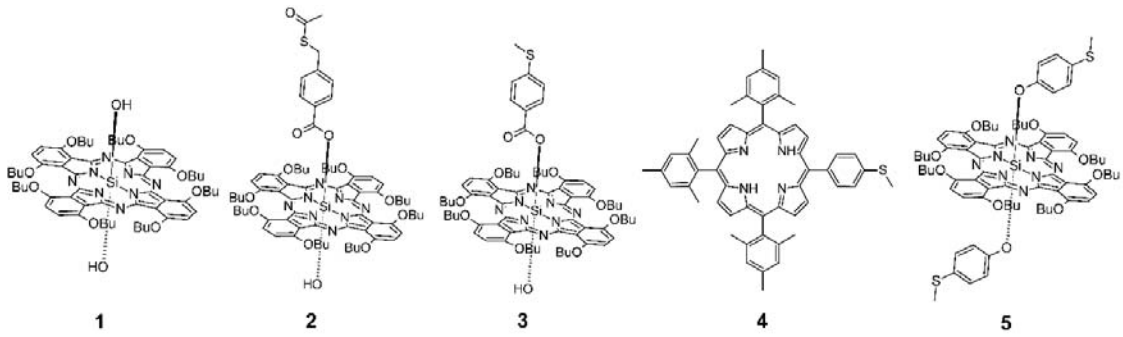

Figure 2: Structures of the silicon phthalocyanine (SiPc) precursor (**1**) of thioester containing SiPc dye **2** and methyl thioether **3** resulting from an esterification reaction of **1**. Structures of a methyl thioether porphyrin (**4**) and a methyl thioether SiPc resulting from an etherification reaction (**5**) of **1**.

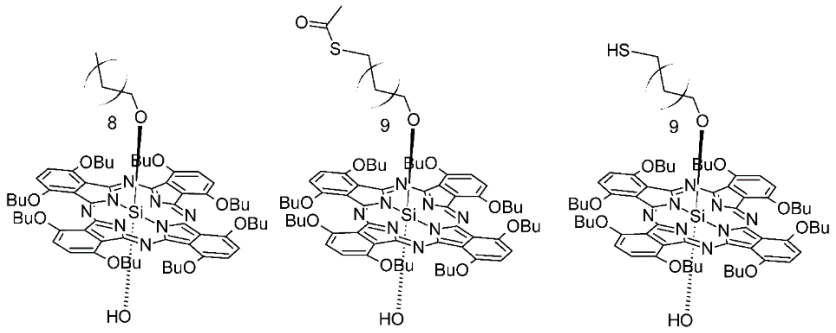

Figure 3. Structure of silicon phthalocyanines (SiPc) **6**, **7**, and **8**.

Materials and Methods

Materials. Pyridine, 2-picoline, distilled methanol, and distilled toluene were dried over activated 4 Å molecular sieves for use in reactions. Tributylamine was passed through activated neutral alumina and stored over activated 4 Å molecular sieves. Toluene, ethyl acetate, hexanes, and dichloromethane (DCM) used for chromatography were distilled. N-bromosuccinimide (NBS) was recrystallized from water before using in reactions. Trichlorosilane, 1,4,8,11,15,18,22,25-octabutoxy-29H,31H-phthalocyanine, 4-methylbenzoic acid, 4-dimethylaminopyridine (DMAP), thionyl chloride, potassium acetate, pyrrole, 4-(methylthio)benzoic acid, 4-(methylthio)benzaldehyde, 2,3-dichloro-5,6-dicyano-1,4-benzoquinone (DDQ), terthiophene, tetraoctyl ammonium bromide (TOAB), sodium borohydride, thioacetic acid, sodium thioacetate, sodium citrate, phenol, acetonitrile, anhydrous N,N-dimethylformaldehyde (DMF), and anhydrous N,N-dimethylacetamide (DMA) were purchased from Sigma-Aldrich and used without further purification. 4-(Methylthio)phenol was purchased from TCI America and used without further purification. Mesityl aldehyde, triethylamine, and carbon tetrachloride were purchased from Alfa Aesar and used without further purification. Chloroauric acid was purchased from Strem Chemicals and used without further purification. Deuterated

chloroform with 0.03% tetramethylsilane was purchased from Sigma-Aldrich and were stored over activated 4 Å molecular sieves and potassium hydroxide pellets at 4 °C. Deuterated methanol with 0.03% tetramethylsilane (TMS) was purchased from Cambridge Isotope Laboratories. Thin layer chromatography plates (250 μm), both fluorescent and non-fluorescent, were purchased from Analtech, Inc. Silica gel (SiliaFlash F60 40-63 μm) used for column chromatography was purchased from SILICYCLE. Size exclusion columns were performed with Sephadex LH-20 from GE Healthcare Life Sciences.

General. Proton nuclear magnetic resonance (^{1}H NMR) spectra were recorded on a 400 MHz Varian Liquid-State spectrometer. NMR samples were dissolved in deuterated chloroform or methanol with 0.03% TMS as an internal reference. Mass spectra were obtained using an Applied Biosystems Voyager-DE STR matrix-assisted laser desorption/ionization time-of-flight spectrometer (MALDI-TOF). The matrix used for all mass spectra samples was terthiophene.

Dihydroxyl-1,4,8,11,15,18,22,25-octabutoxyphthalocyaninatosilicon(IV) (**1**). Compound **1** was obtained following a literature procedure[106].

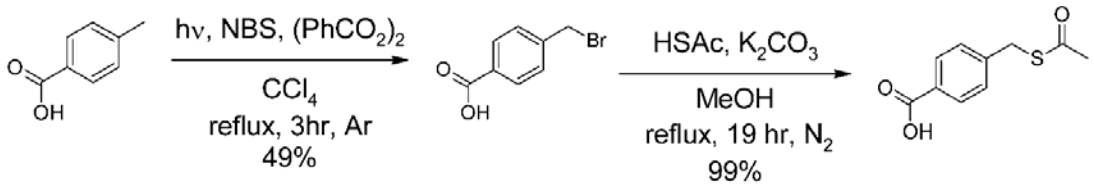

Scheme 1. Synthesis of 4-[(acetylsulfanyl)methyl]benzoic acid from 4-methylbenzoic acid.

4-(Bromomethyl)benzoic acid. This compound was prepared by modifying a published procedure[107]. Benzoyl peroxide (132 mg, 0.54 mmol, 0.04 eq), NBS (2.6 g, 14.7 mmol, 1.0 eq.), and 4-methylbenzoic acid (2.0 g, 14.7 mmol, 1.0 eq.) were dissolved in carbon tetrachloride (50 mL). The reaction mixture was heated to reflux and irradiated with

a 150 W bulb under an argon atmosphere for 4 hours. Once the reaction was complete it was cooled to room temperature and diluted into 150 mL of chloroform. The organic layer was washed twice with 0.2 M HCl (aq), washed once with water, and then washed once with 10% $NaHSO_3$ before drying with sodium sulfate. The organic solvent was removed and the white solid was recrystallized from methanol resulting in 1.56 g of the desired product (49% yield). ^{1}H-NMR (400 MHz, CD_3OD): δ 4.6 (2H, s, Br CH_2), 7.5 (2H, d, Ar H), 8.0 (2H, d, Ar H).

4-[(Acetylthio)methyl]benzoic acid. This compound was prepared by modifying a published procedure[108]. Potassium carbonate (578 mg, 4.18 mmol, 1.2 eq.), thioacetic acid (0.7 mL, 10.5 mmol, 3.0 eq.), and 4-(bromomethyl)benzoic acid (750 mg, 3.40 mmol, 1.0 eq.) were dissolved in 30 mL of distilled methanol. The reaction was heated to reflux under nitrogen and stirred for 19 hours. The reaction was cooled and then quenched with 5 mL of 12 M HCl (aq). The product was extracted with chloroform and the organic layer was washed with water twice before drying with brine and magnesium sulfate. The organic solvent was removed resulting in 712 mg of the product, a white solid (99% yield). ^{1}H-NMR (400 MHz, $CDCl_3$): δ 2.37 (3H, s, S-CH_3), 4.16 (2H, s, S-CH_2), 7.39 (2H, d, J=8.2 Hz, Ar H), 8.03 (2H, d, J=8.0 Hz, Ar H).

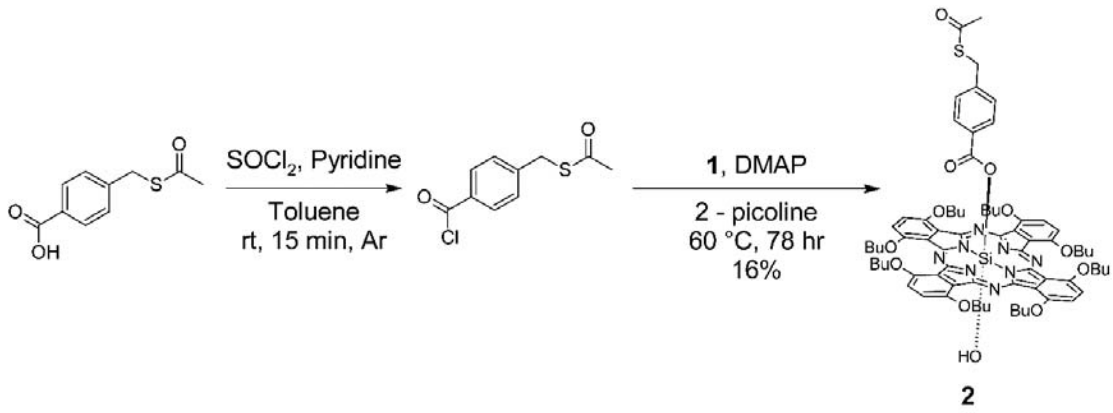

Scheme 2. Acid chloride formation of 4-[(acetylthiol)methyl]benzoic acid and esterification to **1**, for the formation of **2**.

4-[(Acetylthiol)methyl]benzoatehydroxide-1,4,8,11,15,18,22,25-octabutoxy-phthalocyaninatosilicon(IV) (**2**). The benzoic acid, 4-[(acetylthiol)methyl]benzoic acid, (217 mg, 1.03 mmol, 7.9 eq.) was dissolved in 10 mL of dry toluene and 5 mL of dry pyridine. The reaction solution was bubbled with nitrogen for 15 minutes before adding thionyl chloride (0.4 mL, 5.65 mmol, 43 eq.). The reaction stirred at room temperature for 20 minutes forming an orange precipitate. Once the acid chloride was formed the solvent was removed via vacuum and the acid chloride was dissolved in dry 2-picoline. To the solution, SiPc **1** (150 mg, 0.130 mmol, 1.0 eq.) was added and the mixture was allowed to react for 6 hours at 60 °C, and then DMAP (49 mg, 0.40 mmol, 3.0 eq.) was added. The reaction concluded after 72 hours, at which point the solvent was removed under vacuum and the products were purified using silica gel column chromatography with ethyl acetate/ toluene (1:3). This resulted in 27 mg, a 16% yield, of the desired product, a green solid. ^{1}H-NMR (400 MHz, $CDCl_3$): δ 1.05 (24h, t, butoxy CH_3), 1.64 (16H, m, butoxy-3 CH_2), 2.08 (3H, s, S-CH_3), 2.18 (16H, m, butoxy-2 CH_2), 3.51 (2H, s, AcS-CH_2), 4.81 (16H, m, butoxy-1 CH_2), 5.24 (2H, d, J=8.4 Hz, Ar H), 6.17 (2H, d, J=8.4 Hz, Ar H), 7.63 (8H, s, Pc-Ar H); MALDI-TOF-MS m/z: calculated for $C_{74}H_{90}N_8O_{12}SSi$ 1342.62 m/z, observed

1344 m/z, [(4-[(acetylsulfanyl)methyl]benzoate)-SiPc$^+$] 1326 m/z, and [(hydroxide)SiPc$^+$] 1134 m/z; UV/vis (DCM), λ_{max}: 334, 476, 694, and 780 nm.

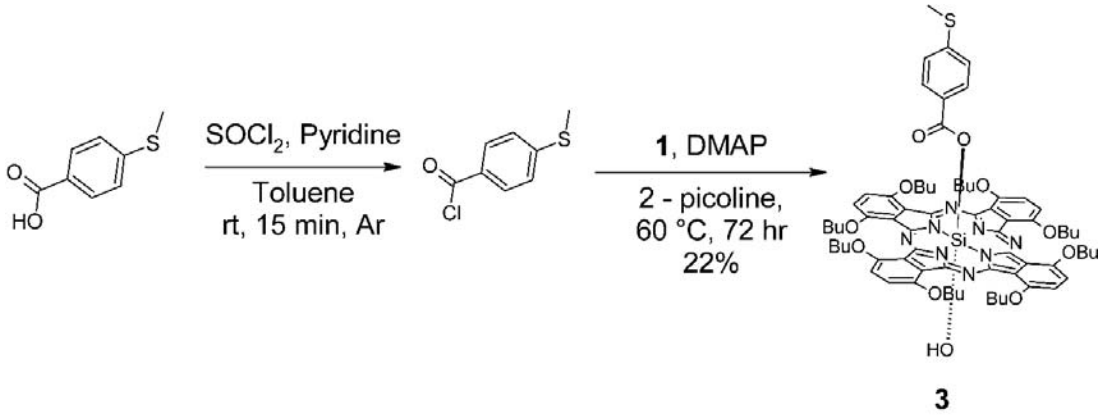

Scheme 3. Acid chloride formation of 4-(methylthiol)-benzoic acid and esterification to **1**, for the formation of **3**.

(4-Methylthiol)benzoatehydroxide-1,4,8,11,15,18,22,25-octabutox-phthalocyaninatosilicon(IV) (**3**). A 1:2 pyridine/toluene solution (15 mL) solution was used to dissolve 4-(methylthiol)benzoic acid (258 mg, 1.3 mmol, 10 eq) before it was bubbled with nitrogen for 15 minutes at room temperature. Then 0.4 mL of thionyl chloride (61 mmol, 467 eq.) was added to the solution and allowed to react for 15 minutes resulting in a yellow-white precipitant and hydrochloric gas. Once the acid chloride was formed the solvent was removed using vacuum. The acid chloride was dissolved into dry 2-picoline (13 mL), then SiPc **1** (150 mg, 0.13 mmol, 1 eq) and DMAP (105 mg, 0.86 mmol, 6.6 eq.) were added to the solution. The green reaction solution was heated to 60 °C and stirred for 72 hours. The solvent was removed, the products were dissolved in DCM and washed with water twice. The organic layer was dried with sodium sulfate before removing the solvent. The mono-coupled product was purified by column chromatography with ethyl acetate/toluene (3:7) as the eluent, resulting in 36 mg of the green solid (22% yield). ^{1}H-NMR (400 MHz, $CDCl_3$): δ 1.03 (24h, t, butoxy CH_3), 1.60 (16H, m, butoxy-3 CH_2), 1.98

(3H, s, S-CH_3), 2.16 (16H, m, butoxy-2 CH_2), 4.77 (16H, m, butoxy-1 CH_2), 5.20 (2H, d, J=8.8 Hz, Ar H), 6.08 (2H, d, J=8.8 Hz, Ar H), 7.60 (8H, s, Pc-Ar H); MALDI-TOF-MS m/z: calculated for $C_{72}H_{88}N_8O_{11}SSi$ 1300.61 m/z, observed 1301.93 m/z, [(4-(methylthiol)benzoate)-$SiPc^+$] 1284.84 m/z, and [(hydroxide)$SiPc^+$] 1134.87 m/z; UV/vis (DCM), λ_{max}: 333, 476, 697, and 781 nm.

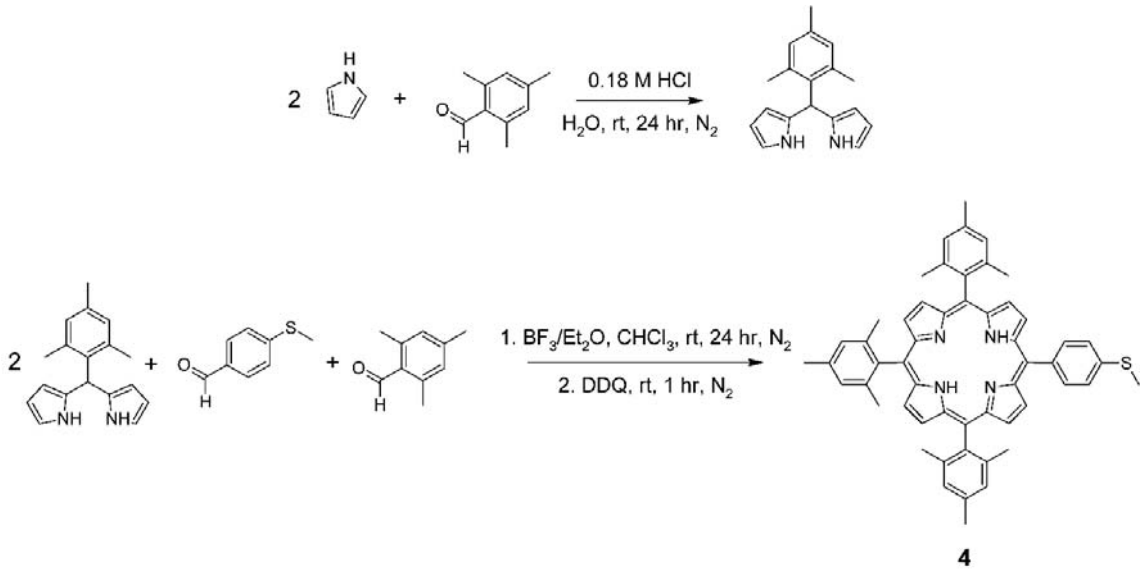

Scheme 4. Synthesis of mesityl-dipyrromethane and tri-mesityl porphyrin **4** using a general Alder-Longo method.

5-(4-Methylmercaptophenyl)-10,15,20-trimesitylporphyrin (4). Compound **4** was synthesized based on a previously published procedure using the Alder-Long synthesis[68, 109]. Freshly distilled pyrrole (3 mL, 45 mmol, 3.0 eq), mesityl aldehyde (2 mL, 15 mmol, 1.0 eq), and 12 M HCl (1.5 mL, 49 mmol, 3.1 eq.) were dissolved in 98.5 mL of water and stirred at room temperature under argon for 20 hours. The solids were filtered and washed with water and 40-60 °C boiling point petroleum ether. The mesityl dipyrromethane (DPM) was eluted from a flash column using hexanes/DCM (3:7) and then the solvent was removed. Two crystallizations using hexane/DCM resulted in 1.58 g of a green solid which was used directly in the next step. Mesityl DPM (700 mg, 2.6 mmol, 2.0 eq), mesityl

aldehyde (0.2 mL, 1.3 mmol, 1.0 eq), 4-(methylthiol)benzaldehyde (0.2 mL, 1.3 mmol, 1.0 eq.), and absolute ethanol (0.2 mL, 3.5 mmol, 2.7 eq.) were dissolved in 240 mL of chloroform and bubbled with argon for 1 hour over ice. Then 25 mL of a 30 mM BF_3/Et_2O (chloroform) was added to the aldehyde-DPM reaction mixture and stirred for 75 minutes under argon. To the dark brown reaction solution DDQ was added and the reaction mixture was exposed to air for the oxidation. After 2 hours the reaction solution was filtered over a pad of silica, it was washed with hexanes/DCM (2:3) until all of the porphyrins were removed, and then the solvent was removed. For easier separations to obtain the desired asymmetrical porphyrin zinc was introduced into the center of the macrocycle by dissolving the porphyrins (12 mg, 0.015 mmol, 1.0 eq) into DCM (5 mL) and methanol (1 mL) and mixing with zinc acetate dehydrate (34 mg, 0.15 mmol, 10 eq) for 2 hours at room temperature. The desired porphyrin was purified by column chromatography using hexanes/DCM (45:65). The zinc was removed in acidic conditions (TFA/DCM) for 4 hours, neutralized, extracted, and then the solvent removed producing the desired porphyrin as a purple solid. ^{1}H-NMR (400 MHz, $CDCl_3$): δ -2.55 (2H, s, NH), 1.83 (18H, s, mesityl CH_3), 2.60 (9H, s, mesityl CH_3), 2.73 (3H, s, S-CH_3), 7.55 (6H, s, mesityl-Ar H), 7.60 (2H, d, MeS-Ar H), 8.08 (2H, d, MeS-Ar H), 8.60 (4H, s, β-pyrrole), 8.65 (2H, d, β-pyrrole), 8.77 (2H, d, β-pyrrole); MALDI-TOF-MS m/z: calculated for $C_{54}H_{50}N_4S$ 1394.63 m/z, observed 1256.65 m/z; UV/vis (1:4 ethyl acetate/acetonitrile) λ_{max} 417, 513, 590, and 647 nm.

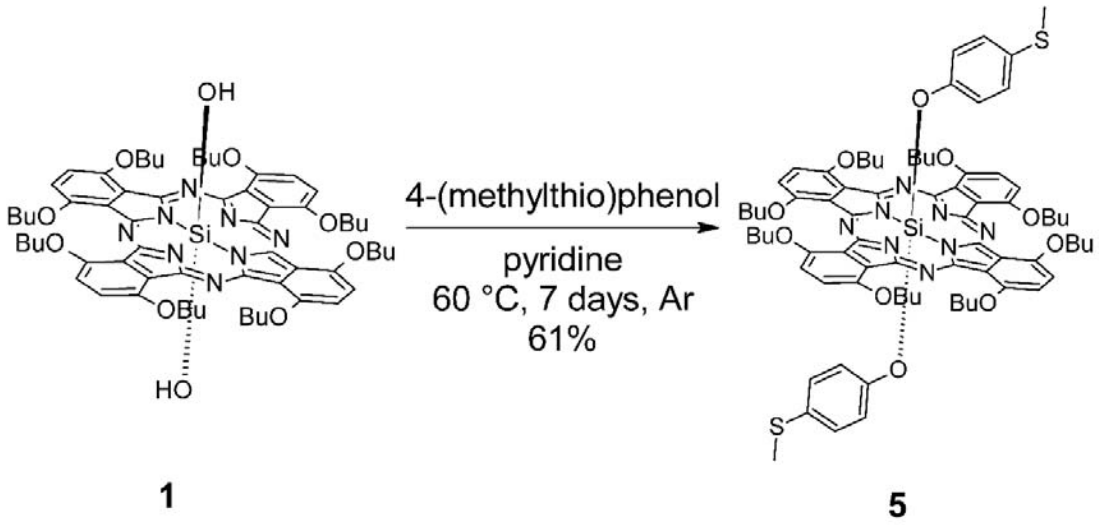

1 **5**

Scheme 5. Synthesis of silicon phthalocyanine **5** from **1**.

Bis-(4-(methythio)-phenol)-1,4,8,11,15,18,22,25-octabutoxyphthalocyaninato-silicon(IV) (**5**). 4-(Methylthio)phenol (567 mg, 4.04 mmol, 46 eq.) and SiPc **1** (100 mg, 0.087 mmol, 1.0 eq.) were dissolved in 5 mL of dry pyridine and bubbled with argon for 15 minutes before heating to 60 °C and stirring for 7 days. The solvent was removed using vacuum and the green solid was purified using silica column chromatography with ethyl acetate/toluene (1:2) as the eluent. This resulted in 68 mg of the product (61% yield). ^{1}H-NMR (400 MHz, $CDCl_3$): δ 1.06 (24H, t, butoxy CH_3), 1.67 (16H, m, butoxy-3 CH_2), 1.76 (6H, s, S-CH_3), 2.12 (16H, m, butoxy-2 CH_2), 2.82 (4H, d, J=8.4 Hz, Ar H), 4.77 (16H, t, butoxy-1 CH_2, 5.55 (4H, d, J=8.4 Hz, Ar H), 7.55 (8H, s, Pc-Ar H); MALDI-TOF-MS m/z: calculated for $C_{78}H_{94}N_8O_{10}S_2Si$ 1394.63 m/z, observed 1256.65 m/z [(4-(methylthio)-phenol)-$SiPc^+$]; UV/vis (DCM) λ_{max} 339, 475, 695, and 781 nm.

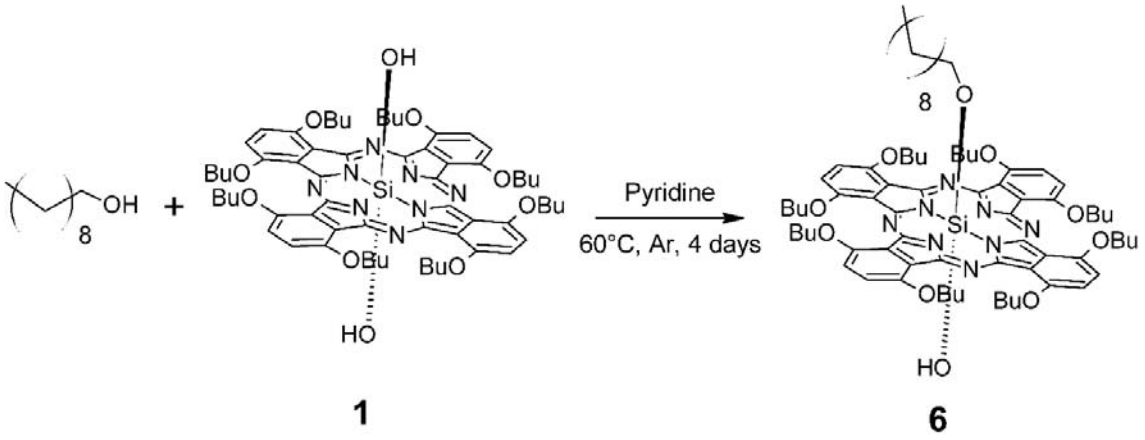

Scheme 6. Synthesis of silicon phthalocyanine **6** from **1**.

Decanolhydroxide-1,4,8,11,15,18,22,25-octabutoxyphthalocyaninatosilicon(IV) (**6**). The reagents, SiPc **1** (50 mg, 0.04 mmol, 1.0 eq.) and 1-decanol (12 μL, 0.26 mmol, 6.5 eq), were dissolved in 4 mL of dry pyridine. The green solution was bubbled with argon for 30 minutes before heating to 60 °C for 4 days. After cooling to room temperature, the solvent was removed, then the green product was dissolved in DCM and washed twice with water. Then the organic layer was washed with brine and dried with sodium sulfate before removing the solvent. The desired product was purified by silica gel column chromatography starting with 1:4 ethyl acetate/toluene as the eluent and slowly increasing the polarity to 2:3 ethyl acetate/toluene. ^{1}H-NMR (400 MHz, $CDCl_3$): δ -1.72 (2H, t, n-decyl-1 CH_2), -1.45 (2H, p, n-decyl-2 CH_2), -1.14 (2H, p, n-decyl-3 CH_2), -0.22 (2H, p, n-decyl-4 CH_2), 0.26 (2H, p, n-decyl-5 CH_2), 0.54 (2H, p, n-decyl-6 CH_2), 0.73 (2H, p, n-decyl-7 CH_2), 0.75 (2H, t, n-decyl-10 CH_3), 0.79 (2H, p, n-decyl-8 CH_2), 1.03 (24h, t, butoxy CH_3), 1.08 (2H, p, n-decyl-9 CH_2), 1.62 (16H, m, butoxy-3 CH_2), 2.23 (12H, m, butoxy-2 CH_2), 4.85 (12H, m, butoxy-1 CH_2), 7.62 (8H, s, Pc-Ar H); MALDI-TOF-MS m/z: calculated for $C_{74}H_{102}N_8O_{10}Si$ 1290.74 m/z, observed 1290.84 m/z, [(n-decyl)-$SiPc^+$]

1273.98 m/z, and [(hydroxide)-SiPc^{+}] 1333.78 m/z; UV/vis (ethanol) λ_{max} 335, 465, 682, and 766 nm.

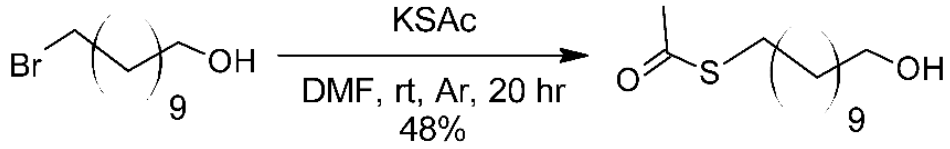

Scheme 7. Synthesis of S-(11-hydroxyundecyl)thioacetate.

S-(11-hydroxyundecyl)thioacetate. This compound was synthesized based on a previously published procedure by M. Wijtmans *et al.*[110]. 11-Bromoundecanol (1.0 g, 4.0 mmol, 1.0 eq.) and potassium thioacetate (0.941 g, 8 mmol, 2.0 eq.) were dissolved in 20 mL of anhydrous DMF. The reaction mixture was stirred at room temperature, for 24 hours under argon before quenching the reaction with water. The product was extracted with diethyl ether, which was brown in color, and washed with water several times before drying with magnesium sulfate. Once the solvent was removed an amber brown liquid resulted and the white product was crystalized from diethyl ether and hexanes (0.498 g, 50% yield). ^{1}H-NMR (400 MHz, $CDCl_3$): δ 1.22 (14H, m, n-decyl-3 to 9 CH_2), 1.56 (4H, m, n-decyl-2 and 10 CH_2), 2.32 (3H, s, SAc CH_3), 2.86 (2H, t, n-decyl-11 CH_2), 3.64 (2H, q, n-decyl-1 CH_2).

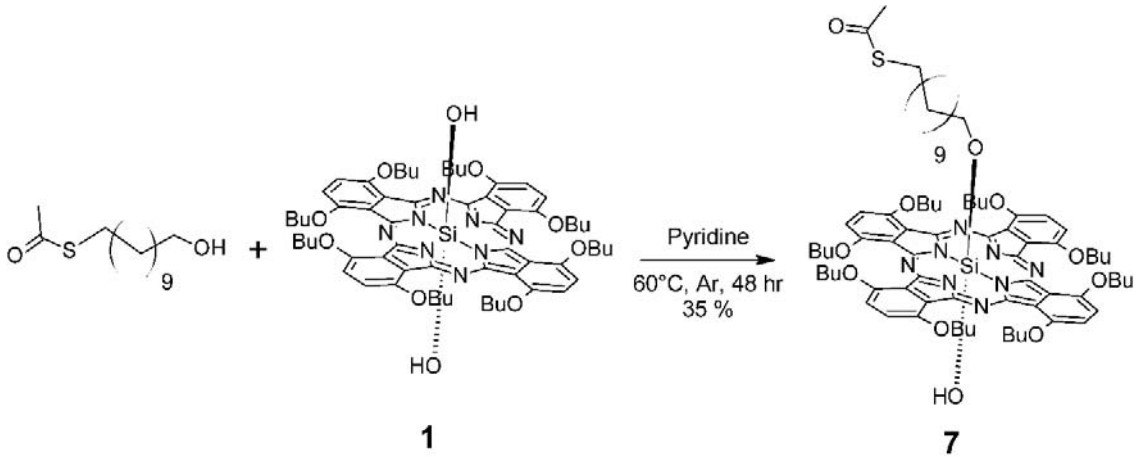

Scheme 8. Synthesis of silicon phthalocyanine **7** from **1**.

S-(11-hydroxyundecyl)thioacetatehydroxide-1,4,8,11,15,18,22,25-octabutoxy-phthalocyaninatosilicon(IV) (**7**). S-(11-hydroxyundecyl)thioacetate (30 mg, 0.12 mmol, 3.0 eq.) and SiPc **1** (50 mg, 0.04 mmol, 1.0 eq.) were dissolved in 4 mL of dry pyridine and bubbled with argon for 30 minutes. The dark green reaction mixture was stirred at 60 °C for 4 days and monitored by TLC for product formation. The pyridine was removed before purifying the desired product by column chromatography using ethyl acetate/toluene (3:7) as the eluent, which afforded 17.7 mg of the dark green solid (35% yield). ^{1}H-NMR (400 MHz, $CDCl_3$): δ -1.73 (2H, t, n-undecyl-1 CH_2), -1.46 (2H, p, n-undecyl-2 CH_2), -1.14 (2H, p, n-undecyl-3 CH_2), -0.23 (2H, p, n-undecyl-4 CH_2), 0.26 (2H, p, n-undecyl-5 CH_2), 0.54 (2H, p, n-undecyl-6 CH_2), 0.79 (2H, p, n-undecyl-7 CH_2), 0.96 (2H, p, n-undecyl-8 CH_2), 1.08 (24H, t, butoxy CH_3), 1.13 (2H, p, n-undecyl-9 CH_2), 1.42 (2H, p, n-undecyl-10 CH_2), 1.65 (16H, m, butoxy-3 CH_2), 2.20 (12H, m, butoxy-2 CH_2), 2.28 (3H, s, SAc CH_3), 2.77 (2H, t, n-undecyl-11 CH_2), 4.87 (12H, t, butoxy-1 CH_2), 7.63 (8H, s, Pc-Ar H); MALDI-TOF-MS m/z: calculated for $C_{77}H_{106}N_8O_{11}SSi$ 1378.75 m/z, observed 1378.70 m/z, [(S-(11-hydroxyundecyl)thioacetate)-$SiPc^+$] 1361.75 m/z, and [(hydroxide)-$SiPc^+$] 1133.60 m/z; UV/vis (ethyl acetate) λ_{max} 331, 666, and 744 nm.

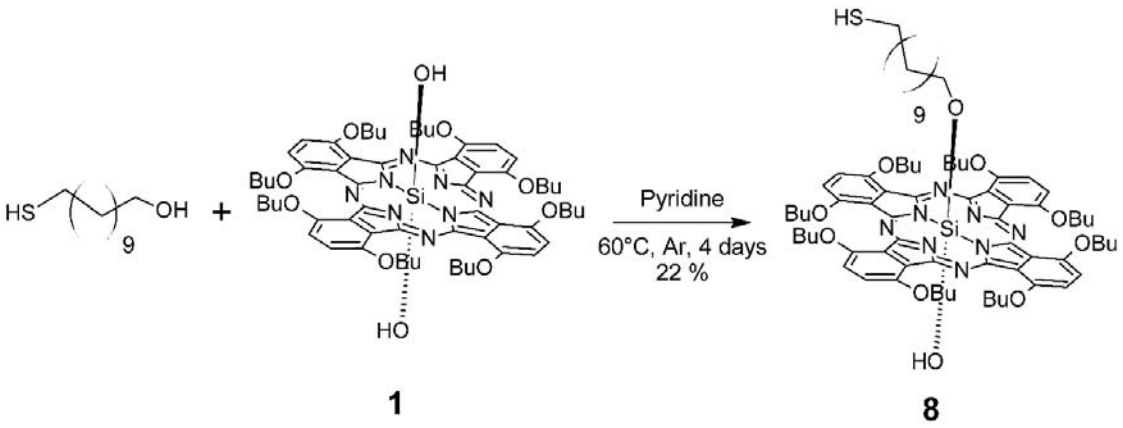

Scheme 9. Synthesis of silicon phthalocyanine **8** from **1**.

11-Mercaptoundecanolhydroxide-1,4,8,11,15,18,22,25-octabutoxy-phthalocyaninatosilicon(IV) (**8**). The reagents, SiPc **1** (400 mg, 0.35 mmol, 1.0 eq.) and 11-mercaptoundecanol (286 mg, 1.4 mmol, 4.0 eq), were dissolved in 10 mL of dry pyridine. The green solution was bubbled with argon for 30 minutes before heating to 60 °C for 4 days. After cooling to room temperature, the green product was dissolved in DCM and washed three times with dilute HCl until the pH was neutral. Then the organic layer was dried with a brine wash and sodium sulfate before removing the solvent. The desired product was purified by column chromatography using triethylamine/ethyl acetate/toluene (0.5:24.5:75) as the eluent. This afforded a dark green, waxy solid (103 mg, 22% yield). ^{1}H-NMR (400 MHz, $CDCl_3$):δ -1.72 (2H, t, n-undecyl-1 CH_2), -1.46 (2H, p, n-undecyl-2 CH_2), -1.14 (2H, p, n-undecyl-3 CH_2), -0.22 (2H, p, n-undecyl-4 CH_2), 0.26 (2H, p, n-undecyl-5 CH_2), 0.54 (2H, p, n-undecyl-6 CH_2), 0.80 (2H, p, n-undecyl-7 CH_2), 0.95 (2H, p, n-undecyl-8 CH_2), 1.08 (24h, t, butoxy CH_3), 1.15 (2H, p, n-undecyl-9 CH_2), 1.46 (2H, p, n-undecyl-10 CH_2), 1.67 (16H, m, butoxy-3 CH_2), 2.23 (12H, m, butoxy-2 CH_2), 2.42 (2H, t, n-undecyl-11 CH_2), 4.89 (12H, t, butoxy-1 CH_2), 7.64 (8H, s, Pc-Ar H); MALDI-TOF-MS m/z: calculated for $C_{86}H_{125}N_8O_{10}SSi$ 1522.87 m/z, observed 1522.43 m/z, [(11-

mercaptoundecanol)-SiPc^{+}] 1320.25 m/z, and [(hydroxide)-SiPc^{+}] 1134.05 m/z; UV/vis (DCM) λ_{max} 336, 467, 683, and 766 nm.

Synthesis of gold nanoparticles.

Unprotected AuNP. Unprotected gold nanoparticles were synthesized photochemically by Erica Wee at the University of Ottawa, using a previously published method[111]. The size was confirmed to be 20 nm by scanning electron microscopy (Figure 4) and it had a concentration of 0.3 mM AuNP (aq). A stock of the AuNP dilute in 1:4 water/acetonitrile was made to attach the SiPc molecules. Stock solutions of the unprotected AuNP in 1:1 ethanol/water were made by centrifuging the AuNP (aq) solution, removing half the volume of supernatant, replacing it with 200 proof ethanol, and then suspending the nanoparticles via sonication.

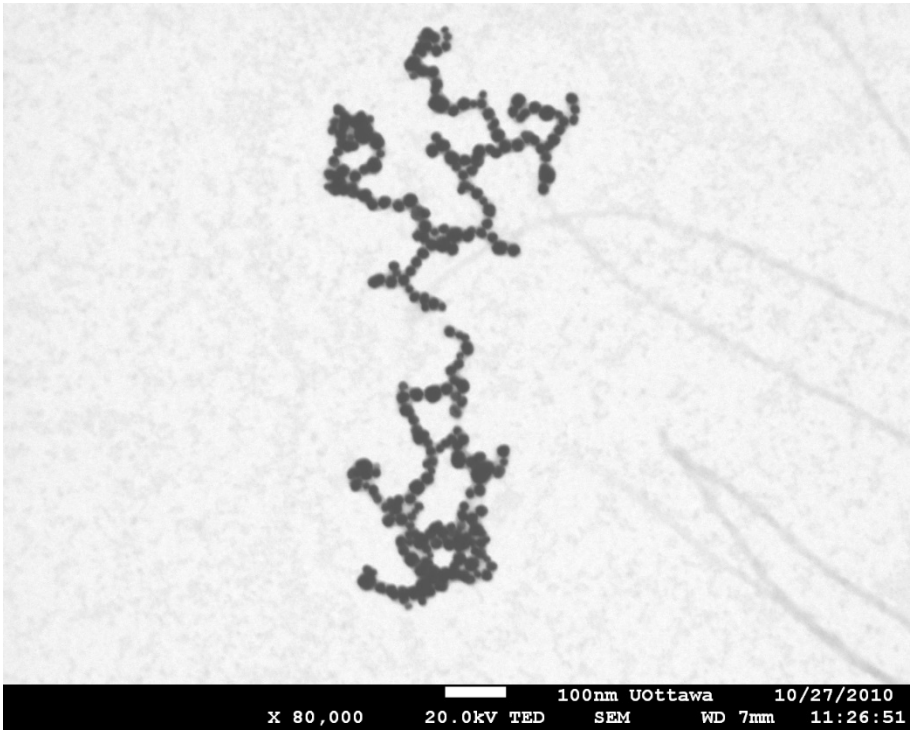

Figure 4. Scanning electron microscopy image of unprotected AuNP have an average 20 nm from the University of Ottawa.

General method for monoprotected clusters (MPC). The MPC were obtained following a literature procedure[112]. Chloroauric acid (80.8 mg, 0.234 mmol, 1.0 eq.) was dissolved in 7.8 mL of water and stirred at room temperature In a separate container tetraoctyl ammonium bromide (TOAB; 332 mg, 1.03 mmol, 4.4 eq.) was dissolved in distilled toluene before adding to the chloroauric acid solution. This created a two phase solution in which the aqueous layer turned from yellow to clear and the organic layer turned red. Then the thiol capping group (0.234 mmol, 1.0 eq.) was added to the two-phase solution causing the organic layer to turn from red to orange. After 20 minutes of stirring, granular sodium borohydride (100 mg, 2.64 mmol, 11.3 eq.) dissolved in 6.6 mL of water was slowly added to the two phase reaction, over 20 second duration, resulting in bubbling and the organic layer to change from orange to purple-brown. This two-phase solution was stirred vigorously for 1 hour at room temperature before washing the excess ligands, salts, and TOAB from the MPCs.

MPC with 1-octanethiol capping group. To the two-phase solution (toluene with TOAB and water with chloroauric acid from the general method) 1-octanethiol (40.6 μL, 0.234 mmol, 1.0 eq.) was added. Once the MPC were formed purification was performed by removing the aqueous layer and then aggregating the MPCs in cold toluene overnight. Then the purple precipitate was filtered and washed with copious amounts of water and ethanol. The purple solid was then dissolved in DCM, for storage and experiments.

MPC with 11-mercaptoundecanol capping group. To the two-phase solution 11-mercaptoundecanol (47.8 mg, 0.234 mmol, 1.0 eq.) was added. Once the MPC were formed purification was performed by filtering and washing with water and toluene. The purple solid was then dissolved in a minimal amount of ethanol, aggregated with DCM, filtered,

washed with DCM, and then the purple solid was dissolved in ethanol again for experiments.

MPC with SiPc 8 and 1-octanethiol as capping groups. To the two-phase solution 1-octanethiol (36 μL, 0.207 mmol, 0.88 eq.) and 40 μL a 30 mM (toluene) solution of SiPc **8** (0.027 mmol, 0.12 eq.) were added. Purification was performed by filtering and washing with water and toluene after the MPC were formed. The purple solid was then dissolved in a minimal amount of DCM, aggregated with ethanol, filtered, washed with ethanol, and then the purple solid was dissolved in DCM again for experiments.

MPC with SiPc 8 and 11-mercaptoundecanol as capping groups. 11-Mercaptoundecanol (15 mg, 0.734 mmol, 0.88 eq.) and 40 μL a 30 mM (toluene) solution of SiPc **8** (0.027 mmol, 0.12 eq.) were added to the two-phase solution. Once the MPC were formed the aqueous layer was removed and the organic layer dried. The purple solid was then dissolved in a minimal amount of ethanol, aggregated with 1:1 DCM/hexanes, filtered, washed with ethanol, and then the purple solid was dissolved in ethanol again for experiments.

MPC with SiPc 8 as a capping group. To the two-phase solution 290 μL of a 30 mM SiPc **8** toluene solution (0.028 mmol, 0.13 eq.) was added. Once the MPC were formed the organic layer was removed and the dried. The dark blue solid was then dissolved in a minimal amount of toluene, aggregation was attempted with DCM and hexanes but this resulted in an insoluble oily solid.

Citrate stabilized AuNP. Citrate stabilized AuNP in water were synthesized based on a previously published procedure[113]. Chloroauric acid (10 mg, 0.029 mmol) was dissolved in 100 mL water and then heated in a flask with stirring to 100 °C. Then 10 mL

of 1% sodium citrate was added to the solution turning the solution a purple-blue color and the reaction solution was stirred for one hour. This resulted in a surface plasmon band absorption at 525 nm and 30 nm nanoparticles by TEM (Figure 5).

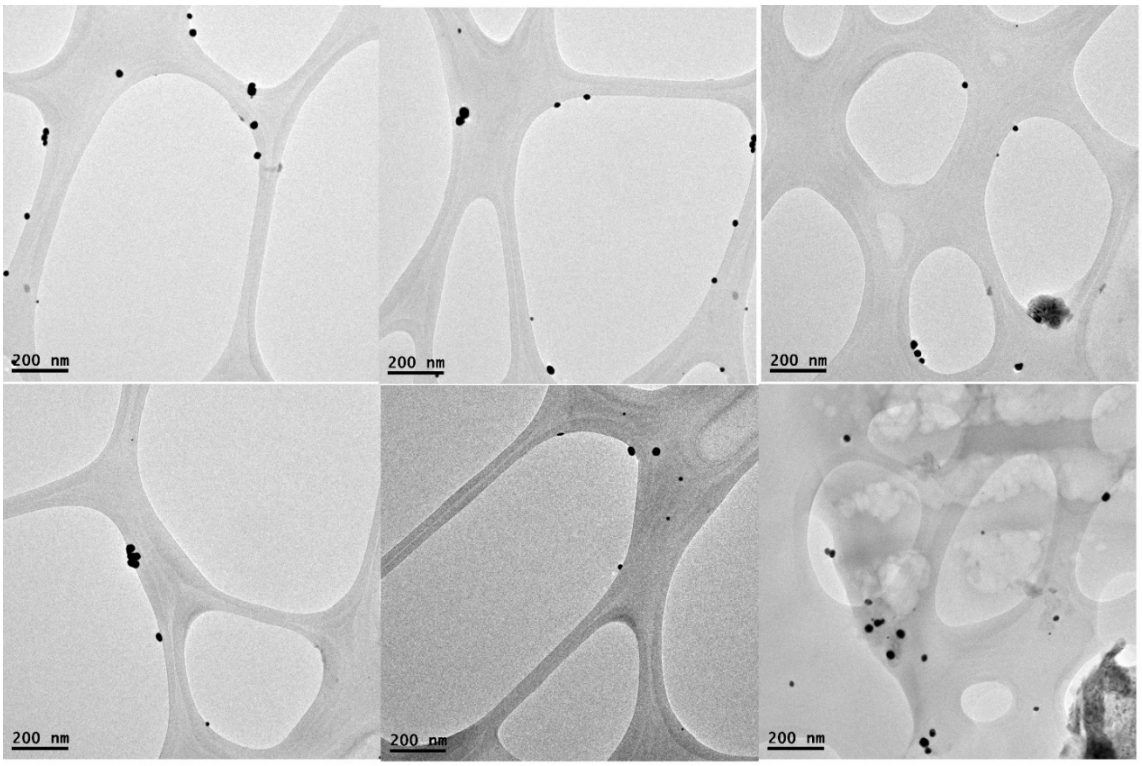

Figure 5. TEM micrographs of citrate stabilized AuNP with an approximately 30 nm diameter.

Attachment of silicon phthalocyanines to gold surfaces.

Unprotected AuNP. One mM stock solutions of SiPc **1** and SiPc **4** in ethyl acetate were made for attaching the SiPc to unprotected AuNP. Six samples were made: 1) solvent control with 1:4 ethyl acetate/acetonitrile, 2) SiPc **1** control with 200 µL of the SiPc **1** stock solution and 800 µL of acetonitrile, 3) SiPc **4** control with 200 µL of the SiPc **4** stock solution and 800 µL of acetonitrile, 4) AuNP control with 200 µL acetonitrile and 800 µL of the AuNP stock solution in acetonitrile, 5) SiPc **1** control with 200 µL of the SiPc stock solution and 800 µL of the AuNP stock solution, and 6) 200 µL of the SiPc **4** stock solution

mixed with 800 μL of the AuNP stock solution. The samples were diluted 1:30 to measure the absorption and emission spectra were measured after the reaction mixed at room temperature without exposure to light.

AuNP in 1:1 ethanol/water were combined with 0.015, 0.030, and 0.060 mM aqueous solutions of 4-(methylthiol)phenol or phenol. The samples were mixed and then monitored over several hours and days using absorption spectroscopy.

Stock solutions of SiPc **7**, 1-octanethiol, and S-(11-hydroxyundecyl)thioacetate in acetonitrile were made and then added to aqueous solutions of the unprotected AuNP resulting in six samples with a 1:100 acetonitrile/water solution: 1) unprotected AuNP, 2) 2.35 μM 1-ocatanethiol, 3) 0.185 μM S-(11-hydroxyundecyl)thioacetate, 4) 0.228 μM S-(11-hydroxyundecyl)thioacetate and 42.6 μM 1-octanethiol, 5) 0.233 μM SiPc **7**, and 6) 42.6 μM 1-octanethiol and 0.233 μM SiPc **7**. These solutions were allowed to mix for 4 hours before they were centrifuged, then the supernatant was removed and replaced with ethyl acetate. This was allowed to sit overnight in the dark before examining by TEM microscopy, absorption and emission spectroscopy.

Six 1 mL samples of the unprotected AuNP (1:1 ethanol/water) with various concentrations of protecting ligands were made and their absorption spectra were observed over time: 1) 10 mM S-(11-hydroxyundecyl)thioacetate, 2) 1.0 mM S-(11-hydroxyundecyl)thioacetate, 3) 0.1 mM S-(11-hydroxyundecyl)thioacetate, 4) 10 mM 6-mercaptohexanol, 5) 1.0 mM 6-mercaptohexanol, and 6) 0.1 mM 6-mercaptohexanol.

Mixed monolayer samples using 1:1 or 1:9 molar ratios of SiPc **7** and 6-mercaptohexanol, totaling 1.0 mM of the ligands, were mixed with AuNP in 1:1

ethanol/water for 4 hours before centrifuging and washing with ethanol two times. Their absorption and emission spectra were measured.

Monoprotected clusters. Attachment of SiPc **1** to MPC capped with 11-mercaptoundecanol was attempted. The MPC (1.5 mg) and 2.5 mg of SiPc **1** were dissolved in 0.5 mL of dry pyridine and stirred under an argon atmosphere in the dark at 50 °C for 3 days. The reaction solution was dissolved in 1 mL ethanol and the excess SiPc **1** was separated from the MPC using a size exclusion column in ethanol. The MPCs (confirmed by absorption spectroscopy and TLC as a dark purple immobile base spot) eluted first as a dark green-brown band and was followed by a green band containing the excess SiPc **1**. Reproducibility of this separation proved difficult.

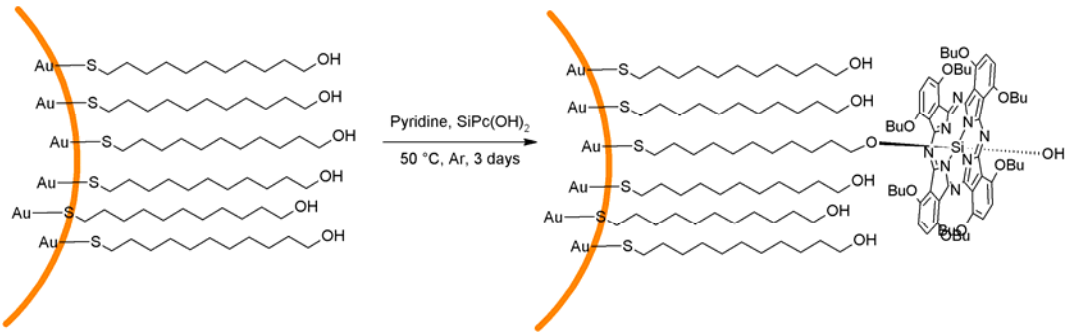

Scheme 10. Reaction method for attaching the SiPc **1** to an 11-mercaptoundecanol MPC (orange) as a mixed monolayer on AuNP.

Surface modification of citrate stabilized AuNP. 11-Mercaptoundecanol and SiPc **8** were dissolved in DMA and then added to the citrate stabilized AuNP in water for a total volume of 4 mL with a 1:3 DMA/water or 100% ethanol solution. Three mixtures containing different ratios of SiPc **8** and 11-mercaptoundecanol were made: 1) 11 µM 11-mercaptoundecanol and 25 µM SiPc **8** for a 5:9 ratio, 2) 26 µM 11-mercaptoundecanol and 2.6 µM SiPc **8** for a 10:1 ratio, and 3) 26 µM 11-mercaptoundecanol and 0.26 µM SiPc **8** for a 5:9 ratio 100:1. These samples were kept under an argon atmosphere and in the dark

to prevent degradation and oxidation. After seven days in these conditions the samples were purified centrifuged, supernatant removed, dissolved in small volumes (0.25 mL) of ethanol. This process was repeated again to remove excess ligands before submitting the sample to a Sephadex LH-20 size exclusion column, in 1:3 DMA/water or ethanol, resulting in three visible bands. Only the 5:9 mixed monolayer ratio resulted in the first band that contained the desired AuNP and SiPc, the remaining samples aggregated at the top of the size exclusion column and did not elute from the column.

Ligand exchange with MPC. MPC with 1-octanethiol (1.5 mg) were dissolved in 1.0 mL DCM and MPCs capped with 11-mercaptoundecanol (1.5 mg) were dissolved in 1.0 mL of ethanol. To each MPC solution, 1.0 mg of SiPc **8** was added and the solutions were bubbled with argon for 10 minutes to remove oxygen. They were kept in sealed vials in the dark for 4 days with stirring. The samples were purified using size exclusion columns with their respective solvents, DCM or ethanol.

Patterned gold surfaces. Glass slides with patterned gold surfaces were made using lithographic techniques in the James Watt Nanofabrication Center at the University of Glasgow (Figure 6).

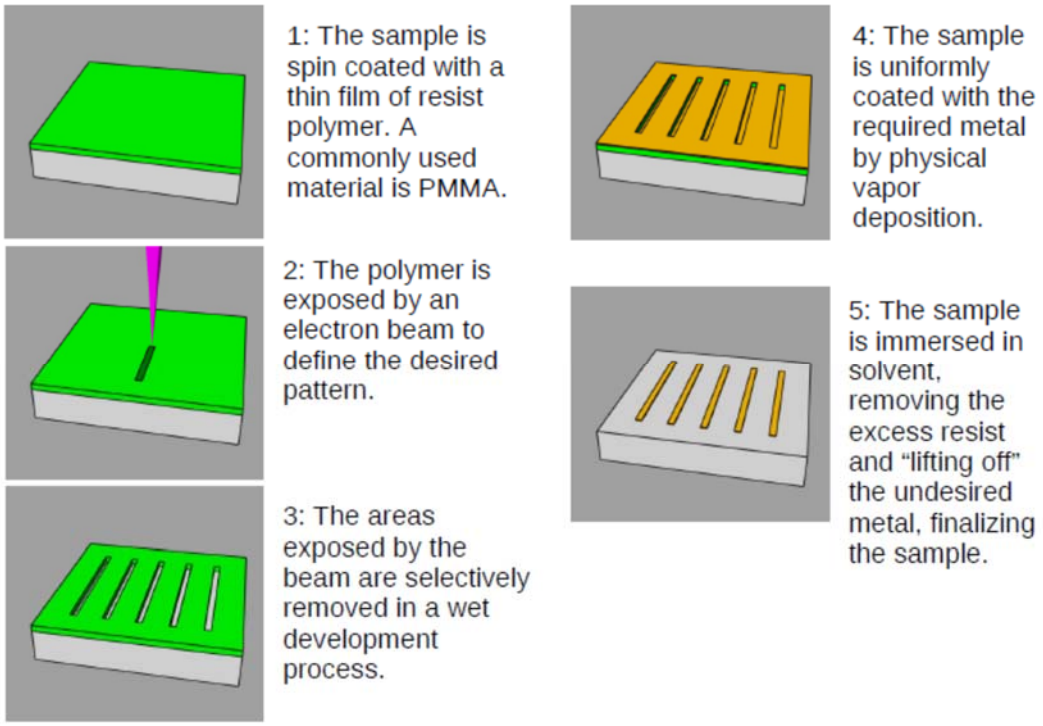

Figure 6. Fabrication process used to make the gold slide pattern at the James Watt Nanofabrication Center, Glasgow, UK.

Then patterned surfaces were washed with piranha solution (1:1 hydrogen peroxide and concentrated sulfuric acid), washed with copious amounts of water, and dried using a flow of nitrogen before soaking in solutions containing SiPc **8**. Eight different samples were made using two different concentrations (1.0 mM and 10 μM), two different supporting ligands (decanethiol and 11-mercaptoundecanol), and two different ratios (1:10 and 1:100) of the SiPc **8** and the supporting ligand in ethanol solutions. In addition, eight controls were made: 1) untreated slide, 2) ethanol solution, 3) 1.0 mM SiPc **8**, 4) 10 μM SiPc **8**, 5) 1.0 mM 1-octanethiol, 6) 10 μM 1-octanethiol, 7) 1.0 mM 11-mercaptoundecanol, and 8) 10 μM 11-mercaptoundecanol. The solutions were bubbled with argon before mixing and soaking the slides for at least 4 days under argon atmosphere. Before measuring their fluorescence, the slides were rinsed with ethanol, then they were

rinsed with DCM, they were sonicated in a DCM solution for 1 minute, rinsed a second time with DCM, and then dried with a compressed nitrogen.

Transmission electron microscopy. TEM micrographs were collected using a Phillips CM200 TEM at 200 kV. The AuNPs were placed onto a carbon coated copper grid (Canemoco, Lakefield, QC, Canada) by dipping the grids in to the solution and air drying. Images were acquired with the Gatan Orius CCD camera.

FTIR spectroscopy. FTIR spectra were obtained using a Thermo Scientific Nicolet 380 spectrometer taken at ambient conditions. Spectra were measured using the Omnic program that came with the spectrometer.

Absorption and fluorescence spectroscopy. Absorption spectra were measured on a Shimadzu UV-3101PC UV-vis-NIR spectrometer. Steady-state fluorescence spectra were measured using a Photon Technology International MP-1 spectrometer and corrected for detection system response. Excitation was provided by a 75 W xenon-arc lamp and single grating monochromator. Fluorescence was detected 90^{o} to the excitation beam via a single grating monochromator and an R928 photomultiplier tube having S-20 spectral response and operating in the single photon counting mode.

In order to determine the correct fluorescence the absorption was converted to optical density for the measured excitation and emission wavelengths using equation 1. The corrected fluorescence (F_{corr}) was calculated using equation 2, where observed fluorescence (F_{em}) is multiplied by the antilog of the average of optical density for the excited and emission wavelengths. The corrected fluorescence was calculated for the samples where the SiPc is attached to the MPC ($F_{Corr}^{MPC\&SiPc}$) and for the SiPc **1** ($F_{Corr}^{SiPc(OH)_2}$). The percentage of emission was calculated by the usual percentage equation 3.

$$OD = 1 - 10^{-Abs} \quad (1)$$

$$F_{Corr} = F_{em} * 10^{\frac{OD_{ex}+OD_{em}}{2}} \quad (2)$$

$$\%Emi = 100\% * \frac{F_{Corr}^{MPC\&SiPc}}{F_{Corr}^{SiPc(OH)_2}} \quad (3)$$

Fluorescence decay measurements were performed by the time-correlated single-photon-counting method (TCSPC). The excitation source was a fiber supercontinuum laser based on a passive mode-locked fiber laser and a high-nonlinearity photonic crystal fiber super-continuum generator (Fianium SC450). The laser provided 6-ps pulses at a repetition rate variable between 0.1 – 40 MHz. The laser output was sent through an Acousto-Optical Tunable Filer (Fianium AOTF) to obtain excitation pulses at desired wavelength. Fluorescence emission was detected at the magic angle (54.7°) using a double grating monochromator (Jobin Yvon Gemini-180) and a microchannel plate photomultiplier tube (Hamamatsu R3809U-50). The instrument response function was 35-55 ps. The spectrometer was controlled by software based on the LabView programming language and data acquisition was done using a single photon counting card (Becker-Hickl, SPC-830).

All TCSPC and transient absorption data were globally analyzed using locally written software (ASUFIT)[59] developed under MATLAB (Mathworks Inc.) environment. The model and procedure for global fitting have been described in detail in reference[114]. These global analysis procedures have been extensively reviewed and random errors associated with the reported lifetimes obtained from fluorescence and transient absorption measurements are typically ≤ 5%.

Fluorescence confocal microscope imaging instrumentation was previously reported by Krajnik *et al*.[115]. The same instrumental set-up, without the solid immersion lens, was used to measure fluorescent maps and lifetime decays on the patterned gold surfaces.

Results & Discussion

Synthesis of silicon phthalocyanine dyes. In order to attach Pc molecules with the macrocycle parallel to the gold surface, thiols would need to be attached to the axial position of a Pc ring through the silicon atom. The silicon atom was introduced into the macrocycle of the tetrapyrrole in the presence of base and then treated with water and a base resulting in dihydroxy SiPc **1**[106]. A variety of molecules were attached to the axial position of the SiPc. All but two of them were commercially available: 4-[(acetylthiol)methyl]benzoic acid was synthesized from 4-methylbenzoic acid via bromination[107] and then thioacetate substitution[108], (Scheme 1) and S-(11-hydroxyundecyl)thioacetate was synthesized from a procedure published by Wijtmans *et al*.[110]. Based on previous procedures for attaching acids to the axial position of a SiPc, 4-[(acetylthiol)methyl]benzoic acid and 4-(methylthiol)benzoic acid were converted to the acid chloride and covalently bound to SiPc **1** using DMAP to catalyze the esterification reaction[103] to produce **2** (Scheme 2) and **3** (Scheme 3). The porphyrin **4** was synthesized from mesityl dipyrromethane and a thioether aldehyde to produce an asymmetric porphyrin based on a previously published procedure[68, 109]. 1-Decanol, 4-(methylthio)-phenol, S-(11-hydroxyundecyl)thioacetate, and 11-mercaptoundecanol were axially attached through an ether linkage to the SiPc using heat and in pyridine to make **5** (Scheme 5), **6** (Scheme 6), **7** (Scheme 8), and **8** (Scheme 9), respectively, which was based on previously developed

procedures by our research group[106]. During these axial reactions it is possible to make the di-coupled product as well as the desired mono-coupled product. Formation of the di-coupled product was more favorable in these etherification reactions, based on the TLC analysis. This was particularly evident when reacting 4-(methiolthio)phenol to SiPc **1**; the major product was the di-coupled product SiPc **4**, little of the mono-coupled product was isolated. With careful separation using column chromatography it was possible to separate the mono-coupled products from the di-coupled products, however this decreased the yield.

Successful synthesis of the SiPc with axial substituents was evident by the upfield shifting of the protons on benzene or aliphatic protons. For SiPc **2**, **3**, and **5**, the benzene ring was situated at different distances in the shielding region of the macrocycle[116]. When adding long aliphatic alcohols, 1-decanol, 11-mercaptoundecanol, and S-(11-hydroxyundecyl)thioacetate the shielding due to the ring currents was also observed. For example, the proton NMR for 11-mercaptoundecanol does not differentiate or separate the methylene protons on carbons 3 to 9, but in the presence of the SiPc each of the methylene groups is separated and measured at different ppm (Figure 7). This is a distinct characteristic of the desired molecule and provides evidence that the product was synthesized successfully.

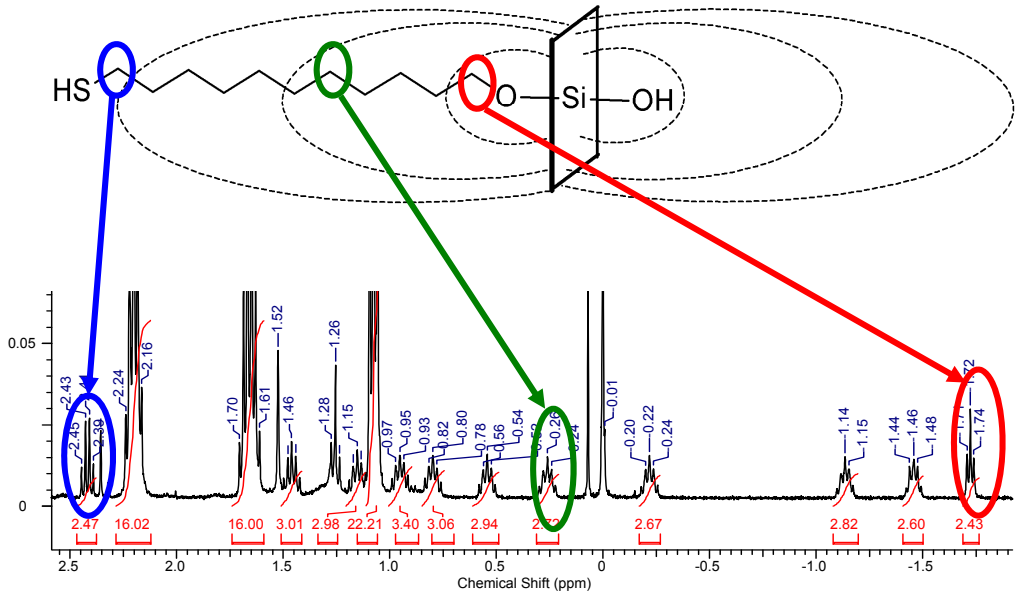

Figure 7. A section of the proton NMR spectra ($CDCl_3$, TMS standard) of SiPc **8** demonstrating the upfield shift of the 11-mercaptoundecanol methylene protons in the ring-currents (dashed curves) of the silicon phthalocyanine represented by the square.

Attachment of SiPc with short linkers to gold surfaces. Attempts to attach SiPc **4** to unprotected AuNP were made. First, the solvent of the AuNP had to adjust for the SiPc to interact and preferentially bind with the surface. The AuNP were synthesized in water, in which SiPc is not soluble. So the AuNP were diluted into acetonitrile and then later mixed with ethyl acetate containing the SiPc for a final 1:1:4 solution of water/ethyl acetate/acetonitrile. The absorption and emission spectra of the AuNP with SiPc **1** and SiPc **4** were compared (Figure 8). SiPc **4** has a Q_x maximum absorption at 783 nm, but after mixing with the unprotected AuNP this Q band shifted to 758 nm. The emission spectra also blue shifted from 828 nm to 791 and formed a second peak at 828 nm. Both the absorption and emission spectra matched SiPc **1** after the SiPc **4** bound to the nanoparticles. Also, the fluorescent lifetimes of the SiPc **4** and SiPc **1** with and without the AuNP were measured using TCSPC (Table 1). SiPc **4** alone had a lifetime of 1.1 ns, but when it was mixed with the AuNP it was 2.2 ns and matched the decay lifetime of the SiPc **1** with and

without the AuNP. The presence of the AuNP did not affect the SiPc **1** because the emission and fluorescence lifetime decays did not change, however the SiPc **4** did change and had characteristics similar to the SiPc **1** in the presence of the AuNP. From these measurements we speculated that when SiPc **4** attached to the AuNP surface, this interaction caused the 4-(methylthio)phenol group to dissociate from the SiPc within one minute of mixing (Figure 9).

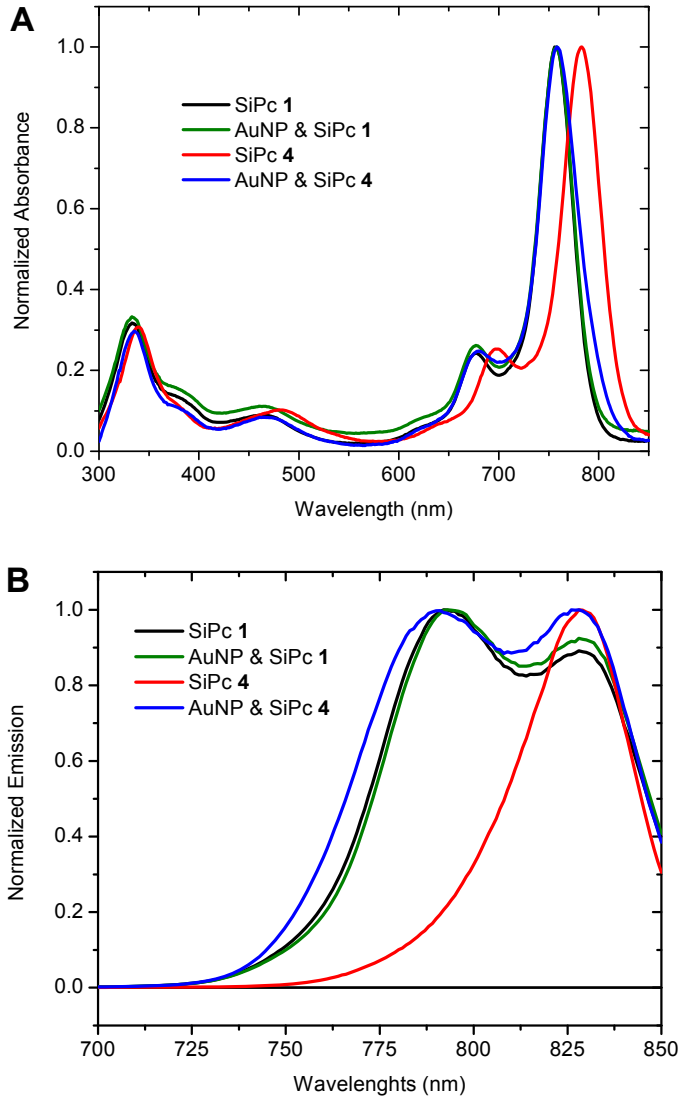

Figure 8. Normalized absorption (A) and emission spectra (excited at 340 nm) (B) of SiPc **1**, SPc **4**, mixtures of AuNP and SiPc **1**, and AuNP and SiPc **4** two hours after mixing in solution (1:1:4 water/ethyl acetate/acetonitrile).

Table 1. TCSPC results of two SiPc with and without AuNP treatment. Samples were in 1:4 ethyl acetate/acetonitrile solvent, excited at 430 nm, and the emission was measured at 830 nm. All lifetimes contained a single component.

Conditions	SiPc **4**	SiPc **1**
Molecule in solution	1.1 ns	2.4 ns
Molecule with AuNP	2.2 ns	2.4 ns

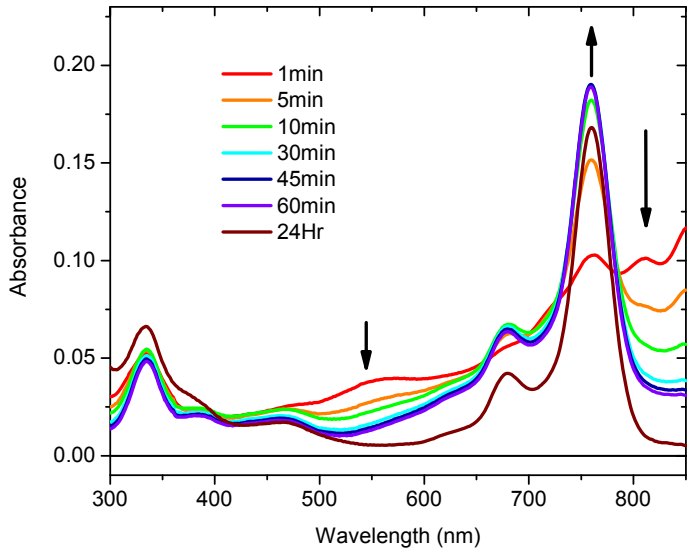

Figure 9. Absorbance spectra over 24 hours of SiPc **4** and AuNP mixed in 1:4 ethyl acetate/acetonitrile. Arrows indicate increases in the 759 nm peak and the decrease of the 811 and 545 nm absorption bands.

The surface plasmon band (SPB) provides information about the surface of the AuNP. When adding ligands to the surface the SPB red shifts due to an increase in the electronic density at the surface[100, 111]. A red shift of the SPB occurred in solutions of AuNP and 4-(methylthio)phenol alone (Figure 10A) and in the presence of SiPc **4** (Figure 10B). Thioethers are known to bind to the gold surfaces[99], but it is possible that the phenol of 4-(methylthio)phenol could also attach to the surface. The affinity of the phenol to the AuNP surfaces was tested and found that the phenol group does not interact with the AuNP surface (Figure 10C). Thus the methylthiol group was responsible for the SPB shift in

solutions of 4-(methylthio)phenol and AuNP. This further supported the fact that the 4-(methylthio)phenol bound to the surface of the AuNP and the SiPc **4** degraded to SiPc **1** which diffused into solution. This short linker was not suitable for binding SiPc to gold surfaces.

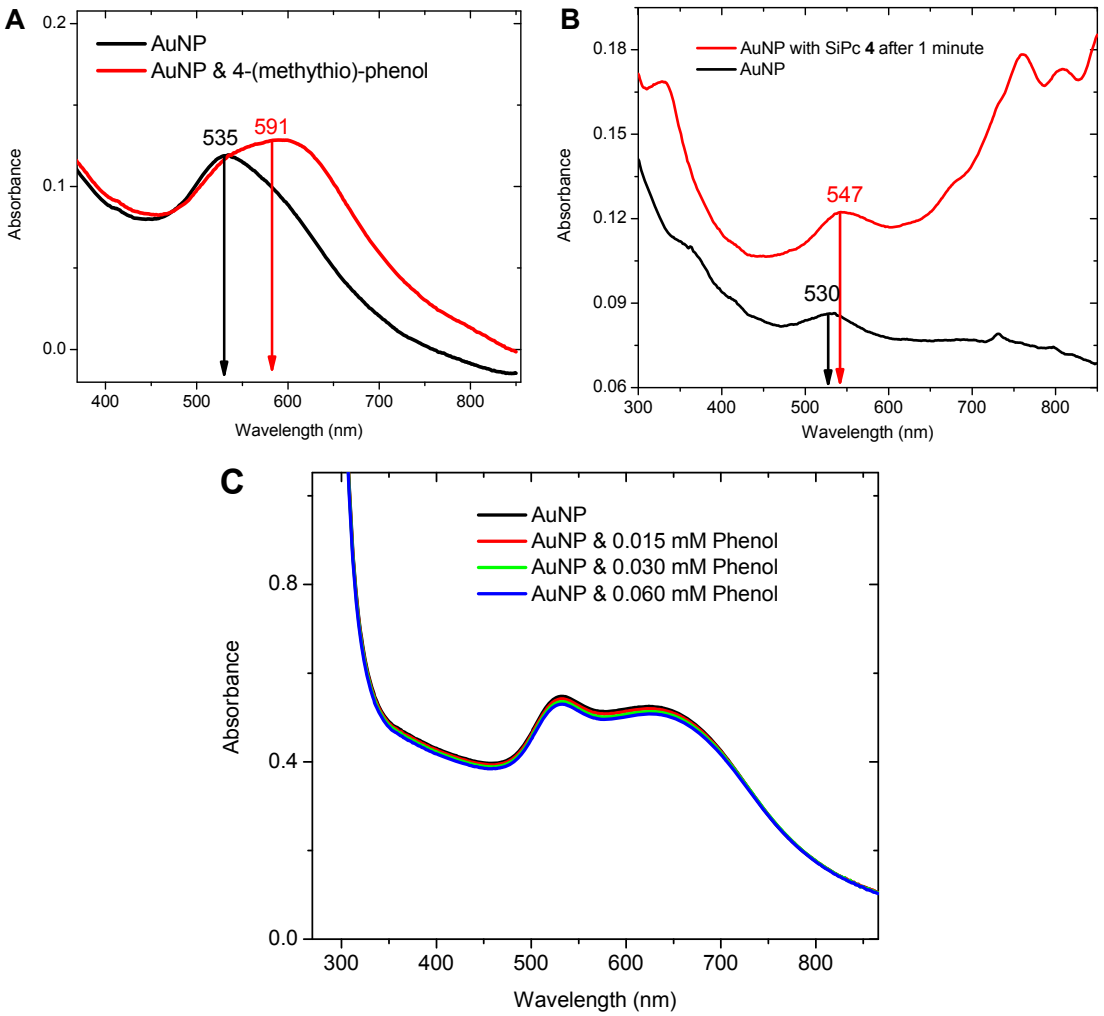

Figure 10. The surface plasmon absorbance spectra of AuNP mixed with 0.015 mM 4-(methylthio)phenol in a 1:1 water/ethanol solution (A) and the surface plasmon of the AuNP in the presence of SiPc **4** in a 1:4 ethyl acetate/acetonitrile solution (B). Various concentrations phenol (aq) were tested on the AuNP in the 1:1 ethanol/water solution (C).

When SiPc **4** was mixed with AuNP, the dye degraded into its precursor SiPc **1** and the 4-(methylthio)phenol linker remained bound to the AuNP. This was confirmed by shifts

in the absorption spectra over time, shifts in the emission spectra, and lengthening of the fluorescent lifetimes which matched SiPc **1**. We speculated that when the 4-(methylthio)phenol linker attached to the AuNP the electronic environment changed and weakened the silicon ether bond such that the ether reaction was reversed and SiPc **1** was released into solution. It seemed that the benzene linker was too electronically coupled to the gold surface, which might have affected the fluorescence had the dye remained bound to the surface. It is also possible that the surface of the unprotected AuNP is very acidic, which would facilitate the decoupling of the SiPc from 4-(methylthio)phenol.

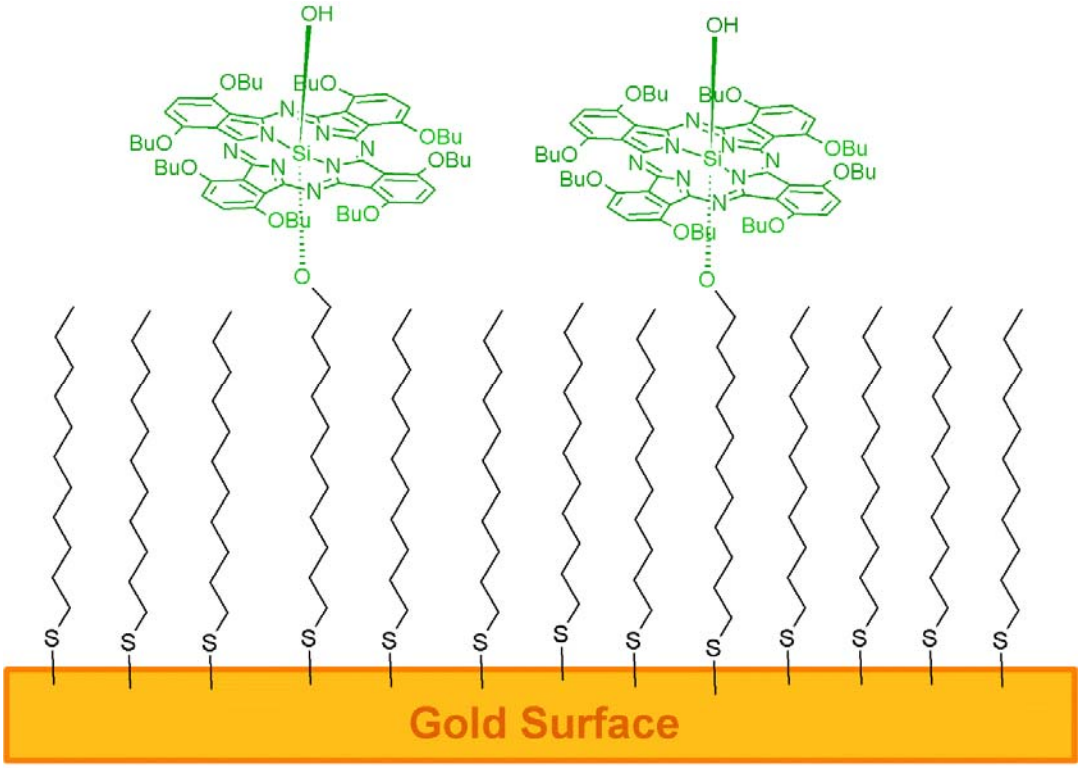

Figure 11. Proposed mixed self-assembling monolayer with deprotected SiPc **7** or SiPc **8** and a supporting ligand, 1-decanethiol, on the gold surface.

Simultaneously while research on AuNP was being conducted at Arizona State University, research for attaching the dyes **2**, **3**, **4**, and **5** to flat, gold surfaces in self-assembling monolayers (SAM) was performed at Osaka University by Professor Hideki

Hashimoto's research group. Results communicated to us indicated that the SiPc and porphyrin dyes, with these short rigid linkers did not bind well to flat gold surfaces. In addition to the poor binding to gold surfaces, the fluorescence of the molecules that bound to the surface was quenched. Quenching was most likely due to the short distance between the Pc dye and the gold surface. This caused us to reconsider the design of the dyes for this project, and a new strategy was proposed to increase the distance and to reduce quenching effects. A mixed monolayer was proposed for attaching the dye through a long aliphatic chain (Figure 11). Supporting alkanethiols will be used to support the aliphatic linkage and to maximize the distance between the dye and the gold surface. Two, new axially substituted SiPc were successfully made for binding to gold surfaces, they consisted of a long alkane linker with a thioacetate (**7**) or a thiol functional group (**8**). Samples of these new compounds were sent to Professor H. Hashimoto's laboratory in Japan and Professor R. Cogdell's research laboratory in Scotland for attachment to patterned gold surfaces, while research on AuNP continued at Arizona State University.

Attachment of SiPc with long linkers to gold nanoparticles. Experiments to attach the SiPc dyes with longer linkers as part of a mixed monolayer were attempted on unprotected AuNP. S-(11-hydroxyundecyl)thioacetate caused shifts in the SPB similar to 1-octanethiol, which is a common capping group for AuNP (Figure 12). This indicates that S-(11-hydroxyundecyl)thioacetate was able to bind to the surface and change the electronic environment on the surface. This also suggests that SiPc **7** should bind to the surface through this thioacetate group in the presence of the unprotected AuNP as well.

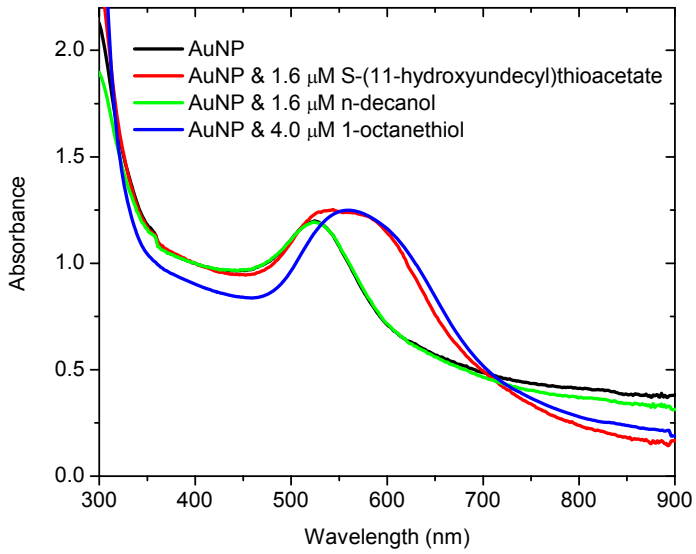

Figure 12. Absorption spectra of S-(11-hydroxyundecyl)thioacetate, n-decanol, and 1-octanethiol binding to unprotected AuNP in 1:1 ethanol/water.

Six samples were made with combinations of SiPc **7**, 1-octanethiol, and S-(11-hydroxyundecyl)thioacetate in 1:100 acetonitrile/water solution with unprotected AuNP. They were mixed for 3 hours resulting in shifts of the SPB demonstrating that the ligands were interacting with the AuNP (Figure 13A). Theoretically, after the nanoparticles are protected with nonpolar ligands they should be more soluble in organic solvents[100], so the AuNP were centrifuged and the solvent was replaced with ethyl acetate. Once the protected AuNP were in ethyl acetate the absorbance was much lower and the SPB were much broader, possibly due to aggregation (Figure 13B). The absorption spectra after washing also did not have SiPc absorption and they also had no fluorescence (Figure 13C).

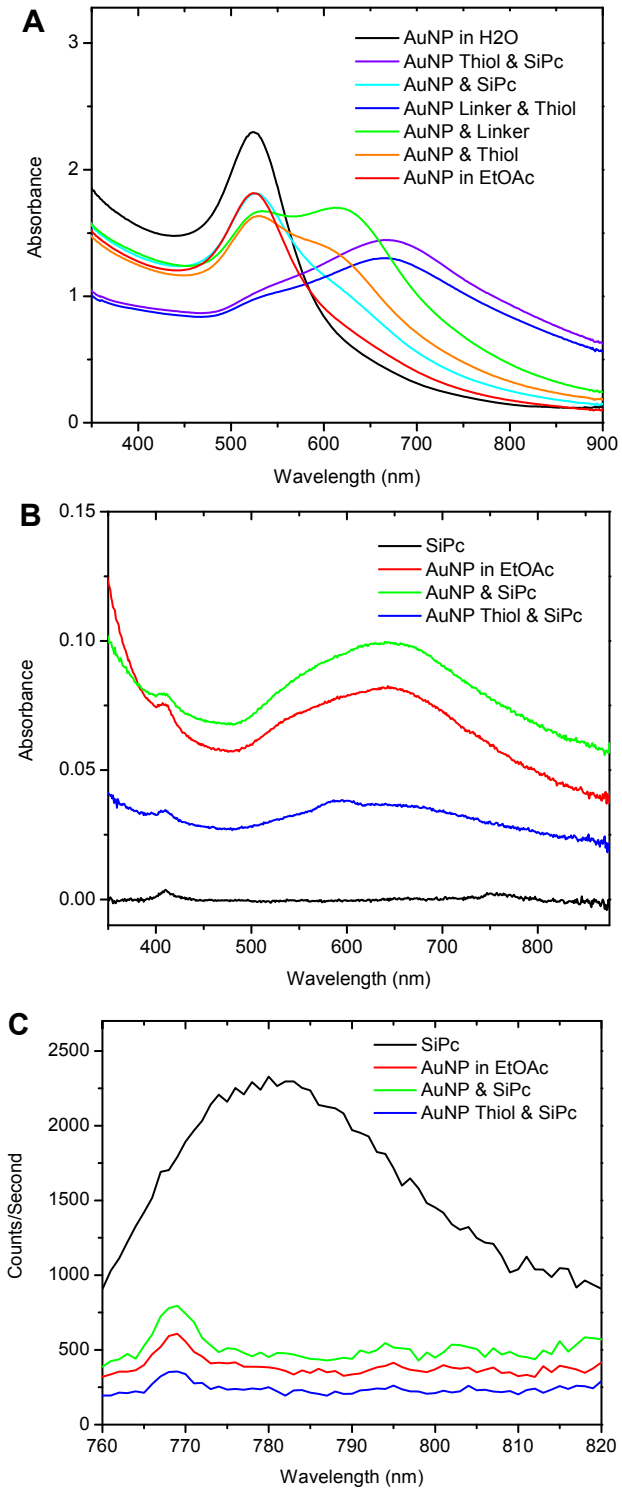

Figure 13. (A) Three hours after mixing the unprotected AuNP with different combinations of 1-octanethiol (thiol), S-(11-hydroxyundecyl)thioacetate (linker) and SiPc **7** in solution. (B) Absorption spectra after 48 hours in solution after removing water and replacing with ethyl acetate this sample was analyzed using fluorescence spectroscopy (C) exciting at 420 nm.

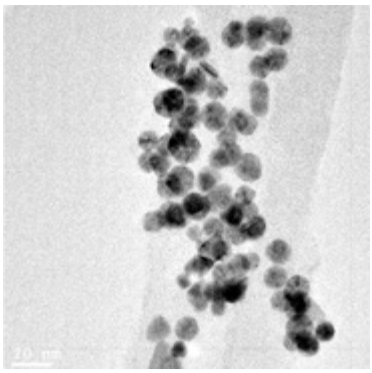

Sample 1: AuNP

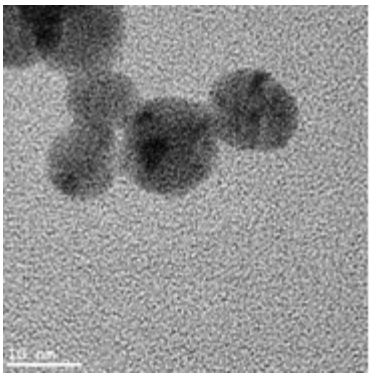

Sample 2: 2.35 μM 1-octanethiol

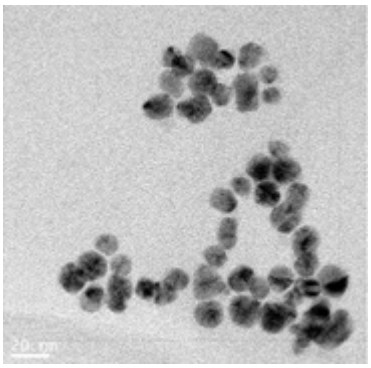

Sample 3: 0.185 μM S-(11-hydroxyundecyl) thioacetate

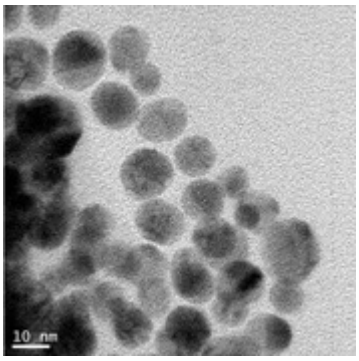

Sample 4: 0.228 μM S-(11-hydroxyundecyl) thioacetate, 42.6 μM 1-ocatanethiol

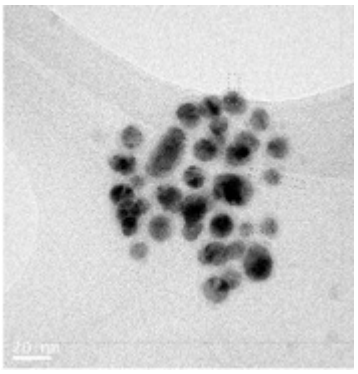

Sample 5: 0.233 μM SiPc **7**

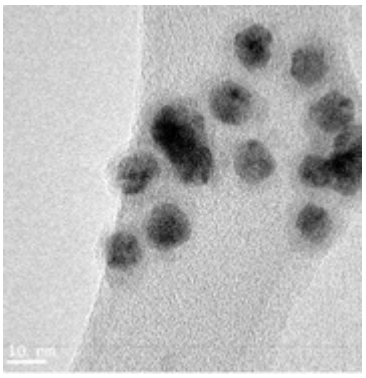

Sample 6: 42.6 μM 1-octanethiol, 0.233 μM SiPc **7**

Figure 14. Transmission electron microscopy (TEM) micrographs from six unprotected AuNP samples in 1:100 acetonitrile/water mixtures and then transferred to ethyl acetate.

Transmission electron microscopy (TEM) images measured what appeared to be a monolayer on the outside of the AuNP in the presence of 0.228 μM S-(11-hydroxyundecyl)thioacetate (Figure 14). There were also thicker and darker monolayer surrounding the AuNP with 42.6 μM 1-octanethiol, and thicker monolayers with 0.233 μM SiPc **7** and 42.6 μM 1-octanethiol, and 0.233 μM SiPc **7** (Figure 14). Attempts to reproduce these samples were difficult both in small (1 mL) and moderate (10 mL) sample sizes. Either way, the sample conditions were unable to attach SiPc **7** to the surface and the

samples tended to aggregate in solution, which may have been why it was difficult to reproduce or create large amounts of these samples.

A common problem with the unprotected AuNP is that they would aggregate and settle to the bottom of the solution if the conditions or the capping groups are not compatible. The long aliphatic linker attached axially to the SiPc made the molecule more hydrophobic, which made dissolving it even more difficult than before when the linkers were shorter and less saturated. So a hydrophilic supporting group, 6-mercaptohexanol, was used to coat the surface of the AuNP to make the surface more polar and to help with solubility. Ligands were tested to increase the stability of the nanoparticles and to reduce the dramatic shifts in the SPB, which are associated with aggregation and precipitation out of solution. Both S-(11-hydroxyundecyl)thioacetate and 6-mercaptohexanol were studied to see if they would stabilized the AuNP at three different concentrations over time (Figure 15). 6-Mercaptohexanol at 10 mM had shifted the SPB the least and kept the SPB absorption relatively stable. This appeared to be a good ligand to use so mixed monolayers using 6-mercaptohexanol ligands with SiPc **7** in 1:1 ethanol/water were attempted at higher concentrations than previously attempted. This still resulted in poor solubility, low levels of absorbance and fluorescence (Figure 16). Low levels of fluorescence and fluorescent artifacts from the solvent made fluorescent lifetime decay measurements for quenching using TCSPC studies more complicated. Even though more polar protecting groups were tested and used the AuNP continued to settle in the solution and ceased to be a colloidal solution when mixed with the polar solvents. Transferring the AuNP into organic polar solvents (i.e. ethanol or ethyl acetate) after adding organic protecting groups did not

improve the sample quality. In attempts to improve the system, alternative AuNPs were made and attempted to attach the SiPcs with longer aliphatic linkers in a mixed monolayer.

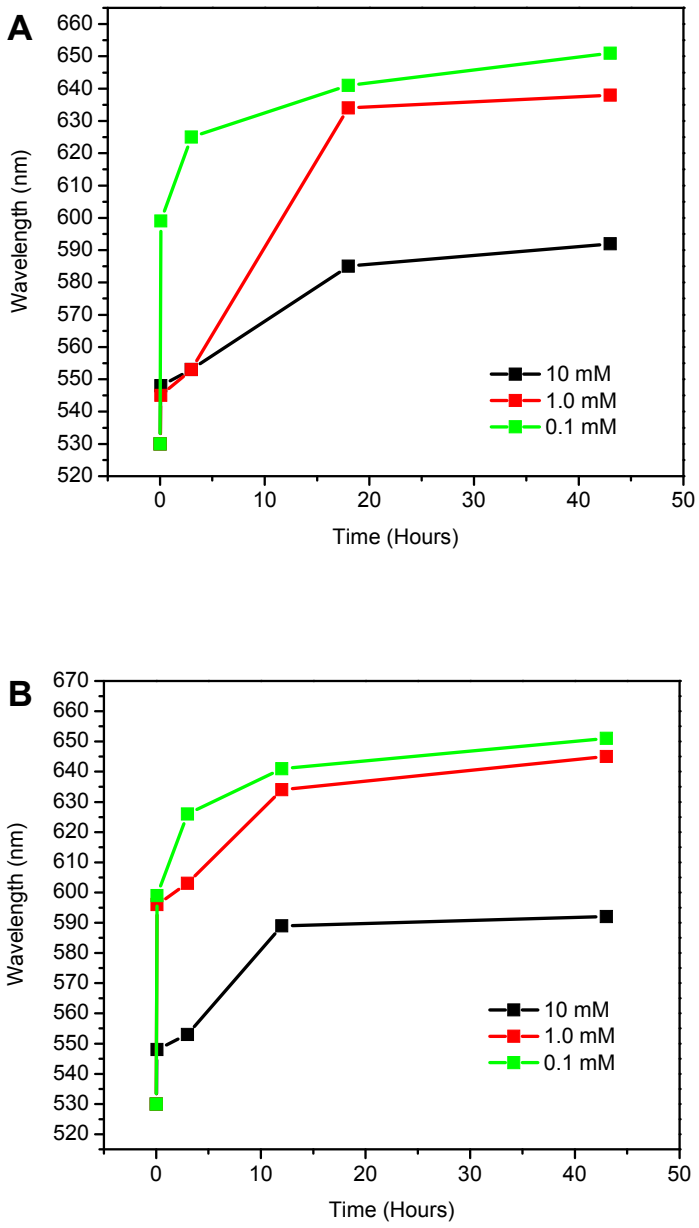

Figure 15. Maximum wavelength of absorption by the AuNP surface plasmon band in the presence of S-(11-hydroxyundecyl)thioacetate (A) and 6-mercaptohexanol (B) ligands over time.

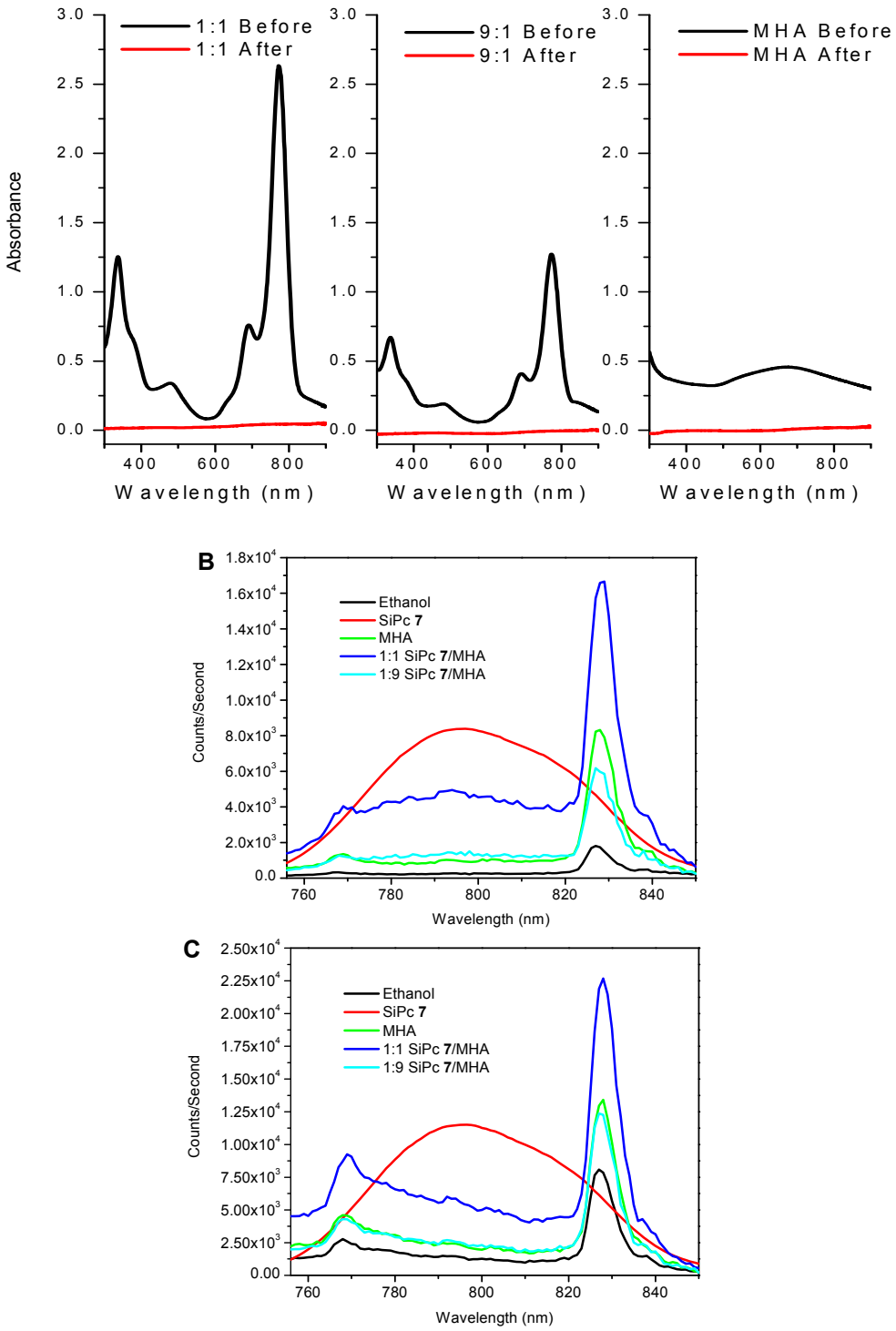

Figure 16. Absorbance spectra (A) before and after centrifuging and washing different ratios (1:1, 1:9) of mixed monolayer formations on AuNP using SiPc **7** and 6-mercaptohexanol (MHA) supporting ligand in 1:1 ethanol/water. Emission spectra excitation at 330 nm (B) and 670 nm (C) of mixed monolayer formation after washing with ethanol with fluorescent artifacts at 765 and 825 nm.

AuNP can be functionalized with different protecting groups using the Brust method[112], which results in monoprotected clusters (MPC). One method included making MPC with the 11-mercaptoundecanol linker using the Brust method and then covalently attaching the SiPc **1** to the nanoparticle using the pyridine reaction conditions used in solution (Scheme 10). The excess SiPc **1** was removed by size exclusion chromatography and small samples of the SiPc attached to the MPC were confirmed by absorption and emission spectroscopy (Figure 17). When an alkane was added to the axial position of SiPc **1**, such as n-decanol in SiPc **6**, the Q_x band red shifts ~4 nm (Figure 18). This same red shift in the absorption spectra is seen in the fractions of the size exclusion column that contain both SiPc and MPC absorbance, which supports the formation of the ether bond on the edges of the MPC.

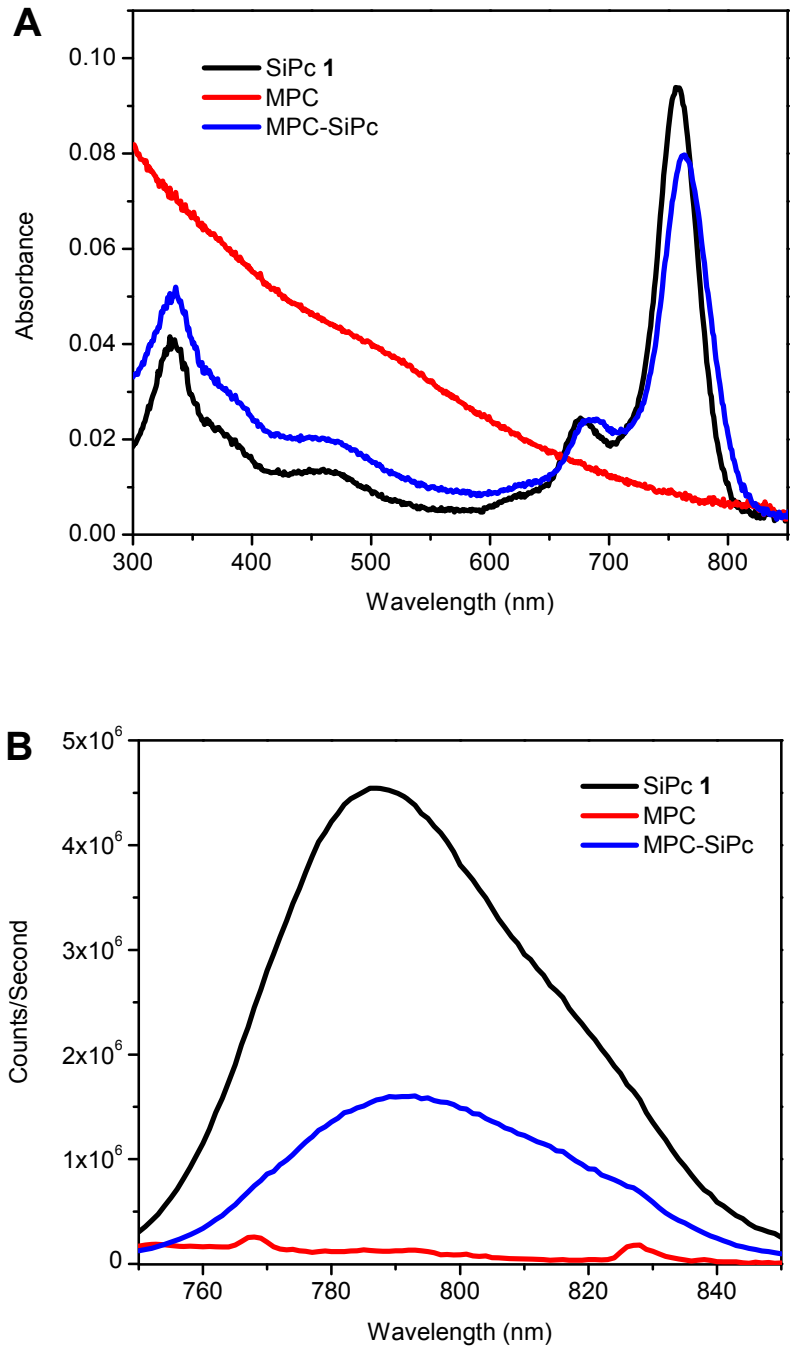

Figure 17. Absorption (A) and emission (B) spectra (excitation at 740 nm) of the MPC with SiPc **1** synthetically attached in ethanol.

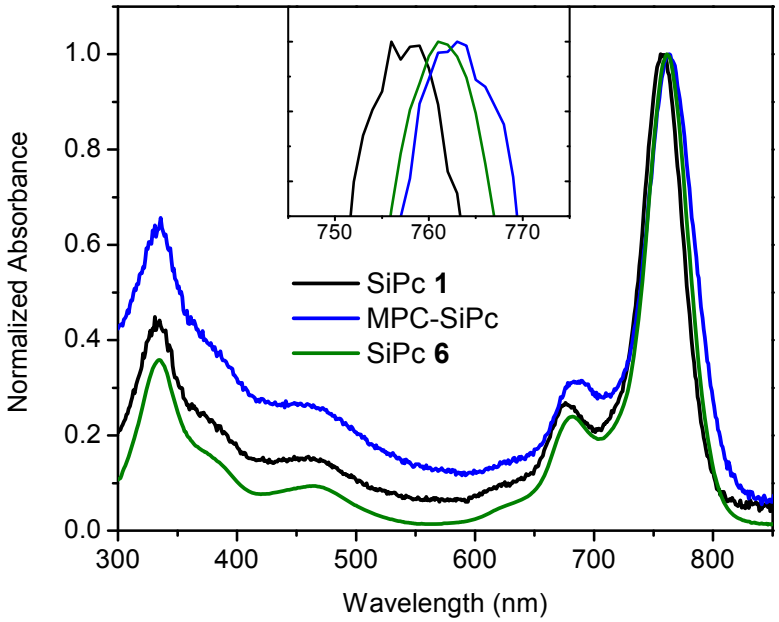

Figure 18. Normalized absorption spectrum to the Q_x band (inset) of the SiPc **1**, SiPc **6**, and SiPc attached to the MPC in ethanol.

In addition, FTIR vibrational spectra of the SiPc covalently bound to the MPC measured new vibrations that correspond to Si-O-C bonds (Figure 19), which is the new bond formed between the SiPc **1** hydroxide and the alcohol of the 11-mercaptoundecnaol on the MPC. The Si-OH bending mode around 800 cm^{-1} is enhanced in the SiPc attached MPC (MPC-SiPc) sample compared to SiPc **1** because of the asymmetry around the central silicon atom when it is axially bound to the MPC. There is also an increase in the O-C stretching from the undecanol group at 1260 cm^{-1}. When comparing to SiPc **1** and the MPCs there is no Si-O-C bond, therefor the presence of this bond is evidence that the reaction worked and that the SiPc is attached to the AuNP.

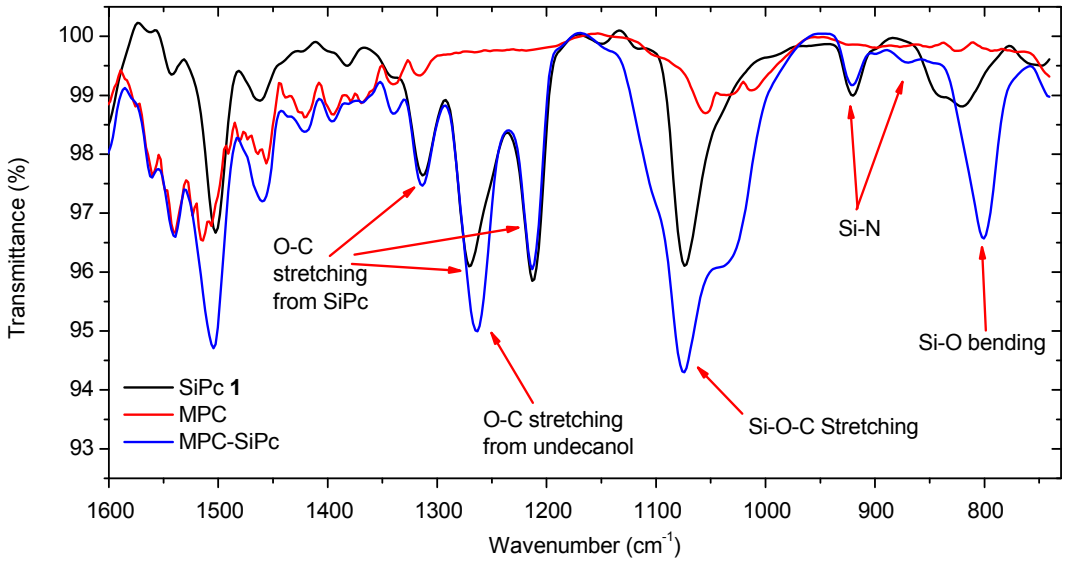

Figure 19. FTIR spectrum of the SiPc **1** and MPC with 11-mercaptoundecanol capping groups before and after synthesis with SiPc **1**.

After we confirmed that the SiPc was attached through an ether bond to the MPC we analyzed the fluorescence emitted on the nanoparticle compared to being in solution (Table 2). The nanoparticle quenched 70% of the SiPc fluorescence; we only saw ~30% of the remaining fluorescence when we compared the dye in solution by itself (Figure 17B). The fluorescence was measured at three different wavelengths to see if the gold plasmon had any effect on the fluorescence. It is possible that the quenching was greater with 460 nm excitation because the plasmon absorbs around 525 nm, but this did not happen because the amount of quenching was essentially the same for the three measured wavelengths. Attempts to repeat this procedure was not successful and often led to aggregated nanoparticles that did not elute from size exclusion columns. Thus this was not a reliable method for attaching SiPc to AuNP, however we did learn that the fluorescence was not totally quenched.

Table 2. Calculated fluorescence quenching of SiPc on the MPC in ethanol at different excitation wavelengths.

Excite λ	460 nm	675 nm	740 nm
% SiPc **1** Emission	29%	27%	25%

The Turkevick method was also used to make larger, 30 nm, AuNP with citrate as the stabilizing groups[113]. Thiol molecules would replace the weaker citrate ligands since the thiolate tends to have a stronger bond with the gold surface[99]. Aqueous solutions of AuNP were combined with solutions of the 11-mercaptoundecanol and SiPc **8** in DMA for a 1:4 DMA/water solution. This solution was left to incubate under inert (argon atmosphere) conditions for three days before washing with ethanol and purifying with a size exclusion column. Several samples containing different ratios of the supporting ligand and SiPc **8** were tried however only the samples with a 5:9 ratio produced samples that could be purified by size exclusion column. During the purification process the first band that eluted contained both the AuNP SPB and the SiPc absorption characteristics (Figure 20A). The corrected emission spectrum matched the emission spectra of SiPc **8** in solution and shows 40% fluorescence (Figure 21B). The TCSPC lifetime decay measurements of the SiPc **8** in DMA (2.17 ns) and SiPc **8** on the larger AuNP in 1:4 DMA/water resulted in three decay lifetimes (1.92 ns, 74%; 1.00 ns, 15%; 0.07 ns, 14%). Multiple lifetimes for the SiPc may have been due to the limited solubility it has in the DMA/water mixture. Because SiPc was not water soluble and it should have been attached to the AuNP surface, but it is possible that there may be a mixture of SiPcs interacting with the AuNP resulting in different decay lifetimes in the AuNP-SiPc sample.

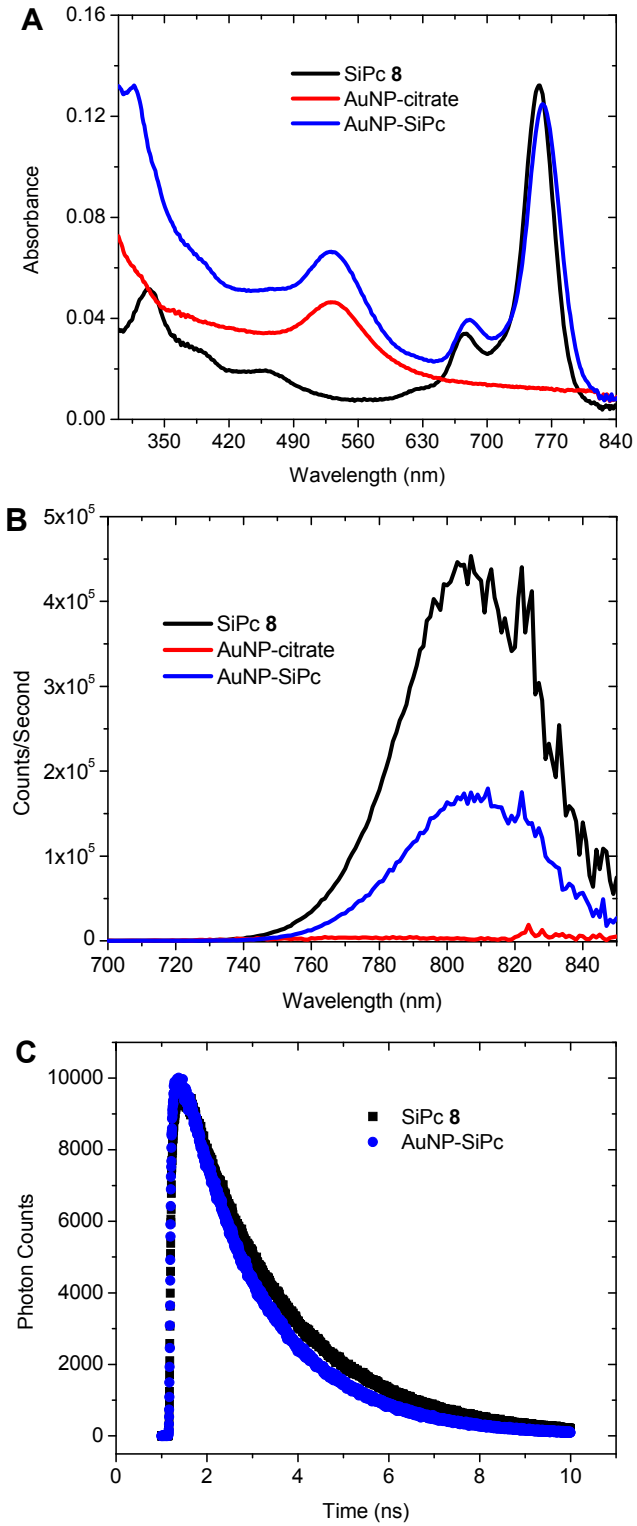

Figure 20. Absorption (A) and emission (B) spectra (excited at 680 nm) of AuNP covered with a mixed monolayer of 11-mercaptoundecanol and SiPc **8** in DMA. Kinetic trace (C) from TCSPC (770 nm excitation, observed at 810 nm) of SiPc **8** and AuNP with a mixed monolayer containing 11-mercaptoundecanol in 1:4 DMA/water and SiPc **8** in DMA.

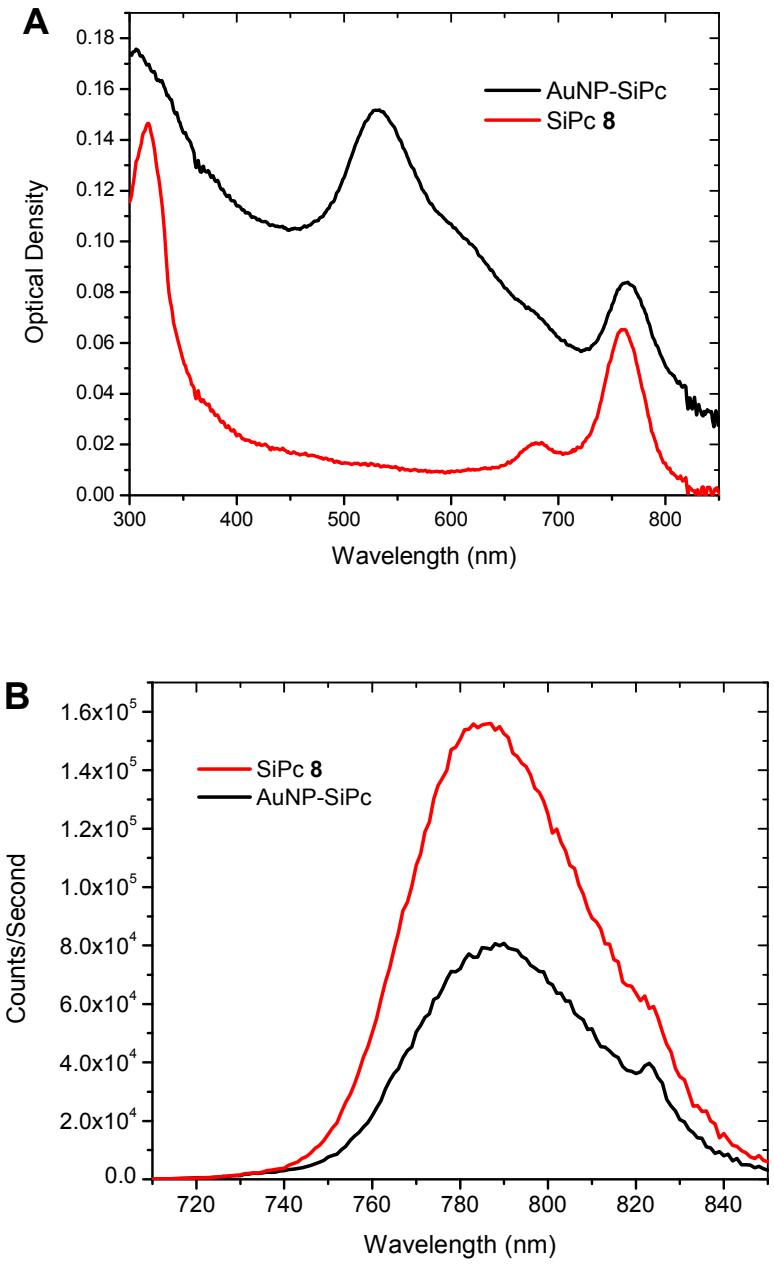

Figure 21. Absorption (A) and emission (B) spectra (λ_{ex} = 675 nm) of the purified citrate stabilized AuNP modified with 11-mercaptoundecanol in ethanol.

The experiment was repeated in ethanol, which improved the solubility of the SiPc and AuNP based on the clear SPB at 530 nm and Q_x features in the absorption spectrum (Figure 21A). However, the fluorescence was still quenched by 44% (Figure 22B). TCSPC

decays measured two decay lifetimes for the SiPc in ethanol (2.14 ns, 54%; 1.15 ns, 46%). But SiPc on the AuNP also had two lifetimes and the shorter decay lifetime had a larger contribution than the SiPc in solution (2.19 ns, 30%; 1.22 ns, 70%). Only shifts in the SPB and the separation of AuNP from excess SiPc provide evidence that the SiPc was attached to the surface, thus the amount of fluorescence observed may be a mixture of SiPc in solution as well as on the surface of the AuNP. This complicated our measurements and made this method less reliable for attaching SiPc larger AuNP.

An additional strategy for attaching molecules to the surface of nanoparticles is by ligand exchange. MPCs with 1-octanethiol and 11-mercaptoundecanol were mixed in solutions with SiPc **8** for several days. It was expected that some of the original MPC ligands should diffuse off of the surface and be replaced by SiPc **8**[99]. The samples were purified using size exclusion columns to remove the excess SiPc. MPCs with 11-mercaptoundecanol eluted two bands off the column. The first was brown-green and had traces of SiPc based on the absorption spectrum (Figure 22A), and the second band was green from the excess SiPc **8** that was not attached to the MPC. The fluorescence spectrum of SiPc **8** mixed with the same MPC in solution without time for ligand exchange had a much higher intensity of fluorescence, while the SiPc which had performed ligand exchange was only 9% of the fluorescence (Figure 22B). TCSPC measurements of the same SiPc mixed with MPCs were compared with the fluorescent lifetimes obtained from the ligand exchanged dyes, both had one lifetime that fit a 1.72 ns decay (Figure 22C).

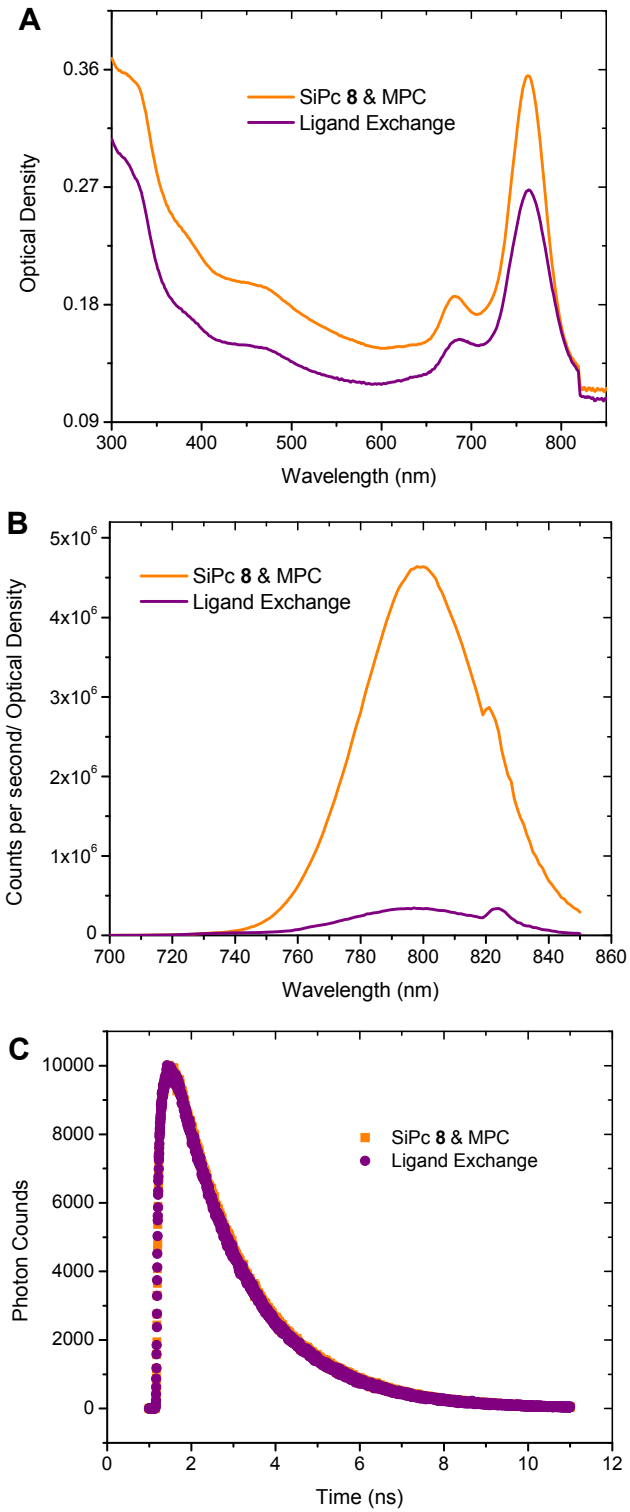

Figure 22. Absorption (A) and corrected emission (B) spectra of the purified MPC with 11-mercaptoundecanol in ethanol after ligand exchange experiments. Kinetic trace (C) from the TCSPC experiments (in ethanol, λ_{ex} = 760 nm, λ_{obs} = 820 nm) shows the same single lifetime decay of 1.72 ns.

Based on the fluorescence spectrum and the lifetime decay results from the two populations of SiPc, one of the populations was responsible for all of the fluorescence that was observed and was not quenched by the nanoparticle, perhaps due to its loose association with the surface. The other population was able to absorb light but was closer to the AuNP such that all of the fluorescence was quenched and was not observed in the steady state or TCSPC experiments. Just as in the previous samples with larger AuNP the only confirmation that we had that the SiPc was bound to the nanoparticle was that it eluted together on the size exclusion column and that the absorption features were present.

MPCs with 1-octanethiol that underwent ligand exchange with SiPc **8** eluted as one brown-green band from the size exclusion column. An additional size exclusion column was performed in attempts to separate the excess SiPc, however only one band eluted with the MPC and SiPc absorption features (Figure 23A), so it was concluded that all the SiPc had bound to the MPC. The steady state fluorescence spectrum of SiPc **8** in the presence of the 1-octanethiol MPCs and the SiPc attached by ligand exchange had minimal fluorescence quenching; 98% of the SiPc fluorescence was observed in the purified MPC after ligand exchange with SiPc **8** (Figure 23B). The fluorescence decay was the same on the MPC as it was in solution with MPC present (Figure 23C). Additional surface characterization would be needed to confirm that the SiPc was attached to the MPC. If SiPc **8** is attached to the surface of the AuNP this would be a reliable way of attaching SiPc to MPC with minimal fluorescence quenching.

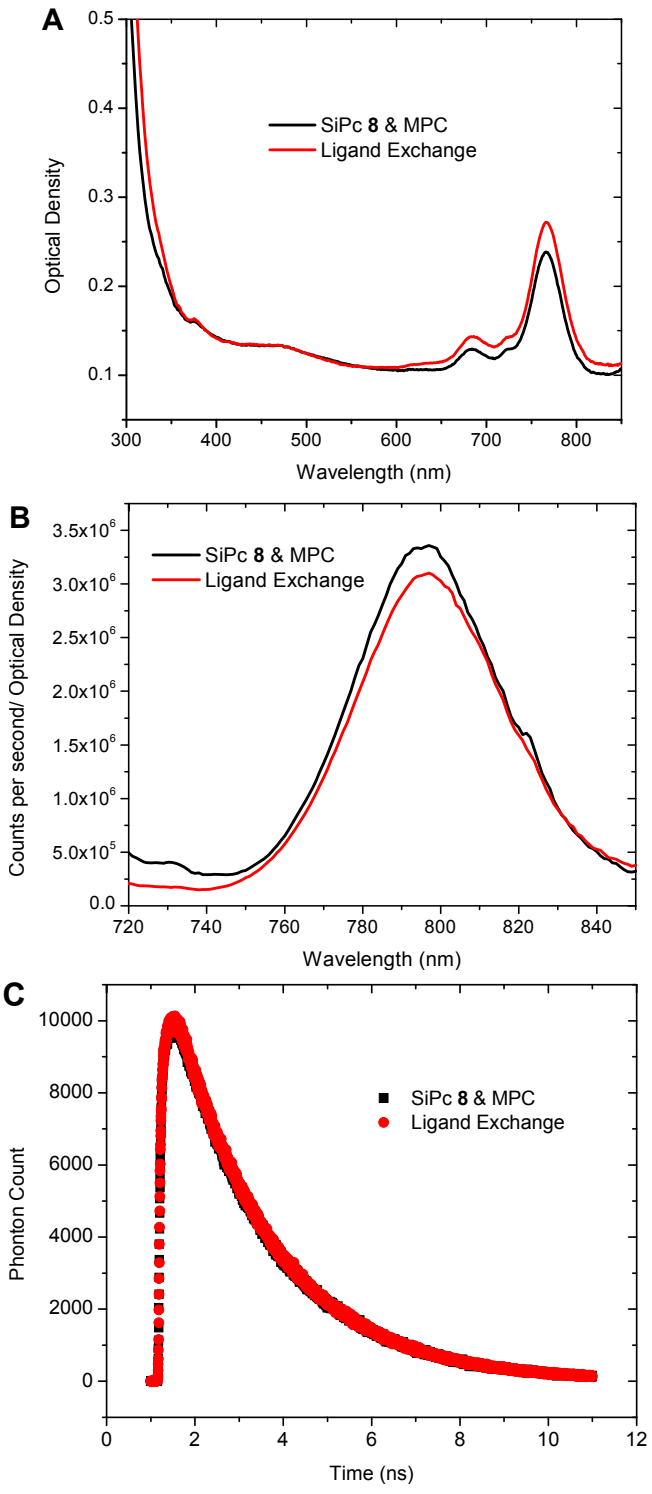

Figure 23. Absorption (A) and emission (B) spectra (λ_{ex} = 760 nm) of the purified MPC with 1-octanethiol in DCM after ligand exchange experiments. Kinetic trace (C) from the TCSPC experiments (in DCM, excite at 760 nm, observed 820 nm) shows the same single lifetime decay of 2.18 ns.

A final attempt to attach SiPc **8** to an AuNP was made by synthesizing the MPC in the presence of SiPc **8** and supporting ligands, 1-octanethiol and 11-mercaptoundecanol. The reactions retained the green color, meaning that the SiPc was able to withstand the reduction of the gold salt to nanoparticles, however after purification by aggregating and washing the nanoparticles there was no trace of the SiPc by absorption spectroscopy (Figure 24), thus this method was not successful.

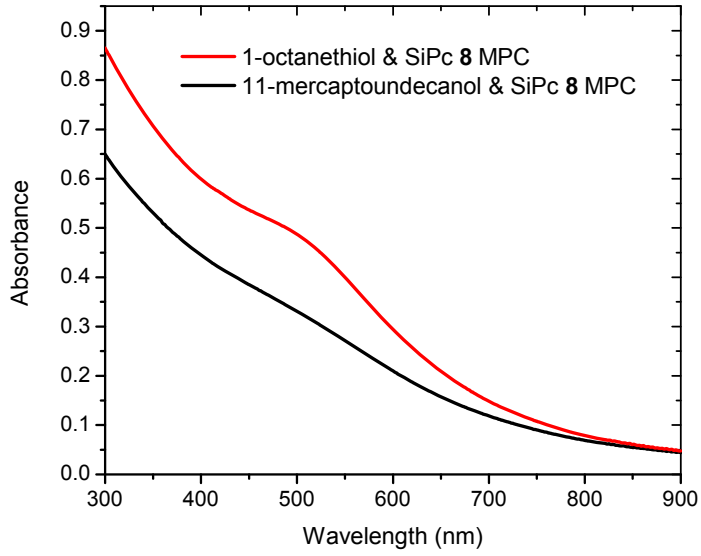

Figure 24. Absorption spectrum of MPC synthesized in the presence of 11-mercaptoundecanol or 1-octanethiol and SiPc **8** as capping groups.

Attachment of SiPc with long linkers to flat gold surfaces. Patterned gold surfaces were printed via lithographic methods at the University of Glasgow, Scotland (Figure 7), which contained various sizes of gold suns with smiles printed on glass slides (Figure 25). These slides were washed in piranha solution before soaking them in solutions with thiol protecting groups and SiPc dyes for four days to form a SAM. In addition, the solutions were bubbled with argon and kept under argon atmosphere to prevent the oxidation of the sulfur groups[99]. Professor Richard Cogdell's research group in Scotland

made several different samples using compound **8** on patterned gold and the fluorescence mapping was measured through a new collaboration with Professor Sebastian Mackowski's group at the Nicolaus Copernicus University, Poland. Initially, SiPc **8** was attached to the gold surface through ligand exchange procedure using decanethiol as the initial and supporting ligand. This produced emission images with a lower intensity on the patterned gold compared with the emission intensity outside the pattern (Figure 26). It was speculated that the SiPc may be quenched by the gold patterns, which would match many of the result measured on AuNP using different methods and sizes.

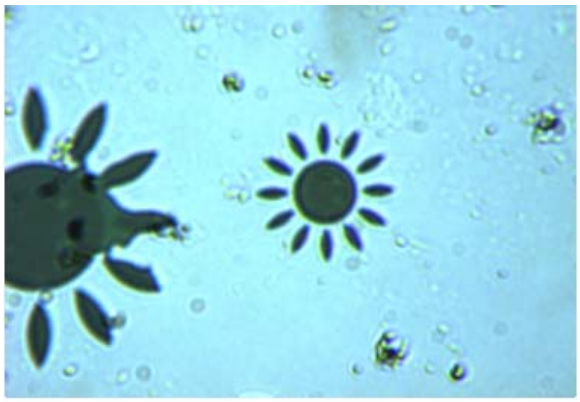

*Figure 25***.** Confocal microscope images of the gold pattern.

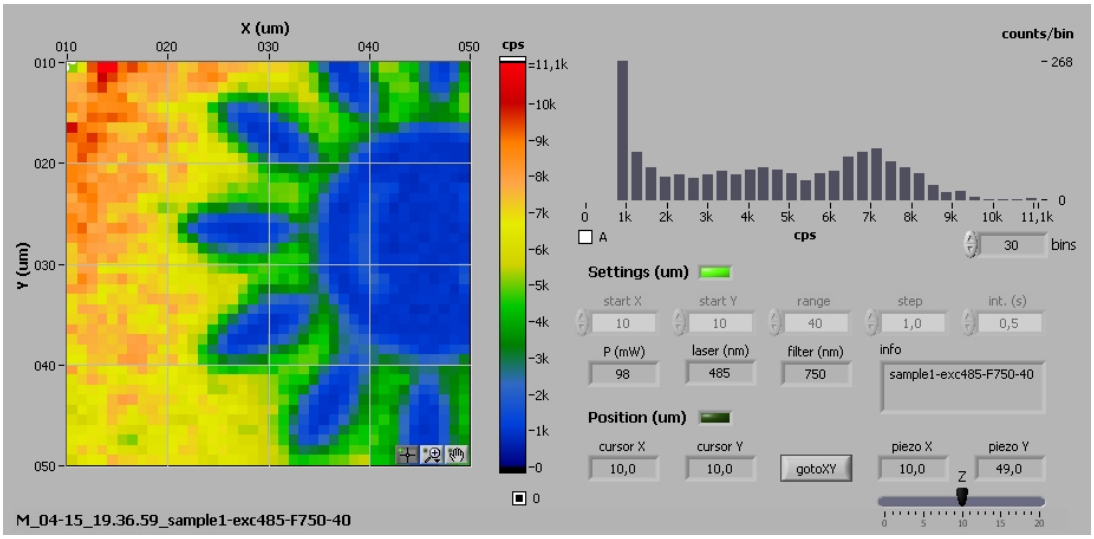

*Figure 26***.** Confocal microscope emission intensity maps of a sample prepared by ligand exchange with 1-octanethiol on gold patterns (λ_{ex} = 485 nm).

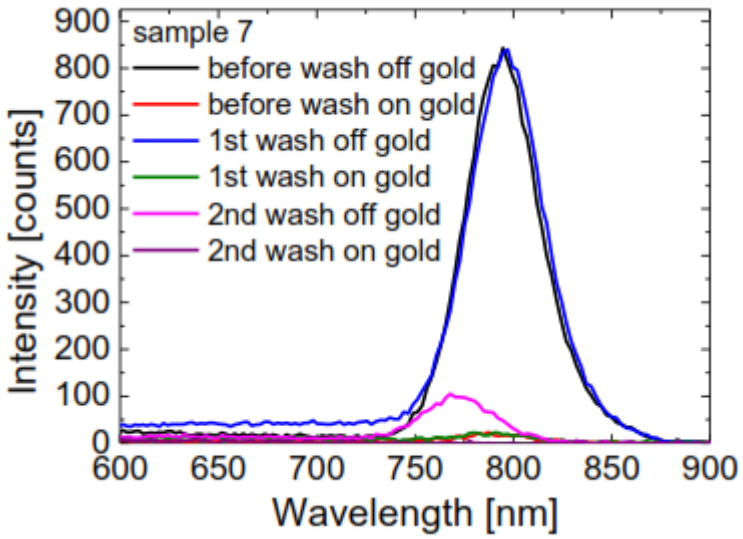

Figure 27. Fluorescence spectra when excited at 485 nm and 800-40 filter of Sample 7 (total concentration 1.0 mM with a 1:100 mixture of SiPc **8** and decanethiol) during the first wash with ethanol and a second wash with DCM.

An alternative method of making a mixed SAM was performed using several different ratios and concentrations of supporting ligands with SiPc **8**. These co-adsorption mixtures were made in Scotland and allowed to adsorb to the gold patterned slides over 4 days before measuring the emission maps and fluorescent lifetimes in Poland. Before measuring the 2-D fluorescence images the slides were washed with ethanol and DCM, and then dried under a stream of nitrogen. It was found that the solvent used for washing the slides made a difference on the intensity of fluorescence measured, and that DCM was the most effective for removing excess SiPc from the slides (Figure 27). There were higher levels of fluorescence on the glass slide and lower levels of fluorescence on the gold surface for all samples (Figure 28). This implies that by altering that concentration, ratio, and type of supporting ligands (11-mercaptoundecanol and decanethiol) did not make a difference on the behavior on the gold surface. The fluorescent lifetime was measured both on and off of the gold pattern on Sample 7 (Figure 30). This resulted in the same lifetime decay (~3.1

ns), thus the fluorescence was not quenched by the gold and was not the reason for lower levels of fluorescence on the gold patterns. Additional samples, including the previous ligand exchange sample and un-patterned bulk gold, were checked for fluorescence quenching on the gold surfaces which did not result in shorter fluorescent lifetime decay constants (Figure 30). The gold pattern and bulk gold do not quench the phthalocyanine fluorescence, thus a SiPc long alkane thiol appears to be an improved structure for adsorbing SiPcs to patterned gold surfaces.

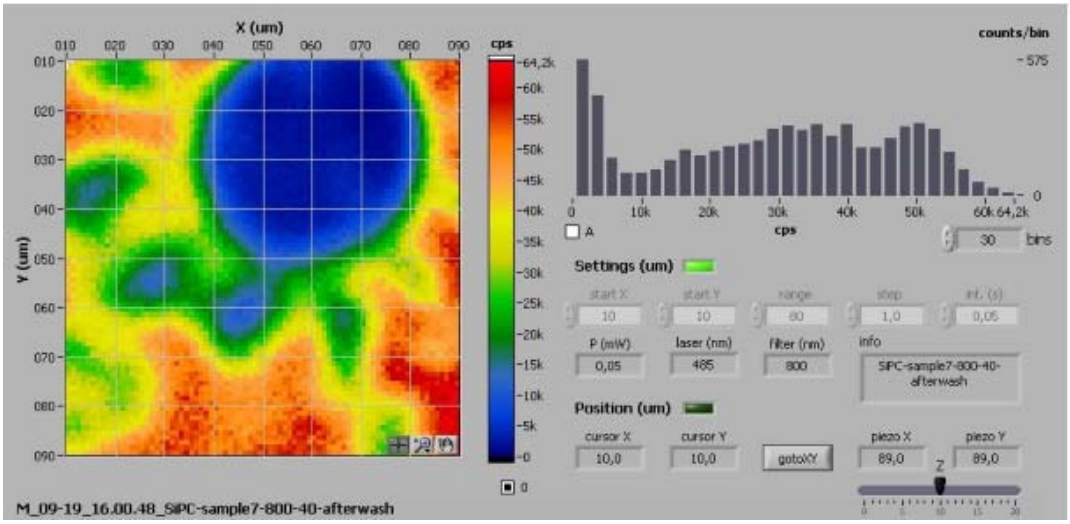

*Figure 28***.** Confocal microscope emission intensity maps of sample 7 (1.0 mM 1:100 SiPc **8** and decanethiol) prepared by co-adsorption on the gold patterns (λ_{ex} = 485 nm).

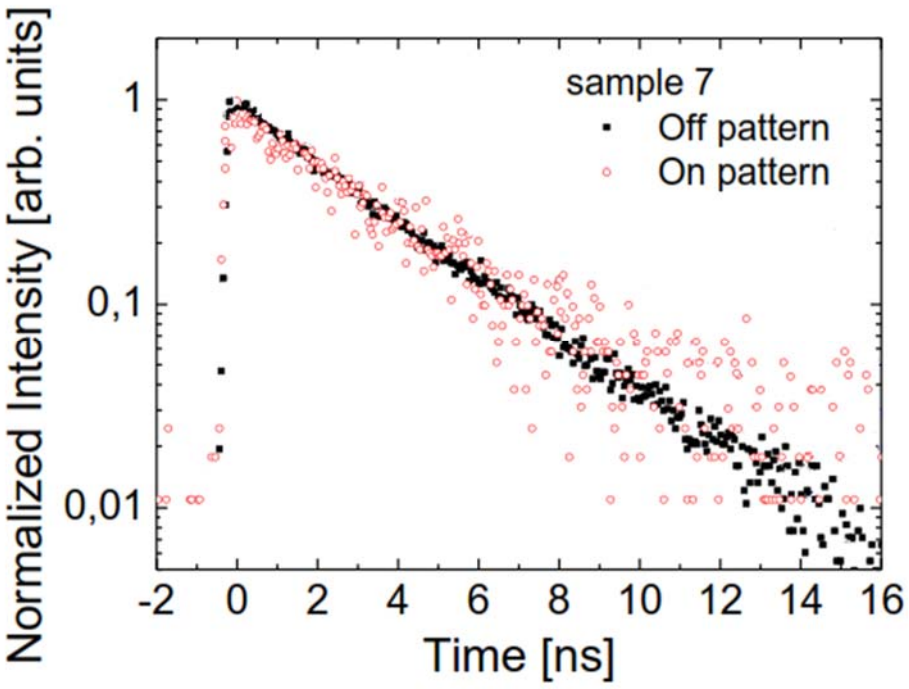

Figure 29. The fluorescence lifetime decay curves of Sample 7 (total concentration 1.0 mM with a 1:100 mixture of SiPc **8** and decanethiol) on and off the gold pattern.

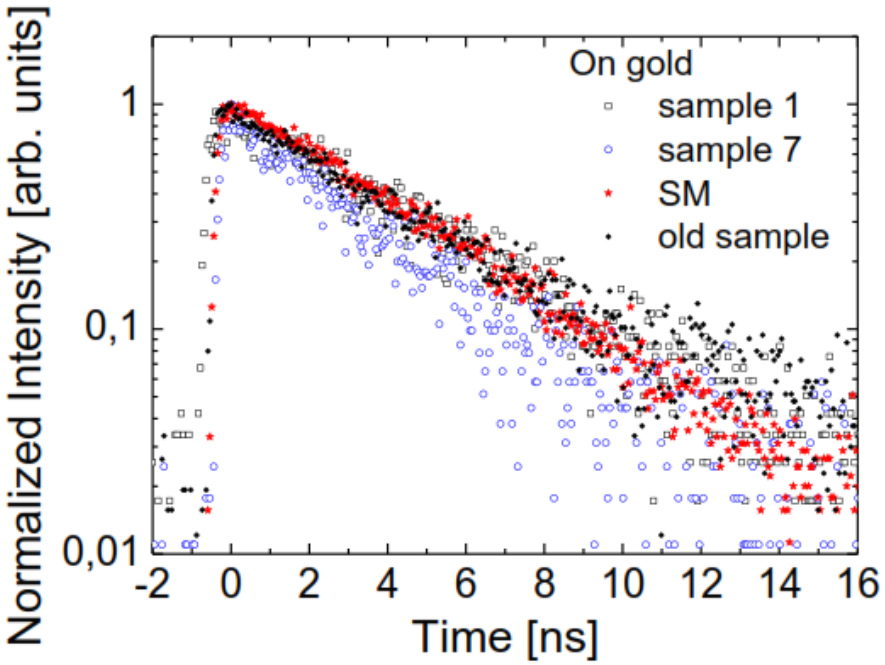

Figure 30. The fluorescence lifetime decay curves of 10 µM of SiPc **8** (Sample 1), total concentration 1.0 mM with a 1:100 mixture of **6** and decanethiol (Sample 7), SiPc **8** dried onto un-patterned bulk 30 nm thick gold (SM), and a previous sample soaked in a DCM solution of SiPc **8** (old sample from Figure 27).

From these observations it was also concluded that the lower level of fluorescence observed on the gold pattern was due to a lower number of Pc molecules on the gold surface compared to the glass surface. It was hypothesized that cleaning the gold with piranha solution etches the glass around the gold pattern creating crevices for the SiPc to non-specifically adsorb. Alternative materials, like quartz and silicon, are being tested for low levels of non-specific adsorption so that it can be used as a substrate for printing the gold pattern and specifically adsorbing the SiPc to the gold.

Conclusion

Several different attempts were made to attach SiPc molecules to different types of AuNP. First, unprotected AuNP in aqueous solution degraded SiPc **4**. Then SiPcs with longer linkers had solubility issues with the aqueous solutions of AuNP, so MPCs with organic protecting ligands were synthesized for their solubility in organic solvents. These MPCs were reacted with SiPc **1** for the formation of the Si-O-C bond had promising fluorescent results, but purification and reproducibility proved difficult. A ligand exchange method was attempted with 1-octanethiol and 11-mercaptoundecanol capped MPCs, where SiPc **8** was purified with the MPC, but the connectivity to the AuNP was not proven even with the improved fluorescence emission. Attaching SiPc **8** to larger citrate covered AuNP resulted in samples that had poor solubility and reproducibility. Lastly, MPC were made in the presence of capping groups that included thiol functionalized SiPc (**8**). The dye withstood the highly reducing environment, but the purification was unsuccessful. Some promising results regarding the fluorescence on these smaller AuNP provided some evidence that the longer linkers would work with flat gold surfaces.

Initial experiments, performed in Japan, on flat gold surfaces with shorter linkers quenched the fluorescence of the first set SiPc synthesized. After modifying the SiPcs with longer, aliphatic linkers, fluorescence was observed on patterned gold surfaces and the fluorescence lifetime was not quenched by the presence of the gold pattern. However, the 2D fluorescence images measured in Poland had higher intensities of fluorescence on the glass areas outside of the gold pattern. It seems that SiPc **8** does not selectively bind to the gold pattern and has an affinity for the glass slide due to etching by the piranha solution. Alternative materials, such as quartz, are currently being investigated for printing gold patterns and then adhering the SiPc to the gold surface. With this modification we hope to see higher selectivity for the gold surface and a higher intensity of fluorescence on the gold pattern. This work is still in progress.

By attempting to attach SiPc molecules to AuNP and patterned gold surfaces it is important to consider the connectivity, solubility, and selectivity of the chromophores. These experiments have advanced our understanding of how to address the initial problems in fabricating soft nanotechnology.

Acknowledgements

This project was funded by the Human Frontiers Science Project Grant Number RGP0005. We gratefully acknowledge the use of facilities within the Le Roy Erying Center for Solid State Science at Arizona State University.

REFERENCES

1.(a) Blankenship, R. E.; Tiede, D. M.; Barber, J.; Brudvig, G. W.; Fleming, G.; Ghirardi, M.; Gunner, M. R.; Junge, W.; Kramer, D. M.; Melis, A.; Moore, T. A.; Moser, C. C.; Nocera, D. G.; Nozik, A. J.; Ort, D. R.; Parson, W. W.; Prince, R. C.; Sayre, R. T., Comparing Photosynthetic and Photovoltaic Efficiencies and Recognizing the Potential for Improvement. *Science* **2011,** *332* (6031), 805-809; (b) Concepcion, J. J.; House, R. L.; Papanikolas, J. M.; Meyer, T. J., Chemical approaches to artificial photosynthesis. *Proc. Natl. Acad. Sci.* **2012,** *109* (39), 15560-15564; (c) Grätzel, M., Photoelectrochemical cells. *Nature* **2001,** *414* (6861), 338-344; (d) Gust, D.; Moore, T. A.; Moore, A. L., Molecular mimicry of photosynthetic energy and electron transfer. *Acc. Chem. Res.* **1993,** *26* (4), 198-205; (e) Gust, D.; Moore, T. A.; Moore, A. L., Mimicking Photosynthetic Solar Energy Transduction. *Acc. Chem. Res.* **2000,** *34* (1), 40-48; (f) Gust, D.; Moore, T. A.; Moore, A. L., Solar Fuels via Artificial Photosynthesis. *Acc. Chem. Res.* **2009,** *42* (12), 1890-1898; (g) Hambourger, M.; Moore, G. F.; Kramer, D. M.; Gust, D.; Moore, A. L.; Moore, T. A., Biology and technology for photochemical fuel production. *Chem. Soc. Rev.* **2009,** *38* (1), 25-35; (h) Rybtchinski, B.; Wasielewski, M. R., Artificial Photosynthesis for Solar Energy Conversion. In *Fundamentals of Materials for Energy and Sustainability*, Ginley, D.; Cahen, D., Eds. Cambridge University Press: 2012; pp 349-364; (i) Sherman, B. D.; Vaughn, M. D.; Bergkamp, J. J.; Gust, D.; Moore, A. L.; Moore, T. A., Evolution of reaction center mimics to systems capable of generating solar fuel. *Photosynth. Res.* **2014,** *120* (1), 59-70.

2.Moore, T. A.; Moore, A. L.; Gust, D., Artificial photosynthesis combines biology with technology for sustainable energy transformation. *AIP Conf. Proc.* **2013,** *1519* (1), 68-72.

3.Lovley, D. R.; Ueki, T.; Zhang, T.; Malvankar, N. S.; Shrestha, P. M.; Flanagan, K. A.; Aklujkar, M.; Butler, J. E.; Giloteaux, L.; Rotaru, A.-E.; Holmes, D. E.; Franks, A. E.; Orellana, R.; Risso, C.; Nevin, K. P., Geobacter: The Microbe Electric's Physiology, Ecology, and Practical Applications. In *Adv. Microb. Physiol.*, Robert, K. P., Ed. Academic Press: London, 2011; Vol. Volume 59, pp 1-100.

4. (a) Polívka, T.; Frank, H. A., Molecular Factors Controlling Photosynthetic Light Harvesting by Carotenoids. *Acc. Chem. Res.* **2010,** *43* (8), 1125-1134; (b) Polívka, T.; Sundström, V., Ultrafast Dynamics of Carotenoid Excited States−From Solution to Natural and Artificial Systems. *Chem. Rev. (Washington, DC, U. S.)* **2004,** *104* (4), 2021-2072.

5. (a) Dirks, G.; Moore, A. L.; Moore, T. A.; Gust, D., Light Absortion and Energy Transfer in Polyene-Porphyrin Esters. *Photochem. Photobiol.* **1980,** *32* (2), 277-280; (b) Moore, A. L.; Dirks, G.; Gust, D.; Moore, T. A., Energy Transfer from Carotenoid Polyenes to Porphyrins: A Light-Harvesting Antena. *Photochem. Photobiol.* **1980,** *32* (5), 691-695.

6. (a) Frank, H. A.; Chadwick, B. W.; Jin Oh, J.; Gust, D.; Moore, T. A.; Liddell, P. A.; Moore, A. L.; Makings, L. R.; Cogdell, R. J., Triplet-triplet energy transfer in B800–850 light-harvesting complexes of photosynthetic bacteria and synthetic carotenoporphyrin molecules investigated by electron spin resonance. *Biochimica et Biophysica Acta (BBA) - Bioenergetics* **1987,** *892* (3), 253-263; (b) Gust, D.; Moore, T. A.; Bensasson, R. V.; Mathis, P.; Land, E. J.; Chachaty, C.; Moore, A. L.; Liddell, P. A.; Nemeth, G. A., Stereodynamics of intramolecular triplet energy transfer in carotenoporphyrins. *J. Am. Chem. Soc.* **1985,** *107* (12), 3631-3640; (c) Liddell, P. A.; Nemeth, G. A.; Lehman, W. R.; Joy, A. M.; Moore, A. L.; Bensasson, R. V.; Moore, T. A.; Gust, D., Mimicry of Carotenoid Function in Photosynthesis: Synthesis and Photophysical Properties of a Carotenopyropheophorbide. *Photochem. Photobiol.* **1982,** *36* (6), 641-645; (d) Moore, A. L.; Joy, A.; Tom, R.; Gust, D.; Moore, T. A.; Bensasson, R. V.; Land, E. J., Photoprotection by Carotenoids During Photosynthesis: Motional Dependence of Intramolecular Energy Transfer. *Science* **1982,** *216* (4549), 982-984; (e) Moore, T. A.; Gust, D.; Moore, A. L., The Function of Carotenoid Pigments in Photosynthesis and their Possible Involvement in the Evolution of Higher Plants. In *Carotenoids*, Krinsky, N.; Mathews-Roth, M.; Taylor, R., Eds. Springer US: New York, 1989; pp 223-228.

7. Gust, D.; Moore, T. A.; Moore, A. L.; Devadoss, C.; Liddell, P. A.; Hermant, R.; Nieman, R. A.; Demanche, L. J.; DeGraziano, J. M.; Gouni, I., Triplet and singlet energy transfer in carotene-porphyrin dyads: role of the linkage bonds. *J. Am. Chem. Soc.* **1992,** *114* (10), 3590-3603.

8. Polívka, T.; Sundström, V., Dark excited states of carotenoids: Consensus and controversy. *Chem. Phys. Lett.* **2009,** *477* (1–3), 1-11.

9. Macpherson, A. N.; Liddell, P. A.; Kuciauskas, D.; Tatman, D.; Gillbro, T.; Gust, D.; Moore, T. A.; Moore, A. L., Ultrafast Energy Transfer from a Carotenoid to a Chlorin in a Simple Artificial Photosynthetic Antenna. *J. Phys. Chem. B* **2002,** *106* (36), 9424-9433.

10. Gouterman, M., Spectra of porphyrins. *J. Mol. Spectrosc.* **1961,** *6* (0), 138-163.

11. Marino-Ochoa, E.; Palacios, R.; Kodis, G.; Macpherson, A. N.; Gillbro, T.; Gust, D.; Moore, T. A.; Moore, A. L., High-efficiency Energy Transfer from Carotenoids to a Phthalocyanine in an Artificial Photosynthetic Antenna. *Photochem. Photobiol.* **2002,** *76* (1), 116-121.

12. Cogdell, R. J.; Gall, A.; Köhler, J., The architecture and function of the light-harvesting apparatus of purple bacteria: from single molecules to in vivo membranes. *Q. Rev. Biophys.* **2006,** *39* (3), 227-324.

13.Kodis, G.; Herrero, C.; Palacios, R.; Mariño-Ochoa, E.; Gould, S.; de la Garza, L.; van Grondelle, R.; Gust, D.; Moore, T. A.; Moore, A. L.; Kennis, J. T. M., Light Harvesting and Photoprotective Functions of Carotenoids in Compact Artificial Photosynthetic Antenna Designs. *J. Phys. Chem. B* **2004,** *108* (1), 414-425.

14.Berera, R.; van Stokkum, I. H. M.; Kodis, G.; Keirstead, A. E.; Pillai, S.; Herrero, C.; Palacios, R. E.; Vengris, M.; van Grondelle, R.; Gust, D.; Moore, T. A.; Moore, A. L.; Kennis, J. T. M., Energy Transfer, Excited-State Deactivation, and Exciplex Formation in Artificial Caroteno-Phthalocyanine Light-Harvesting Antennas. *J. Phys. Chem. B* **2007,** *111* (24), 6868-6877.

15.van Stokkum, I. H. M.; Larsen, D. S.; van Grondelle, R., Global and target analysis of time-resolved spectra. *Biochim. Biophys. Acta* **2004,** *1657*, 82-104.

16. Papagiannakis, E.; Kennis, J. T. M.; van Stokkum, I. H. M.; Cogdell, R. J.; van Grondelle, R., An alternative carotenoid-to-bacteriochlorophyll energy transfer pathway in photosynthetic light harvesting. *Proc. Natl. Acad. Sci.* **2002,** *99* (9), 6017-6022.

17.Kloz, M.; Pillai, S.; Kodis, G.; Gust, D.; Moore, T. A.; Moore, A. L.; Grondelle, R. v.; Kennis, J. T. M., New light-harvesting roles of hot and forbidden carotenoid states in artificial photosynthetic constructs. *Chemical Science* **2012,** *3* (6), 2052-2061.

18. (a) Krueger, B. P.; Scholes, G. D.; Fleming, G. R., Calculation of Couplings and Energy-Transfer Pathways between the Pigments of LH2 by the ab Initio Transition Density Cube Method. *J. Phys. Chem. B* **1998,** *102* (27), 5378-5386; (b) Scholes, G. D.; Jordanides, X. J.; Fleming, G. R., Adapting the Förster Theory of Energy Transfer for Modeling Dynamics in Aggregated Molecular Assemblies. *J. Phys. Chem. B* **2001,** *105* (8), 1640-1651.

19.(a) Kodis, G.; Liddell, P. A.; de la Garza, L.; Clausen, P. C.; Lindsey, J. S.; Moore, A. L.; Moore, T. A.; Gust, D., Efficient Energy Transfer and Electron Transfer in an Artificial Photosynthetic Antenna−Reaction Center Complex. *J. Phys. Chem. A* **2002,** *106* (10), 2036-2048; (b) Kuciauskas, D.; Liddell, P. A.; Lin, S.; Johnson, T. E.; Weghorn, S. J.; Lindsey, J. S.; Moore, A. L.; Moore, T. A.; Gust, D., An Artificial Photosynthetic Antenna-Reaction Center Complex. *J. Am. Chem. Soc.* **1999,** *121* (37), 8604-8614.

20.(a) Strachan, J.-P.; Gentemann, S.; Seth, J.; Kalsbeck, W. A.; Lindsey, J. S.; Holten, D.; Bocian, D. F., Effects of Orbital Ordering on Electronic Communication in Multiporphyrin Arrays. *J. Am. Chem. Soc.* **1997,** *119* (46), 11191-11201; (b) Yang, S. I.;

Seth, J.; Balasubramanian, T.; Kim, D.; Lindsey, J. S.; Holten, D.; Bocian, D. F., Interplay of Orbital Tuning and Linker Location in Controlling Electronic Communication in Porphyrin Arrays. *J. Am. Chem. Soc.* **1999,** *121* (16), 4008-4018; (c) Yang, S. I.; Seth, J.; Strachan, J.-P.; Gentemann, S.; Kim, D.; Holten, D.; Lindsey, J. S.; Bocian, D. F., Ground and excited state electronic properties of halogenated tetraarylporphyrins. Tuning the building blocks for porphyrin-based photonic devices. *J. Porphyrins Phthalocyanines* **1999,** *3* (2), 117-147.

21. (a) Garg, V.; Kodis, G.; Liddell, P. A.; Terazono, Y.; Moore, T. A.; Moore, A. L.; Gust, D., Artificial Photosynthetic Reaction Center with a Coumarin-Based Antenna System. *J. Phys. Chem. B* **2013,** *117* (38), 11299-11308; (b) Kodis, G.; Terazono, Y.; Liddell, P. A.; Andréasson, J.; Garg, V.; Hambourger, M.; Moore, T. A.; Moore, A. L.; Gust, D., Energy and Photoinduced Electron Transfer in a Wheel-Shaped Artificial Photosynthetic Antenna-Reaction Center Complex. *J. Am. Chem. Soc.* **2006,** *128* (6), 1818-1827; (c) Terazono, Y.; Kodis, G.; Liddell, P. A.; Garg, V.; Moore, T. A.; Moore, A. L.; Gust, D., Multiantenna Artificial Photosynthetic Reaction Center Complex. *J. Phys. Chem. B* **2009,** *113* (20), 7147-7155; (d) Terazono, Y.; Moore, T. A.; Moore, A. L.; Gust, D., Light Harvesting, Excitation Energy/Electron Transfer, and Photoregulation in Artificial Photosynthetic Systems. In *Multiporphyrin Arrays: Fundamentals and Applications*, Kim, D., Ed. Pan Stanford Publishing: Singapore, 2012.

22. Gust, D.; Kramer, D.; Moore, A.; Moore, T. A.; Vermaas, W., Engineered and Artificial Photosynthesis: Human Ingenuity Enters the Game. *MRS Bulletin* **2008,** *33* (04), 383-387.

23. Demmig-Adams, B.; Adams, W. W., Antioxidants in Photosynthesis and Human Nutrition. *Science* **2002,** *298* (5601), 2149-2153.

24. Niyogi, K. K., PHOTOPROTECTION REVISITED: Genetic and Molecular Approaches. *Annual Review of Plant Physiology and Plant Molecular Biology* **1999,** *50* (1), 333-359.

25.(a) Baroli, I.; Do, A. D.; Yamane, T.; Niyogi, K. K., Zeaxanthin Accumulation in the Absence of a Functional Xanthophyll Cycle Protects Chlamydomonas reinhardtii from Photooxidative Stress. *The Plant Cell* **2003,** *15* (4), 992-1008; (b) Havaux, M.; Niyogi, K. K., The violaxanthin cycle protects plants from photooxidative damage by more than one mechanism. *Proc. Natl. Acad. Sci.* **1999,** *96* (15), 8762-8767.

26. Hermant, R. M.; Liddell, P. A.; Lin, S.; Alden, R. G.; Kang, H. K.; Moore, A. L.; Moore, T. A.; Gust, D., Mimicking carotenoid quenching of chlorophyll fluorescence. *J. Am. Chem. Soc.* **1993,** *115* (5), 2080-2081.

27. Holt, N. E.; Zigmantas, D.; Valkunas, L.; Li, X.-P.; Niyogi, K. K.; Fleming, G. R., Carotenoid Cation Formation and the Regulation of Photosynthetic Light Harvesting. *Science* **2005,** *307* (5708), 433-436.

28. Cardoso, S. L.; Nicodem, D.; Moore, T. A.; Moore, A. L.; Gust, D., Synthesis and Fluorescence Quenching Studies of a Series of Carotenoporphyrins with Carotenoids of Various Lenghts. *J. Braz. Chem. Soc.* **1996,** *7* (4), 19-30

29. Fungo, F.; Otero, L.; Durantini, E.; Thompson, W. J.; Silber, J. J.; Moore, T. A.; Moore, A. L.; Gust, D.; Sereno, L., Correlation of fluorescence quenching in carotenoporphyrin dyads with the energy of intramolecular charge transfer states. Effect of the number of conjugated double bonds of the carotenoid moiety. *Phys. Chem. Chem. Phys.* **2003,** *5* (3), 469-475.

30.Berera, R.; Herrero, C.; van Stokkum, I. H. M.; Vengris, M.; Kodis, G.; Palacios, R. E.; van Amerongen, H.; van Grondelle, R.; Gust, D.; Moore, T. A.; Moore, A. L.; Kennis, J. T. M., A simple artificial light-harvesting dyad as a model for excess energy dissipation in oxygenic photosynthesis. *Proc. Natl. Acad. Sci.* **2006,** *103* (14), 5343-5348.

31.Ruban, A. V.; Berera, R.; Ilioaia, C.; van Stokkum, I. H. M.; Kennis, J. T. M.; Pascal, A. A.; van Amerongen, H.; Robert, B.; Horton, P.; van Grondelle, R., Identification of a mechanism of photoprotective energy dissipation in higher plants. *Nature* **2007,** *450* (7169), 575-578.

32. Frank, H.; Cua, A.; Chynwat, V.; Young, A.; Gosztola, D.; Wasielewski, M., Photophysics of the carotenoids associated with the xanthophyll cycle in photosynthesis. *Photosynth. Res.* **1994,** *41* (3), 389-395.

33.(a) Bautista, J. A.; Connors, R. E.; Raju, B. B.; Hiller, R. G.; Sharples, F. P.; Gosztola, D.; Wasielewski, M. R.; Frank, H. A., Excited State Properties of Peridinin: Observation of a Solvent Dependence of the Lowest Excited Singlet State Lifetime and Spectral Behavior Unique among Carotenoids. *J. Phys. Chem. B* **1999,** *103* (41), 8751-8758; (b) Frank, H. A.; Bautista, J. A.; Josue, J.; Pendon, Z.; Hiller, R. G.; Sharples, F. P.; Gosztola, D.; Wasielewski, M. R., Effect of the Solvent Environment on the Spectroscopic Properties and Dynamics of the Lowest Excited States of Carotenoids. *J. Phys. Chem. B* **2000,** *104* (18), 4569-4577.

34.Kloz, M.; Pillai, S.; Kodis, G.; Gust, D.; Moore, T. A.; Moore, A. L.; van Grondelle, R.; Kennis, J. T. M., Carotenoid Photoprotection in Artificial Photosynthetic Antennas. *J. Am. Chem. Soc.* **2011,** *133* (18), 7007-7015.

35. Maiuri, M.; Snellenburg, J. J.; van Stokkum, I. H. M.; Pillai, S.; WongCarter, K.; Gust, D.; Moore, T. A.; Moore, A. L.; van Grondelle, R.; Cerullo, G.; Polli, D., Ultrafast Energy Transfer and Excited State Coupling in an Artificial Photosynthetic Antenna. *J. Phys. Chem. B* **2013,** *117* (46), 14183-14190.

36. (a) Liao, P.-N.; Pillai, S.; Gust, D.; Moore, T. A.; Moore, A. L.; Walla, P. J., Two-Photon Study on the Electronic Interactions between the First Excited Singlet States in Carotenoid−Tetrapyrrole Dyads. *J. Phys. Chem. A* **2011,** *115* (16), 4082-4091; (b) Liao, P.-N.; Pillai, S.; Kloz, M.; Gust, D.; Moore, A.; Moore, T.; Kennis, J. M.; Grondelle, R.; Walla, P., On the role of excitonic interactions in carotenoid–phthalocyanine dyads and implications for photosynthetic regulation. *Photosynth. Res.* **2012,** *111* (1-2), 237-243.

37.Bode, S.; Quentmeier, C. C.; Liao, P.-N.; Hafi, N.; Barros, T.; Wilk, L.; Bittner, F.; Walla, P. J., On the regulation of photosynthesis by excitonic interactions between carotenoids and chlorophylls. *Proc. Natl. Acad. Sci.* **2009,** *106* (30), 12311-12316.

38.Straight, S. D.; Kodis, G.; Terazono, Y.; Hambourger, M.; Moore, T. A.; Moore, A. L.; Gust, D., Self-regulation of photoinduced electron transfer by a molecular nonlinear transducer. *Nat. Nanotechnol.* **2008,** *3* (5), 280-283.

39.(a) Tian, L.; van Stokkum, I. H. M.; Koehorst, R. B. M.; Jongerius, A.; Kirilovsky, D.; van Amerongen, H., Site, Rate, and Mechanism of Photoprotective Quenching in Cyanobacteria. *J. Am. Chem. Soc.* **2011,** *133* (45), 18304-18311; (b) Wilson, A.; Punginelli, C.; Gall, A.; Bonetti, C.; Alexandre, M.; Routaboul, J.-M.; Kerfeld, C. A.; van Grondelle, R.; Robert, B.; Kennis, J. T. M.; Kirilovsky, D., A photoactive carotenoid protein acting as light intensity sensor. *Proc. Natl. Acad. Sci.* **2008,** *105* (33), 12075-12080.

40.Terazono, Y.; Kodis, G.; Bhushan, K.; Zaks, J.; Madden, C.; Moore, A. L.; Moore, T. A.; Fleming, G. R.; Gust, D., Mimicking the Role of the Antenna in Photosynthetic Photoprotection. *J. Am. Chem. Soc.* **2011,** *133* (9), 2916-2922.

41. Ramel, F.; Birtic, S.; Cuiné, S.; Triantaphylidès, C.; Ravanat, J.-L.; Havaux, M., Chemical Quenching of Singlet Oxygen by Carotenoids in Plants. *Plant Physiol.* **2012,** *158* (3), 1267-1278.

42. Gust, D.; Moore, T. A.; Moore, A. L.; Krasnovsky, A. A.; Liddell, P. A.; Nicodem, D.; DeGraziano, J. M.; Kerrigan, P.; Makings, L. R.; Pessiki, P. J., Mimicking the photosynthetic triplet energy-transfer relay. *J. Am. Chem. Soc.* **1993,** *115* (13), 5684-5691.

43.(a) Liddell, P. A.; Barrett, D.; Makings, L. R.; Pessiki, P. J.; Gust, D.; Moore, T. A., Charge separation and energy transfer in carotenopyropheophorbide-quinone triads. *J. Am. Chem. Soc.* **1986,** *108* (17), 5350-5352; (b) Schenck, C. C.; Mathis, P.; Lutz, M.; Gust, D.; Moore, T. A., TRIPLET STATE OF BACTERIOCHLOROPHYLL AND CAROTENOID IN BACTERIAL REACTION CENTERS. *Biophys. J.* **1983,** *41* (2, Part 2), 113a-160a.

44.Yeates, T. O.; Komiya, H.; Chirino, A.; Rees, D. C.; Allen, J. P.; Feher, G., Structure of the reaction center from Rhodobacter sphaeroides R-26 and 2.4.1: protein-cofactor (bacteriochlorophyll, bacteriopheophytin, and carotenoid) interactions. *Proc. Natl. Acad. Sci.* **1988,** *85* (21), 7993-7997.

45.Bensasson, R. V.; Land, E. J.; Moore, A. L.; Crouch, R. L.; Dirks, G.; Moore, T. A.; Gust, D., Mimicry of antenna and photo-protective carotenoid functions by a synthetic carotenoporphyrin. *Nature* **1981,** *290* (5804), 329-332.

46. Gall, A.; Berera, R.; Alexandre, Maxime T. A.; Pascal, Andrew A.; Bordes, L.; Mendes-Pinto, Maria M.; Andrianambinintsoa, S.; Stoitchkova, Katerina V.; Marin, A.; Valkunas, L.; Horton, P.; Kennis, John T. M.; van Grondelle, R.; Ruban, A.; Robert, B., Molecular Adaptation of Photoprotection: Triplet States in Light-Harvesting Proteins. *Biophys. J.* **2011,** *101* (4), 934-942.

47. (a) Frank, H. A.; Machnicki, J.; Friesner, R., Energy Transfer between the Primary Donor Bacteriochlorophyll and Carotenoids in Rhodopseudomonas sphaeroides. *Photochem. Photobiol.* **1983,** *38* (4), 451-455; (b) Schenck, C. C.; Mathis, P.; Lutz, M., Triplet Formation and Triplet Decay in Reaction Centers from the Photosynthetic Bacterium Rhodopseudomonas sphaeroides. *Photochem. Photobiol.* **1984,** *39* (3), 407-417.

48.(a) Blankenship, R. E., Chemically induced magnetic polarization in photosynthetic systems. *Acc. Chem. Res.* **1981,** *14* (6), 163-170; (b) Blankenship, R. E., *Moleclar Mechanims of Photosynthesis*. Blackwell Science: Hong-Kong, 2002; (c) Thurnauer, M. C.; Katz, J. J.; Norris, J. R., The triplet state in bacterial photosynthesis: Possible mechanisms of the primary photo-act. *Proc. Natl. Acad. Sci.* **1975,** *72* (9), 3270-3274.

49.(a) Carbonera, D.; Di Valentin, M.; Corvaja, C.; Agostini, G.; Giacometti, G.; Liddell, P. A.; Kuciauskas, D.; Moore, A. L.; Moore, T. A.; Gust, D., EPR Investigation of Photoinduced Radical Pair Formation and Decay to a Triplet State in a Carotene−Porphyrin−Fullerene Triad. *J. Am. Chem. Soc.* **1998,** *120* (18), 4398-4405; (b) Kuciauskas, D.; Liddell, P. A.; Lin, S.; Stone, S. G.; Moore, A. L.; Moore, T. A.; Gust, D., Photoinduced Electron Transfer in Carotenoporphyrin−Fullerene Triads: Temperature and Solvent Effects. *J. Phys. Chem. B* **2000,** *104* (18), 4307-4321.

50. Maeda, K.; Henbest, K. B.; Cintolesi, F.; Kuprov, I.; Rodgers, C. T.; Liddell, P. A.; Gust, D.; Timmel, C. R.; Hore, P. J., Chemical compass model of avian magnetoreception. *Nature* **2008,** *453* (7193), 387-390.

51. Moore, T. A.; Moore, A. L.; Gust, D., The design and synthesis of artificial photosynthetic antennas, reaction centres and membranes. *Philosophical Transactions of the Royal Society of London. Series B: Biological Sciences* **2002,** *357* (1426), 1481-1498.

52.Foote, C. S., *Free radicals and biological systems*. Academic Press: New York, 1976; Vol. 2.

53. (a) Mathis, P.; Butler, W. L.; Satoh, K., Carotenoid Triplet State and Chlorophyll Fluorescence Quenching in Chloroplasts and Subchloroplast Particles. *Photochem. Photobiol.* **1979,** *30*, 603-314; (b) Monger, T. G.; Cogdell, R. J.; Parson, W. W., Triplet states of bacteriochlorophyll and carotenoids in chromatophores of photosynthetic bacteria. *Biochimica et Biophysica Acta (BBA) - Bioenergetics* **1976,** *449* (1), 136-153.

54. (a) Angerhofer, A.; Bornhäuser, F.; Gall, A.; Cogdell, R. J., Optical and optically detected magnetic resonance investigation on purple photosynthetic bacterial antenna complexes. *Chem. Phys.* **1995,** *194* (2–3), 259-274; (b) Bittl, R.; Schlodder, E.; Geisenheimer, I.; Lubitz, W.; Cogdell, R. J., Transient EPR and Absorption Studies of Carotenoid Triplet Formation in Purple Bacterial Antenna Complexes. *J. Phys. Chem. B* **2001,** *105* (23), 5525-5535.

55. (a) Peterman, E. J.; Dukker, F. M.; van Grondelle, R.; van Amerongen, H., Chlorophyll a and carotenoid triplet states in light-harvesting complex II of higher plants. *Biophys. J.* **1995,** *69* (6), 2670-2678; (b) Vos, R.; Carbonera, D.; Hoff, A. J., Microwave and optical spectroscopy of carotenoid triplets in light-harvesting complex LHC II of spinach by absorbance-detected magnetic resonance. *Appl. Magn. Reson.* **1991,** *2* (2), 179-202.

56.(a) Gust, D.; Moore, T. A., Mimicking Photosynthetic Electron and Energy Transfer. In *Adv. Photochem.*, John Wiley & Sons, Inc.: 2007; pp 1-65; (b) Moore, T. A.; Gust, D.; Mathis, P.; Mialocq, J.-C.; Chachaty, C.; Bensasson, R. V.; Land, E. J.; Doizi, D.; Liddell, P. A.; Lehman, W. R.; Nemeth, G. A.; Moore, A. L., Photodriven charge separation in a carotenoporphyrin-quinone triad. *Nature* **1984,** *307* (5952), 630-632.

57.Gunter, M. J.; Robinson, B. C., A synthesis of purpurin derivatives substituted at the 6,16-meso positions. *Tetrahedron Lett.* **1990,** *31* (2), 285-288.

58. Gust, D.; Moore, T. A.; Moore, A.; Liddeli, P. A., Synthesis of carotenoporphyrin models for photosynthetic energy and electron transfer. *Methods Enzymol.* **1992,** *213* (Carotenoids Part A), 87-100.

59. http://www.public.asu.edu/~laserweb/asufit/asufit.html.

60. Christensen, R., The Electronic States of Carotenoids. In *The Photochemistry of Carotenoids*, Frank, H.; Young, A.; Britton, G.; Cogdell, R., Eds. Springer Netherlands: 1999; Vol. 8, pp 137-159.

61.Koyama, Y.; Takatsuka, I.; Nakata, M.; Tasumi, M., Raman and infrared spectra of the all-trans, 7-cis, 9-cis, 13-cis and 15-cis isomers of β-carotene: Key bands distinguishing stretched or terminal-bent configurations form central-bent configurations. *J. Raman Spectrosc.* **1988,** *19* (1), 37-49.

62. (a) Hashimoto, H.; Koyama, Y., Time-resolved resonance Raman spectroscopy of triplet .beta.-carotene produced from all-trans, 7-cis, 9-cis, 13-cis, and 15-cis isomers and high-pressure liquid chromatography analyses of photoisomerization via the triplet state. *J. Phys. Chem.* **1988,** *92* (8), 2101-2108; (b) Hashimoto, H.; Koyama, Y.; Hirata, Y.; Mataga, N., S1 and T1 species of .beta.-carotene generated by direct photoexcitation from the all-trans, 9-cis, 13-cis, and 15-cis isomers as revealed by picosecond transient absorption and transient Raman spectroscopies. *J. Phys. Chem.* **1991,** *95* (8), 3072-3076; (c) Mukai-Kuroda, Y.; Fujii, R.; Ko-chi, N.; Sashima, T.; Koyama, Y.; Abe, M.; Gebhard, R.; van der Hoef, I.; Lugtenburg, J., Changes in Molecular Structure upon Triplet Excitation of All-trans-Spheroidene in n-Hexane Solution and 15-cis-Spheroidene Bound to the Photo-Reaction Center from Rhodobacter sphaeroides As Revealed by Resonance-Raman Spectroscopy and Normal-Coordinate Analysis†. *J. Phys. Chem. A* **2002,** *106* (14), 3566-3579; (d) Ohashi, N.; Ko-Chi, N.; Kuki, M.; Shimamura, T.; Cogdell, R. J.; Koyama, Y., The structures of S0 spheroidene in the light-harvesting (LH2) complex and S0 and T1 spheroidene in the reaction center of Rhodobacter sphaeroides 2.4.1 as revealed by Raman spectroscopy. *Biospectroscopy* **1996,** *2* (1), 59-69; (e) Rondonuwu, F. S.; Taguchi, T.; Fujii, R.; Yokoyama, K.; Koyama, Y.; Watanabe,

Y., The energies and kinetics of triplet carotenoids in the LH2 antenna complexes as determined by phosphorescence spectroscopy. *Chem. Phys. Lett.* **2004,** *384* (4-6), 364-371.

63. Alexandre, M. T. A.; Lührs, D. C.; van Stokkum, I. H. M.; Hiller, R.; Groot, M.-L.; Kennis, J. T. M.; van Grondelle, R., Triplet State Dynamics in Peridinin-Chlorophyll-a-Protein: A New Pathway of Photoprotection in LHCs? *Biophys. J.* **2007,** *93* (6), 2118-2128.

64. Demchenko, A. P., *Introduction to Fluorescence Sensing*. Springer Netherlands: 2009.

65. Turro, N. J.; Ramamurthy, V.; Scaiano, J. C., *Modern Molecular Photochemistry of Organic Molecules*. University Science Books: Sausalito, California, 2010.

66. (a) Gradinaru, C. C.; Kennis, J. T. M.; Papagiannakis, E.; van Stokkum, I. H. M.; Cogdell, R. J.; Fleming, G. R.; Niederman, R. A.; van Grondelle, R., An unusual pathway of excitation energy deactivation in carotenoids: Singlet-to-triplet conversion on an ultrafast timescale in a photosynthetic antenna. *Proc. Natl. Acad. Sci.* **2001,** *98* (5), 2364-2369; (b) Šlouf, V.; Fuciman, M.; Dulebo, A.; Kaftan, D.; Koblížek, M.; Frank, H. A.; Polívka, T., Carotenoid Charge Transfer States and Their Role in Energy Transfer Processes in LH1–RC Complexes from Aerobic Anoxygenic Phototrophs. *J. Phys. Chem. B* **2012,** *117* (38), 10987-10999.

67. Dirks, G. W. I. Energy Transfer From Carotenoids To Porphyrins II. Stereochemistry of Oligomeric Proteins. Arizona State University, 1980.

68. Lindsey, J. S., Synthetic Routes to meso-Patterned Porphyrins. *Acc. Chem. Res.* **2009,** *43* (2), 300-311.

69. Wahadoszamen, M.; Berera, R.; Ara, A. M.; Romero, E.; van Grondelle, R., Identification of two emitting sites in the dissipative state of the major light harvesting antenna. *Phys. Chem. Chem. Phys.* **2012,** *14* (2), 759-766.

70. (a) Novoderezhkin, V. I.; van Grondelle, R., Physical origins and models of energy transfer in photosynthetic light-harvesting. *Phys. Chem. Chem. Phys.* **2010,** *12* (27), 7352-7365; (b) van Amerongen, H.; Valkunas, L.; Van Grondelle, R., *Photosynthetic Excitons*. World Scientific: 2000; (c) van Grondelle, R.; Novoderezhkin, V. I., Energy transfer in photosynthesis: experimental insights and quantitative models. *Phys. Chem. Chem. Phys.* **2006,** *8* (7), 793-807.

71. Frank, H. A.; Cogdell, R. J., Carotenoids in Photosynthesis. *Photochem. Photobiol.* **1996,** *63* (3), 257-264.

72.(a) Niyogi, K. K., Safety valves for photosynthesis. *Current Opinion in Plant Biology* **2000,** *3* (6), 455-460; (b) Ruban, A. V.; Johnson, M. P.; Duffy, C. D. P., The photoprotective molecular switch in the photosystem II antenna. *Biochimica et Biophysica Acta (BBA) - Bioenergetics* **2012,** *1817* (1), 167-181.

73.(a) Ahn, T. K.; Avenson, T. J.; Ballottari, M.; Cheng, Y.-C.; Niyogi, K. K.; Bassi, R.; Fleming, G. R., Architecture of a Charge-Transfer State Regulating Light Harvesting in a Plant Antenna Protein. *Science* **2008,** *320* (5877), 794-797; (b) Pascal, A. A.; Liu, Z.; Broess, K.; van Oort, B.; van Amerongen, H.; Wang, C.; Horton, P.; Robert, B.; Chang, W.; Ruban, A., Molecular basis of photoprotection and control of photosynthetic light-harvesting. *Nature* **2005,** *436* (7047), 134-137.

74. (a) Hudson, B. S.; Kohler, B. E., A low-lying weak transition in the polyene α,ω-diphenyloctatetraene. *Chem. Phys. Lett.* **1972,** *14* (3), 299-304; (b) Schulten, K.; Karplus, M., On the origin of a low-lying forbidden transition in polyenes and related molecules. *Chem. Phys. Lett.* **1972,** *14* (3), 305-309.

75.(a) Cerullo, G.; Polli, D.; Lanzani, G.; De Silvestri, S.; Hashimoto, H.; Cogdell, R. J., Photosynthetic Light Harvesting by Carotenoids: Detection of an Intermediate Excited State. *Science* **2002,** *298* (5602), 2395-2398; (b) Marek, M. S.; Buckup, T.; Motzkus, M., Direct Observation of a Dark State in Lycopene Using Pump-DFWM. *J. Phys. Chem. B* **2011,** *115* (25), 8328-8337; (c) Ostroumov, E.; Müller, M. G.; Marian, C. M.; Kleinschmidt, M.; Holzwarth, A. R., Electronic Coherence Provides a Direct Proof for Energy-Level Crossing in Photoexcited Lutein and β-Carotene. *Phys. Rev. Lett.* **2009,** *103* (10), 108302.

76. Liddell, P. A.; Kuciauskas, D.; Sumida, J. P.; Nash, B.; Nguyen, D.; Moore, A. L.; Moore, T. A.; Gust, D., Photoinduced Charge Separation and Charge Recombination to a Triplet State in a Carotene−Porphyrin−Fullerene Triad. *J. Am. Chem. Soc.* **1997,** *119* (6), 1400-1405.

77. Manzoni, C.; Polli, D.; Cerullo, G., Two-color pump-probe system broadly tunable over the visible and the near infrared with sub-30fs temporal resolution. *Rev. Sci. Instrum.* **2006,** *77* (2), -.

78. Polli, D.; Lüer, L.; Cerullo, G., High-time-resolution pump-probe system with broadband detection for the study of time-domain vibrational dynamics. *Rev. Sci. Instrum.* **2007,** *78* (10), -.

79. Snellenburg, J. J.; Laptenok, S. P.; Seger, R.; Mullen, K. M.; Van Stokkum, I. H., Glotraran: A Java-Based Graphical User Interface fro the R Package TIMP. *J. Stat. Softw.* **2012,** *49* (3), 1-23.

80. (a) de Weerd, F. L.; van Stokkum, I. H. M.; van Grondelle, R., Subpicosecond dynamics in the excited state absorption of all-trans-β-Carotene. *Chem. Phys. Lett.* **2002,** *354* (1–2), 38-43; (b) Polli, D.; Cerullo, G.; Lanzani, G.; De Silvestri, S.; Hashimoto, H.; Cogdell, R. J., Carotenoid-Bacteriochlorophyll Energy Transfer in LH2 Complexes Studied with 10-fs Time Resolution. *Biophys. J.* **2006,** *90* (7), 2486-2497.

81.Savolainen, J.; Buckup, T.; Hauer, J.; Jafarpour, A.; Serrat, C.; Motzkus, M.; Herek, J. L., Carotenoid deactivation in an artificial light-harvesting complex via a vibrationally hot ground state. *Chem. Phys.* **2009,** *357* (1–3), 181-187.

82.Papagiannakis, E.; van Stokkum, I. H. M.; Vengris, M.; Cogdell, R. J.; van Grondelle, R.; Larsen, D. S., Excited-State Dynamics of Carotenoids in Light-Harvesting Complexes. 1. Exploring the Relationship between the S1 and S* States. *J. Phys. Chem. B* **2006,** *110* (11), 5727-5736.

83. Krueger, B. P.; Scholes, G. D.; Jimenez, R.; Fleming, G. R., Electronic Excitation Transfer from Carotenoid to Bacteriochlorophyll in the Purple Bacterium Rhodopseudomonas acidophila. *J. Phys. Chem. B* **1998,** *102* (12), 2284-2292.

84. (a) Macpherson, A. N.; Arellano, J. B.; Fraser, N. J.; Cogdell, R. J.; Gillbro, T., Efficient Energy Transfer from the Carotenoid S2 State in a Photosynthetic Light-Harvesting Complex. *Biophys. J.* **2001,** *80* (2), 923-930; (b) Wohlleben, W.; Buckup, T.; Herek, J. L.; Cogdell, R. J.; Motzkus, M., Multichannel Carotenoid Deactivation in Photosynthetic Light Harvesting as Identified by an Evolutionary Target Analysis. *Biophys. J.* **2003,** *85* (1), 442-450.

85.Savolainen, J.; Dijkhuizen, N.; Fanciulli, R.; Liddell, P. A.; Gust, D.; Moore, T. A.; Moore, A. L.; Hauer, J.; Buckup, T.; Motzkus, M.; Herek, J. L., Ultrafast Energy Transfer Dynamics of a Bioinspired Dyad Molecule. *J. Phys. Chem. B* **2008,** *112* (9), 2678-2685.

86. Cong, H.; Niedzwiedzki, D. M.; Gibson, G. N.; LaFountain, A. M.; Kelsh, R. M.; Gardiner, A. T.; Cogdell, R. J.; Frank, H. A., Ultrafast Time-Resolved Carotenoid to-Bacteriochlorophyll Energy Transfer in LH2 Complexes from Photosynthetic Bacteria. *J. Phys. Chem. B* **2008,** *112* (34), 10689-10703.

87. Papagiannakis, E.; Das, S. K.; Gall, A.; van Stokkum, I. H. M.; Robert, B.; van Grondelle, R.; Frank, H. A.; Kennis, J. T. M., Light Harvesting by Carotenoids Incorporated into the B850 Light-Harvesting Complex from Rhodobacter sphaeroides R-26.1: Excited-State Relaxation, Ultrafast Triplet Formation, and Energy Transfer to Bacteriochlorophyll. *J. Phys. Chem. B* **2003,** *107* (23), 5642-5649.

88.Wohlleben, W.; Buckup, T.; Hashimoto, H.; Cogdell, R. J.; Herek, J. L.; Motzkus, M., Pump−Deplete−Probe Spectroscopy and the Puzzle of Carotenoid Dark States. *J. Phys. Chem. B* **2004,** *108* (10), 3320-3325.

89. (a) Kingma, H.; van Grondelle, R.; Duysens, L. N. M., Magnetic-field effects in photosynthetic bacteria. II. Formation of triplet states in the reaction center and the antenna of Rhodospirillum rubrum and Rhodopseudomonas sphaeroides. Magnetic-field effects. *Biochimica et Biophysica Acta (BBA) - Bioenergetics* **1985,** *808* (3), 383-399; (b) Rademaker, H.; Hoff, A. J.; Van Grondelle, R.; Duysens, L. N. M., Carotenoid triplet yields in normal and deuterated Rhodospirillum rubrum. *Biochimica et Biophysica Acta (BBA) - Bioenergetics* **1980,** *592* (2), 240-257.

90.Niedzwiedzki, D.; Koscielecki, J. F.; Cong, H.; Sullivan, J. O.; Gibson, G. N.; Birge, R. R.; Frank, H. A., Ultrafast Dynamics and Excited State Spectra of Open-Chain Carotenoids at Room and Low Temperatures. *J. Phys. Chem. B* **2007,** *111* (21), 5984-5998.

91. Palacios, R. E.; Kodis, G.; Herrero, C.; Ochoa, E. M.; Gervaldo, M.; Gould, S. L.; Kennis, J. T. M.; Gust, D.; Moore, T. A.; Moore, A. L., Tetrapyrrole Singlet Excited State Quenching by Carotenoids in an Artificial Photosynthetic Antenna†. *J. Phys. Chem. B* **2006,** *110* (50), 25411-25420.

92. Engel, G. S.; Calhoun, T. R.; Read, E. L.; Ahn, T.-K.; Mancal, T.; Cheng, Y.-C.; Blankenship, R. E.; Fleming, G. R., Evidence for wavelike energy transfer through quantum coherence in photosynthetic systems. *Nature* **2007,** *446* (7137), 782-786.

93.Collini, E.; Wong, C. Y.; Wilk, K. E.; Curmi, P. M. G.; Brumer, P.; Scholes, G. D., Coherently wired light-harvesting in photosynthetic marine algae at ambient temperature. *Nature* **2010,** *463* (7281), 644-647.

94.Calhoun, T. R.; Ginsberg, N. S.; Schlau-Cohen, G. S.; Cheng, Y.-C.; Ballottari, M.; Bassi, R.; Fleming, G. R., Quantum Coherence Enabled Determination of the Energy Landscape in Light-Harvesting Complex II. *J. Phys. Chem. B* **2009,** *113* (51), 16291-16295.

95. (a) Sherman, B.; Vaughn, M.; Bergkamp, J.; Gust, D.; Moore, A.; Moore, T., Evolution of reaction center mimics to systems capable of generating solar fuel. *Photosynth. Res.* **2014,** *120* (1-2), 59-70; (b) Tsao, J.; Lewis, N.; Crabtree, G., Solar FAQ. Energy, D. o., Ed. Sandia National Laboratory, 2006.

96.Law, C. J.; Roszak, A. W.; Southall, J.; Gardiner, A. T.; Isaacs, N. W.; Cogdell, R. J., The structure and function of bacterial light-harvesting complexes (Review). *Mol. Membr. Biol.* **2004,** *21* (3), 183-191.

97.(a) Berman, H. M.; Westbrook, J.; Feng, Z.; Gilliland, G.; Bhat, T. N.; Weissig, H.; Shindyalov, I. N.; Bourne, P. E., The Protein Data Bank. *Nucleic Acids Res.* **2000,** *28* (1), 235-242; (b) Papiz, M. Z.; Prince, S. M.; Howard, T.; Cogdell, R. J.; Isaacs, N. W., The Structure and Thermal Motion of the B800–850 LH2 Complex from Rps. acidophila at 2.0 Å Resolution and 100 K: New Structural Features and Functionally Relevant Motions. *J. Mol. Biol.* **2003,** *326* (5), 1523-1538.

98.Scheuring, S.; Lévy, D.; Rigaud, J.-L., Watching the components of photosynthetic bacterial membranes and their in situ organisation by atomic force microscopy. *Biochimica et Biophysica Acta (BBA) - Biomembranes* **2005,** *1712* (2), 109-127.

99. Love, J. C.; Estroff, L. A.; Kriebel, J. K.; Nuzzo, R. G.; Whitesides, G. M., Self-Assembled Monolayers of Thiolates on Metals as a Form of Nanotechnology. *Chem. Rev. (Washington, DC, U. S.)* **2005,** *105* (4), 1103-1170.

100. Andrews, D.; Gaburro, Z.; Prodi, L.; Battistini, G.; Dolci, L.; Montalti, M.; Zaccheroni, N., Luminescence of Gold Nanoparticles. In *Frontiers in Surface Nanophotonics: Principles and Applications*, Springer: Berlin 2007; Vol. 133, pp 99-128.

101.Kriegisch, V.; Lambert, C., Self-Assembled Monolayers of Chromophores on Gold Surfaces

Supermolecular Dye Chemistry. Würthner, F., Ed. Springer Berlin / Heidelberg: 2005; Vol. 258, pp 585-585.

102.Cook, M. J.; Hersans, R.; McMurdo, J.; Russell, D. A., Self-assembled monolayers of phthalocyanine derivatives on glass and silicon. *J. Mater. Chem.* **1996,** *6* (2), 149-154.

103.Mariño-Ochoa, E.; Palacios, R.; Kodis, G.; Macpherson, A. N.; Gillbro, T.; Gust, D.; Moore, T. A.; Moore, A. L., High-efficiency Energy Transfer from Carotenoids to a Phthalocyanine in an Artificial Photosynthetic Antenna. *Photochem. Photobiol.* **2002,** *76* (1), 116-121.

104.Li, Z.; Lieberman, M.; Hill, W., XPS and SERS Study of Silicon Phthalocyanine Monolayers: Umbrella vs Octopus Design Strategies for Formation of Oriented SAMs. *Langmuir* **2001,** *17* (16), 4887-4894.

105. Hutchings, G. J.; Brust, M.; Schmidbaur, H., Gold-an introductory perspective. *Chem. Soc. Rev.* **2008,** *37* (9), 1759-1765.

106.Bergkamp, J. J.; Sherman, B. D.; Mariño-Ochoa, E.; Palacios, R. E.; Cosa, G.; Gust, D.; Moore, T. A.; Moore, A. L., Synthesis and characterization of silicon phthalocyanines bearing axial phenoxyl groups for attachment to semiconducting metal oxides. *J. Porphyrins Phthalocyanines* **2011,** *15*, 943-950.

107. Schuster, M. C.; Mann, D. A.; Buchholz, T. J.; Johnson, K. M.; Thomas, W. D.; Kiessling, L. L., Parallel Synthesis of Glycomimetic Libraries: Targeting a C-Type Lectin. *Org. Lett.* **2003,** *5* (9), 1407-1410.

108. Han, C.-C.; Balakumar, R., Mild and efficient methods for the conversion of benzylic bromides to benzylic thiols. *Tetrahedron Lett.* **2006,** *47* (47), 8255-8258.

109. Gryko, D. T.; Clausen, C.; Lindsey, J. S., Thiol-Derivatized Porphyrins for Attachment to Electroactive Surfaces. *J. Org. Chem.* **1999,** *64* (23), 8635-8647.

110. Wijtmans, M.; Rosenthal, S. J.; Zwanenburg, B.; Porter, N. A., Visible Light Excitation of CdSe Nanocrystals Triggers the Release of Coumarin from Cinnamate Surface Ligands. *J. Am. Chem. Soc.* **2006,** *128* (35), 11720-11726.

111.(a) Marin, M. L.; McGilvray, K. L.; Scaiano, J. C., Photochemical Strategies for the Synthesis of Gold Nanoparticles from Au(III) and Au(I) Using Photoinduced Free Radical Generation. *J. Am. Chem. Soc.* **2008,** *130* (49), 16572-16584; (b) McGilvray, K. L. Photochemical Strategies for the Synthesis of Gold Nanoparticles. University of Ottawa, Ottawa, 2010; (c) McGilvray, K. L.; Decan, M. R.; Wang, D.; Scaiano, J. C.,

Facile Photochemical Synthesis of Unprotected Aqueous Gold Nanoparticles. *J. Am. Chem. Soc.* **2006,** *128* (50), 15980-15981.

112.Brust, M.; Walker, M.; Bethell, D.; Schiffrin, D. J.; Whyman, R., Synthesis of thiol-derivatised gold nanoparticles in a two-phase Liquid-Liquid system. *J. Chem. Soc., Chem. Commun.* **1994,** (7), 801-802.

113.(a) Turkevich, J.; Garton, G.; Stevenson, P. C., The color of colloidal gold. *Journal of Colloid Science* **1954,** *9* (Supplement 1), 26-35; (b) Turkevich, J.; Stevenson, P. C.; Hillier, J., A study of the nucleation and growth processes in the synthesis of colloidal gold. *Discussions of the Faraday Society* **1951,** *11*.

114.Hernandez, L. I.; Godin, R. P.; Bergkamp, J. J.; Llansola-Portoles, M. J.; Sherman, B. D.; Tomlin, J.; Kodis, G.; Méndez-Hernández, D. D.; Bertolotti, S.; Chesta, C.; Mariño-Ochoa, E.; Moore, A. L.; Moore, T. A.; Cosa, G.; Palacios, R. E., Spectral Characteristics and Photosensitization of TiO2 Nanoparticles in Reverse Micelles by Perylenes. *J. Phys. Chem. B* **2013,** *117* (16), 4568-4581.

115.Krajnik, B.; Schulte, T.; Piątkowski, D.; Czechowski, N.; Hofmann, E.; Mackowski, S., SIL-based confocal fluorescence microscope for investigating individual nanostructures. *Central European Journal of Physics* **2011,** *9* (2), 293-299.

116.Koyama, T.; Suzuki, T.; Hanabusa, K.; Shirai, H.; Kobayashi, N., A comparison of the loop-current effect of silicon phthalocyanine and silicon naphthalocyanine rings on their axial ligands. *Inorg. Chim. Acta* **1994,** *218* (1-2), 41-45.

117. Pillai, S. Design and Synthesis of Artificial Photosynthetic Molecules to Mimic Aspects of Natural Photosynthetic Mechanisms. Ph.D., Arizona State University, Ann Arbor, 2011.

APPENDIX A

SYNTHESIS AND TRIPLET CHARACTERIZATION OF 12 DOUBLE BOND CAROTENOPHTHALOCYANINE DYAD

Introduction

Chapter 1 discussed the importance of photoprotection and how carotenoids provide this function in natural and artificial systems. Chapters 2 and 3 analyzed several carotenoid containing dyads for their triplet energy transfers and triplet states. The last set of dyads in Chapter 3 contained three carotenophthalocyanine dyads with carotenoids containing different numbers of polyene bonds (9 to 11 db). Just as the energy levels of carotenoids vary by length for singlet energy transfer the change in length was investigated to understand how it may affect the coupled carotenoid triplet state. An additional dyad, the 12 db carotenophthalocyanine (**C12Pc**), was synthesized by Smitha Pillai and its carotenoid triplet state was characterized. In this appendix, the triplet character of this dyad in relation to the other carotenophthalocyanine dyads was investigated

Materials and Methods

Materials. The same materials for organic synthesis were state in Chapter 5.

Methods. The same absorption and transient absorption measurements and data analysis were stated in Chapter 3.

Synthesis. The synthesis of the 12 db carotenophthalocyanine followed the same method of extending the length of the apo-carotenoid using repeated Wittig, reduction, and oxidation reactions (Scheme 1) was based on previously published procedures[28, 117]. Then an EDCI and DMAP amide coupling reaction was used to bond the amino zinc phthalocyanine with the carotenoid acid (Scheme 2) using previously published procedures[117].

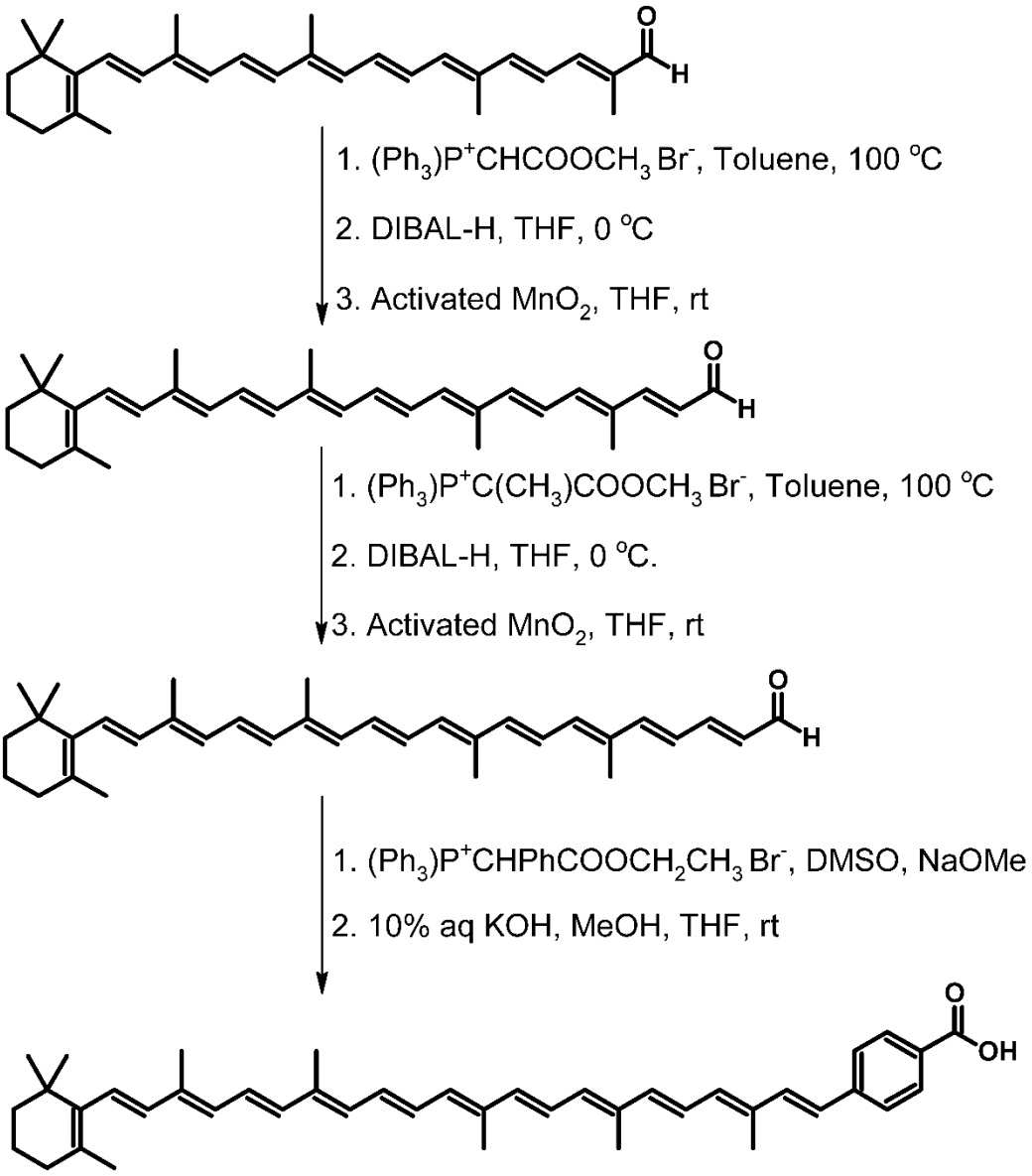

Scheme 1. Synthetic scheme for synthesizing a 12 db apo-carotenoid benzoic acid.

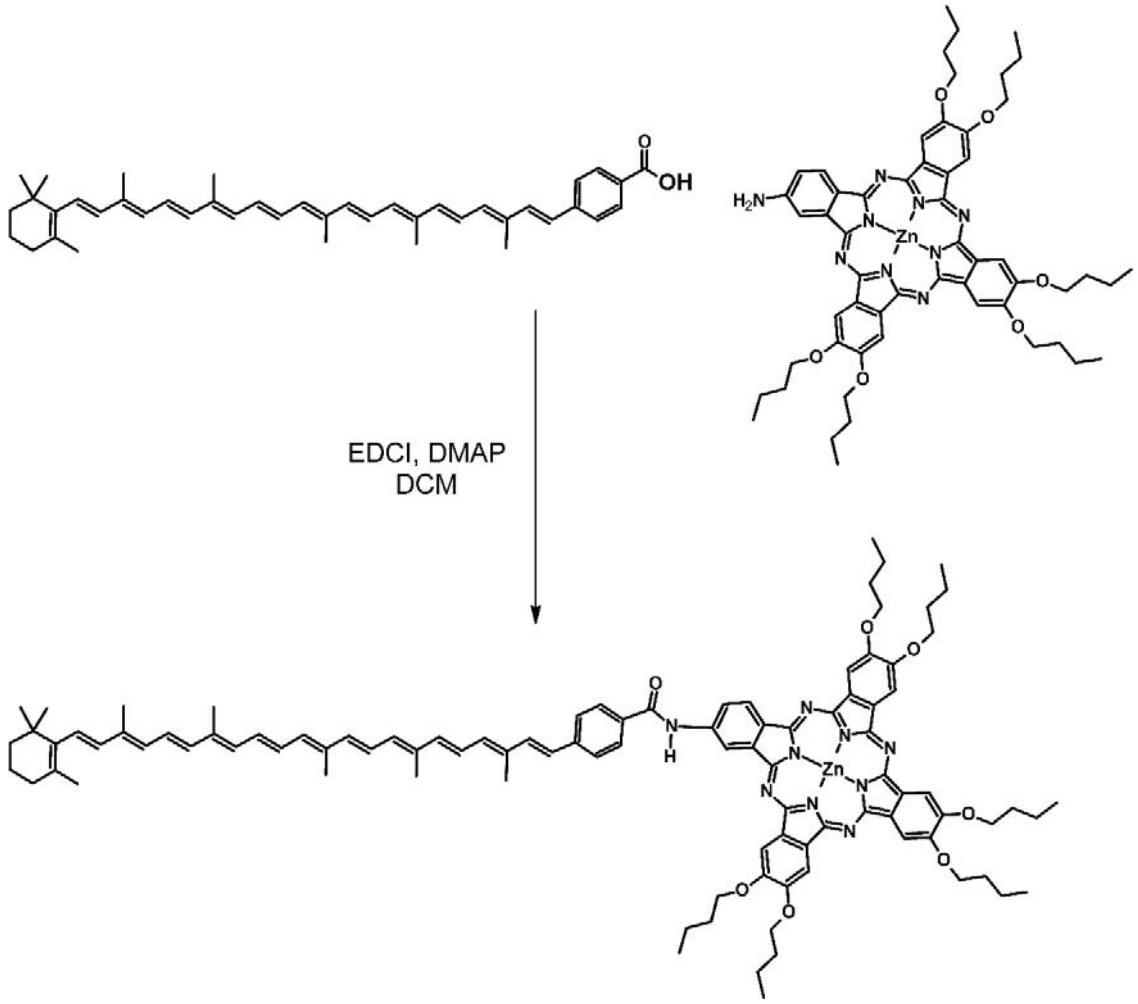

Scheme 2. Synthesis of the 12 db carotenophthalocyanine dyad.

Results & Discussion

From Figure 1A there are features of both the carotenoid between 400 and 550 nm, and the zinc phthalocyanine around 350 nm and between 600 and 700 nm. This spectrum is very similar to the previous dyads (Figure 1B), the only difference is that the 12 db carotenoid is red shifted due to its extended conjugation with the twelfth db and phenyl ring.

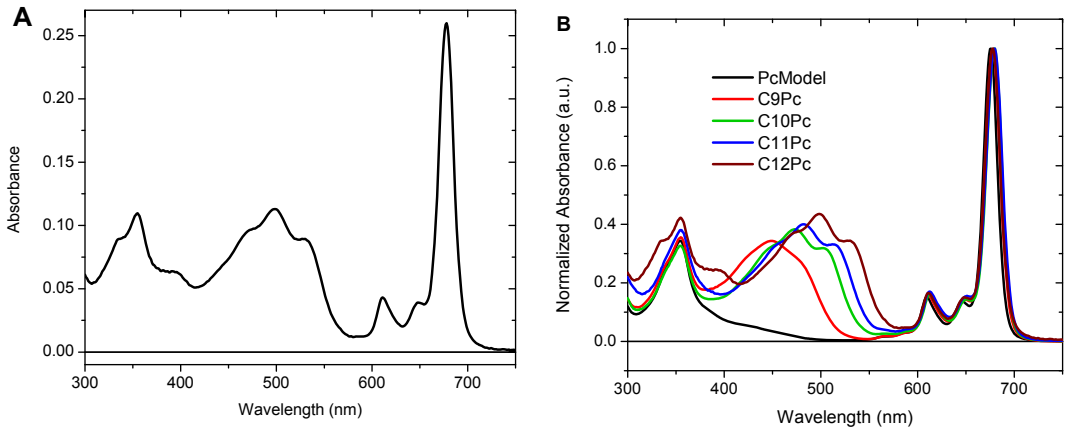

Figure 1. Absorbance spectrum of the 12 db carotenophthalocyanine, **C12Pc**, (A) and the absorbance spectrum of the Pc model and the other carotenophthalocyanine dyads from Chapter 3 in methyl-THF (B).

Since the phthalocyanine triplet was not observed it was assumed that after exciting the phthalocyanine moiety to the singlet excited state, it intersystem crossed to the triplet state, and then the phthalocyanine transferred its energy to the carotenoid faster than the detection limit of the nanosecond transient absorption instruments. This is the same as with the shorter dyads (see Chapter 3). The carotenoid triplet state spectrum (Figure 2) had a carotenoid bleach at 490 nm and photoinduced absorption at 525 nm, and decays in 3.45 μs. In addition, there was a very small photoinduced bleach at 675 nm, which corresponds to the phthalocyanine Q_x band. There was a constant lifetime that has the same spectral features as the phthalocyanine model (Chapter 3, Figure 25), which decayed slower than the time window observed.

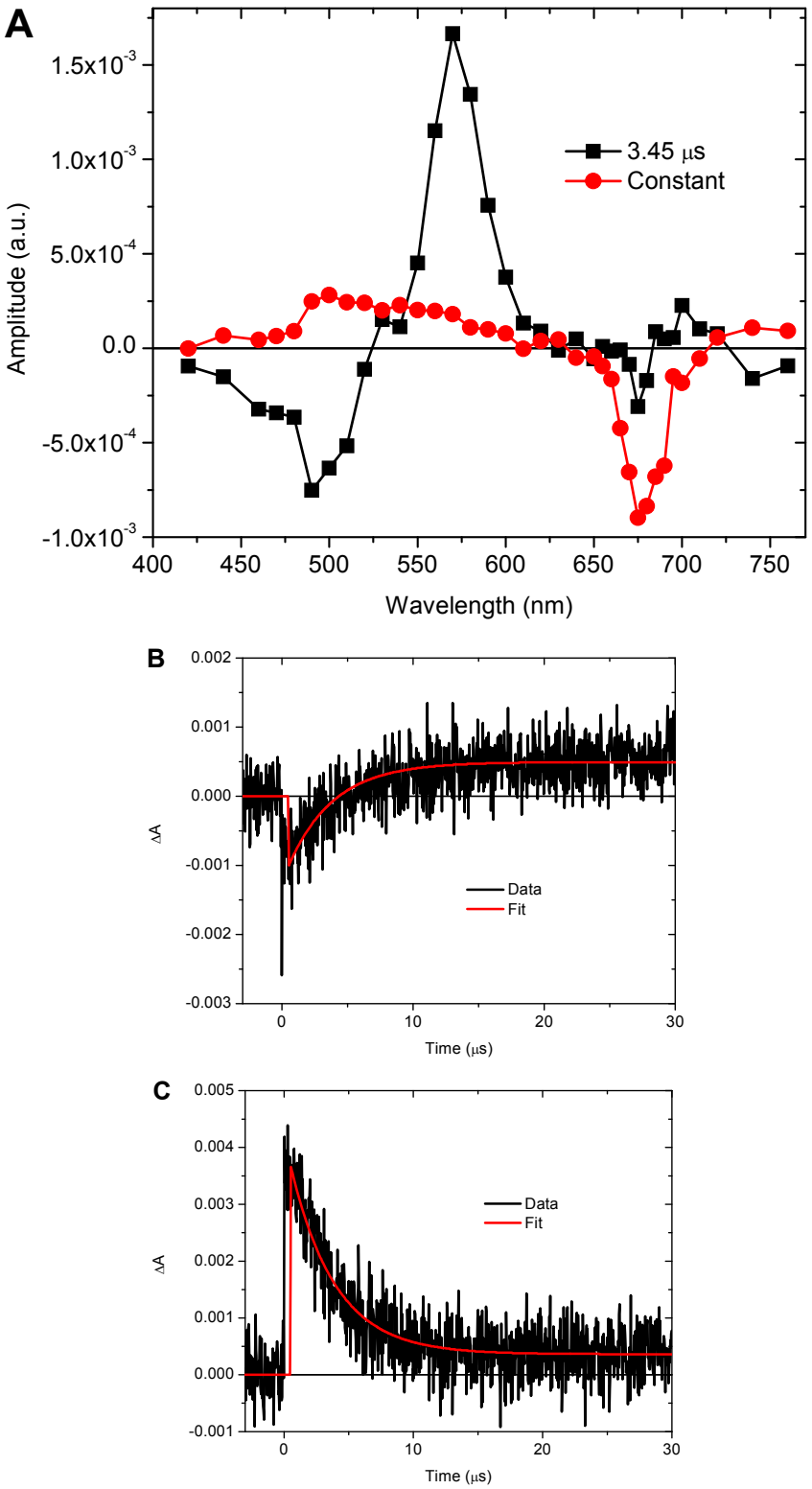

Figure 2. DAS of (A) and the kinetic traces measured at 490 nm (B) and 570 nm (C) resulted from exciting **C12Pc** at 610 and 675 nm in argon saturated methyl-THF.

The 12 db dyad was normalized to the carotenoid bleach at 480 nm and compared with the other carotenophthalocyanine dyads (Figure 3). This longer dyad has a much smaller contribution of the phthalocyanine Q_x bleach than the 10 and 11 db carotenoids, but it has the same intensity as **C9Pc**. This may be due to the phenyl ring that separates the carotenoid and the phthalocyanine, which is a major structural difference between this longer dyad. The phenyl ring could reduce the coupling between the chromophores and increase their separation. Another explanation is that the phenyl ring extends the conjugation of the carotenoid giving it electronic properties of a long carotenoid. Assuming the later, the lower energy level may not interact well with the phthalocyanine Q band and thus have less contribution to the carotenoid triplet state. Either explanation would describe why the phthalocyanine contribution is less for **C12Pc**.

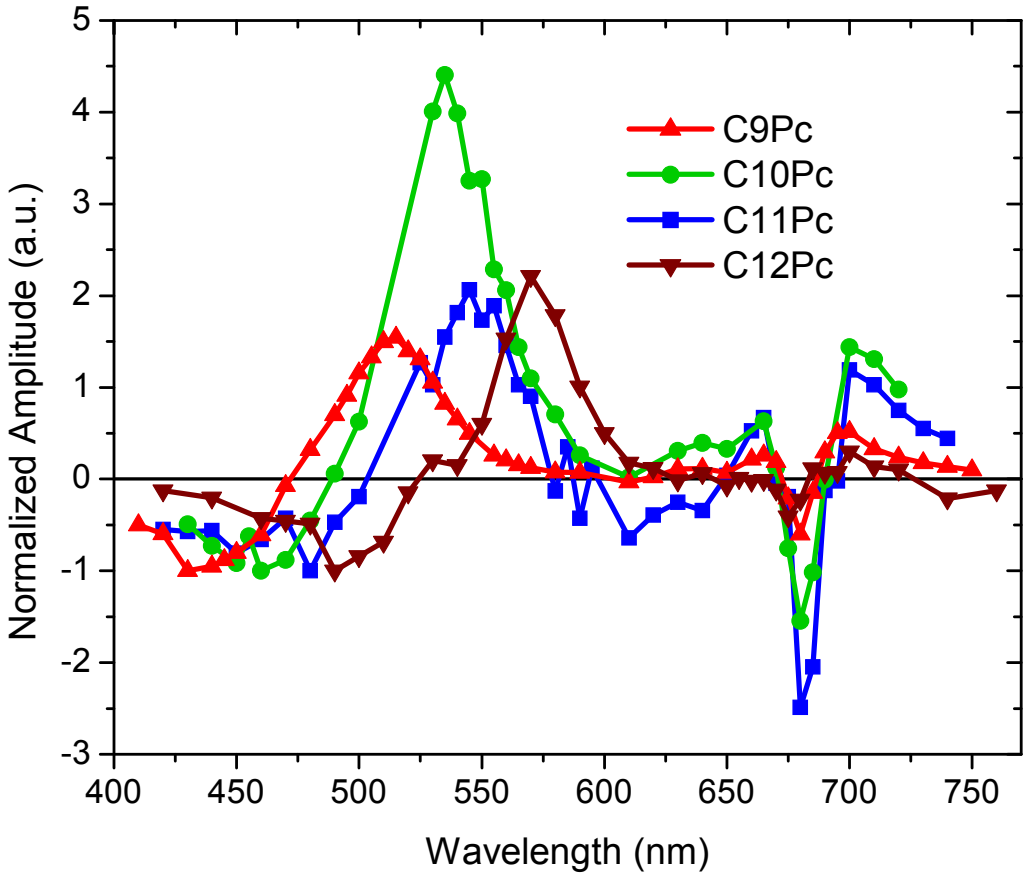

Figure 3. Combined DAS of the CarPc dyads from 9 db to 12 db normalized to the carotenoid bleach.

Table 1. Numbers are based on the carotene decay component (between 4-8 μs) from the DAS and are calculated by dividing the ΔA of the Pc Q_x bleach (680 nm) by the ΔA of carotene triplet bleach (435 to 490 nm).

LENGTH OF CAROTENE	CAROTENE BLEACH/ PC Q_X BLEACH RATIO
9db	0.60
10db	1.54
11db	2.49
12db + Phenyl	0.41

APPENDIX B

SYNTHESIS AND CHARACTERIZATION OF AN ETHER CAROTENOPHTHALOCYANINE DYAD

Introduction

All of the artificial photosynthetic carotenophthalocyanine dyads studied so far contain amide or amine bonds that lead to strong electronic coupling between the two chromophores. For comparison, a dyad containing a 10 db apo-carotenoid covalently bonded to a zinc phthalocyanine through an ether bond was made (Figure 1). A method for making this less coupled dyad and spectroscopic characterization are reported.

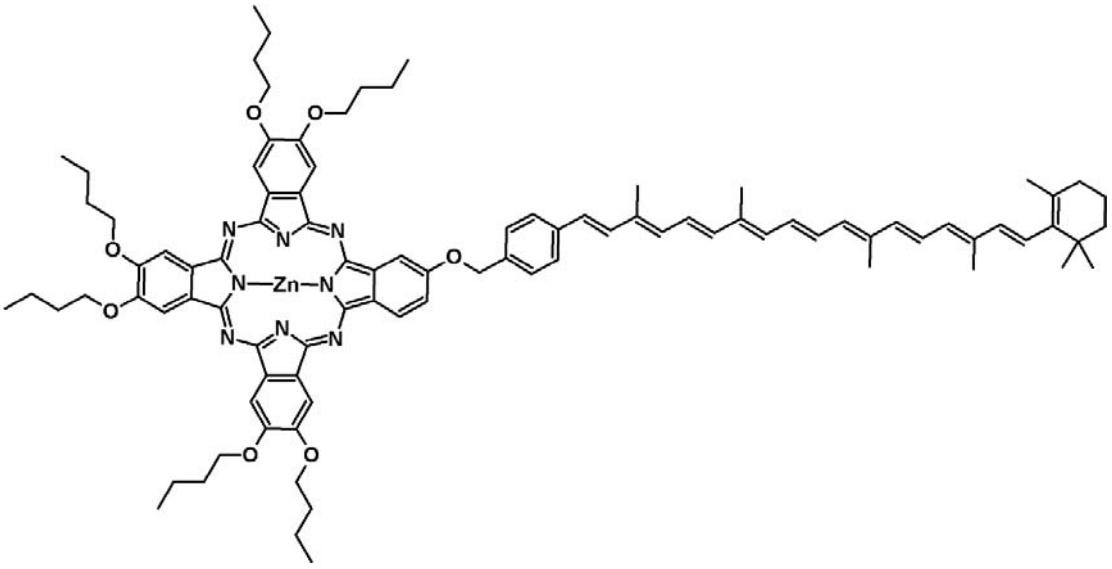

Figure 1. Molecular structure of the ether carotenophthalocyanine.

Materials and Methods

Materials. The same materials for organic synthesis were descrubed in Chapter 5. Dimethylethanolamine (DMAE) was dried over activated 4 Å molecular sieves for use in the reactions. Acetone was distilled for gel silica chromatography. Triphenyl phosphine, ethyl-‘4-(bromomethyl)benzoate, sodium methoxide, apo-8’-carotenal, diisobutyl-aluminium hydride (DIBAL), phosphorous tetraiodide, and zinc chloride were purchased from Sigma-Aldrich and used without further purification 4-Hydroxy phthalonitrile was purchased from TCI America and used without further purification. 4,5-Dibutoxy

phthalonitrile was synthesized from catechol using a previously established method[117]. Ampules of deuterated THF (THF-d^8) was purchased from Cambridge Isotope Laboratories.

Zinc 2-amino-9,10,16,17,23,24-hexabutoxyphthalocyanine (ZnPc). Zinc chloride (100 mg, 0.8 mmol, 1.1 eq), 4-hydroxy phthalonitrile (200 mg, 1.4 mmol, 2.0 eq), and 4,5-dibutoxy phthalonitrile (377 mg, 1.4 mmol, 2.0 eq) were dissolved in 15 mL of dry DMAE. The reaction mixture was heated to reflux and stirred under nitrogen 16 hours. After the reaction solution was cooled to room temperature the solution was washed with water and the blue-green zinc phthalocyanine was extracted with ethyl acetate and small amounts of methanol. The organic layer was dried with brine solution and sodium sulfate before removing the solvent. This resulted in a mixture of zinc phthalocyanines as a blue-green solid. The asymmetrical zinc phthalocyanine was purified by regular silica column chromatography using 1% methanol, 4% acetone, 95% dichloromethane up to 1% methanol, 9% acetone, 90% dichloromethane. Crystallization from dichloromethane to methanol yielded 63.2 mg (8%) of the desired product. ^{1}H-NMR (400 MHz, THF-d^8): δ 1.2 (18h, t, butoxy CH_3), 1.8 (12H, m, butoxy-3 CH_2), 2.1 (12H, m, butoxy-2 CH_2), 4.6 (12H, m, butoxy-1 CH_2), 7.5 (1H, d, J=8 Hz, Pc-H), 8.6-8.7 (6H, m, Pc-H), 9.1 (1H, d, J=8 Hz, Pc-H), 9.2 (1H, s, Pc-H); MALDI-TOF-MS m/z: calculated for $C_{56}H_{64}N_8O_7Zn$ 1024.41 m/z, observed 1024.87 m/z; UV/vis (methyl-THF) 354, 608, and 674 nm.

((4-Ethyoxycarbonyl)phenyl)methyl)triphenylphosphonium bromide. Triphenyl phosphine (2.50g, 9.5 mmol) and ethyl-‘4-(bromomethyl)benzoate were dissolved in dry toluene and heated to 80 °C overnight. This formed a white insoluble salt which was filtered and washed with toluene to afford a quantitative yield. ^{1}H-NMR (400

MHz, $CDCl_3$): δ 1.36 (3H, t, CH_3), 1.84 (2H, s, benzyl-CH_2), 4.32 (2H, q, COO-CH_2), 5.64 (2H, q, Ar-H), 7.23 (2H, m, Ar-H), 7.59-7.64 (6H, m, P^+-Ar), 7.72-7.80 (9H, m, P^+-Ar); MALDI-TOF-MS m/z: calculated for $C_{28}H_{26}O_2P$ 425.17 m/z, observed 425.27 m/z.

7'-Apo-7'-(4-ethylbenzoate)-β-carotene. Sodium methoxide (202 mg, 3.74 mole) and ((4-ethyoxycarbonyl)phenyl)methyl)triphenylphosphonium bromide (1.56 g, 3.67 mole) were dissolved in dry DMSO and stirred at room temperature for 30 minutes to form the phosphonium ylide. Apo-8'-carotenal (600 mg, 1.44 mmol) was added to the light-orange phosphonium ylide solution turning the reaction solution a dark red color. The reaction solution was stirred for 3 hours at room temperature under an argon atmosphere. Once the reaction was complete, the carotenoid was extracted using DCM and washed 3 times. The organic layer was dried with brine and sodium sulfate before removing the solvent. This resulted in a *cis/trans* mixture of the desired carotenoid. The *trans* isomer was isolated using a silica column with DCM/hexanes as the eluent and recrystallization from DCM/methanol. ^{1}H-NMR (400 MHz, $CDCl_3$): δ 1.03 (6H, m, CH_3-16C and CH_3-17C), 1.40 (3H, t, COOEt-CH_3), 1.45-1.50 (2H, m, CH_2-2C), 1.60-1.63 (2H, m, CH_2-3C), 1.72 (3H, s, CH_2-19C), 1.98-2.05 (12H, m, CH_3-18, CH_3-20C, CH_3-19'C, CH_2-4C), 4.37 (2H, q, COO-CH_2), 6.10-6.70 (13H, m, vinyl H), 7.00 (1H, d, J=16Hz, vinyl H), 7.45 (2H, m, benzene), 7.98 (2H, m, benzene); MALDI-TOF-MS m/z: calculated for $C_{40}H_{50}O_2$ 562.38 m/z, observed 562.62 m/z; UV/vis (DCM) 481 and 510 nm, (methyl-THF) 476 and 506.

7'-Apo-7'-(4-phenylmethanol)-β-carotene. The carotenoid ester (81 mg, 0.143 mmol) was dissolved in freshly distilled THF, then it was bubbled with nitrogen and cooled to 0° C. To the carotenoid solution a hexane solution of DIBAL (2.5 mL of 1 M) was added

and allowed to stir at 0° C for 30 minutes. After the completion of the reaction was achieved (monitored by silica TLC with 100% $CHCl_3$) the reaction was quenched with additions of methanol and then water as it warmed to room temperature. The carotene was extracted using ethyl acetate and washed with water and brine before drying with magnesium sulfate. The solvent was removed resulting in the desired product as a light orange solid was afforded a quantitative yield. ^{1}H-NMR (400 MHz, $CDCl_3$): δ 1.03 (6H, m, CH_3-16C and CH_3-17C), 1.45-1.48 (2H, m, CH_2-2C), 1.58-1.63 (2H, m, CH_2-3C), 1.72 (3H, s, CH_2-19C), 1.97-2.04 (12H, m, CH_3-18, CH_3-20C, CH_3-19'C, CH_2-4C), 4.68 (2H, s, benzyl-CH_2), 6.13-6.70 (13H, m vinyl H), 6.90 (1H, d, J=16Hz, vinyl H), 7.31 (2H, m, benzene), 7.42 (2H, m, benzene); MALDI-TOF-MS m/z: calculated for $C_{35}H_{48}O_2$ 520.37 m/z, observed 520.43 m/z; UV/vis (methyl-THF) 467 and 497 nm.

7'-Apo-7'-(4-iodomethylphenyl)-β-carotene. The carotenoid alcohol (185 mg, 0.355 mmol, 1.0 eq.) was dissolved into 10 mL of dry carbon disulfide. The carotenoid solution was bubbled with nitrogen for 30 minutes at 0° C. Phosphorous tetraiodide (89 mg, 0.156 mmol, 0.44 eq.) was added to the carotene solution and stirred at 0° C, under nitrogen, for 90 minutes. The reaction was monitored by TLC using 100% DCM to determine its reaction completion. After 2 hours the reaction was quenched, with anhydrous potassium carbonate and then a saturated aqueous solution of potassium carbonate. The carotenoid products were extracted with DCM and washed with water. The carotenoid solution was treated with brine and then dried magnesium sulfate before removing the solvent, resulting in an orange solid. The solid was further purified using a short pad of silica and a 1:1 hexanes/DCM solution to remove the starting material and polar side-products. The purification resulted in a yellow solid (78 mg, 27%). ^{1}H-NMR

(400 MHz, $CDCl_3$): δ 1.03 (6H, m, CH_3-16C and CH_3-17C), 1.45-1.50 (2H, m, CH_2-2C), 1.60-1.63 (2H, m, CH_2-3C), 1.72 (3H, s, CH_2-19C), 1.93-2.03 (12H, m, CH_3-18, CH_3-20C, CH_3-19'C, CH_2-4C), 4.48 (2H, s, benzyl-CH_2), 6.10-6.70 (13H, m vinyl H), 6.90 (1H, d, J=16Hz, vinyl H), 7.34 (4H, m, benzene); MALDI-TOF-MS m/z: calculated for $C_{38}H_{47}I$ 630.27 m/z, observed 630.46 and 503.36 [-I].

Ether CarPc Dyad. ZnPc (37 mg, 0.036 mmol, 1.5 eq.) and sodium methoxide (5 mg, 0.036 mmol, 1.5 eq) were dissolved in 5 mL of nitrogen bubbled, dry DMSO (sonication was briefly used). The phenoxide anion was allowed to form while stirring at room temperature under nitrogen flow. Then 7'-apo-7'-(4-iodomethylphenyl)-β-carotene (15 mg, 0.024 mmol, 1.0 eq) was dissolved into 2 mL of nitrogen saturated, dry toluene before added to the phthalocyanine solution. The reaction was stirred at room temperature, under nitrogen flow for 1 hour before quenching the reaction by an addition of water. The products were extracted with ethyl acetate and the organic layer washed with water twice, then the organic layer was treated with brine and dried with magnesium sulfate. The solvent was removed leaving a green solid. Silica column purification of the dyad was performed under nitrogen using 1:9 ethyl acetate/toluene solution to remove starting materials. This yielded 3 mg (13%) of the dyad. ^{1}H-NMR (400 MHz, THF-d^8): δ 1.0 (6H, m, CH_3-16C and CH_3-17C), 1.2 (18h, t, butoxy CH_3), 1.5 (6H, m, CH_2-2C), 1.8 (12H, m, butoxy-3 CH_2), 2.0 (12H, m, CH_3-18, CH_3-20C, CH_3-19'C, CH_2-4C), 2.1 (12H, m, butoxy-2 CH_2), 4.6 (12H, m, butoxy-1 CH_2), 5.6 (2H, s, benzyl-CH_2), 6.1-7.2 (14H, m vinyl H), 7.7 (4H, d, Car-1',2',3',4'), 8.7 (6H, m, Pc-Ar H), 9.1 (1H, s, Pc-Ar H), 9.7 (1H, s, Pc-Ar H), 10.8 (1H, s, Pc-Ar H); MALDI-TOF-MS m/z: calculated for $C_{94}H_{110}N_8O_7Zn$ 1526.78 m/z, observed 1526.83; UV/vis (methyl-THF) 355, 467, 496, 608 and 674 nm.

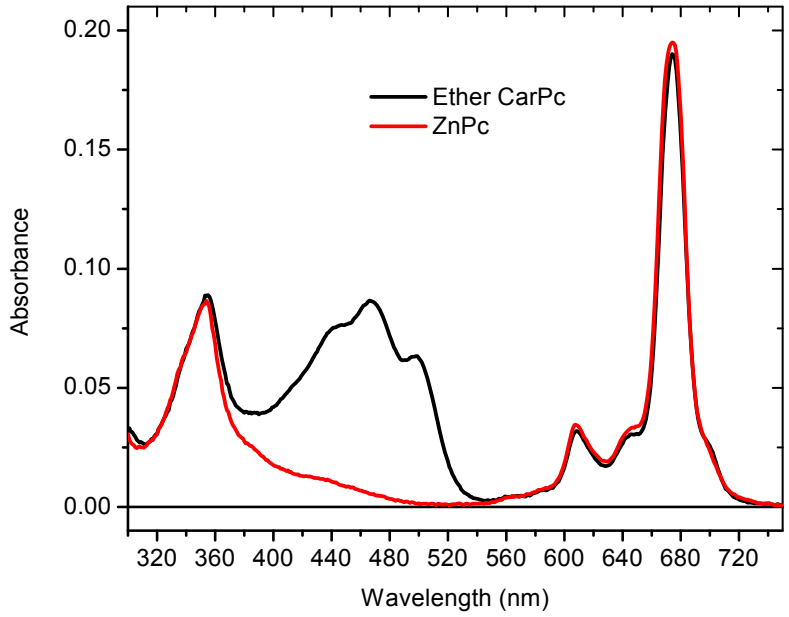

Figure 2. Absorption (A) spectrum of the ether carotenoporphyrin (CarPc) and ZnPc in methyl-THF.

Methods. The same absorption, fluorescence, and transient absorption measurements and data analysis were performed as in Chapter 4.

Results

The absorption spectrum of the ether dyad is atypical for a carotenophthalocyanine dyad because the Q bands did not red shifted compared to previous carotenophthalocyanine dyads. The red shift has always been explained as an extension of the phthalocyanine conjugation by an amine or amide bond. Since there is a saturated methylene ester on the periphery of the phthalocyanine the conjugation is not extended and the Q bands occur at the same wavelengths as the ZnPc precursor.

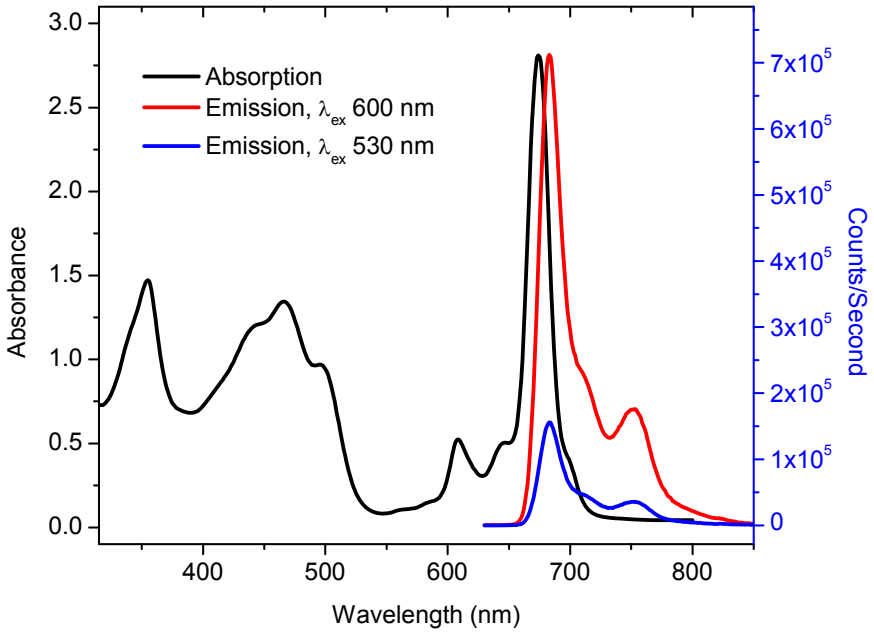

Figure 3. Absorption and emission spectra at different excitation wavelengths of the ether carotenophthalocyanine dyad in methyl-THF.

Upon exciting the phthalocyanine at 600 nm, the emission spectra has a maximum emission at 683 nm with a shoulder at 753 nm. The 10 db carotenoid in the ether dyad could theoretically transfer the exited energy state to a phthalocyanine via singlet-singlet energy transfer[30]. By exciting the dyad at 530 nm, a wavelength where the ZnPc does not absorb (Figure 2), the phthalocyanine emission spectrum is observed (Figure 3). This emission is only 16% of the fluorescence observed when exciting the dyad at 600 nm, after adjusting for the change in optical density. This was a crude measurement for understanding the antenna ability of the carotenoid in this dyad, thus an excitation spectrum and ultrafast transient absorption spectroscopy would need to be performed to understand the energy transfer events occurring in this new dyad.

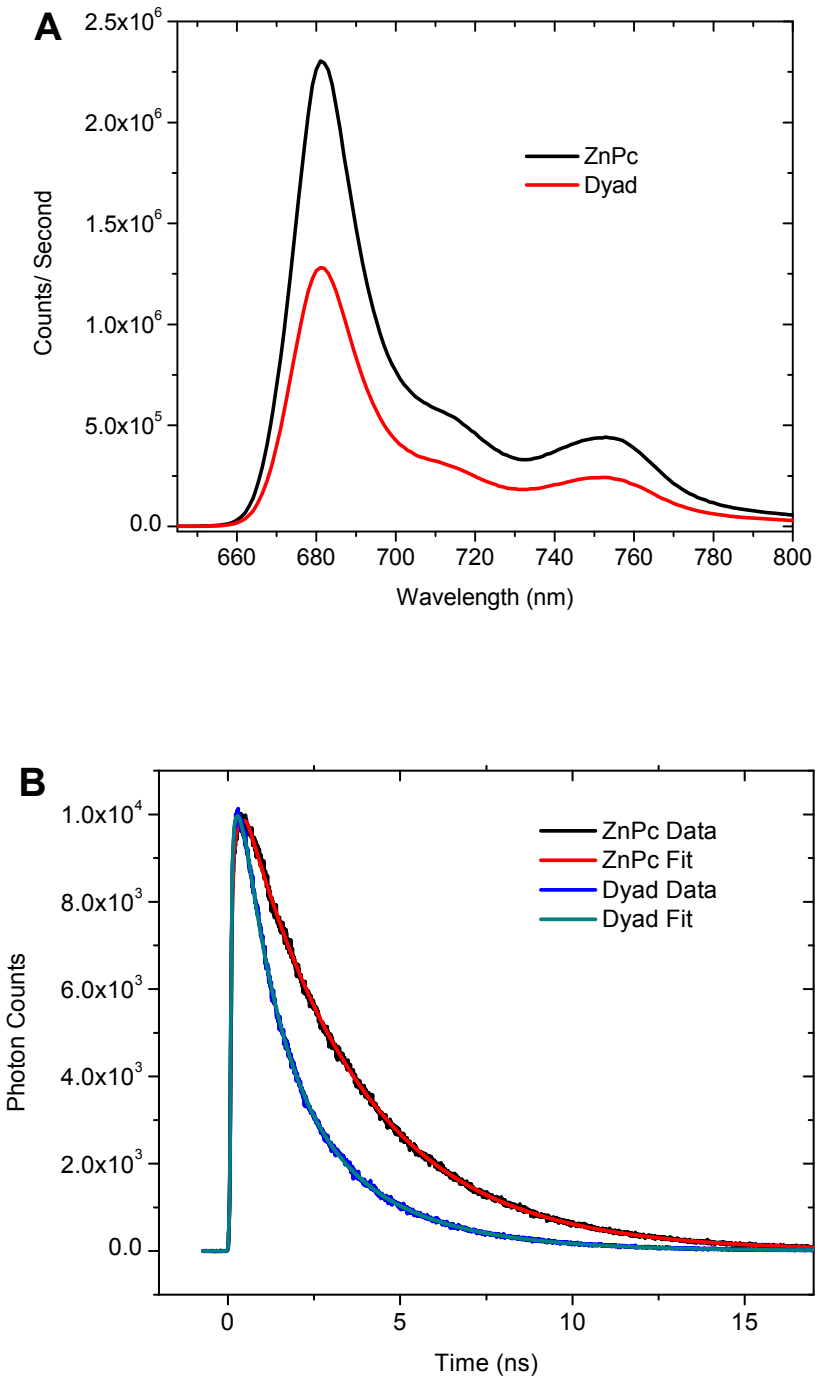

Figure 4. Emission spectra (λ_{ex} = 600 nm, A) and fluorescent decay kinetic (λ_{ex} = 609 nm, λ_{obs} = 750 nm) of the ZnPc and ether carotenophthalocyanine dyad in methyl-THF.

Upon exciting the ZnPc and the ether CarPc there was a significant decrease in the amount of fluorescence observed. Only 56% of the fluorescence was observed in the dyad compared to the phthalocyanine in methyl THF. This is most likely due to quenching by the carotenoid, since 10 db carotenoids are capable of quenching the fluorescence of phthalocyanines. TCSPC also evidenced this quenching of the phthalocyanine fluorescence in the presence of a carotenoid. The ZnPc had a single component that decays in 3.4 ns, while the dyad had two shorter components (2.8 ns, 43%; 1.1 ns, 57%). Ultrafast transient absorption spectroscopy would clarify which carotenoid state is responsible for the fluorescence quenching of the phthalocyanine.

The ether dyad triplet state was measured using transient absorption spectroscopy. First the phthalocyanine was excited to form the singlet excited phthalocyanine, which intersystem crosses to the phthalocyanine triplet in the ultrafast timescale. This triplet state was measured using transient absorption spectroscopy, it decays in 94 ns as the carotenoid triplet state rises (Figure 5). The carotenoid triplet state has distinct absorption and bleach features that decay in 5 μs after relaxing from a non-relaxed state in 1.25 μs. The phthalocyanine triplet was similar to the phthalocyanine triplet measured in Chapter 3 (Figure 25) with an intense Q_x bleach centered at 680 nm. There was a small amount of the phthalocyanine Q_x photoinduced bleach during the non-relaxed and relaxed carotenoid triplet states, so there may be a minimal amount of coupling between the phthalocyanine and the carotenoid in the triplet state. The constant lifetime is from remaining triplet phthalocyanine and has minimal contribution.

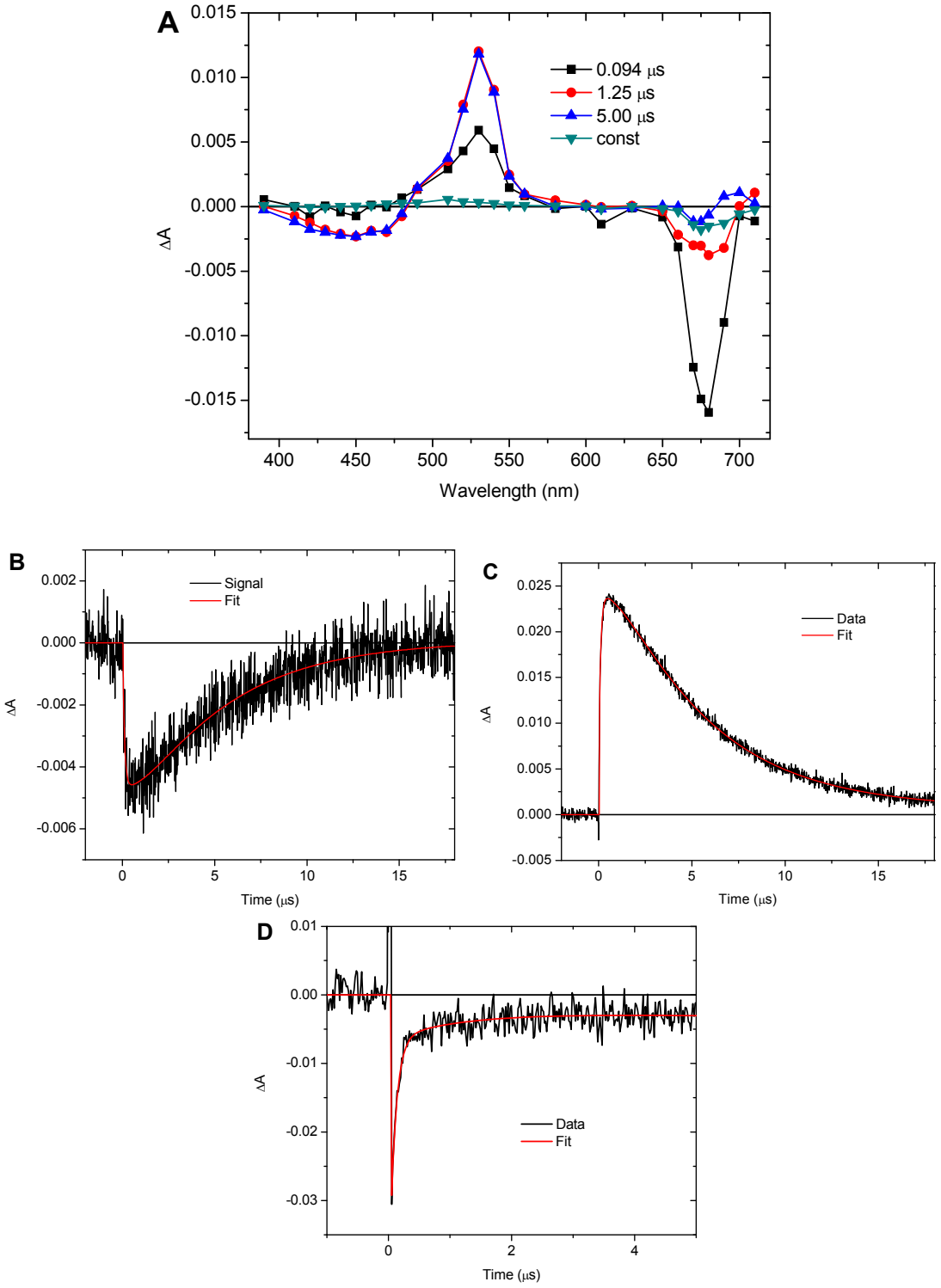

Figure 5. Transient spectrum at 5 ns delay time (A) and kinetic traces at 450 nm (B), 540 nm (B), and 675 nm (C) resulted from the ether CarPc excited at 608 or 675 nm in argon saturated methyl-THF.

APPENDIX C

COPYRIGHT PERMISSION

Copyright Permission for Chapter 4

PERMISSION/LICENSE IS GRANTED FOR YOUR ORDER AT NO CHARGE

This type of permission/license, instead of the standard Terms & Conditions, is sent to you because no fee is being charged for your order. Please note the following:

- Permission is granted for your request in both print and electronic formats, and translations.
- If figures and/or tables were requested, they may be adapted or used in part.
- Please print this page for your records and send a copy of it to your publisher/graduate school.
- Appropriate credit for the requested material should be given as follows: "Reprinted (adapted) with permission from (COMPLETE REFERENCE CITATION). Copyright (YEAR) American Chemical Society." Insert appropriate information in place of the capitalized words.
- One-time permission is granted only for the use specified in your request. No additional uses are granted (such as derivative works or other editions). For any other uses, please submit a new request.

BACK CLOSE WINDOW